Seismic Progressive Collapse of Reinforced Concrete Frame Structures using the Applied Element Method

A thesis submitted for the degree of Doctor of Philosophy in the School of the Built Environment of Heriot-Watt University

By

Samah AlHafian

(BSc Structural Eng., Damascus University)

(MSc Earthquake Eng., Damascus University)

November 2013

To my loving family and best friends

in Damascus, Syria

for their support and love

Abstract

Collapse of reinforced concrete structures under earthquakes is the main reason for life loss. Thus, avoiding structural collapse under strong earthquakes is the aim of seismic codes. The aim of the current study is to lead to an improved understanding of the seismic progressive collapse behaviour of reinforced concrete frame structures and to identify the most important parameters that should be considered in seismic progressive collapse analysis. The Applied Element Method, AEM, is an innovative method for direct progressive collapse simulation, in which strong geometric nonlinearity, element separation and collision can automatically be considered. Most previous studies focused on side-sway collapse modes only and indirectly checked for vertical collapse modes.

A validation of the AEM for seismic progressive collapse simulation has been carried out. The AEM models of three different frame structures have been validated by comparing the analytical and experimental results. The results have indicated that the AEM can simulate the structure response from linear range up to collapse reasonably well.

Sensitivity studies have been conducted to rank the material parameters most important to the collapse process in terms of the time at incipient collapse and to investigate their effects on the possible failure modes. The results show that the most important parameters are the parameters that can alter the failure mode.

An investigation on the effect of inclusion of the vertical ground motions on the collapse capacity and the possible failure modes has been performed. Considering vertical ground motions in collapse assessment of irregular frame structures has led to a decrease in the collapse capacity and to modifications in the possible failure mechanisms resulting in vertical rather than side-sway collapse modes.

A correlation study for investigation of the effect of using different intensity measures, fifteen spectrum and structure based intensity measures, for scaling far- and near-field ground motions for seismic assessment of mid-rise frame structures has been carried out. Employing intensity measures that account for the spectral shape has led to a considerably better correlation with the engineering demand parameters than utilizing intensity measures that are based on a single spectral value or a combination of two spectral values.

Acknowledgments

I would like to express my gratitude to Prof. Ian M. May for his support and guidance during the completion of this work. I am greatly thankful to Prof. Omar Laghrouche for his encouragement during this work.

I would like also to thank my friend and colleagues in Heriot-Watt University for their moral support and useful suggestions, in particular; Sarah Nodwell, Muhammad Aslam Bhutto and Nawras Hamdan.

I am deeply thankful to my beloved family for their continuous love, support and prayers throughout every minute in my study.

Special thanks to Prof. Mohammed Al-Samara for his encouragement throughout my study. Also, I would like to thank Dr Yasser Helal for providing me with the experimental data of the first test. I would like to express my deepest thank to Prof. Yong Lu for providing me with the experimental data of the second and third tests.

Finally, this research was funded by Damascus University. This financial support is gratefully acknowledged. In addition, I would like to acknowledge the use of the academic license of the Extreme loading for structures software provided by Applied Science International LLc.

Table of Contents

List of Tables

List of Figures

Notation

AEM: Applied element method.

IAEM: Improved applied element method.

FOSM: First-order second-moment method.

ASOSM: Approximate second-order second-moment method.

DEM: Distinct element method.

MDEM: Modified distinct element method.

EDEM: Extended distinct element method.

FEM: Finite element method.

VFIFE: Vector form intrinsic finite element method.

ASI: Adaptively shifted integration.

PEER: Pacific earthquake engineering research centre.

OpenSees: Open system for Earthquake Engineering simulation.

PGA: Peak ground acceleration.

IM: Intensity measure.

EDPs: Engineering demand parameters.

DM: Damage measure.

DV: Decision variables.

IDA: Incremental dynamic analysis.

MAF: Mean annual frequency of collapse.

MCE: Maximum considered earthquake.

PSHA: Probabilistic seismic hazard analysis.

SHA: Seismic hazard analysis.

DSHA: Deterministic seismic hazard analysis.

CMS-ε: Conditional mean spectrum including epsilon.

UHS: Uniform hazard spectrum.

CDF: Cumulative distribution function of the collapse capacities.

RC: Reinforce concrete.

ELS: Extreme loading for Structures.

FEMA: The U.S. Federal Emergency Management Agency.

EC8: Eurocode 8.

SD: Standard deviation.

COV: Coefficient of variation.

S: Soil profile.

EPA: Effective peak acceleration.

EPV: Effective peak velocity.

HI: Housner intensity.

I_A: Arias intensity.

VSI: Velocity spectrum intensity.

ASI: Acceleration spectrum intensity.

CAV: Cumulative absolute velocity.

I_c : Characteristic intensity.

I_F: Index for ground motion damage potential that considers PGV and significant duration.

IEPA: Improved effective peak acceleration.

IEPV: Improved effective peak velocity.

GMSM: Ground motion selection and modification methods.

MIV: Maximum incremental velocity.

PRDR: The peak roof drift.

PIDR: The peak inter-storey drift ratio.

E_i: Hysteretic energy dissipated in i excursion .

E_t: Reference hysteretic energy dissipation capacity.

E_j: Hysteretic energy dissipated in all excursions prior to i excursion.

c: An exponent to define the deterioration rate.

δ_c/δ_y: Ductility capacity.

K_e: Initial stiffness.

$K_s = \alpha_s K_e$: Hardening stiffness.

$K_c = \alpha_c K_e$: Post-capping stiffness.

F_r: Residual strength branch.

P: Axial compression load.

$f_c^{'}$: Concrete compressive strength.

A_{st}: Shear reinforcement area within spacing s.

f_{yt}: Yield strength of transverse reinforcement.

A_g: The cross-section area.

ρ": Transverse reinforcement ratio.

v: Nominal shear stress.

θ: Critical crack angle.

d_c: The core depth measured in the direction of the applied shear.

δ_a: The drift at axial failure.

δ_x: The drift at shear failure.

K_n: Stiffness of the normal spring.

K_s: Stiffness of the shear spring.

d: The distance between springs.

t: Element thickness.

a: The length of the representative area.

E: Young's modulus of the material.

G: the shear modulus of the material.

ρ: Material density.

ξ: Damping ratio.

ω_1 The first natural frequency.

[M]: Mass matrix.

[K] Matrix of the global nonlinear stiffness.

[U]: Displacement vector.

D_t: The contact time.

r : Rebound factor.

R_G: The residual load vector due to geometric changes.

R_M: The residual load vector due to the cracking or incompatibility between the spring stress and the corresponding strain.

n: The ratio between loading and unloading stiffness.

σ_P: The major principal stress.

β: The angle of the local crack.

f_c (MPa): Compressive concrete strength.

f_t (MPa): Tensile concrete strength.

E_c (MPa): Initial modulus of elasticity of concrete.

f_y (MPa): Yield strength of longitudinal reinforcement.

f_u (MPa): Ultimate strength of longitudinal reinforcement.

u : Ultimate strain of longitudinal reinforcement.

f_{ys} (MPa): Yield strength of transverse reinforcement.

f_{us} (MPa): Ultimate strength of transverse reinforcement.

u_s: Ultimate strain of transverse reinforcement,

$f_{c,c}$: Compressive concrete strength of columns.

$f_{c,b}$: Compressive concrete strength of beams.

$E_{c,c1}$: Initial modulus of elasticity of concrete of first-storey columns.

D_b: Bracketed durations.

D_u: Uniform durations.

D_s: Significant durations.

D_{a5-95}: The significant duration as the time interval between 5% and 95% of the total integral of the square of the acceleration, velocity or displacement .

$D_{a0.5-95}$: The significant duration estimated between 0.5% and 95% of the Arias intensity.

$D_{a0.5-97.5}$: The significant duration estimated between 0.5 and 97.5 of the Arias intensity.

R: Epicentral distance.

M: Moment magnitude of earthquake.

H: The case where only the horizontal component is applied

H+V: The case of utilising the vertical and horizontal component together.

V/H: The ratio of the vertical to horizontal components.

$\varepsilon_{Sa}, \varepsilon$: Epsilon, The number of standard deviations between the spectral acceleration of the selected un-scaled ground motion at a given period and the median spectral acceleration at the same period calculated from attenuation function.

η: Eta, Spectral shape as a linear combination of two epsilons ε_{Sa} and ε_{PGV}.

ε_{PGV}: Peak ground velocity epsilon.

m^*: The equivalent mass of the SDOF system.

T^*: Elastic period of the idealised bilinear system.

T_{crack}: Cracked period.

T_1 : Initial period.

T_f : Elongated period.

T_{max}: Maximum period.

T_{dam}: Damage period.

d_y: Yield displacement.

A_y: Yield strength.

D_G: Ultimate stiffness degradation index.

$D_{G,f}$: Final softening index.

$D_{G,pl}$: Plastic softening index.

$D_{G,m}$: Maximum softening index.

R^2: Coefficient of determination.

P: Pearson's correlation coefficient.

$s_a(T_1, 5\%)$: The 5% damped spectral acceleration at the first-mode of the structure.

$s_a(T_1)$: The 5% damped spectral acceleration at the first-mode of the structure.

$S_{a,cordova}$: Two-parameter intensity measure.

$IM_{1E\&2E}$, $IM_{1I\&2E}$, IM_{1I}, IM_{1E}, IM_{1eff} and IM_{1eq}: Spectral displacement intensity measures.

S_{di}: Inelastic spectral displacement.

Δ_{mean}: The average elastic spectral displacement over a range of periods.

$S_a(T_{crack})$: Spectral acceleration at the cracked period of the structure.

$S_a(T_*)$: Spectral acceleration at the nonlinear period of the structure determined based on pushover analyses.

$S_a(T_0 - T_y)$: Spectral acceleration over a range of periods.

$S_{a,avg}(T_1, \dots, T_n)$: The geometric mean of spectral acceleration values over a specific period range.

N_p: Spectral shape proxy.

I_{NP} : Scalar intensity measure.

Unnormalised I_a: Acceleration spectrum intensity measure.

I_a: Acceleration spectrum intensity measure.

I_{am}: Improved acceleration spectrum intensity measure.

IM_{Nc}: Displacement-based scalar intensity measure.

IM_c: Displacement-based scalar intensity measure for collapse case.

Chapter 1 Introduction

1.1 Background

Partial and/or total collapses of structures are often the main cause of loss of life during strong earthquakes. Therefore, preventing structural collapse has been the primary goal of seismic design. In post-earthquake reconnaissance reports, it has been revealed that the most common reasons for the collapse of reinforced concrete structures during earthquakes are poor nonlinear behaviour and corresponding unfavourable energy dissipation mechanisms. Example of this are the Izmit earthquake, in Turkey, 1999 (Sezen et al., 2000, Sezen et al., 2003) and the Bam earthquake, in Iran, 2003 (Ahmadizadeh and Shakib, 2004). Failure in columns, failure in slab-column connections and/or in beam-column joints initiate most collapses. These often arise from structural deficiencies; for example, insufficient reinforcement or poor detailing in the joints, columns with light transverse confinement, weak or soft storeys, strong-beam with weak-columns, and poor design and construction quality.

The seismic collapse of structures is defined as the inability of a structural system or a large part of it to sustain gravity loads under earthquake loading (Elwood and Moehle, 2003). Different mechanisms can cause a structure to collapse. Earthquake loading can trigger a global dynamic instability mechanism or a vertical collapse mode. A large side-sway displacement of single or multiple storeys generally initiates the former. This can be due to a combination of P-delta effects and with the effects of the strength and stiffness deterioration of the structural components (Ibarra and Krawinkler, 2005). The latter may occur because of the loss of the axial capacity of vertical members following the development of shear failure (Elwood and Moehle, 2003).

Several examples of partial or global structural collapse of reinforced concrete, RC, buildings under past earthquakes are depicted in Figures 1-1, 1-2 and 1-3.

Figure 1-1: Vertical collapse of a building during Kobe earthquakes,1995 (Moehle et al., 2002)

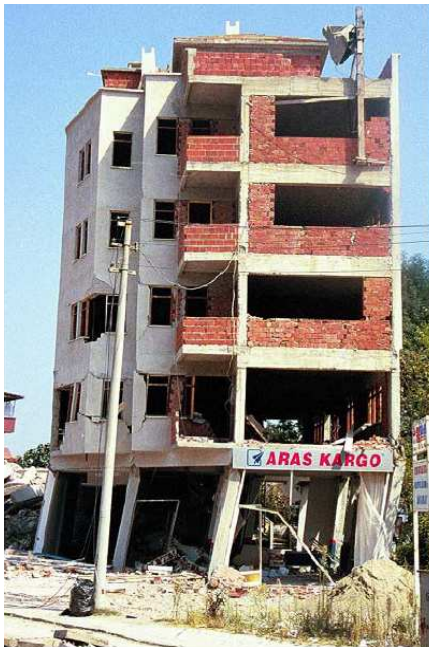

Figure 1-2: Formation of a soft-storey mechanism (Sezen et al., 2000)

Figure 1-3: Collapse due to a soft-storey mechanism (Ahmadizadeh and Shakib, 2004)

1.2 Overview of the problem

Most studies of structural progressive collapse have focused on collapse under impact and blast loads (Vlassis, 2007, Kaewkulchai and Willamson, 2003). However, seismic progressive collapse of structures has received a minimal attention. Although there are some similarities between the collapse behaviour of structures under extreme loadings, earthquake and impact loads; the spread of damage throughout structures is significantly different. Generally, the entire structure is severely damaged under seismic loadings. Following member separation due to earthquake loading, gravity loads carried by a member are redistributed to neighbouring structural members, which are often also damaged. These dynamic redistributed loads can exceed the residual strength capacity of the adjacent members leading to progressive collapse. In contrast, the damage under blast loads is more localised and adjacent members are often intact and consequently more capable of sustaining the redistributed loads (Wibowo and Lau, 2009). In addition, the duration of seismic loads is much longer than that of impact loads. In the case of the seismic progressive collapse of structures, the structures are simultaneously subjected to seismic and gravity loads, which then affect the overall structural performance.

Most studies concerning the seismic collapse of structures have focused on side-sway collapse (Haselton et al., 2008b, Ibarra and Krawinkler, 2005, Krawinkler et al., 2009, Zareian and Krawinkler, 2009, Zareian et al., 2008). It is possible that collapse of a structure will contain both side-sway and gravity components. This is an area, which has not been fully investigated. Based on damage observations from past earthquakes, it has been found that earthquake loading can result in the loss of multiple axial load-carrying members within the structure leading to partial or total vertical collapse, especially in buildings designed according to older codes of practice (Moehle et al., 2002). The failure of corner columns on upper storeys caused by earthquake loads often leads to two-way cantilever mechanisms (Gurley, 2008). Different seismic collapse modes can then be triggered (Starossek, 2007). In order to address collapse modes, which cannot be directly simulated by the available analytical tools, Aslani and Miranda developed fragility functions for incorporating shear failure or axial failure in non-ductile columns and also failure in slab-column connections (Aslani and Miranda, 2005). However, this method did not consider the interaction between structural members and hence neglected proper consideration of the capacity of the entire

system. The collapse of structures does not occur due to the loss of a member or the exceeding of a specific limit state of drift (Sezen et al., 2000). The capacity of an entire structural system to sustain large deformations following member separation, and the corresponding redistribution of internal forces within a structure are the main aspects that control collapse modes. Thus, collapse behaviour is very complicated due to the interaction between the vertical and lateral capacities of the structure (Elwood and Moehle, 2003). The ductility and strength of the entire structural system affects the propagation of damage. In addition, the effects of the dynamic redistribution of internal forces and impact forces can dramatically alter failure modes.

There are no accurate analytical tools that can simulate all of the collapse phenomena and capture the interaction between the structure vertical and lateral capacity (Comartin, 2001). A new method called the Applied Element Method, AEM, has recently been developed for direct collapse simulation (Tagel-Din and Meguro, 1999a). The AEM can reliably take into account both potential local and global dynamic instability collapse mechanisms, involving impact between elements and the following redistribution of forces. By using this method in this study, the effects of various input variables on the collapse process, not been previously addressed due to the limitation of the available analytical tools, can be investigated.

1.3 Objectives

The main purpose of the present study is to lead to an improved understanding of the progressive collapse behaviour of reinforced concrete frame structures under earthquake loadings using nonlinear dynamic analyses and to identify the most important parameters that should be considered in seismic progressive collapse analysis. The parameters include material properties, vertical ground motion components and the intensity measure for scaling ground motion real records.

The results of nonlinear time history analysis for predicting the response of reinforced concrete, RC, structures is heavily dependent on the input data; such as characteristics of the input ground motions and the structural system properties. In order to understand collapse behaviour, there is a need to investigate the effects of uncertainties in the input quantities on

the collapse process involving, collapse mechanisms, the collapse potential and the time at incipient collapse.

The required input data can be classified in two groups. The first group relates to seismic loadings, both the vertical and horizontal components of ground motions. The second group involves the input parameters, material properties and mass, which define stiffness, strength and the deformation capacity of the structural system. The AEM model is based on the constitutive relationship of the concrete and steel materials. The element stiffness, strength and deformation capacity are inherent in the model and they are associated with the material properties. The input parameters, which strongly affect the collapse process, need to be determined and the influences of correlations between random variables for different structural members and for different storeys should be examined.

The findings from these investigations can lead to a better understanding of the effect of these various key parameters and their significant impact on the collapse process. Thus, the parameters required to conduct seismic collapse analysis will be determined. It can lead to a better seismic design and to more effective seismic retrofit strategies. To achieve the objectives of this study, the methodology adopted is as follows:

- To review former experimental collapse investigations.
- To review the analytical tools available for collapse analysis.
- To provide a review of the background of the Applied Element Method.
- To validate the AEM for seismic progressive collapse by comparing the AEM models with the experimental results obtained in previous studies.
- To assess the seismic collapse behaviour of the two RC frame structures that were designed and detailed according to EC 8.
- To investigate the effects of uncertainty in different key parameters, for two structural systems, on collapse behaviour by using sensitivity analyses and then establishing the order of importance of these parameters to control the progressive collapse behaviour of RC frame structures.
- To illustrate the important influence of the correlation between the different variables associated with structural members for different storeys on the collapse process, collapse modes and the time at incipient collapse.

- To evaluate the effects of vertical ground motions on seismic collapse potential, as well as the possible collapse mechanisms for the two RC frame structures.
- To investigate the effects of using different ground motion scaling methods on the response of RC structures in terms of three different engineering demand parameters, the peak roof drift, the peak inter-storey drift ratios and damage indices based on the changes in the first natural period of a structure for different levels of nonlinear response.

1.4 Content of the thesis

The focus of this work is on the seismic progressive collapse behaviour of RC frame structures with emphasis on the effects of different sources of uncertainties on the collapse process. The Extreme Loading for Structures software, ELS, which is based on the Applied Element Method, has been used to simulate the collapse response for the selected frame structures. This thesis is organised into eight chapters as follows:

Chapter 1 presents the background and an overview of the problem and the main objectives of the study. The content of this work is summarised in this Chapter.

Chapter 2 begins with a summary of the experimental work regarding seismic performance, followed by a comprehensive review of currently available analytical tools for collapse simulation. Current seismic collapse assessment methods are also briefly described in this Chapter.

Chapter 3 provides the background to the Applied Element Method. In particular, the element formulation for a large deformation analysis, the numerical techniques adopted to solve collision and contact problems. The material models and the failure criteria adopted in this method are also presented. The procedures for the validation and application of the AEM are also summarised in this Chapter. In addition, the simplifying assumptions made when applying this method, and the limitations and advantages of the AEM are given.

Chapter 4 covers with the validation of the AEM models for three shake-table tested RC frame structures by comparing the analytical nonlinear response of these structures obtained from AEM analyses with the experimental results from tests performed by other researchers

in terms of storey-displacement time histories, inter-storey drift ratios and natural periods. Detailed descriptions of shake-table tests are given. Nonlinear time history analyses have been performed using Extreme Loading for Structures software. The AEM models for the selected structures are described in detail, followed by comparisons between the analytical and experimental results.

Chapter 5 begins with an overview of some previous studies accounting for the effects of two different sources of uncertainty on seismic performance. A brief summary of the three most common methods used in this field is provided. These methods are the first-order second-moment method, FOSM, the approximate second-order second-moment method, ASOSM, and Tornado Diagram analyses. The random variables to be used in this study are described. Deterministic sensitivity analyses carried out in order to determine and to rank the most important random variables to the collapse process are also described. Three types of correlation between the random variables were considered as presented in the sensitivity studies: correlation between random parameters for a single member, correlation between random parameters for different members, and correlation between random parameters for different storeys. The process of the selection of the seismic input for the sensitivity studies is discussed. The concepts of mechanism control and the effects of the strong-column weak-beam strength ratio on the collapse capacity of structures are explained. The results of the sensitivity analyses, in terms of the time at incipient collapse and collapse modes are discussed in detail.

Chapter 6 reviews previous research focused on the effects of vertical ground motions on the seismic performance of structures. The characteristics of vertical ground motions are presented. The method used for selecting and scaling ground motion records is discussed. The approach adopted to determine the collapse capacity of selected structures and the definition of the collapse limit state are given. The levels of seismic intensity are selected. The influences of the inclusion of vertical ground motions on collapse capacity, as well as on the failure modes are explained in detail. Then, conclusions are given.

Chapter 7 deals with the selection and scaling ground motion methods for seismic collapse assessments. A review of selection of ground motion methods for nonlinear dynamic analysis is given. The most up to date scaling ground motion approaches for seismic assessment are summarised. A number of studies concerning the effects of using different

scaling methods on structural performance are reviewed. Then, the structural models selected and analyses of these models are described. The two sets of ground motion records employed in this study are listed, and regression analyses carried out to investigate the effects of using different intensity measures, IM, on three engineering demand parameters are described. The regression results for different intensity measures are compared with the results obtained using the spectral acceleration at the fundamental period of the structure as an intensity measure and conclusions are given.

Chapter 8 summarises the main conclusions drawn from the present investigations into the effects of different sources of uncertainties on the seismic progressive collapse behaviour of RC frame structures designed according to EC 8 provisions. In addition, recommendations for further research are given.

Chapter 2 Literature review

2.1 Introduction

Structural collapse occurs during earthquakes not only in structures designed according to old codes, but also in structures that satisfy modern seismic code provisions (Villaverde, 2007). Post-earthquake reconnaissance of structures can provide insight into the common collapse modes (Moehle and Mahin, 1991). Site damage investigations of RC structures following devastating earthquakes, in combination with data obtained from experimental work and seismic tests, are essential to achieving an understanding of the seismic performance of buildings near to or beyond the initiation of the collapse stage, in order to identify safety margins. Monitoring the real response of structures in situation where actual strong earthquakes, characterised by a low probability of occurrence, can be very difficult. Numerical simulation tools validated by experimental data are also important. Contributions towards improving collapse assessment methods have been made by several researchers in relation to different issues associated with collapse assessment (Elwood and Moehle, 2003, Ibarra and Krawinkler, 2005); for example, quantifying P-Delta effects, developing hysteretic models to account for deterioration in strength and stiffness, developing component models for shear failure and/or axial load failure and integrating the key factors affecting collapse process into a unified seismic assessment method.

This literature review is divided into three parts. The first part details the role of seismic testing in checking the reliability of numerical simulation tools and in reproducing the observable damage patterns in the progression to collapse, and experimental work regarding collapse investigations. The second part provides a review of the analytical tools available for progressive collapse simulation, in particular, the simulation of seismic collapse. A brief summary of the current methods applied for seismic collapse assessment is provided in the third part. The three parts of the literature review can be summarised as: experimental collapse investigations; analytical tools and methods for collapse simulation; and analytical methods for seismic collapse assessment.

2.2 Part I: Experimental collapse investigations

This section reviews the background to experimental work, shaking table tests to collapse and the needs and challenges of experimental work on collapse.

2.2.1 Background to experimental work

The objectives of all experimental work related to collapse analyses and/or collapse assessment can be summarised as follows (Pinto et al., 2004):

1. To validate analytical models or to calibrate the parameters of a model.
2. To validate new analytical procedures.
3. To improve new constitutive laws for materials in order to increase the confidence in innovative materials and methods.
4. To trace the structure's response under a series of ground motions of increasing intensities.

With the aim of assessing the performance of structures, test protocols; such as load intensity and test sequences in the case of validation of multi-level performance should be selected carefully. This is due to the possible effects of cumulative damage on the test results. Thus, the number of tests need to be limited. Furthermore, an appropriate input motion should be chosen (Pinto et al., 2004).

In order to improve understanding of failure mechanisms of structures, and the causes leading to these failure modes, experimental investigations have been conducted on different structural systems or structural members. The following is a summary of shaking table tests that have been used to investigate collapse.

2.2.2 Experimental work associated with collapse investigations

A number of shaking table tests have been performed to date on structural members, structural components, and reduced or full-scale models of structures to investigate the performance of a member in the structure or the entire structure when subjected to earthquake loads. A number of these experimental studies are reviewed below.

Elwood and Moehle conducted two shake table tests for a scale one-storey RC frame, to examine the collapse mechanisms of RC frames containing non-ductile columns (Elwood and Moehle, 2003). In particular, vertical collapse modes were found to occur due to the column shear failure followed by the loss of the column axial capacity. In addition, load redistribution in a two-dimensional structure with alternative load paths was of concern here. The one-half scale specimens were composed of three base-fixed columns connected by a strong beam, as shown in Figure 2-1 (Elwood and Moehle, 2008).

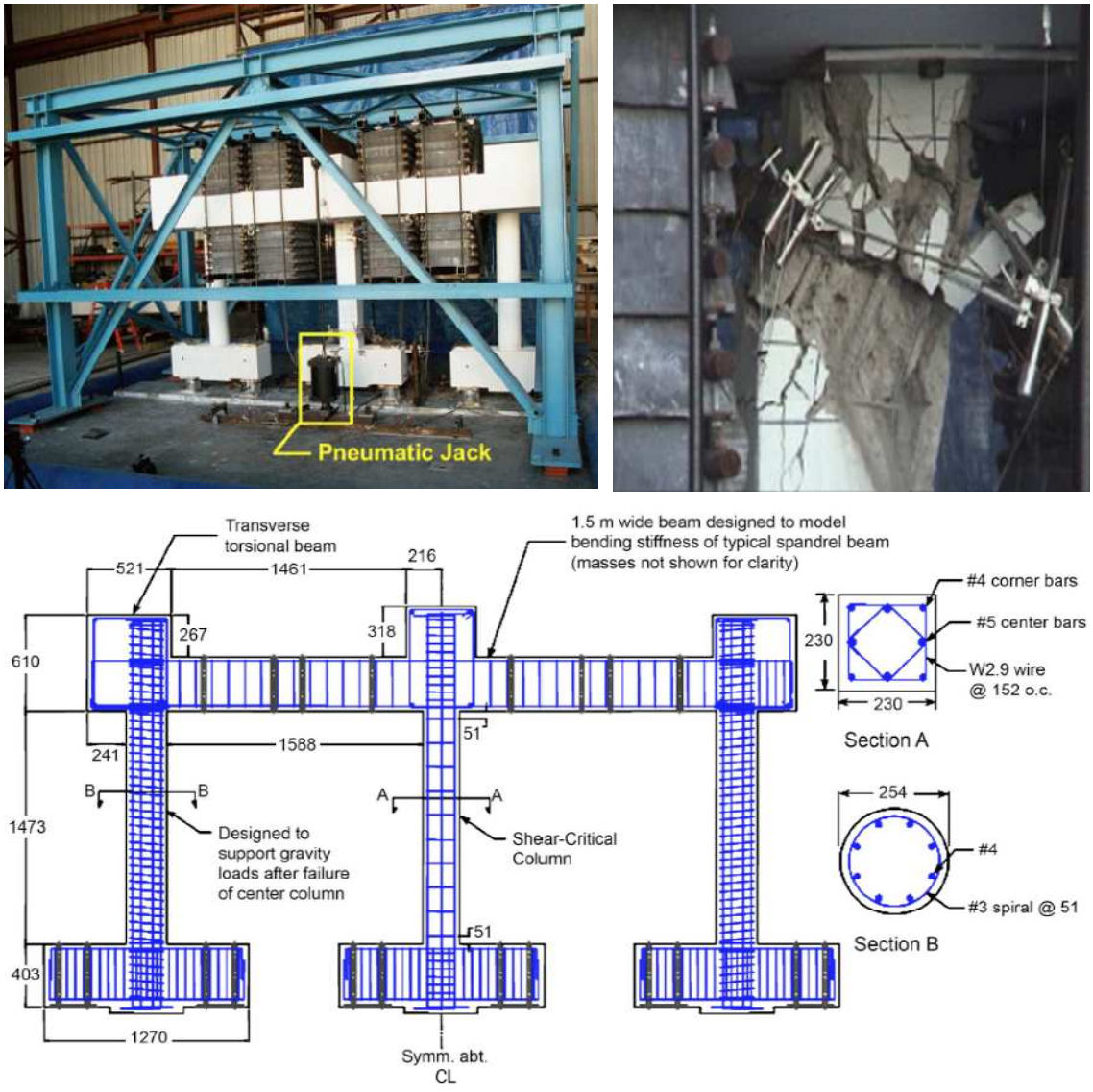

Figure 2-1: Second specimen on shaking table, damage to the top of the centre column of the second specimen at 29.8 sec, and the (Elwood and Moehle, 2008)

The centre column had light transverse reinforcement. Consequently, this design allowed this column to experience shear failure followed by axial failure. It has been stated that the structure's response is sensitive to the applied axial load. A scaled unidirectional ground motion was used as input. Different axial force magnitudes were applied to the centre column in the two specimens. In specimen 1, shear failure, without subsequent axial load failure developed in the centre column; this was compared to the column with higher axial loads in specimen 2, where axial failure occurred at smaller drift ratios. Column shear failure does not necessarily lead to the complete collapse of a structural system; it depends on subsequent load redistribution. When the axial load was redistributed to the adjacent columns during axial failure of the centre column in specimen 2, dynamic amplification of the transferred axial loads to the adjacent columns was observed.

The previously mentioned work was later extended by Ghannoum et al., to improve the understanding of collapse modes of non-ductile RC frame structures (Ghannoum et al., 2008). Dynamic tests on a third-scale three-storey concrete frame with flexure-shear critical columns and ductile columns were carried out on the Berkeley shaking table, Figure 2-2. The three tests to collapse aimed to investigate the effects of local failure, column shear and axial failure, on damage progression and load redistribution within the entire structural system; in addition to the effects of the framing system on the progressive collapse behaviour (Ghannoum and Moehle, 2008a). The results therefore highlighted the effects of neighbouring framing members on collapse behaviour.

Figure 2-2: Specimen on shaking table, frame after collapse and column B1 at end of test 1 (Ghannoum and Moehle, 2008a)

A dynamic test on a 1/3 scale model of a six-storey wall-frame RC structure was carried out under a series of ground motions of increasing intensity (Matsumori et al., 2005). It was found that the shear wall at the first-storey experienced earlier shear failure in contrast to the design results obtained based on a pushover analysis. The reasons for this could be the considerable differences in the dynamic distribution of lateral forces between the test and those considered in the pushover analysis, leading to large shear forces in the first-storey wall. Hence, a nonlinear static analysis cannot reliably predict neither the highly nonlinear response of structures nor their failure mechanisms. This may result from ignoring the cyclic effect, which proved to dominate the seismic performance (Haselton et al., 2009). The dynamic properties changed dramatically during the loading and unloading stages, whereas ground shaking resulting in alterations to the force distribution (Villaverde, 2007).

Hashemi and Mosalam conducted a shaking table test on a scale model of a one-storey RC moment-resisting frame structure containing an infill wall at the University of California in 2005 (Hashemi and Mosalam, 2006). The concern of their study was to investigate the effects of a masonry infill wall on structural behaviour, and to calibrate the models being implemented in the OpenSees program. The test involved three stages. The first stage conducted with the complete collapse of the infill. The behaviour of the frame without infill and the collapse mechanism were investigated during the two other stages. Figure 2-3 shows the damage pattern for the first stage (Hashemi and Mosalam, 2006).

Figure 2-3: Structure tested on shaking table and observed damage of the structure in the first stage (Hashemi and Mosalam, 2006)

The damage in the infill wall can lead to a reduction in structural stiffness and an increase in the fundamental period. It was concluded that infill walls should be taken into consideration in both the design and analysis of structures, due to their important role on the stiffness and strength of structures and on force distribution between structural members.

Although reduced-scale models are cheaper and require less time for construction compared to full-scale tests, the accuracy of the results is often affected by multiple factors; such as the specimen size, similitude rules, control of input and excitation, material properties used, e.g. diameters of reinforcement rebar and concrete mixes, and the accuracy of the data acquisition system. Moreover, certain features are difficult to reproduce in a scale model; for example, bond-slip in RC structures (Xianguo et al., 2004, Garevski et al., 2010). Therefore, full-scale tests are very important to an examination of complex phenomena. For example, this involves the interaction between structural and non-structural members at different performance levels, the effect of RC slabs on damage patterns, and the effects of local damage from individual members on the behaviour of the remaining members, as well as on the global modes of damage experienced by the entire structural system.

A full-scale test on a three-storey steel moment-resisting frame was performed up to failure under quasi-static cyclic loading. The objectives of this were to trace the behaviour of a structure when large deformations occurred near to collapse, and to check the accuracy of a commonly used analytical model (Nakashima et al., 2004). A failure mechanism was developed due to local buckling at the top of the first-storey columns. It was concluded that non-deteriorating models can accurately reproduce structural behaviour up to a level of deformation represented by drift angles of approximately 1/25.

A full-scale four-storey steel structure was tested to complete collapse using the E-Defense three-dimensional shaking table in Japan in 2007. The aim of the test was to assess the structural performance of the steel structures under the design earthquake, and to determine the collapse safety margin (Yamada et al., 2008). Figure 2-4 shows the frame specimen and the failure mode. The frame, which was designed according to current design codes, performed well under the design earthquake. A first-storey collapse mode was observed during a catastrophic earthquake. Collapse occurred due to deterioration in the first-storey columns resulting from local buckling (Keiichiro et al., 2009).

Figure 2-4: Frame specimen and failure mode of specimen at the end of the test (Tuan-Nam and Kasai, 2012)

In 2006, a full-scale six-storey wall-frame structure, designed according to an old code, was tested to collapse at the E-Defense shaking table, with the aim of investigating the collapse behaviour of wall-frame structures involving non-structural components. The test design and procedures for the test were found in (Kabeyasawa et al., 2005). The specimen height was 16 m. A series of ground motions with increasing intensity were employed. The specimen comprised of frames with different characteristics. It was noted that the shear failure of shear walls and short columns triggered a first-storey collapse mechanism (Shirai et al., 2007, Kim et al., 2012), as shown in Figure 2-5.

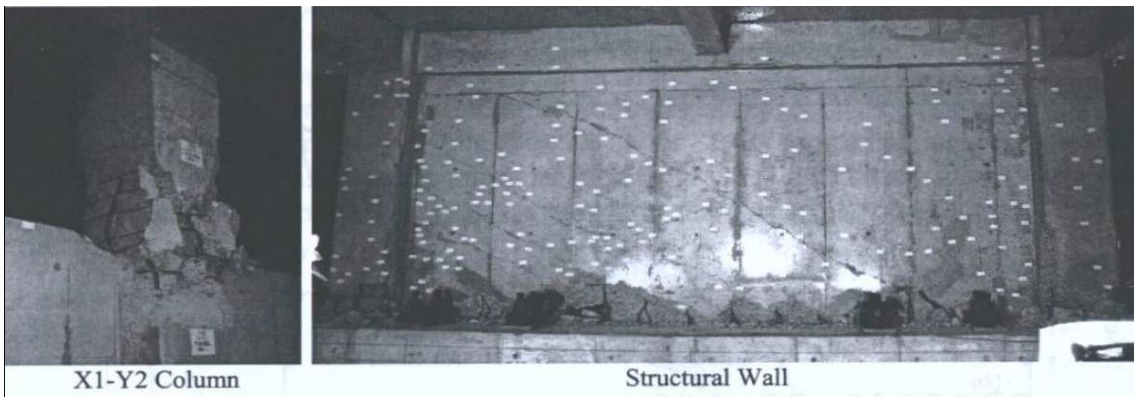

Figure 2-5: Damage in short columns and shear wall (Shirai et al., 2007)

More recently, two scale models for a four-storey steel frame were tested beyond collapse at NEES, at the University at Buffalo, in order to investigate the side-sway collapse

of frame structures (Lignos et al., 2011). It was concluded that the side-sway collapse of structures can be analytically predicted with good accuracy, provided the effects of component deterioration are correctly represented together with P-Delta effects, as these effects dominate structural behaviour near to collapse (Sezen et al., 2000). In addition, it was noted that the frame behaviour prior to collapse had been strongly affected by the load history experienced by each structural component. Consequently, using information obtained from test components and utilising only symmetric cyclic loading histories is not sufficient for calibrating deterioration models for collapse simulation (Lignos et al., 2011). Both models collapsed in a complete three-storey mechanism (Lignos and Krawinkler, 2009), as shown in Figure 2-6.

Figure 2-6: Collapse mechanism of the first frame and collapse mechanism of the second frame 2 (Lignos and Krawinkler, 2009)

Investigations into previous experiments revealed a lack of seismic experimental tests near collapse, in particular, large scale or full-scale tests. This can be attributed to the costly and time consuming nature of large testes. Moreover, many difficulties arise when fabricating and loading the models and recording data. The capacities of available shaking tables are limited in terms of both acceleration and weight. The test height is often restricted due to limitations that affect the laboratory space. Furthermore, most experiments cannot be performed so that they follow the entire collapse process, due to the cost and the risk of damaging the shaking table and neighbouring areas following collision forces (Riddell, 2007). The challenges of experimental work and the needs for future research regarding

seismic risk assessment and performance-based seismic design are summarised as (Pinto et al., 2004, Garevski et al., 2010):

1) Shaking tables with multi-axis input motions.
2) Development of sensor techniques and the enhancement of dynamic controls associated with testing facilities.
3) New advanced facilities capable of testing complex structures.
4) Shaking tables capable of reproducing excitations with a high intensity, in order to trace structural performance from initial damage to collapse.
5) Development in testing procedures, especially tests of non-structural components.
6) Tests on structures containing non-structural elements are required.
7) Field testing to provide more realistic data about the performance of structures and the interaction between their structural members; such as beams, columns and joints at the onset of failure.
8) Advanced instrumentation including digital measuring and visualisation systems are needed for a better estimation of local and global damage.

It is often very difficult to simulate the process of a complete structural collapse and the corresponding failure modes in physical tests. This is because the mechanical behaviour inherited in progressive collapse modes is often very complicated and extremely difficult to quantify in a test (Wang et al., 2006). The generalisation of those collapse modes observed to cases involving large deformation, disconnections and possible subsequent impact from falling elements is also very difficult. Thus, developing efficient tools to generate progressive collapse simulations has become highly desirable in the recent years.

2.3 PART II: Analytical tools and methods for collapse simulation

This section reviews the analytical tools and methods developed for collapse simulation. Based on modelling assumptions, such as discrete or continuum models, the analytical methods for collapse simulations can be categorised into several groups, as discussed in the following sections.

2.3.1 Finite Element Method

The Finite element method, which is based on continuum equations, requires further additional modifications to apply to collapse analyses with strong nonlinearity and discontinuous behaviours. A number of techniques have been proposed by researchers to improve the efficiency of the conventional Finite element method, FEM.

2.3.1.1 Vector Form Intrinsic Finite Element Method

The Vector Form Intrinsic Finite Element, VFIFE, method developed by Ting and his co-workers was extended to a seismic collapse analysis of frame structures, from a continuous to a discontinuous phase (Ting et al., 2004a, Ting et al., 2004b, Shih et al., 2004). This method incorporates material nonlinearity and large deformations and the frame structure is modelled using prismatic elements without mass and discrete mass nodes. The motion for each mass satisfies Newton's second law and Euler's equations. The VFIFE method depends on lumped mass techniques that mean the matrix equations need not be solved. The main difference between this method and the conventional FEM, which is an energy-based method, is that the VFIFE method requires force equilibrium at those nodes that connect structural members during rigid body motion, thus numerical errors resulting from the fictitious unbalanced residual forces can be avoided. The principle of virtual work can then be used to obtain balanced forces at each node. In addition, this method removes rigid body motion for each element, displacements and rotations, redefining a set of deformation coordinates on the element for each time step. Thus, rigid body displacements can be separated from the total element displacements. The accuracy of the VFIFE method has been demonstrated by comparing the results obtained from numerical simulations, using this method with those

obtained from shake table experiments (Wang et al., 2008, Wang et al., 2011). The seismic collapse analysis for a five-storey reinforced concrete frame was performed using the VFIFE method (Wang et al., 2006). A material model with stiffness, strength degrading and pinching was adopted and the damage index modified by Park and Ang (Park et al., 1987) was considered as the component failure criteria. Contact detection was considered for simulating the progressive failure of the structure. Further development is still needed to analyse relatively complicated structures.

2.3.1.2 Adaptively Shifted Integration Technique

A technique called Adaptively Shifted Integration, ASI, has been developed from the shift integration technique for finite element analysis by Toi and Isobe (Toi and Isobe, 1996). A Plastic and dynamic collapse analysis of frame structures can be performed using this technique. The concept of this technique is that numerical integration points for determining stiffness matrices are shifted immediately, following the formation of a fully plastic hinge within an element. Plastic hinges form at both ends and simultaneously the resultant forces are released. The results of a seismic collapse analysis of RC frame structures, performed using this code together with Timoshenko beam elements have indicated the sufficiency of this technique for collapse analyses (Isobe and Tsuda, 2003). The impact between elements can be taken into consideration. However, the accuracy of this technique in the elastic range depends on the selected number of elements per member (Lynn and Isobe, 2007).

The accuracy of the ASI technique in the elastic range has been improved by Lynn and Isobe (Lynn and Isobe, 2007). An ASI-Gauss technique has also been proposed. In this case, two beam elements are required to model a structural member. The position of the numerical integration points for the elastically deformed member is altered. In other words, the evaluation points for the stresses are located at the Gaussian integration points of the member, and are optimal for two-point integration. Thus, accurate bending deformation can be obtained, even when the element behaves elastically. This technique, with member fracture and contact has been applied to impact analyses. The efficiency of using the ASI-GAUSS technique to analyse an RC frame structure from the elastic phase until the point of total collapse under a three-dimensional ground motion in a short CPU time has been proven (Katahira et al., 2008).

2.3.1.3 Commercial software

There are a number of commercial software packages, which can be used for dynamic collapse analysis; such as LS-DYNA3D (Hallquist, 2006) and the OpenSees program (OpenSees, 2005). For example, collapse analysis of the RC bridge due to the Loma Prieta Earthquake was carried out by Sun et al., using the nonlinear explicit finite element code LS-DYNA (Sun et al., 2003a). Reduced integration 8-node solid elements with one Gauss integration point and the user-defined material model, smeared crack in ANSYS/LS-DYNA, were used for modelling the structure. The fracture of the structural elements was modelled by deactivating failed members and multiplying their stiffness with a severe reduction factor. The contact and impact problems were considered using the penalty method. It was indicated that the proposed simulation method can properly predict the collapse process.

A fiber-based model called THUFIBER was developed for modelling reinforced concrete structures, and implemented in MSC.MARC software (Miao et al., 2007). The cyclic behaviour of the reinforced concrete material under earthquake loads can be simulated. Hence, the collapse mechanism and the early failure stage can be properly simulated. Although the structure remains continuous after the occurrence of collapse, the effects of member separation can be implicitly taken into account. Lu et al., proposed the appropriate criterion to deactivate a member when it exceeds its deformation limits using the aforementioned fibre-based model (Lu et al., 2008).

2.3.1.4 OpenSees platform

Analytical models for predicting the side-sway collapse of a structure under a set of ground motions vary from using SDOF to MDOF models for representing the structure. The critical features of progressive collapse simulation tools under earthquake excitation are their ability to model a deterioration in the strength and stiffness of the structural components under seismic loading and to incorporate large deformations, element separation and contact between elements following the removal of an element (Fardis et al., 2010a). Developing such hysteretic models for structural components in moment-resisting frames or wall structures has been the subject of several studies. The Pacific Earthquake Engineering Research Center, PEER, developed an open system for Earthquake Engineering simulation,

OpenSees program (OpenSees, 2005). Several deterioration models were implemented in the OpenSees platform. Some of these models are discussed in the following sections.

2.3.1.4.1 Mehanny-Deierlein model

A damage model was developed by Mehanny and Deierlein (Mehanny and Deierlein, 2001). The Mehanny-Deierlein damage model was based on cumulative member ductility, rather than on dissipated energy. The damage index accounted for the effects of both peak and cumulative plastic deformations in the form of the primary half cycle, PHC, and the following half cycles, FHC. Three calibration coefficients, determined based on experimental data (α, β and γ), in addition to maximum negative and positive plastic rotation capacity ($\theta_{pu}^{+}, \theta_{pu}^{-}$), were required when defining this model; as illustrated in Equation 2-1.

$$DI = \sqrt{\left(\frac{(\theta_p^{+}/\text{current PHC})^{\alpha}+(\sum_{i=1}^{n+}\theta_p^{+}/FHC,i)^{\beta}}{(\theta_{pu}^{+})^{\alpha}+(\sum_{i=1}^{n+}\theta_p^{+}/FHC,i)}\right)^{\gamma}+\left(\frac{(\theta_p^{-}/\text{current PHC})^{\alpha}+(\sum_{i=1}^{n-}\theta_p^{-}/FHC,i)^{\beta}}{(\theta_{pu}^{-})^{\alpha}+(\sum_{i=1}^{n-}\theta_p^{-}/FHC,i)}\right)^{\gamma}} \quad \text{Equation 2-1}$$

Figure 2-7 is an example of different time histories that can be used to explain the difference between primary and follower half cycles.

When the damage index of a component exceeds 1; failure of this component is assumed to occur. Cumulative damage models are used to indicate the degree of component damage. Damage models often fail to account for stiffness and strength reduction resulting from cumulative damage, which result in larger deformations. Increasing the structural deformations due to strength reduction can lead to structural collapse (Ibarra and Krawinkler, 2004). Therefore, deterioration models that explicitly consider these features are required for collapse assessment.

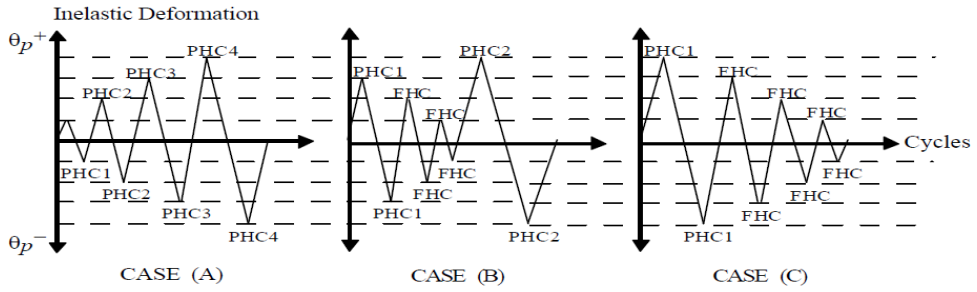

Figure 2-7: Definition of PHCs, FHCs and the local sequence effects (Mehanny, 1999)

Deterioration models for beam-column components

In the case of flexural lumped plastic hinges, two main deterioration modes, monotonic and cyclic deterioration, often occur (Fardis et al., 2010a). As seen in Figure 2-8, deterioration under cyclic loading can be categorised into four modes, namely basic strength deterioration, post-capping strength deterioration following reaching of the capping point, unloading stiffness deterioration, and accelerated reloading stiffness deterioration (Ibarra et al., 2005). All modes with exception to the final one, have been observed in all structural component responses under cyclic loading. As a result of these modes, the initial backbone curve, in other words, the curve under monotonic loading generally differs from the cyclic envelope curve.

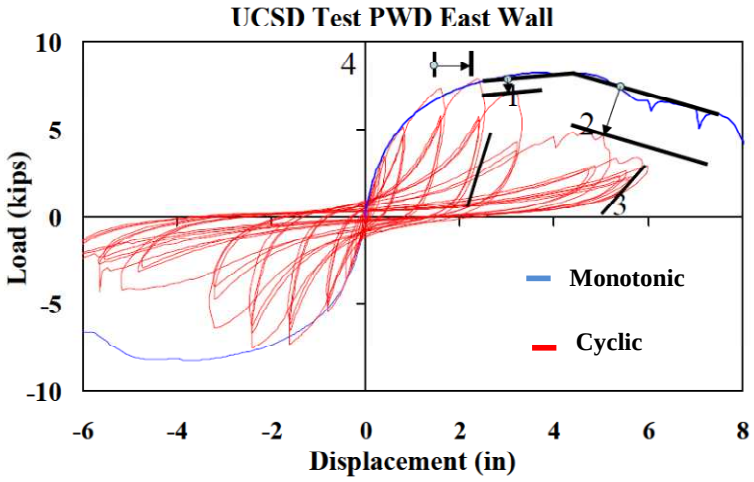

Figure 2-8: Monotonic and cyclic experimental response of a wood specimen (Ibarra et al., 2005)

2.3.1.4.2 Ibarra-Krawinkler deterioration model

Ibarra and Krawinkler have developed plastic hinge models to incorporate the aforementioned deterioration modes and to predict global side-sway collapse (Ibarra and Krawinkler, 2005, Ibarra et al., 2005). The parameters defining the backbone curve of the model are initial stiffness, hardening stiffness, post-capping stiffness, and residual strength branch, as illustrated in Figure 2-9. In this model, the cyclic deterioration of each component is assumed to be independent of loading history, being controlled by a criterion based on a

reference hysteretic energy dissipation capacity, that is similar to the deterioration model developed by (Rahnama and Krawinkler, 1993). An energy-based deterioration parameter defining cyclic deterioration in excursion i, β_i , can be applied for these four deterioration modes. The stiffness or strength value in excursion i can be determined in the form, $F_i = (1 - \beta_i)F_{i-1}$. This parameter can be defined as in Equation 2-2 (Rahnama and Krawinkler, 1993, Ibarra et al., 2005).

$$\beta_i = \left[\frac{E_i}{E_t - \sum_{j=1}^{i} E_j}\right]^c \qquad \text{Equation 2-2}$$

E_i is the hysteretic energy dissipated in i excursion; $E_t = \gamma F_y(\delta_c - \delta_y)$ is the reference hysteretic energy dissipation capacity; E_j is the hysteretic energy dissipated in all excursions prior to i excursion; c is an exponent used to define the deterioration rate; and (δ_c/δ_y) is the ductility capacity.

The parameters defining the deformation of the backbone curve and cyclic deterioration in the Ibarra-Krawinkler model have been calibrated based on experimental data for plywood, masonry, reinforced concrete (Haselton et al., 2008a) and steel structural components (Lignos and Krawinkler, 2009, Lignos and Krawinkler, 2011).

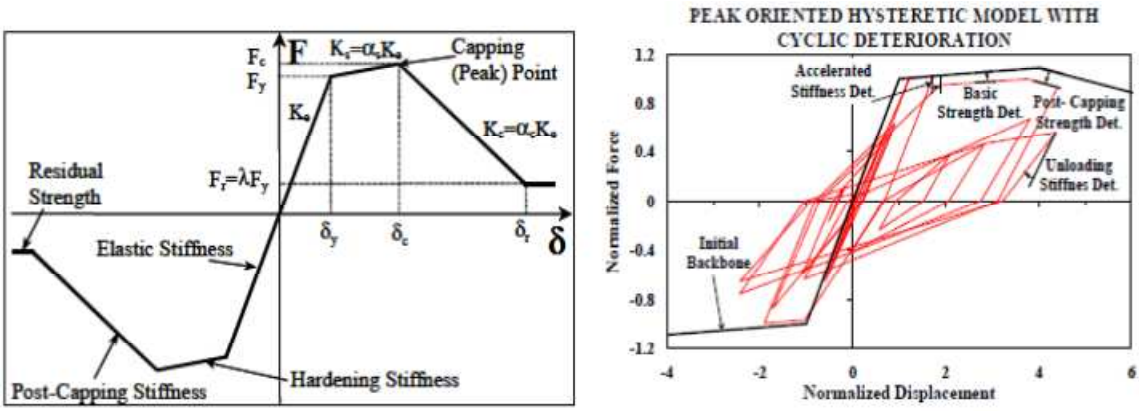

Figure 2-9: Ibarra-Krawinkler model (Ibarra and Krawinkler, 2005)

Lignos and Krawinkler modified the Ibarra-Krawinkler model to represent the asymmetric hysteretic behaviour of a beam-column component, by incorporating residual

strength and different cyclic deterioration rates in positive and negative loading directions. Moreover, an ultimate component deformation with zero strength has also been incorporated (Lignos and Krawinkler, 2009, Lignos and Krawinkler, 2011). The modified model was implemented in the OpenSees platform (OpenSees, 2010).

2.3.1.4.3 Models for shear and axial load failure of RC columns

Several shear models were developed for columns with rectangular cross sections. The focus of recent studies has been on columns with light transverse reinforcement, which have been designed to yield in flexure prior to developing shear failure and then axial load failure. Some examples of these models are discussed in the following section.

Sezen and Moehle calibrated an empirical model for shear column strength based on experimental results (Sezen and Moehle, 2004). The shear strength equation considers shear contributions from transverse reinforcements and concrete. The main parameters in this model are axial compression load, P; concrete compressive strength, f'_c, transverse reinforcement, e.g. A_{st} and f_{yt}, the shear reinforcement area, within spacing s and the yield strength of transverse reinforcement, respectively, the cross-section area, A_g, column aspect ratio and displacement ductility demand.

A model for estimating the deformation at column shear failure has been derived empirically based on experimental data (Elwood and Moehle, 2005b, Elwood and Moehle, 2003). Shear failure is assumed to occur at 20% loss in the peak shear strength. The Equation 2-3 for drift at shear failure is proposed in MPa units. It has been stated that drift, δ_x, increases with increases in the transverse reinforcement ratio, ρ", or decreases in response to shear stress and/or axial stress. v represents nominal shear stress.

$$\delta_x = \frac{3}{100} + 4\rho'' - \frac{1}{42}\frac{v}{\sqrt{f'_c}} - \frac{1}{40}\frac{P}{A_g f'_c} \geq \frac{1}{100} \qquad \text{Equation 2-3}$$

Elwood and Moehle extended the drift capacity model developed for shear failure to account for the loss of axial capacity in shear damaged RC columns (Elwood and Moehle, 2005a). The columns can experience axial failure following the loss of shear capacity. The drift at axial failure, δ_a, was estimated based on shear-friction concepts and experimental investigations in Equation 2-4.

$$\delta_a = \frac{4}{100}\frac{1+\tan^2\theta}{\tan\theta+P\left(\frac{s}{A_{st}f_{yt}d_c\tan\theta}\right)} \quad \text{Equation 2-4}$$

θ is the critical crack angle; and d_c is the core depth measured in the direction of applied shear. This model for shear and axial failure was implemented in OpenSees in 2004.

(Ghannoum and Moehle, 2008a) noted that the shear failure of flexure-shear columns tends to be associated with inelastic rotational demands, rather than the drift demands of those columns, particularly for columns in a frame system. Previous tests were performed on columns with fixed-fixed boundary conditions, where both column end rotations were equal and closely associated with drifts. Ghannoum and Moehle introduced new models for column rotations at shear failure based on regression analyses of experimental data (Ghannoum and Moehle, 2008b). Different rotation measures can be used in these models; such as plastic or elastic rotations.

In generally, the finite element method based on the continuum equations is valid only for structural analyses prior to collapse, because complicated modifications are required to simulate member fractures. Advanced tools accounting for element separation are essential for predicting the complete progressive collapse response of structures under earthquake and for evaluating their capabilities to withstand strong earthquake loading.

2.3.1.5 Models considering element separation

A review of the approaches and tools that can be used to manage element separation during a progressive collapse simulation are introduced in the following section.

In a study reported by Kaewkulchai and Williamson, a lumped plasticity model, which accounts for both strength and stiffness degradation of beam-column elements, and with a damage index based on the maximum deformations and accumulated plastic energy, has been defined for predicting the collapse of planar frame structures (Kaewkulchai and Williamson, 2004). As the damage index of an element reaches a predefined threshold value, the element becomes disconnected from the structural system. After which, the effect of dynamic force redistribution from the lost element is considered by applying external forces at the end nodes, utilising a step function. This approach utilises a static condensation method to modify the member stiffness. Hence, the collapsed element response is tracked without requiring

modification of the number of degrees of freedom, as are the element connectivity relationships arising from element disconnection (Kaewkulchai and Williamson, 2004).

Kaewkulchai and Williamson has extended the previously mentioned method to take into account the effects of the impact of collapsed element on the structure below, by adopting a simplified method based on a low-velocity impact regime, particularly on the transverse impact on flexible bodies, with the assumption of the impact of a perfectly-plastic mass on a damaged member (Kaewkulchai and Williamson, 2006). Hence, local deformations at the impact location can be neglected. The duration of impact has been assumed as negligible, and the immediate velocity change at the impact location has been employed related to the velocities and masses of both falling and impacted elements.

Simulation tools for seismic progressive collapse analyses have been developed by Talaat and Mosalam, in which an algorithm for the automatic sudden removal of a lost member based on principles of dynamic equilibrium has been presented (Talaat and Mosalam, 2008, Mosalam et al., 2008, Talaat and Mosalam, 2009, Fardis et al., 2010b). This formulation, which has been implemented into the OpenSees codes, has been extended to account for the simplified modelling of a collision. The separation takes place when the removal criteria of the damage indices for RC columns, the response of a member is governed either by flexure-axial interaction or by shear-axial interaction, are met. A benchmark problem with noncomplex criteria for element removal has been utilised to verify this algorithm. However, there are some complications associated with the implementation of this technique.

Since plastic hinge models are suitable only to simulate the response of structures prior to element separation, Zhang and Liu have developed a mixed hinge model (Zhang and Liu, 2000). This model is capable of describing three displacement discontinuities (transverse, longitudinal and rotational displacements) in beam-column members, based on singularity functions. In this model, displacement discontinuities are assumed to be concentrated at the member ends. Furthermore, collision effects are also fully considered by imposing conditions of velocity constraint on the system and introducing a Lagrange multiplier to modify kinetic energy (Zhang and Liu, 2000). A numerical simulation of a frame structure under the Wenchuan earthquake has been carried out. The analytical results illustrated the feasibility of this model to account for collision effects (Zhang and Liu, 2008, Zhang and Liu, 2000).

The disadvantage of the method, based on FEM, is that the crack location should be predefined, prior to the collapse analysis, using the FEM. Hence, separation is generally assumed to take place at the element ends using joint elements. Moreover, contact between members is often difficult to accurately account for in this method.

2.3.2 Discrete Analysis Methods

Several discrete analysis methods have been developed for the analysis of discontinuous problems. A review of some of these approaches, as applied to collapse analyses, is provided below:

- The Distinct Element Method, DEM, was proposed by (Cundall and Strack, 1979) for the purpose of simulating the mechanical behaviour of discontinuous material, such as soil and rock. Granular material is modelled as an assembly of rigid elements; each rigid element has a vertical and a horizontal spring.
- The Modified Distinct Element method, MDEM, was developed from the DEM for a fracture analysis of concrete structures (Meguro and Hakuno, 1989).
- The Extended Distinct Element method, EDEM, is a modification of the DEM, undertaken to simulate the bending fracture of reinforced concrete structures, in which circular or spherical elements are used to represent concrete aggregate and pore-springs between those elements are utilised to model binding mortars (Meguro and Hakuno, 1994). This approach has been applied when modelling the collapse modes of several concrete structures under seismic loads (Meguro and Sato, 1996, Hakuno and Meguro, 1993). The EDEM cannot accurately represent local fracture modes. This is because appropriate material properties for determining contact elements are not available. Only the global failure mode of the structure can be predicted; including the effects of contact and collision between the elements (Hakuno and Meguro, 1993).
- The lattice model was proposed by (Sun et al., 2003b) for seismic collapse analysis of reinforced concrete structures using EDEM. Such a structure is assumed to consist of square elements. Each square element consists of six springs and four lumped masses. Reinforcement can be modelled either as an integral model or as a discrete model. Material fracture is based on ultimate strain. As the springs yield and then fracture, the entire process of collapse can be simulated, from the elastic to the

discontinue stage. Contact is considered to occur between masses representing concrete materials only. The advantage of this model is that a shorter CPU time is required, comparative to that needed for the EDEM.

The discrete element methods are time consuming and require detailed modelling. Hence, their suitability is limited to detailed analyses; such as 2 D models or small 3 D models. In addition, these discrete element methods are less accurate than the FEM at the small deformation stage. Also, the accuracy of the analytical results obtained from numerical methods utilising rigid elements is affected by element size, shape and arrangement (Kikuchi et al., 1992).

2.3.3 Coupled Finite Element-Discrete Element Method

The coupled finite element-discrete element method, has the advantages of both finite element and discrete element methods, as proposed by Lu (Lu et al., 2009). This approach has been implemented in existing software MSC.MARC. Multi-layer shell models and fiber models, developed by Lu et al., were used to construct the initial finite element model (Miao et al., 2007, Lu et al., 2008). The progressive collapse of a structure is then simulated by removing those finite elements that reach failure limits and by replacing them with granular discrete elements with an equivalent total mass and volume and with the initial conditions of the deactivated elements. Furthermore, a simple algorithm is used to account for any contact and impact between the elements. It has been concluded that this method can simulate the impact of fragments during collapse better than the finite element method. A numerical example conducted using this approach has indicated the importance of impact and debris effects on the process of collapse (Lu et al., 2009).

2.3.4 Applied Element Method

Tagel-Din and Meguro developed an Applied Element Method for modelling the entire collapse process, starting from crack initiation until complete collapse, with reasonable accuracy in both the small and large deformation ranges (Tagel-Din and Meguro, 1999a). In this method, the structure is modelled as an assembly of small rigid elements, connected together by sets of normal and shear springs. These springs represent the element deformations and stresses. Element separation, the effect of impact loads and rigid body

motion were considered in this approach in a reasonable CPU time, without requiring any previous knowledge of possible failure behaviour. Although the shape of the rigid elements remains unchanged, the behaviour of a set of elements is deformable according to the deformations of the springs surrounding the elements. The accuracy of the AEM for nonlinear analyses has been demonstrated. Reasonable agreement has been observed between the numerical results of an eleven-storey RC frame structure under earthquake loading and those obtained using a shaking table (Meguro and Tagel-Din, 1999a). Wibowo and his co-workers reported that a good estimation of the seismic progressive collapse behaviour of bridge can be achieved by using computer software called the Extreme loading for Structures, ELS, which is based on the AEM (Wibowo et al., 2009). The theory and application of the AEM is described in detail in Chapter 3.

2.4 PART III: Analytical methods for seismic collapse assessment

2.4.1 Analytical methods for seismic collapse assessment

The provisions for performance-based assessment were first specified in FEMA 273/356 (ASCE, 2000, ASCE, 1997) and ATC 40 (ATC, 1996). In the former, the monotonic backbone curves, defining a force-deformation component relationship defined as a function of reinforcement details and seismic demand parameters. The Pacific Earthquake Engineering Research, PEER, Center extended previous work and developed a methodology for seismic collapse assessment integrating possible sources of uncertainty related to the collapse prediction process; e.g. seismic demand and capacity and ground motion intensity (Cornell et al., 2002, Ibarra et al., 2005, Haselton et al., 2007, Zareian and Krawinkler, 2007). Side-sway collapse can be simulated directly; whereas, vertical collapse due to the loss in the column load carrying capacity or failure of the slab-column connection is assessed based on the post processing of simulation data and component damage models (Aslani and Miranda, 2005). The global probabilistic framework for seismic performance assessment involves four processes; seismic hazard analysis, structural response simulation, damage assessment and loss modelling, as related to economic losses and casualties (Deierlein, 2004), as outlined in Figure 2-10. The four outputs obtained during these steps are hazard curves, representing the annual frequency of exceeding different levels of seismic excitation in terms of a ground motion Intensity Measure, IM, Engineering Demand Parameters, EDPs, Damage Measure, DM, and Decision Variables, DV. The focus of this study is on directly predicting collapse capacities; thus, only the most recently methods for assessing the collapse capacities are described below. State of the art available methods for seismic collapse assessment, as developed before 2007 can be found in (Villaverde, 2007). Structural engineering demand parameters can be determined from nonlinear dynamic time history analyses of analytical models involving the features important to collapse simulation.

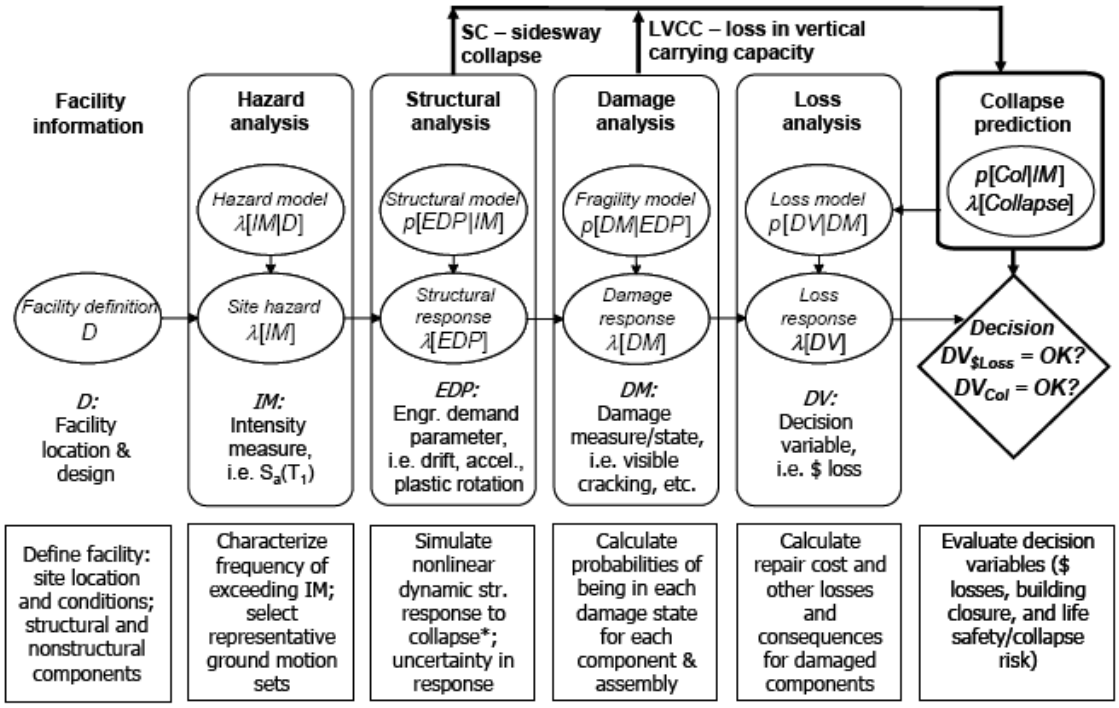

Figure 2-10: PEER probabilistic framework for collapse assessment (Deierlein and Haselton, 2005)

2.4.1.1 Step-by-step analysis

Mehanny and Deierlein developed a methodology for the seismic damage assessment of steel-concrete composite frames, utilising a Mehanny-Deierlein component damage index (Mehanny and Deierlein, 2001). The collapse safety of structures under earthquake loadings can be evaluated by integrating structural component damage indices. The first step of this methodology involves performing time history analyses for a set of ground motions under linearly increasing intensity, in order to calculate the damage indices. Then, for a given record and intensity level, the analytical model is modified to account for any corresponding damage obtained from the IDA, which means updating the geometry of the model in order to consider the permanent deformation obtained at the end of the first analysis and to decrease the element stiffness and strength according to the damage index. Then, for each intensity level, a second-order inelastic static analysis under gravity loads are only carried out for each selected record, using the modified model to determine the stability index, which represents the ratio between the vertical load capacity and the actual gravity load. This index can be

used as a criterion for global failure as it describes the relationship between the collapse capacity and seismic intensity.

2.4.1.2 Incremental dynamic analysis, IDA

An incremental dynamic analysis, IDA, is a powerful method for studying the complete seismic performance of structures in the elastic stage and as they proceed toward global collapse. This method involves conducting a series of nonlinear dynamic analyses under multi-level ground motion intensity. The concept of IDAs was first proposed by Bertero in 1977 (Villaverde, 2007). Then, FEMA, the U.S. Federal Emergency Management Agency, introduced the IDAs guidelines. Recently, (Vamvatsikos and Fragiadakis, 2010, Vamvatsikos and Cornell, 2002) have explained this approach. Thus, a brief description of the IDA is given below.

In this approach, a structural model is subjected to a set of representative ground motion records, the intensity of each is incrementally increased until global collapse of the structure is reached. The IDA curves can then be produced. An IDA curve for each individual record is a plot of a response measure, recorded in an IDA study versus an intensity measure, as shown in Figure 2-11 (Haselton et al., 2008b). The intensity Measure, IM, can be selected as the peak ground acceleration, PGA, or the 5% damped spectral acceleration at the first-mode of the structure, $s_a(T_1, 5\%)$. The damage or response measure, DM, can be as the maximum peak inter-storey drift ratio. Global collapse occurs due to global dynamic instability, when a small increment in the IM-level leads to an unlimited increase in the response measure of the structure. Based on the IDA curve, global dynamic instability for each individual record occurs when the IDA curve becomes flat. Different ground motions with different content frequency lead to different IDA curves. It is worth noting that the IDA curve is not always monotonic due to the scaling up of the record. The effective period of the structure elongates as the structure is subjected to higher cyclic loading in the earliest part of the time history, whereas later cycles may not cause the structure to yield. Hence, the response of the structure to subsequent cyclic loading may change. The output of the IDAs is the mean collapse capacity and the dispersion due to record-to-record variability, RTR. Thus, estimating collapse capacity using IDAs requires a proper IM, which represents the ground motion frequency content associated with a seismic event that will cause collapse of the structure.

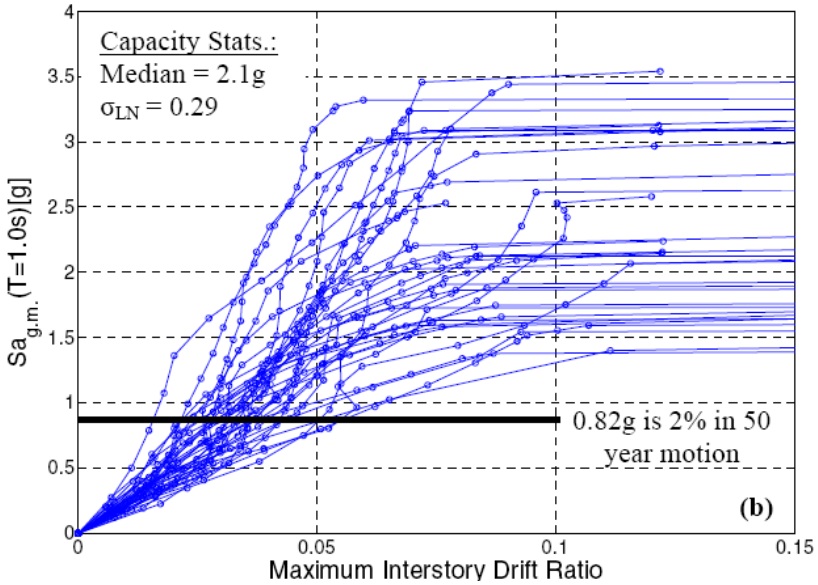

Figure 2-11: Example of IDA for collapse analysis (Haselton et al., 2008b)

Ibarra and Krawinkler developed a methodology for evaluating the seismic side-sway collapse of deteriorating SDOF and MDOF systems using a relative intensity measure and a response measure defined as, $\frac{\delta_{max}}{\delta_d}$, when performing an incremental dynamic analysis (Ibarra and Krawinkler, 2004, Ibarra and Krawinkler, 2005). The relative intensity measure is represented by the ratio between the seismic intensity and the strength parameter of the structure. This relative intensity measure is defined as $\left(\frac{s_a(T_1).\eta}{g}\right)$. $s_a(T_1)$ is the 5% damped spectral acceleration at the first-mode of the structure without the P-Delta effect. $\eta = \frac{V_y}{W}$ is the base shear coefficient; V_y is the yield strength; and W is the structure weight. δ_{max} is the maximum displacement and δ_d is the spectral displacement. The collapse capacities of single-bay generic frames with various numbers of storeys representing different MDOF systems, were investigated using a set of 40 ground motions. In Ibarra and Krawinkler's study, plastic hinges were allowed to form at both ends of all beams but only at the column bases. The assumption made was that the same hysteresis model, which includes monotonic and cyclic strength degradation, was used for all the rotational plastic springs of a structure. The values of the primary parameters used in the modified Ibarra-Krawinkler model (Ibarra et al., 2005) are: $\alpha_s = 0.03, \frac{\delta_c}{\delta_y} = 2, 4$ and $6, \alpha_c = -0.1, -0.3$ and $-0.5, \lambda = 0, \gamma = \infty, 100, 50$ and 25. The same γ is use for all the four deterioration modes. Both, the effect of

ground motion uncertainty on the collapse capacity of MDOF systems and the effect of modelling uncertainties, associated with the above mentioned models, on collapse capacity have been quantified using this methodology. It has been concluded that post-capping stiffness and ductility capacity are the most important parameters. The proposed methodology can be applied to the development of the collapse fragility curves, as well as to evaluation of the mean annual frequency of collapse (Ibarra and Krawinkler, 2005).

2.4.1.3 Stripe analysis method in IDA

The characteristics of ground motion depend on the hazard level. The spectral shape of ground motions representing rare events significantly differs from that of ground motions associated with frequent events. Therefore, the assumption made in the IDA method, when scaling a single set of ground motions in order to represent all hazard levels to provide a proper IM, can result in an overestimation or underestimation of seismic demand. Several studies have found that if the effect of ground motion shape as represented by ε is ignored, then the seismic demand on the structure will be under-estimated for frequent hazard levels and over-estimated for rare hazard levels (Zareian and Krawinkler, 2009, Baker and Cornell, 2005). This problem can be resolved by employing the stripe analysis method as related to IDA, in which different sets of ground motion records, with proper characteristics for different ranges of hazard levels are selected and then each bin is used at the corresponding IM levels. At each stripe level, the ground motion records in the corresponding set are scaled to the desired values of IM. To undertake collapse assessment, the set of records with largest magnitude is then used over the IDA (Haselton et al., 2008b).

2.4.2 Assessment of collapse probability

Collapse performance can be estimated by the probability of collapse at a discrete hazard level; e.g. IM value, the mean annual frequency of collapse, MAF, and the collapse capacity margin. The latter is defined as the ratio between the median collapse capacity and the maximum considered earthquake, MCE, intensity and is generally associated with the 2% in 50-year ground motion intensity level (Zareian et al., 2010). In order to obtain these measures, two key components are necessitated: the seismic hazard curve and the collapse fragility curve.

The hazard curve for a specific site, and the location of the selected structure, represents the relationship between the ground motion intensity measure and the return period of ground motion. The seismic hazard curve for a given IM can be calculated through either seismic hazard maps or probabilistic seismic hazard analysis, PSHA. More information about the PSHA procedures can be found in (Kramer, 1996, McGuire, 2004).

The probability of collapse for a set of ground motions can be computed using either an EDP-based method or an IM-based method. In the EDP-based method, the collapse is assumed to occur when an engineering demand parameter, EDP, exceeds the structure capacity at a given intensity level, $EDP_d \geq EDP_c$. In this case, the engineering demand parameter could be a structural component deformation or a storey drift ratio (Zareian et al., 2010). EDP_c can also be a predefined deterministic value. The collapse probability at a given IM, $P[C/IM]$, can be obtained as in Equation 2-5 (Zareian et al., 2010). $P[\,EDP_c = edp_{ci}]$ represents the probability that capacity is equal to edp_{ci}.

$$P[C/IM = im_i] = P[\,EDP_d \geq EDP_c/IM = im_i] \qquad \text{Equation 2-5}$$

$$= \sum_{\text{all } edp_c} P[\,EDP_d \geq EDP_c/EDP_c = edp_{ci}, IM = im_i]\, P[\,EDP_c = edp_{ci}]$$

Both probabilistic estimations can be obtained using information obtained from the IDA curves. In cases of collapse, EDPs are very sensitive, since small changes in input can significantly alter responses (Ibarra and Krawinkler, 2005). For this reason, collapse capacity is often determined by an IM-based method instead of an EDP-based.

When utilising IM-based method, the collapse capacity of the structure is defined by the maximum ground motion intensity the structural system can sustain without experiencing dynamic instability. This means that the structure is on the verge of collapse but is remaining stable at this intensity; therefore, any small increase in intensity will cause the structure to collapse (Krawinkler et al., 2009). The ground motion intensity is generally measured using spectral acceleration at the fundamental period of the structure, $S_a(T_1)$. The collapse capacity values of a given structure subjected to a set of ground motions can be obtained using the IDA as illustrated in Figure 2-12. The values for collapse capacity are generally assumed to be log-normally distributed (Ibarra and Krawinkler, 2005). The collapse fragility curve is defined as the cumulative distribution function of the collapse capacities, CDF (Ibarra and

Krawinkler, 2005). Figure 2-12 shows the process for determining collapse capacities and corresponding fragility curve (Zareian and Krawinkler, 2009).

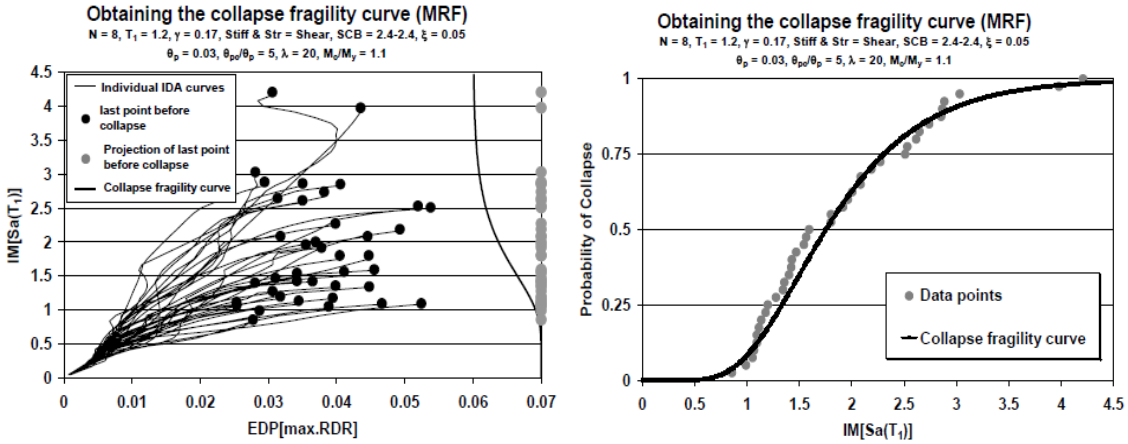

Figure 2-12: Determination of collapse capacities and the corresponding fragility curve (Zareian and Krawinkler, 2009).

The mean annual probability of collapse can be obtained by integrating fragility collapse curves, which incorporate aleatory and epistemic uncertainties, over the hazard curve. Aleatory uncertainty, denoted as β_{UC}, result from record to record variability and can be obtained directly from the cumulative distribution function of the collapse capacities. Epistemic uncertainties, denoted as β_{RC}, due to uncertainty in analytical tools can be obtained using a Monte Carlo simulation or the first-order second-moment method. The collapse probability at a specific hazard level can be directly evaluated from fragility collapse curves (Krawinkler et al., 2009).

2.4.2.1 Combination of different sources of uncertainty

The aim of seismic collapse assessment is to accurately quantify the mean and variability of structure response measures; such as the probability of collapse. Probabilistic approaches for the incorporation and integration of both sources of uncertainties are explained in (Ibarra and Krawinkler, 2005, Zareian and Krawinkler, 2009, Krawinkler et al., 2009). Two common approaches that can be used to incorporate the effects of uncertainty are the mean estimate and the confidence interval methods; provided that both sources of uncertainties are

independent. These two methods are illustrated by the plot of collapse fragilities in Figures 2-13 and 2-14.

The confidence interval method requires determination of the collapse capacity with a certain level of confidence (Ellingwood and Kinali, 2009, Cornell et al., 2002). Firstly, a median fragility curve and the β_{RC} dispersion in it are estimated by employing the median component values in the IDA analysis. The median of this median estimate is treated as a random variable, with a log-normal distribution (Liel et al., 2009). Then, epistemic dispersion is used as the dispersion for the distribution of the median estimate. Prediction at a certain confidence level is made by shifting the median of aleatory distribution to an appropriate percentile on the epistemic distribution according to the chosen confidence level (Zareian et al., 2010), as shown in Figure 2-13. The collapse probability, as well as the rate of collapse, are strongly affected by the choice of confidence level (Liel et al., 2009). Furthermore, distinction between both sources of uncertainties, aleatory and epistemic, is required in this method.

In the mean estimates method for integrating the two uncertainty sources, the median collapse capacity obtained from IDA using median component values is assumed to be unchangeable. Incorporating modelling uncertainties does not affect the median collapse capacity. However, the distribution probability of dispersion can be inflated by using the square-root-of-sum-of-squares for both uncertainties (Liel et al., 2009). The assumptions made in this method are that both uncertainty distributions are log-normal. This method is more stable than the previous approach, which depends on the choice of confidence level prediction, in addition it is not sensitive to classifying uncertainty into different sources (Liel et al., 2009).

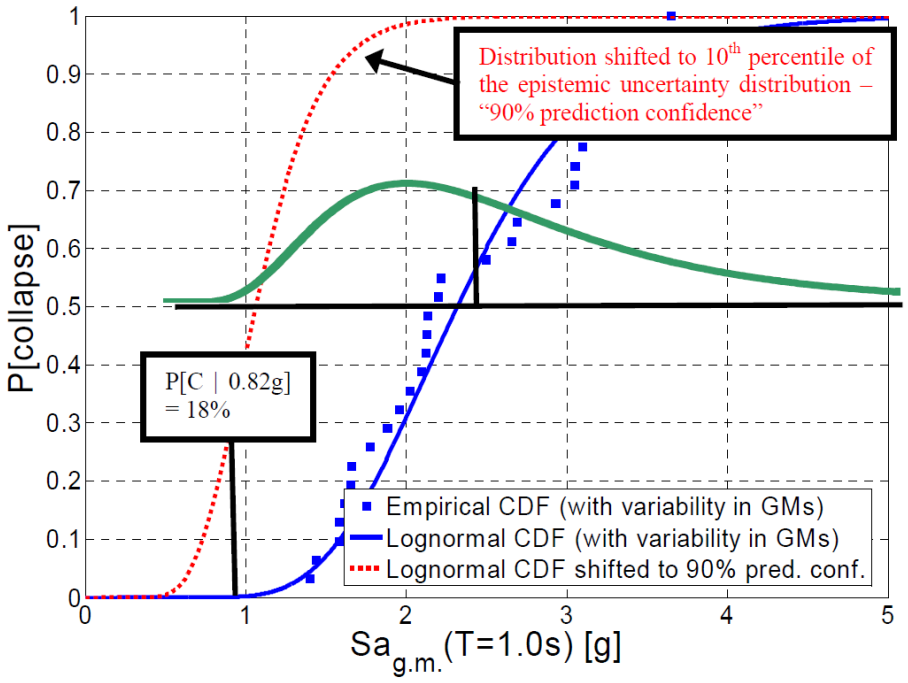

Figure 2-13: Collapse distribution based on the confident level method (Haselton and Deierlein, 2008)

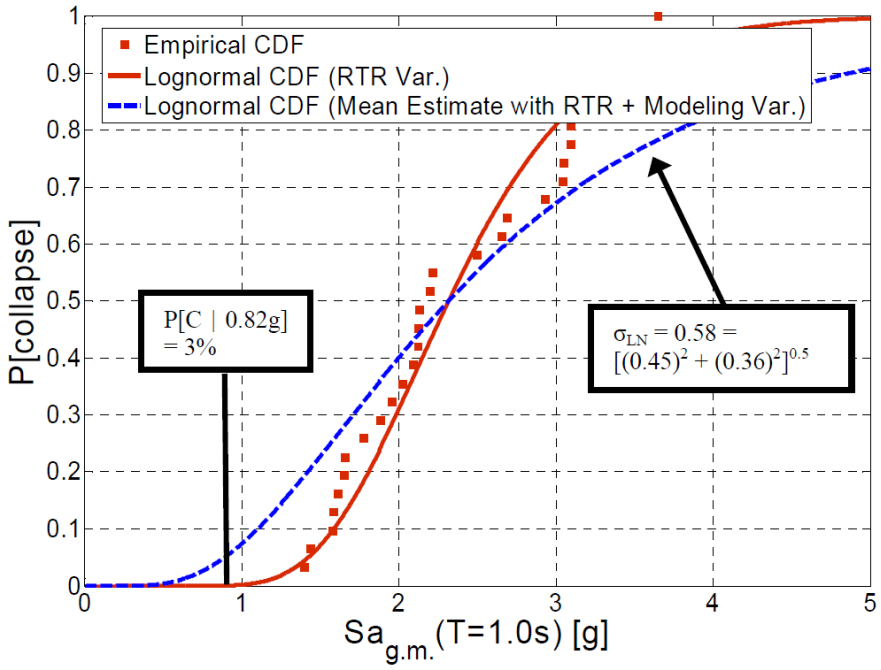

Figure 2-14: Collapse distribution based on the mean method (Haselton and Deierlein, 2008)

Haselton et al., assessed the side-sway collapse capacity of a number of ductile RC frames, designed according to current seismic codes, and accounting for the effects of modelling uncertainties as well as record-to-record variability (Haselton and Deierlein, 2008, Haselton et al., 2011b). 39 pairs of ground motion records have been utilised for performing the IDA in their study. The number of storeys in the structures varied between one and twenty. Based on a site-specific hazard curve corresponding to the Los Angeles site, they found that the collapse probabilities at the MCE are in a range of 0.12 to 0.47, collapse margins are in a range of 1.1 to 2.1 and the MAF of collapse for return periods between 400 and 4500 years are $[2.2 \times 10^{-4} - 25.5 \times 10^{-4}]$. However, these collapse quantities overstate the collapse risk, because the assessments made neglect the effects of ground motion spectral shape. The collapse capacity distribution of each structure has been modified using the method proposed in (Haselton et al., 2011a) to account for ε. Following the $\varepsilon -$ adjustment, the ranges of the previous three measures are $[0.03 - 0.20]$, $[1.4 - 3.4]$ and $[0.7 \times 10^{-4} - 7 \times 10^{-4}]$ for an average return period of 3200 years, respectively. Furthermore, they have investigated the effects of specific design provisions on seismic collapse safety. For example, the requirements of minimum base shear of ASCE 7 in the different editions, 2002 and 2005, the ACI 318 ratio of strong-column week-beam, the building height and strength-irregular design. In general, if modifying a code requirement leads to more localisation of damage in fewer storeys, the inelastic deformation capacity of the structure and thus its collapse resistance will decrease. However, more investigations are still required to quantify these effects.

A similar study regarding the assessment of the collapse capacity of a set of non-ductile RC frame structures, of varying heights from two to twelve storeys, has been carried out by (Liel and Deierlein, 2008, Liel et al., 2011). Material nonlinearities in the beam-column joints, in addition to those in the beams and columns have been considered in the structures analytical models. The plastic rotation capacity and the post-capping stiffness in the non-ductile RC frames were considerably smaller than those in the ductile RC frames. Side-sway collapse was directly simulated using the IDA with a set of 80 ground motions, while vertical collapse due to loss of axial load carrying capacity, following shear failure, was detected by post-processing the IDA results using a component criterion developed by (Aslani and Miranda, 2005) based on median column drift ratio. The results have indicated that incorporating vertical collapse modes leads to a reduction in the structure collapse

capacity of up to 30% compared with the case of only side-sway collapse. The assessment showed that the collapse probabilities at the MCE are in the range of 0.54 to 0.85.

The seismic performance of non-ductile RC frames has been compared with that of ductile frame buildings investigated by (Haselton and Deierlein, 2008, Haselton et al., 2011b). The comparison of results has indicated that the capacity design provisions employed in modern seismic codes have a significant impact on enhancing the collapse capacities of structures and reducing their seismic risk, because they result in better component deformation capacity. The requirement of strong-column weak-beam allows for greater distribution of damage over the entire structure. The collapse margin ratios of ductile RC frames are larger than those of non-ductile RC frames, by a factor of three.

2.5 Significant of the current study

The thesis will describe investigations into the collapse behaviour of reinforced concrete frame structures and the key factors that affect the collapse process. Even though a number of studies have been conducted for collapse assessments, and it can be concluded from the previous review that until now no work has focused on the collapse limit state considering the direct simulation of the different possible failure modes. This modes can involve element separation, the interaction of both vertical and horizontal capacity of the structural system and debris effects. The nonlinear time history analyses have been carried out using the Extreme Loading for Structures, ELS, software (Applied Science International (ASI), 2010). This software depends on the AEM and allows for direct modelling of element separation and element contact. Therefore, some collapse mechanisms; such as pancake collapse mode and vertical collapse mode, due to failure of more than one vertical structural member or vertical and horizontal structural members, which have not been studied before, can be investigated using the AEM. As mentioned earlier, most seismic collapse assessment studies have utilised OpenSees platform or other FEM software for side-sway collapse simulation only. Vertical collapse due to the loss of axial capacity a column has been detected by post-processing the IDA results. It was considered that AEM was more appropriate than FEM for the research described in the thesis because of the way in which separation and contact were modelled in a appropriate way.

Chapter 3 Applied Element Method for seismic collapse analysis

3.1 Introduction

The Applied Element Method, AEM, was developed by Tagel-Din and Meguro (Tagel-Din and Meguro, 1999a). This method combines the advantages of both, the Finite Element Method, FEM, and the Discrete Element Method, DEM. By using the AEM, the response of the structure can be followed all the way to collapse involving the elastic stage, crack initiation and propagation, reinforcement yielding, large deformations, element failure and separation, rigid body motion of falling elements, collision between elements, and impact forces resulting from falling debris, with acceptable accuracy and within a reasonable CPU time. This method can be easily applied to a wide range of applications; both for small and large deformation ranges under static or dynamic loading conditions, and for linear or nonlinear materials.

This chapter summarises the theoretical background to the Applied Element Method, in particular, those aspects associated with seismic progressive collapse analysis. The validation and application of the AEM in different fields are discussed, and the limitations of the AEM and its advantages are presented.

3.2 Element formulation in the AEM

3.2.1 Stiffness matrix

In the AEM, the structure is modelled as an assembly of relatively small rigid elements, as illustrated in Figure 3-1. The elements are connected by sets of three nonlinear springs (one normal and two shear springs) located at contact points, and distributed along the element surfaces. Each set of springs represents the stresses, strains, deformations and failure of a certain volume, an area $(d \times t)$ with length a. The AEM is a stiffness-based method, in which the stiffness of each pair of normal and shear springs connecting the element centrelines is calculated as in Equations 3-1 and 3-2.

$$K_n = \frac{E \times d \times t}{a}$$ Equation 3-1

$$K_s = \frac{G \times d \times t}{a}$$ Equation 3-2

Where K_n is the stiffness of the normal spring; K_s is the stiffness of the shear spring; d is the distance between the springs; t is the element thickness; a is the length of the representative area; and E and G are the Young's modulus and the shear modulus of the material, respectively.

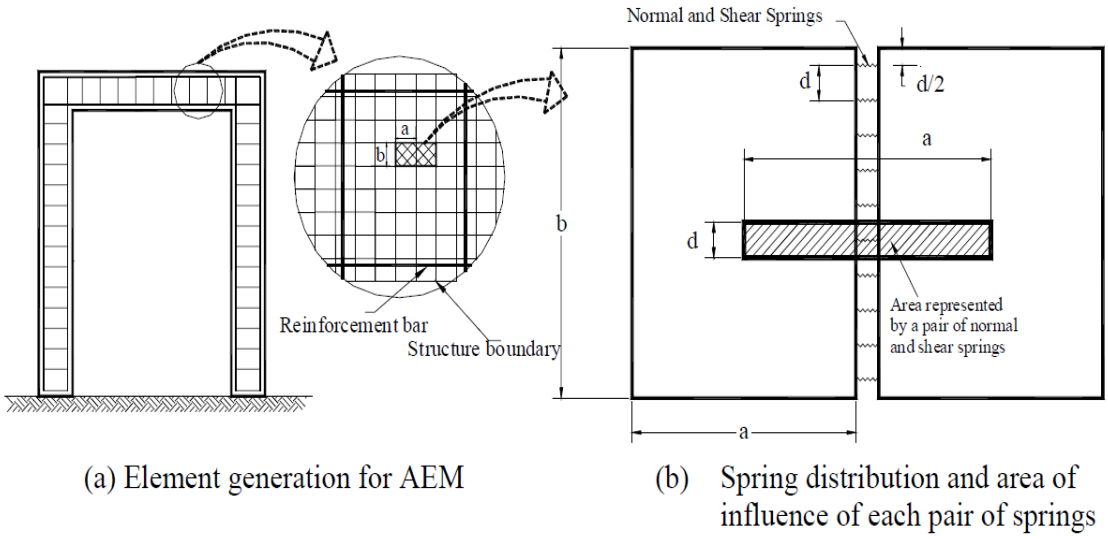

Figure 3-1: Modelling of structure in the AEM (Meguro and Tagel-Din, 1999a)

In the reinforced concrete model, two types of springs are used, namely matrix springs for concrete, and reinforcement springs for steel bars, as shown in Figure 3-2 (Applied Science International (LLC), 2010). Reinforcement springs can be set at the exact location of the steel bars so that all reinforcement details and amounts can be easily considered. In the case of the reinforcement spring, the representative area $(d \times t)$ is replaced by the reinforcement bar area.

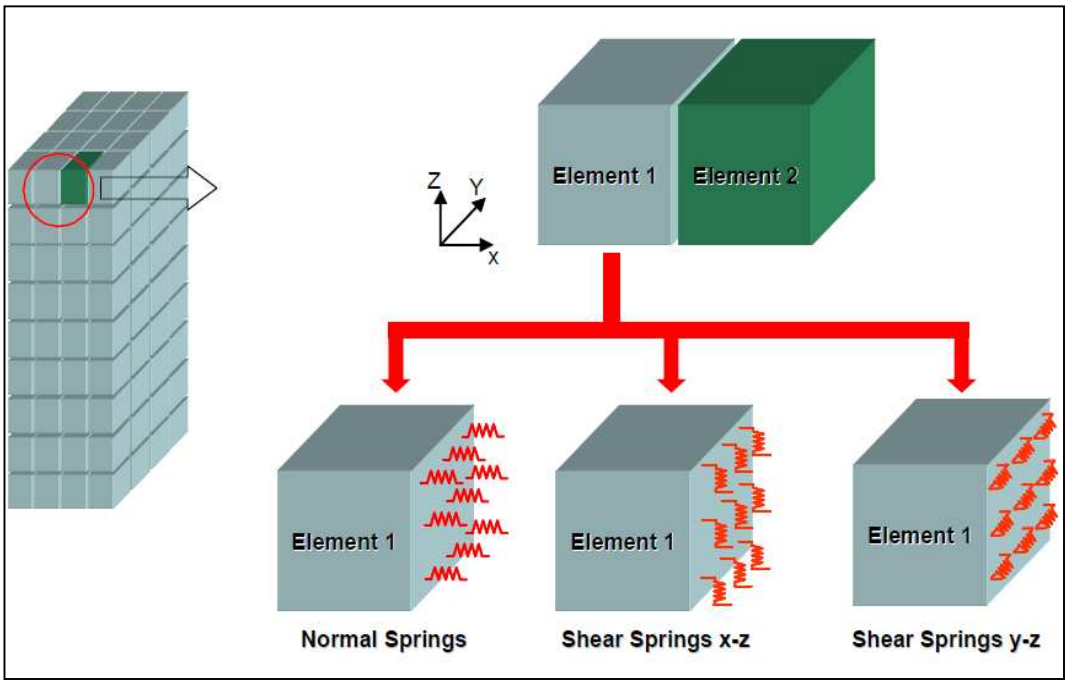

Concrete springs

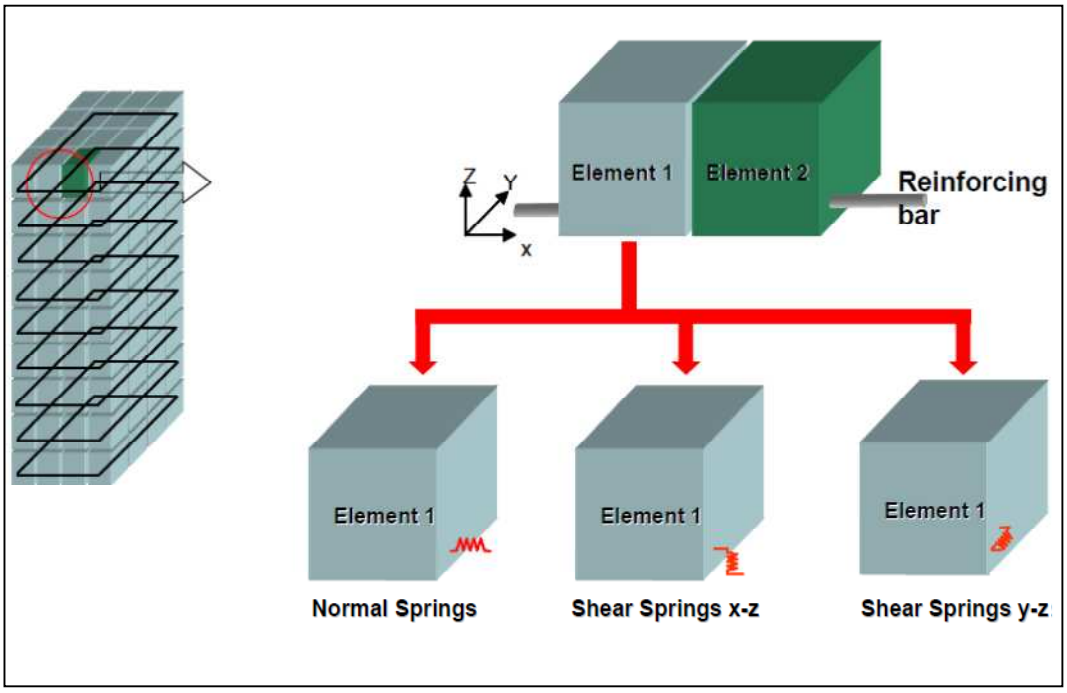

Reinforcement springs

Figure 3-2: Concrete and reinforcement springs (Applied Science International (LLC), 2010)

In general, each element has six degrees of freedom, calculated at the element centre of gravity to represent the rigid body motion of the element. Although the element shape is not deformable and the element moves as a rigid body during analysis, the behaviour of the element assembly is deformable, due to the deformations in the springs distributed around each element.

Although the reinforcement spring and the neighbouring concrete spring have the same strain, relative displacements can occur between reinforcement bars and the surrounding concrete, due to the assumption that the failure of concrete springs occurs prior to the failure of reinforcement springs.

In the two-dimensional model, each element has three degrees of freedom. The size of the element stiffness matrix is 6×6. The element stiffness matrix is determined based on the relative coordinates between the location of the contact points and the element centreline and on the spring stiffness, as shown in Figure 3-3.

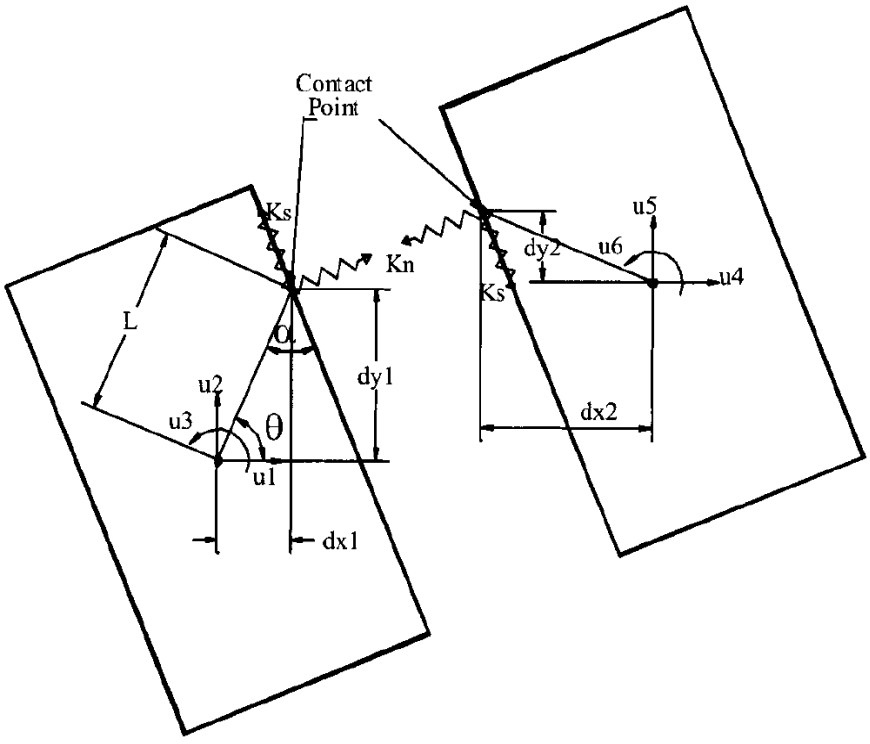

Figure 3-3: Element shape, contact point and DOF (Meguro and Tagel-Din, 2001)

Each component of the element stiffness matrix as it relates to a degree of freedom can be obtained by first applying a unit displacement to the degree of freedom under consideration and then restraining the remaining degrees of freedom. Hence, the resulting forces at the element centroid represent the stiffness matrix component as it corresponds to the DOF. The element stiffness matrix is formulated by combining the contributions of all the spring pairs distributed over the element edges. The overall global stiffness matrix is calculated as the sum of the stiffness matrices of all elements in the system.

Equation 3-3 illustrates one-quarter of the element stiffness matrix. The coefficients of this stiffness matrix, which are related to the three degrees of freedom, u_1, u_2 and u_3, can be determined by assuming that only one pair of springs connects the two elements, and that these springs are in a general position, as shown in Figure 3-3, in order to illustrate the method described above (Meguro and Tagel-Din, 2001).

$$\begin{bmatrix} sin^2(\theta+\alpha)k_n & -k_n sin(\theta+\alpha)cos(\theta+\alpha) & cos(+\alpha)k_s c\ sin(\alpha) \\ +cos^2(\theta+\alpha)k_s & +k_s sin(\theta+\alpha)cos(\theta+\alpha) & -sin(\theta+\alpha)k_n Lcos(\alpha) \\ -k_n sin(\theta+\alpha)cos(\theta+\alpha) & sin^2(\theta+\alpha)k_s & cos(\theta+\alpha)k_n Lcos(\alpha) \\ +k_s sin(\theta+\alpha)cos(\theta+\alpha) & +cos^2(\theta+\alpha)k_n & +sin(\theta+\alpha)k_s Lsin(\alpha) \\ cos(\theta+\alpha)k_s L\ sin(\alpha) & cos(\theta+\alpha)k_n Lcos(\alpha) & L^2cos^2(\alpha)k_n \\ -sin(\theta+\alpha)k_n Lcos(\alpha) & +sin(\theta+\alpha)k_s Lsin(\alpha) & +L^2sin^2(\alpha)k_s \end{bmatrix}$$ Equation 3-3

L is the distance between the spring location and the element centroid, and θ and α are the element orientation angles.

3.2.2 Large deformation analysis

A relatively simple technique called the geometrical residuals technique is adopted in the proposed method to account for geometric nonlinearity. In this technique, the effects of the geometrical changes are accounted for by determining and then redistributing residual forces resulting from the geometrical changes, R_G, and by recalculating the structure stiffness matrix after modifying the structure geometry (Meguro and Tagel-Din, 2002).

The geometrical stiffness matrix, which is very difficult to calculate in the case of element separation and materials that have experienced excessive damage, is not required,

making this method easy to apply to various types of loading conditions and across different structural configurations.

3.2.3 Determination of mass matrix in the AEM

In the AEM, the mass of the rigid element is lumped at the element centre. As the size of the AEM element is relatively small, the effect of the lumped mass is similar to that of a distributed mass. The mass matrix of a square element of thickness t is determined in Equation 3-4 (Tagel-Din and Meguro, 2000b):

$$\begin{bmatrix} M_1 \\ M_2 \\ M_3 \end{bmatrix} = \begin{bmatrix} D^2 \times t \times \rho \\ D^2 \times t \times \rho \\ D^4 \times t \times \rho/6 \end{bmatrix} \quad \text{Equation 3-4}$$

D is the element size, t is the thickness of the element, ρ is the material density, M_1 and M_2 are the element mass in X and Y directions, and M_3 is the element mass relative to the moment of inertia about the axis, which passes through the element centre.

The mass matrix is diagonal positive definite, so the diagonal elements of the mass matrix should also be positive. The addition of the mass matrix to the stiffness matrix in dynamic analysis prevents the occurrence of a singular stiffness matrix, especially where element separation occurs (Tagel-Din and Meguro, 2000b). Element separation is permitted in static analysis, due to the absence of the mass matrix.

3.2.4 Determination of damping matrix in the AEM

In the nonlinear response stage of RC structures, internal damping can arise due to the following (Tagel-Din and Meguro, 2000b):

1. Concrete cracking.
2. Energy dissipation due to the loading and unloading of compression springs.
3. Unloading of reinforcement after yielding.
4. Energy dissipation due to crack opening and closure. Shear stiffness is equal to initial shear stiffness in the case of crack closure. The shear forces that develop through the crack closure process are redistributed, leading to shear energy dissipation during the crack reopening process.

5. Friction between elements during contact.
6. Unloading factors during contact.

The sources of internal damping forces mentioned above, are automatically considered in the nonlinear response of structures using the AEM. In the elastic range, these effects from internal damping forces are neglected. Thus, an external damping matrix, [C], is required at this stage to account for internal damping (Applied Science International (LLC), 2010). The damping matrix is mass proportional and depends on the first mode of vibration, as in Equation 3-5.

$$[C] = 2\xi\omega_1[M] \qquad \text{Equation 3-5}$$

ξ is the damping ratio, and ω_1 is the first natural frequency.

3.3 Eigenvalue analysis

The AEM allows for analysis to be conducted in the frequency domain. The technique of vector iteration with shifts is utilised for Eigenvalue analysis (Tagel-Din and Meguro, 2000b). Using this approach, as many pairs of natural vibration modes and frequencies as required can be obtained; Equation 3-6 shows the case of free vibration with zero damping.

$$\left[\omega^2[M] - [K]\right][U] = 0 \qquad \text{Equation 3-6}$$

ω is the eigenvalue vector, [M] and [K] are the mass and stiffness matrix, and [U] is the displacement vector.

3.4 The numerical technique adopted for solving collision and contact problems

In order to check for collisions between elements in the AEM, a simplifying assumption is made, in which the element shape is assumed to be circular in the 2 D model, as shown in Figure 3-4. This approximation is acceptable since the element size is relatively small, and the assumption can also be applied to large elements, because the element corners are generally broken as a result of stress concentrations during the collision process.

Consequently, only the distance between the element centres is determined to check for re-contact between elements (Tagel-Din and Meguro, 1999a).

To reduce the time required for checking the collisions between elements, the geometrical coordination technique is used. When using this technique, the space is divided by grids of a reasonable size. During the analysis, the geometrical coordinates of each element are determined according to location, which changes during the analysis process, due to geometric nonlinearity. By adopting this technique, collision is checked for between the element and surrounding elements only (Tagel-Din and Meguro, 1999a).

Relatively large incremental times can be used before a collision occurs, while the time increment used during contact should be less than the contact time, D_t, which is a function of the element mass, the stiffness of the collision spring and the rebound factor, r, as illustrated in Equation 3-7. Further details about this factor are provided in Section 3.6.3.

$$\mathrm{D_t} = \frac{\pi}{2}\sqrt{\frac{\mathrm{m}}{\mathrm{k}}}(1 + \mathrm{r}) \qquad \text{Equation 3-7}$$

When a collision occurs, energy is transferred between elements in contact via contact springs, which are generated at the contact point. Linear springs, normal and shear springs are created at each contact point; this makes it possible to represent material behaviour during collision. The direction of the normal spring passes through the centres of both elements, while the direction of the shear spring is perpendicular to the normal spring at the point of contact. Elements may separate and come into contact again, either with the same or different elements.

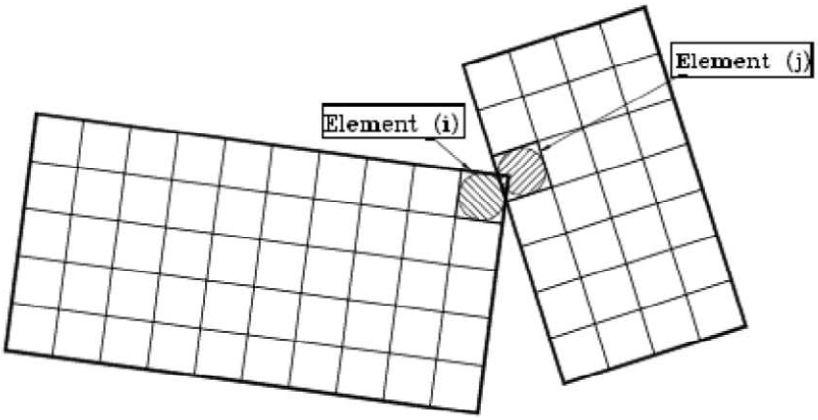

a) Collision between elements (i) and (j)

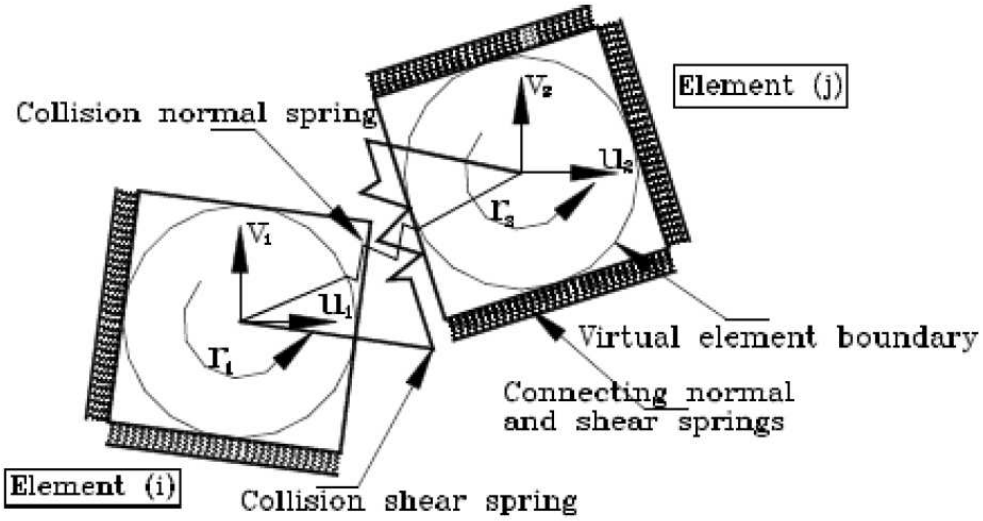

b) Close up of the elements in collision process

Figure 3-4: Collision between elements (Raparla et al., 2011)

3.5 Element formulation in collapse analysis

In the AEM, the dynamic equation of motion under seismic loading is as described in Equation 3-8 (Tagel-Din and Meguro, 1999a):

$$[M]\Delta\ddot{u} + [C]\Delta\dot{u} + [K]\Delta u = \Delta f(t) + R_M + R_G \qquad \text{Equation 3-8}$$

[M] is the mass matrix, [C] is the damping matrix, and [K] is the matrix of global nonlinear stiffness.

$\Delta\ddot{u}, \Delta\dot{u}$ and Δu are the incremental acceleration, velocity, and displacement vectors, respectively.

$\Delta f(t)$ is the incremental applied load vector, $\Delta f(t) = -[M][\Delta\ddot{u}_G]$ in the case of seismic loads and $\Delta\ddot{u_G}$ is the gravity acceleration vector.

R_G is the residual load vector due to geometric changes (Meguro and Tagel-Din, 2002).

R_M is the residual load vector due to cracking or incompatibility between spring stress and the corresponding strain (Meguro and Tagel-Din, 2002). The effects of material nonlinearity are considered in R_M and [K].

The nonlinear Equation 3-8 is solved by a dynamic step-by-step time integration method, the Newmark's Beta method, assuming small deformations during each increment and using a small time increment. This algorithm is numerically stable. Failure and element separation do not lead to a singular matrix in dynamic analysis, since the mass matrix, which is added to the stiffness matrix, results in a positive definite stiffness matrix. As previously mentioned, element separation is not permitted in a static analysis, because the stiffness matrix may become singular.

The numerical procedures for applying this approach are (Tagel-Din and Meguro, 1999a):

1. Solve Equation 3-9 under gravity loads to obtain the displacements, stresses and strains.

$$[K]\Delta u = \Delta f_s \qquad \text{Equation 3-9}$$

Where Δf_s is the incremental static load vector.

2. Assume zero values for R_M and R_G.
3. Choose a value for the time increment to be used in the AEM analysis. A relatively large time increment can be used before the occurrence of a collision. However, the selected time increment should fulfil the assumptions of small deformation theory during each time increment. This requires that the incremental geometrical changes of the structure relative to its global dimensions should be small.
4. Utilise the Newmark's Beta method to solve Equation 3-8 in order to obtain the displacement Δu as in Equation 3-10.

$$\left[\frac{1}{\beta(\Delta t)^2}M + \frac{\gamma}{\beta\Delta t}C + K\right]\Delta u = \Delta f + \left[\frac{1}{\beta\Delta t}M + \frac{\gamma}{\beta}C\right]\dot{u} + \left[\frac{1}{2\beta}M + \left(\frac{\gamma}{2\beta} - 1\right)\Delta tC\right]\ddot{u} \qquad \text{Equation 3-10}$$

5. Modify the geometry of the structure based on the calculated Δu, by adjusting the element locations and orientations.
6. Update the directions of the spring force vectors that correspond to the new element geometry. This modification then generates incompatibility between the applied loads and the calculated stresses, as well as to the damping and inertia forces.
7. Determine the geometrical coordinates of each element.
8. Check whether collisions between each element and the surrounding elements occur or not. if collision occurs, several steps are followed:

- The value of the time increment used during the contact process is reduced. A number of factors should be considered to select a proper value, including: the relative element velocity before and following contact, the energy transmitted during the contact process and the time of contact between elements.
- Three collision springs, a normal one and two shear springs, are established at each contact point, as shown in Figure 3-4. These collision springs are activated during the occurrence of contact and are deactivated when separation occurs by removing them and applying the relevant shear and tension residual forces in reverse directions.
- The global stiffness matrix, which is a sparse matrix, is modified in order to account for changes in the contact between elements, separation and existing contact between elements. For more details about how the sparse global stiffness matrix can be modified see (Tagel-Din and Meguro, 1999a).

9. Check if cracking has occurred and determine the material residual load vectors, R_M.
10. Determine the element force vector, F_m, as the summation of the forces in all the springs surrounding each element, including the collision springs.
11. Calculate the geometrical residual forces, R_G, due to the geometrical changes, using Equation 3-11:

$$R_G = f(t) - [M]\ddot{u} + [C]\dot{u} - F_m \qquad \text{Equation 3-11}$$

12. Calculate the stiffness matrix for the new structure's configuration, including cracking and yielding conditions.
13. Calculate the incremental displacements by solving Equation 3-12.

$$[M]\Delta\ddot{u} + [C]\Delta\dot{u} + [K]\Delta u = \Delta f(t) + R_G \qquad \text{Equation 3-12}$$

14. Calculate the incremental strain and stress in each element.
15. Calculate $\Delta\dot{u}, \Delta\ddot{u}, \dot{u}, \ddot{u}$.
16. Apply the next time increment and repeat the calculation from step 5.

3.6 Material modelling

3.6.1 Concrete models

For cracked and uncracked concrete under compression, the Maekawa model, a path-dependent constitutive model, is adopted, as shown in Figure 3-5 (Maekawa, 1991). This elasto-plastic and fracture model allows for convenient representation of the loading, unloading, and reloading conditions. Calculation of the tangent modulus depends on the strain at the spring location. In order to define the compressive stress-strain envelope, the values of three parameters are required, the initial Young's modulus of concrete, the fracture parameter and the compressive plastic strain. The fracture parameter represents the extent of the internal damage to the concrete.

A minimum value, which is set as equal to 0.1% of the initial spring stiffness, is assumed for the spring stiffness after attaining peak stress, in order to avoid negative values of stiffness. Consequently, the calculated stress and that which corresponds to the spring strain becomes different. To solve this problem, the forces related to residual stresses are applied in a reverse direction in the next loading step.

The transverse reinforcement confines the concrete and increases compressive strength. The effects of biaxial confinement in compression areas are considered in the AEM by adopting the biaxial failure function, as developed by (Kupfer et al., 1969). A modified compressive strength related to each spring, f_{ceq}, is determined utilising Equation 3-13.

$$f_{ceq} = \frac{1+3.65\left(\frac{\sigma_1}{\sigma_2}\right)}{\left(1+\left(\frac{\sigma_1}{\sigma_2}\right)\right)^2} f_c \qquad \text{Equation 3-13}$$

σ_1 and σ_2 are the normal and the secondary stress of the spring, and f_c is the concrete compressive strength.

It is apparent that the spring compressive strength depends strongly on the stress state at the spring location.

For concrete in tension, the stiffness of the concrete springs is assumed constant and set as equal to the initial spring stiffness up to cracking point. After reaching this point, the tensile stress drops to zero and the spring stiffness is assumed to be equal to zero. Residual stresses are then redistributed by applying residual forces in a reverse direction in the next loading step.

The shear model used is shown in Figure 3-6. The shear stiffness is assumed to be linear until cracking. After cracking, shear stiffness is assumed to be zero and shear stresses decrease to a constant value. In order to represent the effects of shear friction and interlocking, a redistributed proportion of the shear stresses, RV, assumed to be 0.5, is considered as shown in Figure 3-6 (Meguro and Tagel-Din, 2001).

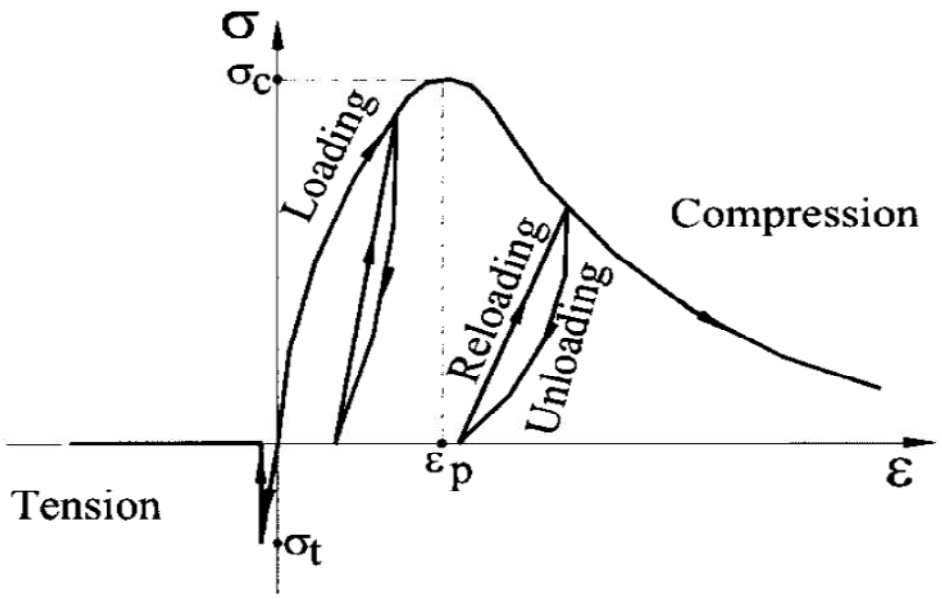

Figure 3-5: Constitutive model for concrete in compression and tension (Tagel-Din and Meguro, 2000b)

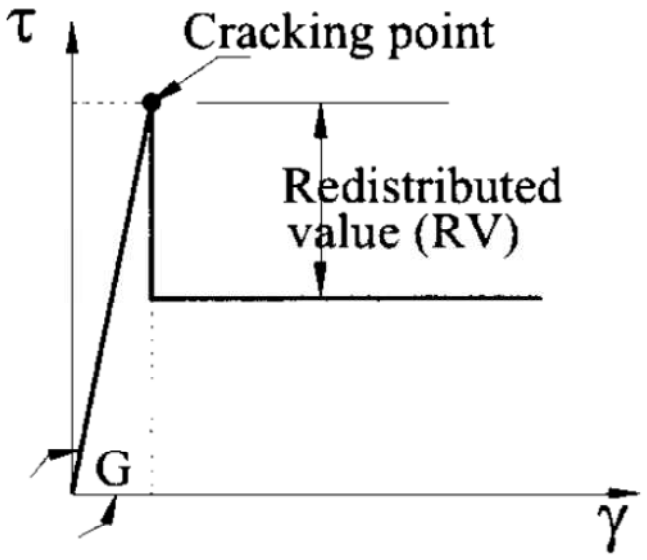

Figure 3-6: Constitutive model for concrete in shear (Meguro and Tagel-Din, 2001)

3.6.2 Reinforcement steel model

The bilinear stress-strain relationship developed by (Ristic et al., 1986) is used for reinforcement, Figure 3-7.

The stiffness of the steel spring after yielding is set to 1% of the initial spring stiffness. Bauschinger's effect and unloading effects are considered. The tangent stiffness is calculated depending on the strain history of the steel spring including loading and unloading effects. The steel spring is assumed to fracture after reaching the failure criterion. When the reinforcement fractures, the residual forces in the reinforcement are redistributed by application of these forces in a reverse direction during the next loading step.

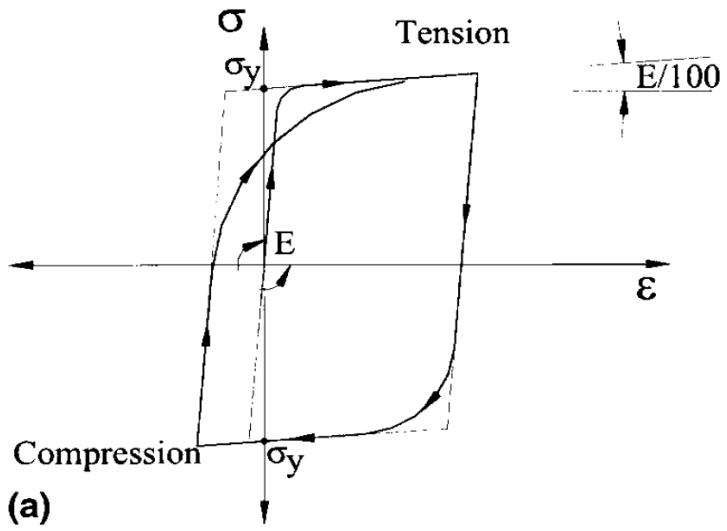

Figure 3-7: Constitutive model for reinforcement used in AEM (Tagel-Din and Meguro, 2000b)

3.6.3 Collision spring

When a collision occurs, energy is transmitted between elements in contact through collision springs, which represent the material behaviour during the collision. Two linear springs, normal and shear springs, are added at each contact point. The stiffness of the normal spring is determined by Equation 3-14 (Tagel-Din and Meguro, 1999a):

$$K = \frac{E \times d \times t}{D}$$ Equation 3-14

E is the minimum value of the Young's modulus of the colliding elements, t is the element thickness, D is the distance between the centres of the contacted elements, and d is the contact distance, which is taken as 10% of the size of the element.

The aim when using normal springs is to transmit the stress waves that result from the impact between elements. Normal springs are not permitted to fail in compression or to have tensile forces. A tensile force means that the elements in contact will separate and the contact springs will be removed and the residual shear and tension forces in the springs redistributed in the following increments (Tagel-Din and Meguro, 1999a).

The stiffness of the shear contact spring, which is affected by friction properties, is assumed to be 1% of the normal spring stiffness because the shear forces transmitted are often less than the normal forces (Tagel-Din and Meguro, 1999a).

Energy dissipated during collision can be determined by using different values for loading and unloading spring stiffness, as shown in Figure 3-8. Using this technique leads to a reduction in the CPU time, since a small value of time increment is only required during contact. "n" is defined as the ratio between loading and unloading stiffness. The relationship between n and the rebound factor, r, which represents the ratio between the relative velocity of the element before and after collision, is defined in Equation 3-15 (Tagel-Din and Meguro, 1999a):

$$r = \frac{1}{\sqrt{n}}$$ Equation 3-15

The value of r is in the range of zero to one and can be determined according to the conservation of momentum. When r and n are equal to one, then no energy will be lost during collision and the velocity before and after collision will remain constant. While all kinetic energy is dissipated during contact in the case of r equals to zero. Having a value of 10 for n indicates that 90% of the element's energy is lost during contact.

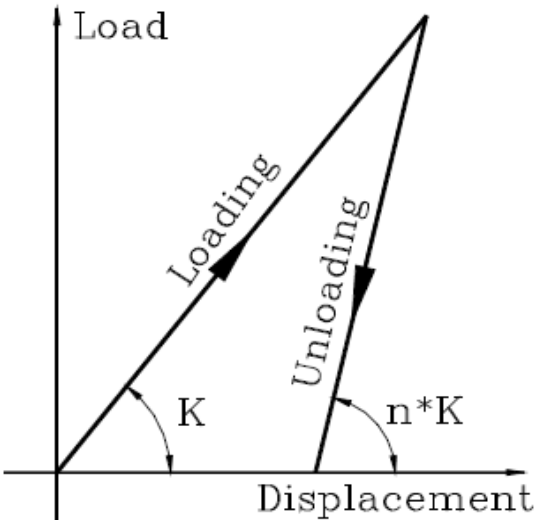

Figure 3-8: Load-displacement relationship of a collision spring (Tagel-Din and Meguro, 1999a)

3.7 Criteria adopted in the AEM

3.7.1 Cracking criterion for concrete

Modelling the diagonal cracking in concrete can be performed by adopting a failure criterion based on principal stresses rather than on the Mohr-Coulomb criterion. The Mohr-Coulomb criterion, which depends on two stress components, normal and shear stresses, is an accurate tool for a structure comprised of elements; such as masonry structures. In the AEM method, structures are virtually divided into elements. Even though normal and shear stress at the element edge change according to the mesh arrangements, principal stresses do not change (Meguro and Tagel-Din, 1999a). Hence, using the Mohr-Coulomb criterion for a continuum material may yield inaccurate results (Tagel-Din and Meguro, 2000c). Principal stresses can be calculated based on spring stresses, since the stresses and strains surrounding each element can be obtained accurately using the AEM (Meguro and Tagel-Din, 1999a).

The stresses at each spring location, which are required for calculating the major principal stress, are σ_1, τ, σ_2 , as shown in Figure 3-9.

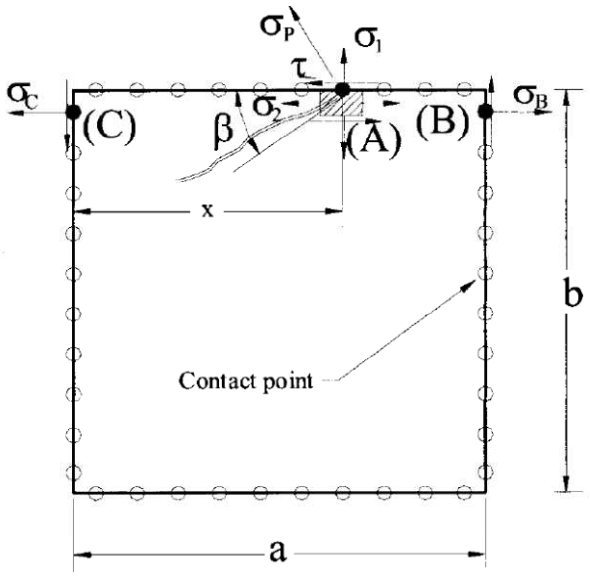

Figure 3-9: Principal stress determination (Tagel-Din and Meguro, 2000c)

The shear stress, τ and normal stress, σ_1 at a contact point; such as A can be found from the normal and shear springs attached at this point. Equation 3-16 shows the technique used for calculating second direct stress, σ_2, depending on normal stresses at two points B and C, as illustrated in Figure 3-9. The principal tension is then determined using Equation 3-17 (Tagel-Din and Meguro, 2000c).

$$\sigma_2 = \frac{x}{a}\,\sigma_B + \frac{(a-x)}{a}\,\sigma_C \qquad \text{Equation 3-16}$$

$$\sigma_P = \left(\frac{\sigma_1+\sigma_2}{2}\right) + \sqrt{\left(\frac{\sigma_1-\sigma_2}{2}\right)^2 + (\tau^2)} \qquad \text{Equation 3-17}$$

When the value of the major principal stress, σ_P, reaches the maximum tensile resistance of concrete, a crack in the concrete is assumed to occur. The forces in both normal and shear springs are then redistributed and reapplied in the reverse direction in the next time increment resulting in zero tension stress on the crack faces, due to the redistribution of all the force in the normal spring. The stiffness of the shear spring is set as equal to zero and a redistributed value, RV, is considered to represent the friction and interlocking effects as previously mentioned. After cracking, the stiffness of concrete springs is then set as equal to zero until the occurrence of crack closure.

For springs in compression, the Mohr-Coulomb failure criterion is adopted to check compression shear failure. A zero value for shear stiffness, with a redistributed value, RV, is utilised when compression shear failure occurs. The angle of the local crack, β, can be found from Equation 3-18 (Tagel-Din and Meguro, 2000c).

$$\tan(2\beta) = \left(\frac{2\tau}{\sigma_1+\sigma_2}\right) \qquad \text{Equation 3-18}$$

The crack direction is parallel to the element edge when the shear stress is equal to zero.

As shown in Figure 3-10, modelling a diagonal crack can be performed in two ways as follows (Tagel-Din and Meguro, 2000c):

1. Dividing the element into two parts. Each part has three degrees of freedom and new springs are generated between the crack surfaces of the two parts. Tension stress redistribution takes place at the plane of principal tension stress and a zero shear plane. This method is accurate for calculating the width and direction of cracks as well as failure due to compression shear. However, it is time consuming because it causes a large increase in the number of elements, in addition to a reduction in the element size due to the existence of cracks. The size of the global stiffness matrix rises rapidly because of the existence of new elements. Calculating the spring stiffness of cracked elements is less accurate than calculating the spring stiffness before cracking, since the springs do not represent a constant area after element separation.
2. Redistributing stresses that result from cracking rather than splitting the element, and setting the stiffness of failed springs equal to zero.

This method is less accurate than the previous one. In this simple method, failure of the attached springs, as they reach the failure criterion, represents failure inside the element. Despite these simplifications, this method still gives reasonable results.

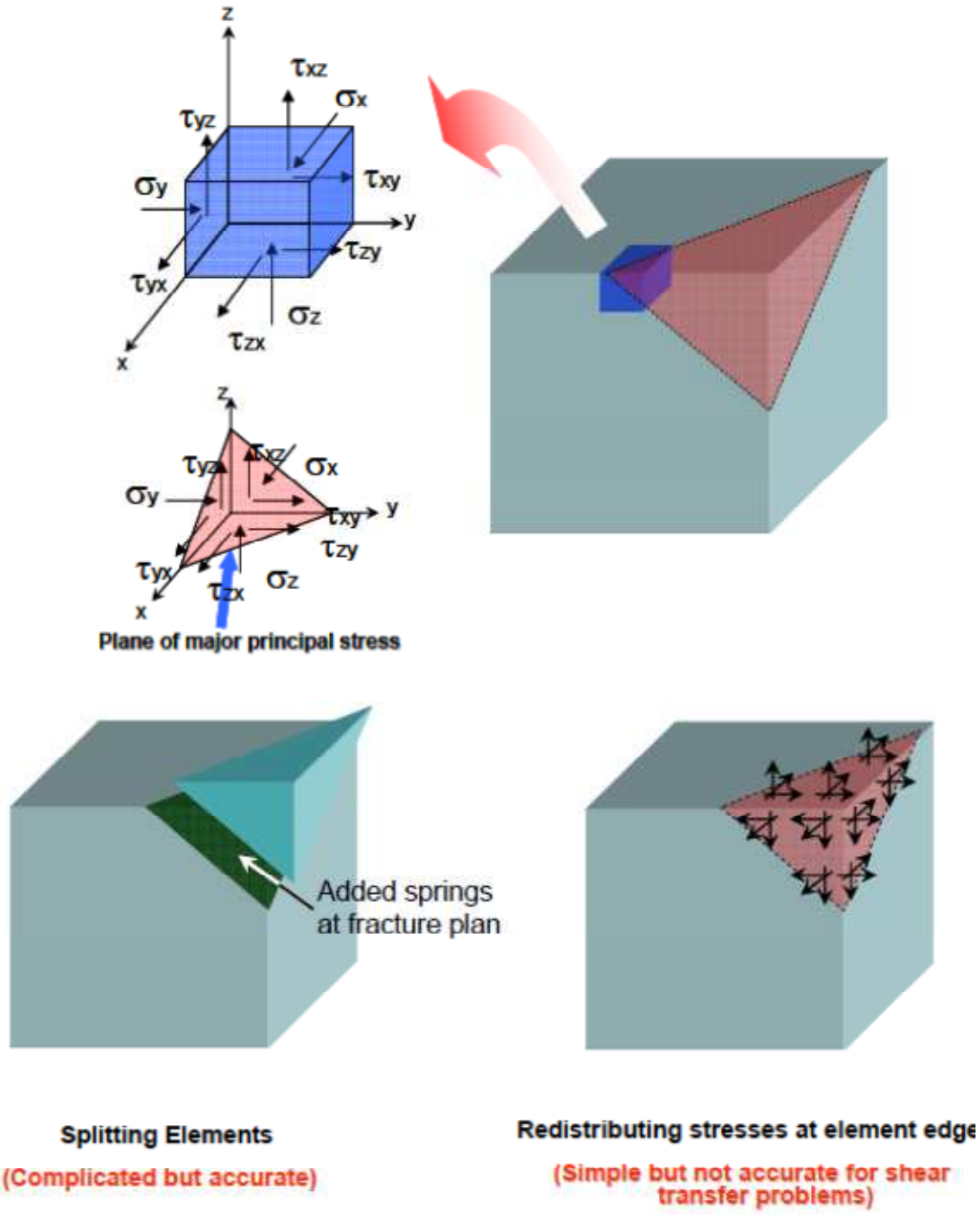

Figure 3-10: Different strategies to deal with cracking (Applied Science International (LLC), 2010)

3.7.2 Failure Criterion for concrete

The average normal strain at each element face is determined from the average of absolute values of strains on this face. When the value of the average strain at the element face exceeds a predefined value, called the separation strain, all the springs attached to this face are considered failed and removed (Applied Science International (LLC), 2010).

3.7.3 Criterion for reinforcement rebar cut

Reinforcement bar springs are assumed to fracture and then cut in either of two cases as follows (Applied Science International (LLC), 2010):

1. When the failure criterion of the steel springs is met, which means the normal stress has reached the specified ultimate stress for the steel material. It is important to note that the bar break occurs due to tension forces only and no failure is permitted in compression.
2. The strain of the concrete springs satisfies the separation limit. In this case, all concrete and reinforcement springs are removed even if the reinforcement springs have compression forces.

3.8 Validation and application of the AEM

A number of studies have been conduced to check the accuracy of the AEM in various fields of application by comparing the AEM analytical results with theoretical and experimental results or those obtained from other numerical methods.

The accuracy of the AEM in the range of small deformations and in the case of static loading conditions has been proven (Meguro and Tagel-Din, 2000, Meguro and Tagel-Din, 2001, Tagel-Din and Meguro, 2000c). Displacements, strains and internal stresses around elements can be obtained accurately using the AEM. A new technique for large deformations for both static and dynamic loading conditions has been implemented in the AEM (Meguro and Tagel-Din, 2002) and it has been indicated that the theoretical and simulation results were comparable.

The buckling and post-buckling responses of different structures have also been examined using AEM in the large deformations range, and good agreement has been observed between the theoretical results and those obtained from the proposed method for buckling modes and loads, as well as the post-buckling behaviour (Meguro and Tagel-Din, 1999b).

It has also been shown that the element size, shape and arrangement do not affect the crack pattern or crack propagation. Hence, the mechanical behaviour of structures including crack opening and closure process can be followed accurately (Meguro and Tagel-Din, 1999a, Meguro and Tagel-Din, 2001).

The effect of the number of contact springs between elements was investigated using 20, 10 connecting springs (Meguro and Tagel-Din, 2000). The rotational stiffness was affected by the number of connecting springs, while the translational stiffness was independent. It was found that using 10 contact springs instead of 20 contact springs to connect the two adjacent faces of the elements does not affect the accuracy of the results (Meguro and Tagel-Din, 2000).

Consideration of Poisson's ratio effect, without increasing the number of degrees of freedom has been taken into account for 2D problems. This can be performed by correlating each element's stiffness matrix to the stiffness matrix of each adjacent element, from all directions using a factor called 'f' to represent continuity and by applying an additional term to the element stiffness matrix (Meguro and Tagel-Din, 2000). For more information about the technique used for accounting for the Poisson's ratio effect, see (Meguro and Tagel-Din, 2000). It has been noted that no significant additional time is needed to account for the Poisson's ratio effect using elements with only 3 DOFs. For 3D problems, the effect of Poisson's is neglected, as it is relatively small.

The AEM has been extended to account for the collision problem (Tagel-Din and Meguro, 1999a). Good agreement was observed when comparing the analytical and theoretical results. It should be emphasised that the behaviour of structures during collapse and collision can be traced effectively with the AEM. It has been proven that element separation, the rigid body motion of falling elements and element collision, either with each other or with the ground, can be followed reliably (Tagel-Din and Meguro, 1999a).

Comparison of the results of the AEM model for a scaled eleven-storey RC structure (1/15) subjected to a series of scaled motions, with those obtained from shaking table experiments has proven that the AEM is an efficient tool for collapse simulation. Even though the experiment was only performed up to the beginning of the collapse, due to the limitations of the capacity of the shaking table used, realistic results were obtained from the collapse simulation using the AEM, with relatively simple models for concrete crushing and reinforcement fracture (Tagel-Din and Meguro, 1999b, Tagel-Din and Meguro, 2000a).

An AEM analysis can be performed either in the time domain or the frequency domain. The accuracy of the AEM for determining the natural frequency of damaged structures prior to collapse has been proven by comparing experimental and numerical results (Uehan and Meguro, 2004b, Uehan and Meguro, 2004a). It has been found that the natural frequency can be used as a measure of damage.

The AEM is not only an effective tool for investigating the progressive collapse of steel, reinforced concrete or masonry structures under different loading conditions, such as: blast, flood (Hamed, 2011), seismic loading or the demolition scenario, but also for assessing the response of structures with different types of strengthening, leading to the selection of the most effective strengthening techniques (Dessouky et al., 2007, Hamed, 2011, Karbassi, 2010, Karbassi and Nollet, 2008, Lupoae et al., 2011, Raparla et al., 2011, Pandey and Meguro, 2004, Worakanchana et al., 2008, Uehan and Meguro, 2004b). Understanding of the collapse process has been the aim of most studies. The conclusions reached in some of these studies have provided direction to improve the design of new structures; offering more effective retrofitting techniques for existing structures or more economical design against progressive collapse by investigating the effects of utilising different retrofitting strategies (Galal and El-Sawy, 2009, Hamed, 2011, Khalil, 2011, Salem et al., 2011, Uehan and Meguro, 2004b). It has been found by Wibowo et al., that the progressive collapse of RC bridges can be reliably predicted using the AEM (Wibowo et al., 2009, Wibowo, 2009).

The accuracy of using AEM for the demolition analysis of reinforced concrete structures has been evaluated by (Lupoae and Bucur, 2009, Sasani, 2008). The AEM results show good agreement with those observed during the actual demolition of full-scale structures.

The AEM allows for the modelling of masonry walls, free standing or inside steel or in reinforced concrete frames. Bricks and mortar can be individually simulated (Guragain et al., 2006, Pandey and Meguro, 2004). The effects of infill walls on the progressive collapse of reinforced concrete structures subjected to blast loads, or due to demolition, have been investigated using the AEM (Lupoae et al., 2011, Sasani, 2008). Based on the AEM results, the load distribution mechanism associated with the vierendeel action of frames can be properly explained and hence understood.

It was proven in comparison with experimental results that the crack pattern and the force-deformation relationship of non-retrofitted masonry walls with different configurations (Pandey and Meguro, 2004) and of retrofitted masonry walls with Polypropylene bands under monotonic and cyclic static loading can be simulated accurately using the AEM (Guragain et al., 2006, Worakanchana et al., 2008).

The Improved Applied Element Method, IAEM, has been developed for collapse analysis of steel structures (Elkholy and Meguro, 2004). Modifications made in the AEM allow simulation of non-rectangular cross-sections utilising large elements, as shown in Figure 3-11. The stiffness of both the normal and shear springs of an element can be determined using a different thickness from that used for calculating the stiffness of the adjacent set of springs connected to the same element as illustrated in Equations 3-19 and 3-20. In addition, the effect of any changes in the thickness of the cross-section is considered when calculating the lumped mass, as illustrated in Equation 3-21.

$$k_n^i = \frac{E \times d \times T_n^i}{a} \qquad \text{Equation 3-19}$$

$$k_s^i = \frac{G \times d \times T_s^i}{a} \qquad \text{Equation 3-20}$$

k_n^i is the stiffness of the i normal spring, k_s^i is the stiffness of the i shear spring, and T_n^i, T_s^i are the thickness represented by the i set of springs for normal and shear springs, respectively.

$$\begin{bmatrix} M_1 \\ M_2 \\ M_3 \end{bmatrix} = \begin{bmatrix} \frac{D^2.\rho}{nsp} \times \sum_{i=1}^{i=nsp} t_i^x \\ \frac{D^2.\rho}{nsp} \times \sum_{i=1}^{i=nsp} t_i^y \\ \frac{D^4 \times \rho}{nsp} \times \sum_{i=1}^{i=nsp} \left(\frac{t_i^x}{12} + \frac{t_i^y}{12} \right) \end{bmatrix} = \begin{bmatrix} D^2 \times \rho \times t_{av} \\ D^2 \times \rho \times t_{av} \\ \frac{D^4 \times \rho}{nsp} \times \sum_{i=1}^{i=nsp} \left(\frac{t_i^x}{12} + \frac{t_i^y}{12} \right) \end{bmatrix} \quad \text{Equation 3-21}$$

t_{av} is the average element thickness, and nsp is the number of pairs of springs connected to the element.

In the IAEM, the plastic zone solution is adopted for modelling the spread of plasticity, assuming that the contact springs are fibers. Good agreements have been observed between the theoretical and the IAEM results for ultimate load-carrying capacity. Further development is still necessary to consider the effects of local and lateral tortional buckling.

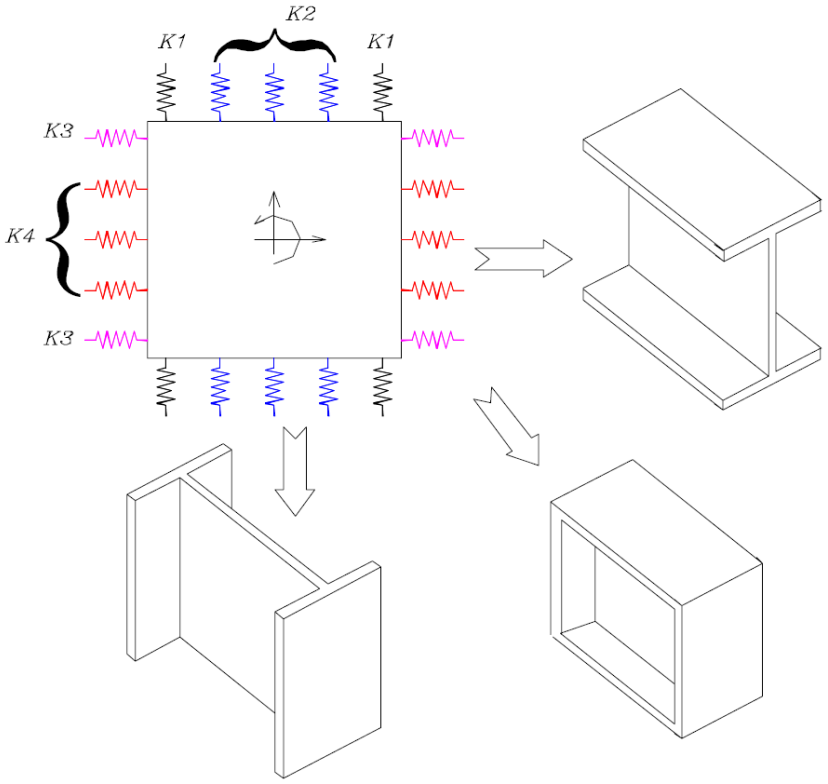

Figure 3-11: Element shape for IAEM (Elkholy and Meguro, 2004)

The capabilities of the AEM, in regards to simulating the highly nonlinear response of a porous glass fiber reinforced polymer, GFRP, barrier subjected to blast loads, has also been also demonstrated based on comparisons with experimental data (Asprone et al., 2010). The

results have indicated that strains and accelerations in the barrier can be predicted well by the AEM.

3.9 Limitations of the AEM method

The material models for concrete and reinforcement in AEM do not consider the effects of the following (Tagel-Din and Meguro, 1999a):

1. Strain rate effects.
2. Tension softening.
3. Spalling of concrete cover, as well as pull out and buckling of reinforcement bar. This is because steel rebar and concrete have the same DOF, as they are modelled by springs attached to rigid elements.
4. An AEM model capable of considering the effects of reinforcement buckling and concrete spalling has been developed and validated under quasi-static cyclic loading for a column specimen, in which, the collapse mainly occurred due to these two effects (Kuroda et al., 2004). This model has not been implemented in Extreme Loading for Structures software yet, since further research is still necessary. Using the developed model, the response of a concrete pier that collapses in a brittle shear mode has also been investigated by (Kuroda et al., 2004). More details about this model are available in (Kuroda et al., 2004).

3.10 Simplifying assumptions in the AEM

Other simplifying assumptions adopted in the AEM are as follows:

1. The duration of the fracture process of springs, concrete or steel, which depends on the value of the post-peak strain, is ignored in this method. Hence, all forces in the failed springs are redistributed in the following time increment, regardless of the post-peak strain value (Tagel-Din and Meguro, 1999a).
2. To avoid overlap between elements in contact, springs in compression are not allowed to fail after reaching a value of 0.01 of the concrete strain (Tagel-Din and Meguro, 1999a).

3. Simulation of crack widths is not very accurate, so shear transfer and shear softening, which depend on the crack width, are only approximately considered (Tagel-Din and Meguro, 2000c).
4. Modelling of compression shear failure is not accurate if the angle β is not approximately zero (Tagel-Din and Meguro, 2000c).

3.11 Advantages of the AEM

The advantage of this numerical technique can be summarised as follows:

1. The numerical method is stable even in the case of collapse and element contact (Tagel-Din and Meguro, 1999a).
2. No previous knowledge about the location and direction of crack propagation or failure modes is required.
3. The effects of falling debris on structural response can be investigated reliably using this method (Tagel-Din and Meguro, 1999a).
4. Reasonable CPU times are required to perform the analyses.
5. Partial as well as total collapse can be simulated.
6. The complete response of a structure from the loading stage until total collapse can be simulated with acceptable accuracy.

3.12 Summary

A detailed description of the theoretical background of the Applied Element method has been provided in this chapter, including element formulation in collapse analysis, material modelling, techniques for solving collision problems and failure criteria. The validation and application of the AEM in different fields have been introduced. The simplification assumptions made in the AEM, in addition to the advantages of using this method, have been presented.

Chapter 4 Validation of Applied Element Method

4.1 Introduction

This Chapter describes the details of analyses carried out for three reinforced concrete, RC, frame structures using the Applied Element Method, AEM. Applied element analyses have been performed on three reinforced concrete, RC, frame structures previously shake-table tested. These three frames are a two-storey one-bay RC frame structure (Chaudat et al., 2005) and two six-storey, three-bay RC plane frames (Lu, 1996, Lu, 2002, Lu et al., 1999). The first frame is an example of an under seismically designed RC frame structure. While the others are examples of RC frames seismically that were designed according to Eurocode 8, EC8 (Eurocode 8 (EC8), 1988 (draft); 1994). The objective of the selection of these three frames is to compare the AEM results with the experimental results reported in other studies (Lu, 2002, Lu et al., 1999, Chaudat et al., 2005), in order to validate the AEM models for modelling highly nonlinear response of structures under seismic loadings and in simulating seismic progressive structural collapse.

The nonlinear response of a structure mainly depends on its structural system, loading pattern, material properties and reinforcement details. Collapse behaviour is expected to be structure-specific. Therefore, the decision was made to choose different prototype structures with at least three-bays, formerly designed and analysed by other researchers, in order to deliver more general conclusions, so that the findings can be applied to any structure. The minimum required number of bays in any prototype structure, in order to capture the important features related to interior and exterior beam-column joints, is three (Liel et al., 2008). A brief description of these three tests is provided.

Extreme Loading for Structure software, ELS, which is based on the AEM, is used as in (Applied Science International (ASI), 2010). A detailed description of the AEM models is presented. In order to validate the AEM models, the analytical results are compared with existing experimental data obtained from previously performed tests. The details of the comparisons for each example are described in this chapter. The effects of failure criteria on

the collapse process are investigated, since these are anticipated to be one of the key parameters that can control the collapse phenomenon.

4.2 Description of shaking table test 1

A test of a full-scale two-storey one-bay RC frame structure was performed on the AZALEE shaking table in the CEA Laboratory in France in 2004 as part of the European ECOLEADER project (European Consortium of Laboratories for Earthquake and Dynamic Experimental Research) (Chaudat et al., 2005). The aim of this test was to understand the seismic performance of existing RC structures, and to assess the efficiency of using carbon fiber reinforced polymer, CFRP, materials as a strengthening technique. The frame structure contained seismically deficient reinforcement details in the beam-column joints, to represent typical existing buildings, designed according to older seismic code provisions. Two series of shaking table tests were conducted. The first series was performed on the bare frame, while the second was carried out on the retrofitted frame. In the first stage, five shaking table tests were carried out until severe damage was observed, in order to predict the actual behaviour of the frame. The main objective of using the initial series in this study is to validate the AEM models at different levels of nonlinearity throughout; by comparing the analytical results obtained by using Extreme Loading for Structures software, with experimental data obtained from the initial shaking table tests. Then, the AEM analysis was extended, and the simulation performed up to the total collapse of the structure, to predict the failure mechanisms of such structures and to investigate the effect of failure criteria on the collapse process.

4.2.1 Details of test 1 and experimental observation

4.2.1.1 Geometry and reinforcement details of the selected structure

The structural system of this test was a one-bay two-storey spatial regular frame. The building was $4260\ \text{mm} \times 4260\ \text{mm}$ in plan with a total height of 6.87 m and a storey height of 3.30 m. All the columns had rectangular cross sections of $260\ \text{mm} \times 260\ \text{mm}$ with longitudinal reinforcements consisting of $8\text{Ø}14$ mm for the first floor columns and $4\text{Ø}14$ mm for the second floor columns. The dimensions of the rectangular beams were $400\ \text{mm} \times 260\ \text{mm}$ and the longitudinal reinforcement was $2 \times 4\text{Ø}14$ mm. The concrete cover was 30 mm. The slab thickness was approximately 120 mm, with two layers of Ø9 mm mesh at

100 mm spacing. Figure 4-1 gives a general view of the test. The dimensions and reinforcement details in the frame are given in Figure 4-2. Complete details of this seismic test can be found in (Chaudat et al., 2005).

Figure 4-1: General view of test 1 (Chaudat et al., 2005)

4.2.1.2 Material properties of the RC frame

The properties of the materials used in the construction of the structure were as follows: the yield and ultimate strength of the longitudinal reinforcement were $f_y = 551$ MPa and $f_u = 656$ MPa, respectively. The yield and ultimate strength of the transverse reinforcements were $f_y = 582$ MPa and $f_u = 644$ MPa, respectively. The modulus of the elasticity of steel was 200000 MPa and its Poisson ratio was set as equal to 0.2. The average compressive strength of concrete, f_c, obtained from 24 cylindrical specimens, was approximately 19.6 MPa and the average modulus of the elasticity of the concrete, E_c, was around 23500 MPa (Chaudat et al., 2005).

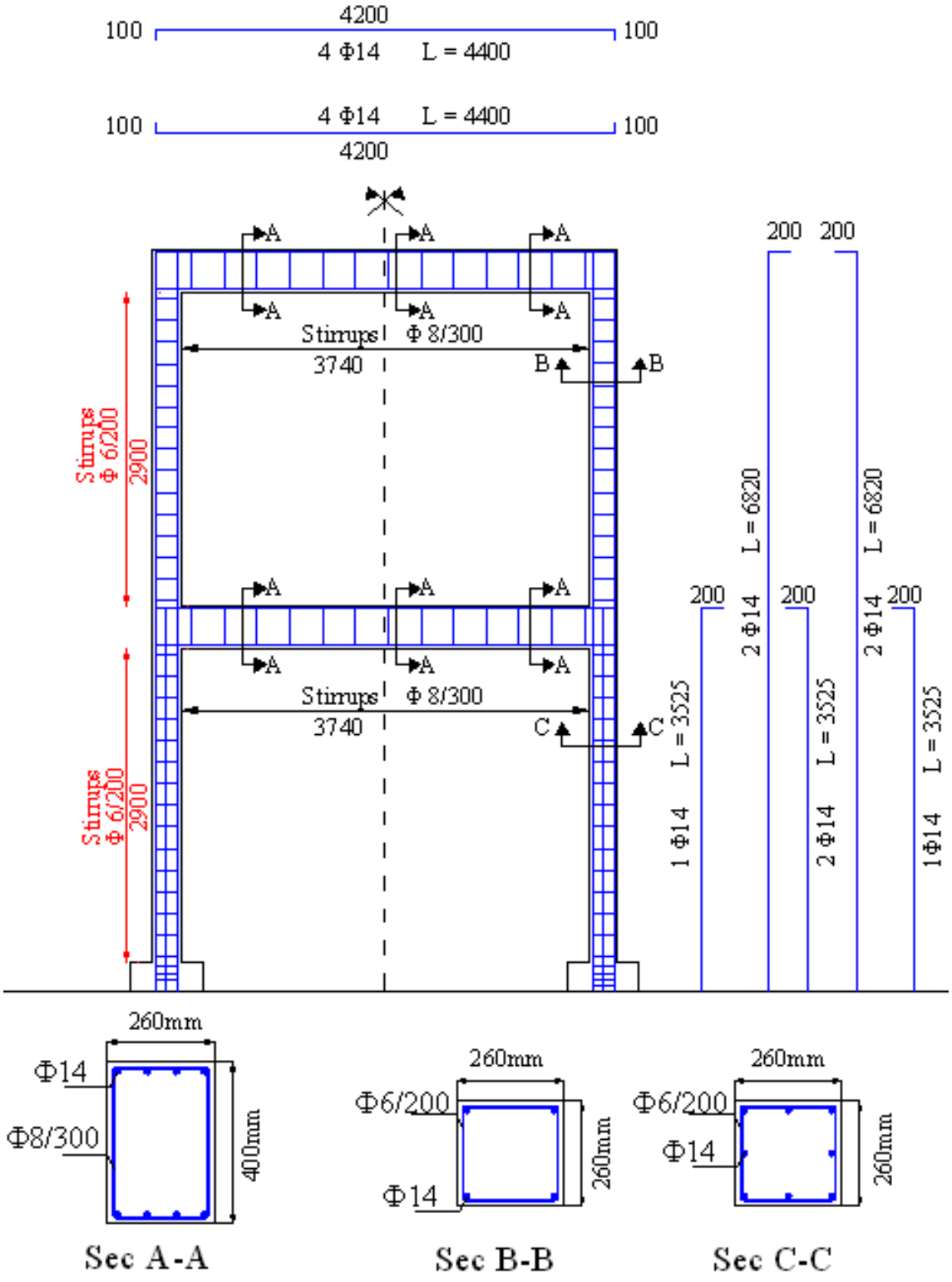

Figure 4-2: Dimensions and reinforcement details of test 1 (Chaudat et al., 2005)

4.2.1.3 Loading of the RC frame

The frame was subjected to its own gravity loads, in addition to a series of excitations with increasing Peak Ground Acceleration, PGA, levels from 0.05 g to 0.4 g. The self-weight of the frame was about 20 tonnes. Live and dead loading conditions were represented by adding two steel plates to each slab. The additional mass, accounting for the live and dead loads, was about 18 ton. The unidirectional excitations used in these seismic tests were five artificially generated accelerograms, and compatible with the EC8 response spectrum for soil profile type C. The PGA of the five accelerograms applied was 0.05 g, 0.10 g, 0.20 g, 0.30 g and 0.40 g.

4.2.1.4 Experimental results

Table 4-1 lists the natural frequencies of the first two modes of vibration of the frame for each test. The first natural frequency dropped from 1.9 HZ prior to the first test to 0.68 HZ after the fifth test (Chaudat et al., 2005).

No damage was observed during the first two seismic tests, PGA= 0.05 g and 0.10 g, in which the response of the frame was almost linear. Damage was initially observed during the third seismic test at PGA= 0.20 g; diagonal cracks appeared in the first storey joints and horizontal cracks under the joints of the second storey, as shown in Figure 4-3. This could be due to the bond-slip of the column reinforcement before yielding (Garcia et al., 2010). More horizontal cracks were detected above the first storey joints in addition to new cracks in all the columns and at the base of column 4 during the 0.3 g seismic test. During 0.4 g test, some cracks were observed around the middle of the column 1 and detachments of concrete were detected at the base of column 4, as shown in Figure 4-4. It is clear that most damage was located in the joints and in the columns.

Table 4-1: Natural frequencies of the frame (Chaudat et al., 2005)

Tests	**The first natural frequency (HZ)**	**The second natural frequency (HZ)**
Before tests	1.9	5.6
After the test at level 0.05 g	1.66	4.88
After the test at level 0.10 g	1.36	4.3
After the test at level 0.20 g	1.07	3.6
After the test at level 0.30 g	0.88	2.64
After the test at level 0.40 g	0.68	2.54

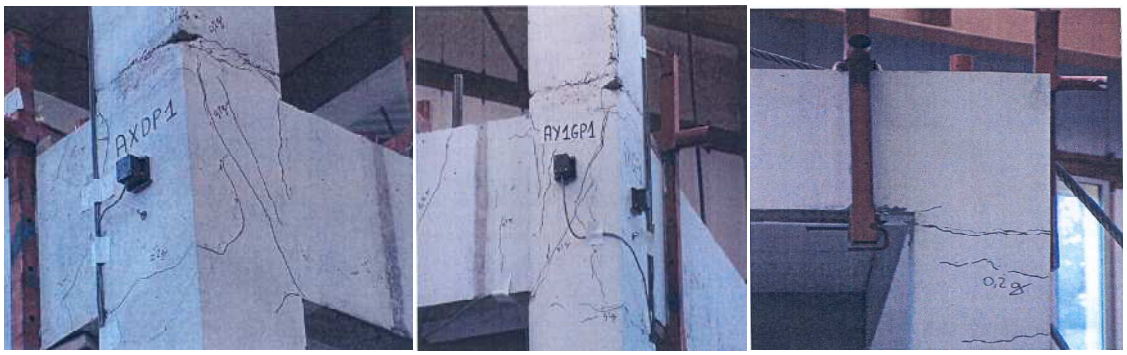

Figure 4-3: Crack following 0.2 g seismic test; column 2 on the first level, column 3 on the first level and column 1 on the second level (Chaudat et al., 2005)

Column 1 Base of column 4

Figure 4-4: Crack following 0.4 g seismic test (Chaudat et al., 2005)

4.2.2 AEM model of test 1

A three-dimensional model of the bare frame structure has been created using the Extreme Loading for Structure, ELS, software, based on the applied element method adopting a discrete cracking approach (Applied Science International (LLC), 2010). By using the AEM, structural behaviour can be automatically traced throughout all the response stages, including elastic, crack initiation, reinforcement yielding, element separation and collision as well as the effect of debris loading on the structural system (Tagel-Din and Meguro, 1999a). Appropriate values for the material parameters, as observed during the test, have been used in the AEM model to achieve comparisons between the experimental and analytical results. The results obtained from the AEM analyses have been compared with the experimental data in terms of the first two periods of vibration, maximum inter-storey drift ratio and storey displacement records. These comparisons aim to demonstrate the reliability and accuracy of the AEM model for simulating the seismic response of frame structures, until total collapse.

In AEM, the structure is discretised into a series of relatively small rigid elements connected together along their faces by a set of nonlinear normal and shear springs, representing the material behaviour and located at contact points (Meguro and Tagel-Din, 2000). Each of the columns and beams in the structure was divided into $10 \times 5 \times 5$ and $10 \times 3 \times 5$ equal elements, respectively. The mesh size used in modelling the slabs was $10 \times 10 \times 1$ equal elements. The contribution of the slabs to the capacity of the structure to resist collapse under seismic loadings was considered. The elements were connected together using sets of three contact springs (normal and two shear springs), to represent the stresses and deformations of the elements based on the characteristics of the concrete and reinforcement materials. The structure was modelled using 3400 three-dimensional cubical sub-elements. A mesh sensitivity check of the AEM model was carried out. A new AEM model was created with columns and beams divided into $20 \times 10 \times 10$ and $20 \times 6 \times 10$ equal elements, respectively. The analytical results for the storey displacement of both models for the first two loading stages were compared. It was found that the mesh size adopted yields accurate results. 10 sets of contact springs were assigned to each two adjacent element interfaces resulting in 239824 springs in the entire model. All the reinforcement details, longitudinal and transverse reinforcement of the beams and columns, were explicitly modelled ,as well as the slab reinforcement, as shown in Figure 4-5, in which the concrete in two columns and

beams, as well as the concrete in the first storey slab were removed to show the reinforcement details of these members. Steel springs representing the reinforcement bars were automatically assigned to the interfaces of the elements at the exact location of the steel bars.

The material properties used in the AEM model are shown in Table 4-2. The concrete was represented by matrix springs and the reinforcement by bar springs. In the AEM, fully nonlinear path-dependent constitutive models are adopted for concrete. The Maekawa compression model, an elasto-plastic and a fracture model, were utilised for concrete in compression (Okamura and Maekawa, 1991). While for concrete in tension, a linear stress–strain relationship was used, until the occurrence of cracking, when the stress fell to zero. For the reinforcing bar, the model presented by (Ristic et al., 1986) was adopted.

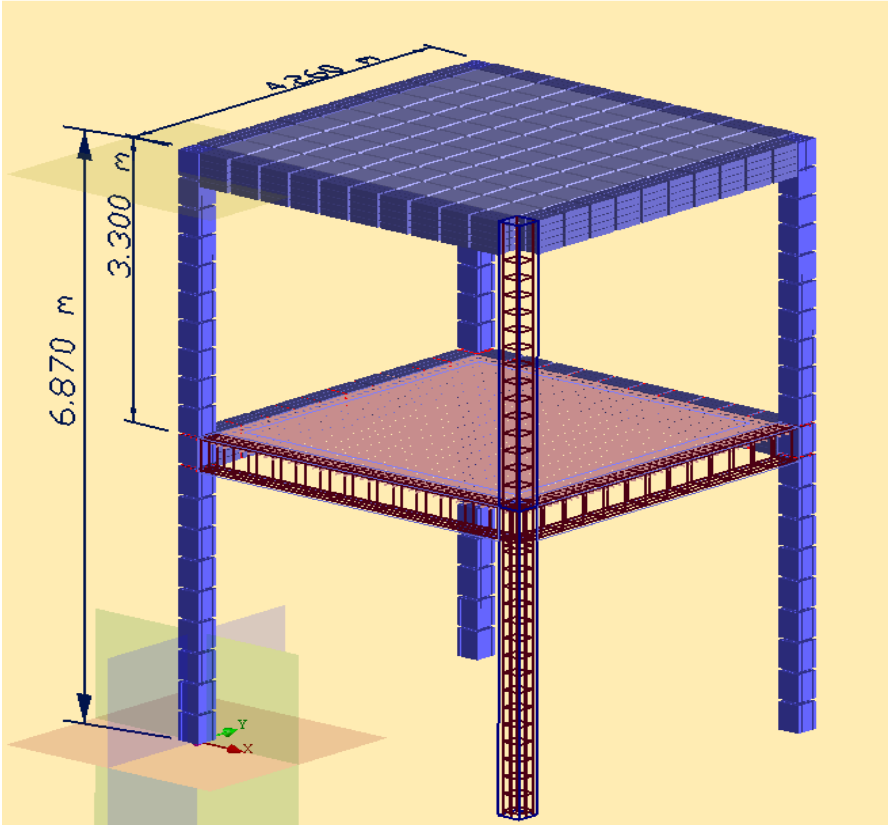

Figure 4-5: AEM model of test 1

Table 4-2: Material parameters used in the AEM model

Material properties	**Concrete**	**Steel (longitudinal-transverse)**
Young's modulus (MPa)	23500	200000
Shear modulus (MPa)	9038.46	76923
Tensile strength (MPa)	2.07	551-582
Compressive strength (MPa)	19.60	
Separation strain	0.1	0.2
Friction coefficient	0.8	0.8
Ultimate strain		0.1
Ultimate strength /Tensile yield stress		1.19-1.106
Post yield stiffness ratio		0.01

The concrete density for the beams and columns was assumed as equal to $25\ \mathrm{kN/m^3}$. The slab weight was increased to account for dead and live loads. Distributed masses and weights have been used. Hence, the density of the slab concrete were taken as $85.4\ \mathrm{kN/m^3}$ instead of $25\ \mathrm{kN/m^3}$, in order to account for the additional weight of the steel plates.

The analysis was performed in a similar manner to the seismic test. The nonlinear response of the structure is very complicated due to damage accumulation, which is considered automatically in the AEM model. The first loading stage was the self-weight stage, in order to account for the effect of the gravity loads, in particular, the initial deformations and the concrete cracking. The earthquake excitations were applied in the same sequence as the seismic tests from a PGA level of 0.05 g in the second stage to a PGA level of 0.4 g in the sixth stage. The duration of each input motion was increased from 40.98 sec to 55 sec with a zero acceleration amplitude loading, as shown in Figure 4-6, in order to allow the structural response to dampen. The acceleration signal measured at the middle of the shaking table was used as the input ground motion in the analytical model instead of the shaking table input signal. The frequency content of these excitations is almost the same, but their amplitudes differ. Large displacement effects were considered in the analyses. A loading time step of 0.01 sec was used for the first three stages, and the time step was then decreased to 0.005 for the remaining stages, in which the structural behaviour became highly nonlinear. The recorded CPU time of the total nonlinear dynamic analysis of these excitations with a 275 sec duration is about 50 hours, which is a relatively short time with regard to the

structure dimensions, mesh size, loading scenario, loading time step and highly nonlinear response of the structure. An eigenvalue analysis was carried out to investigate the structure natural periods of vibration, which change according to the extent of the structural damage.

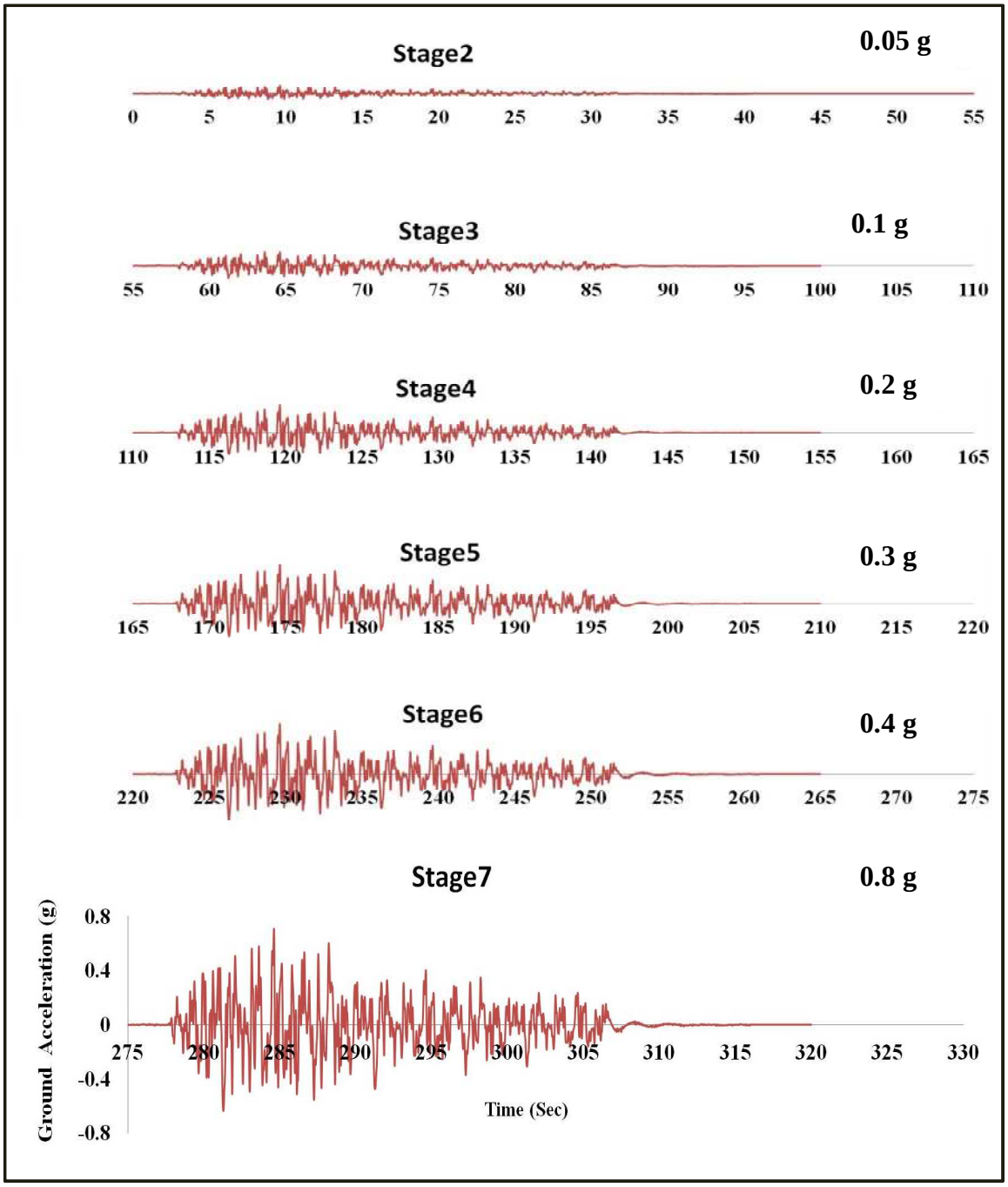

Figure 4-6: Input ground motions used in the AEM models

As far as damping is concerned, the analyses were conducted three times with different damping parameters according to the level of nonlinearity observed during the seismic tests. Since no damage was observed during the first two seismic tests for PGA levels of 0.05 and 0.1 g, the structural behaviour of the frame was almost linear in these low-intensity ground motion cases and so the effect of the internal damping was not included. Damping is therefore modelled as external damping, which is mass proportional and depends on the first mode of vibration. The elastic damping ratio for the first mode of vibration was assumed to be 0.01 for a PGA level of 0.2 g and 0.02 for PGA levels smaller than 0.2 g. In contrast, the effects of internal damping, as previously explained in Section 3.2.4, are dominant in the nonlinear stage of structural behaviour. Therefore, the analysis was repeated using a zero value for the external damping in the case of the seismic tests, with PGA levels larger than 0.2 g. The inherent damping, due to the material nonlinearities was sufficient in the nonlinear analysis and resulted in reasonable energy dissipation, as mentioned in the ELS technical manual (Applied Science International (LLC), 2010).

4.2.3 Comparison of AEM and experimental results

4.2.3.1 Storey-displacements

Figure 4-7 and Figure 4-8 compare the analytical and experimental displacement records for the first and second storeys at the PGA levels of 0.05 g and 0.1 g, respectively. As can be seen, there is good agreement between the experimental and analytical results throughout almost the entire time duration of this ground motion. This indicates that the AEM model can capture the linear behaviour of the structure with high accuracy.

Regarding Figure 4-8, small differences in responses are observed from 75 to 80 sec. However, it is apparent that the values for the maximum displacements, as obtained from both the test and the analytical model are almost the same. The predicted peak displacement of the second storey is only about 4% larger than the measured value. While the calculated maximum displacement of the first floor is about 10% larger than the corresponding measured ones.

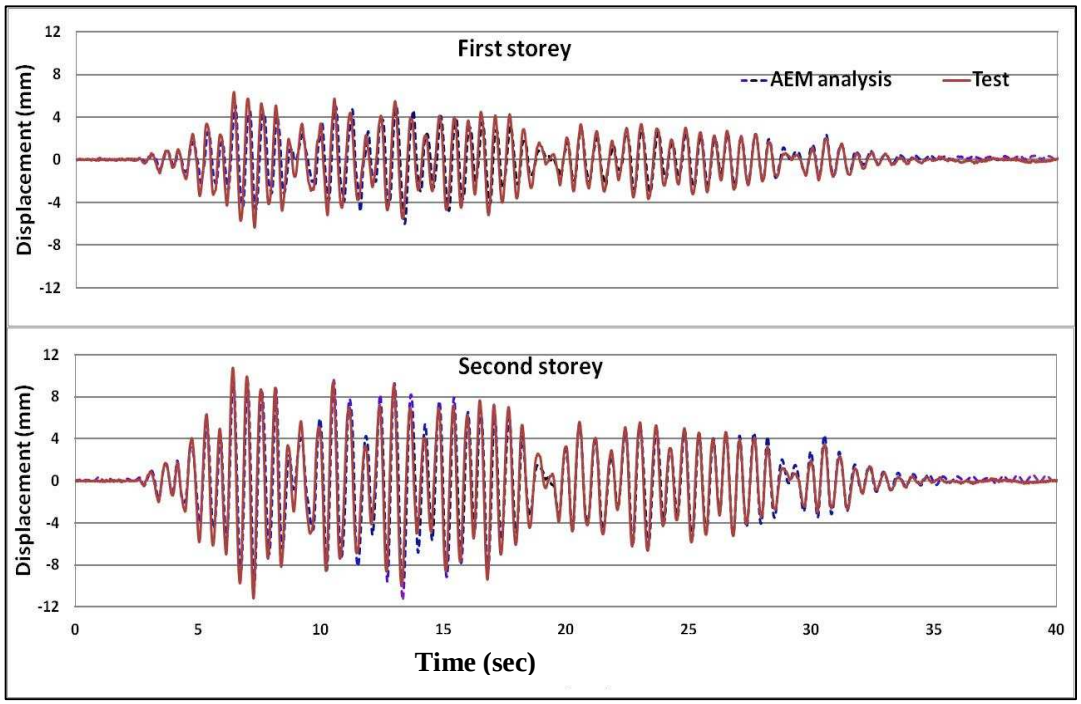

Figure 4-7: Displacement response for 1st and 2nd storeys at a PGA level of 0.05 g

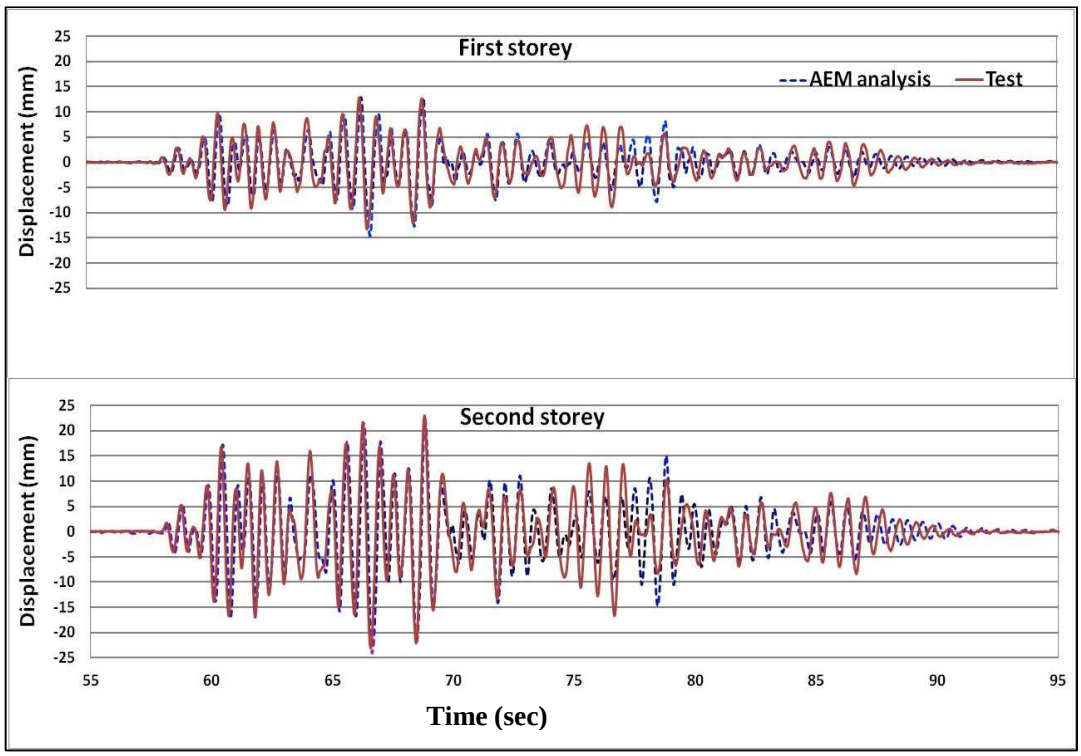

Figure 4-8: Displacement response for 1st and 2nd storeys at a PGA level of 0.1 g

Figure 4-9 shows that there are small differences in the phase between the experimental and analytical results after reaching the peak displacement at PGA levels of 0.2 g. This may be because of the additional measured deformations, due to bar slippage prior to the yielding of reinforcement (Garcia et al., 2010), which cannot be accurately simulated in the AEM model. This is because the rebar and the surrounding concrete are modelled using the same element, but with different springs. Thus, they have the same degrees of freedom (Tagel-Din and Meguro, 1999a). In addition, changes in the natural period of the frame due to the reduction in its stiffness could contribute to the phase lag. The structure stiffness may be reduced due to joint damage occurring during the test, which could not be modelled accurately in the AEM model. The analytical model is still capable of predicting the peak displacement with an error of less than 20%.

The experimental and analytical response histories, at PGA levels 0.3 g and 0.4 g are plotted in Figure 4-10 and Figure 4-11, respectively. In Figure 4-10, the experimental displacement record of the second storey is only presented up to 248.0 sec, due to failure of the displacement transducer at this time (Garcia et al., 2010). Thus, a relatively small test detail of the time history response of the frame has been lost.

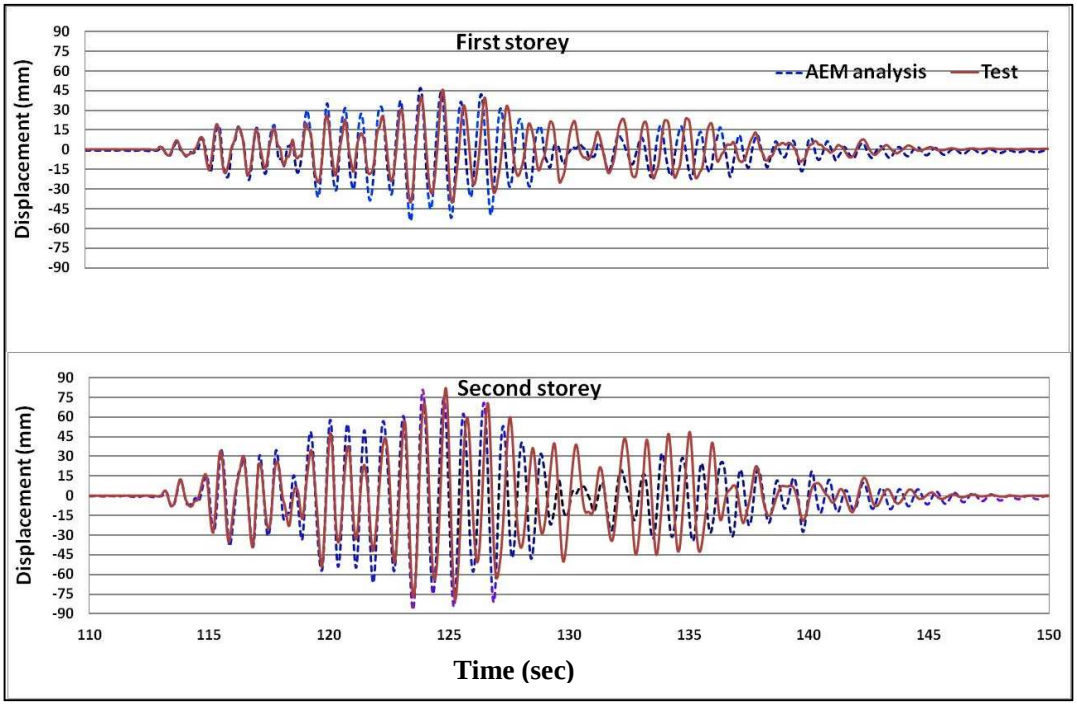

Figure 4-9: Displacement response for 1st and 2nd storeys at a PGA level of 0.2 g

Although the cumulative error increases following each stage, the overall response of the structure can still be estimated with a reliable accuracy. As can be seen in Figure 4-10 and 4-11, the top storey displacements are almost the same, but the analytical displacements overestimate the corresponding measured displacements at the first storey. This could be attributable to the relatively simple modelling of the joint shear cracking in the AEM and its effects on the global response. Joint damage in existing RC structures leads to mixed local and global failures, rather than a pure global failure mechanism. It was observed during the seismic test that the majority of the damage was concentrated in the beam-column joints, due to the lack of transverse reinforcement in the joint region. The interaction of the shear damage in these joints, and the flexural hinging of the adjacent columns may affect the damage mechanism and delay to some extent the formation of a single soft-storey mechanism (Calvi et al., 2002a, Calvi et al., 2002b). Based on experimental investigation and analytical studies using both models with and without modelling the joint behaviour, Calvi et al., found that the deformation demand in reinforced concrete existing structures, which concentrates in the joint regions due to the occurrence of joint shear cracking, often leads to a considerable change in the rotation demand place on the surrounding structural members.

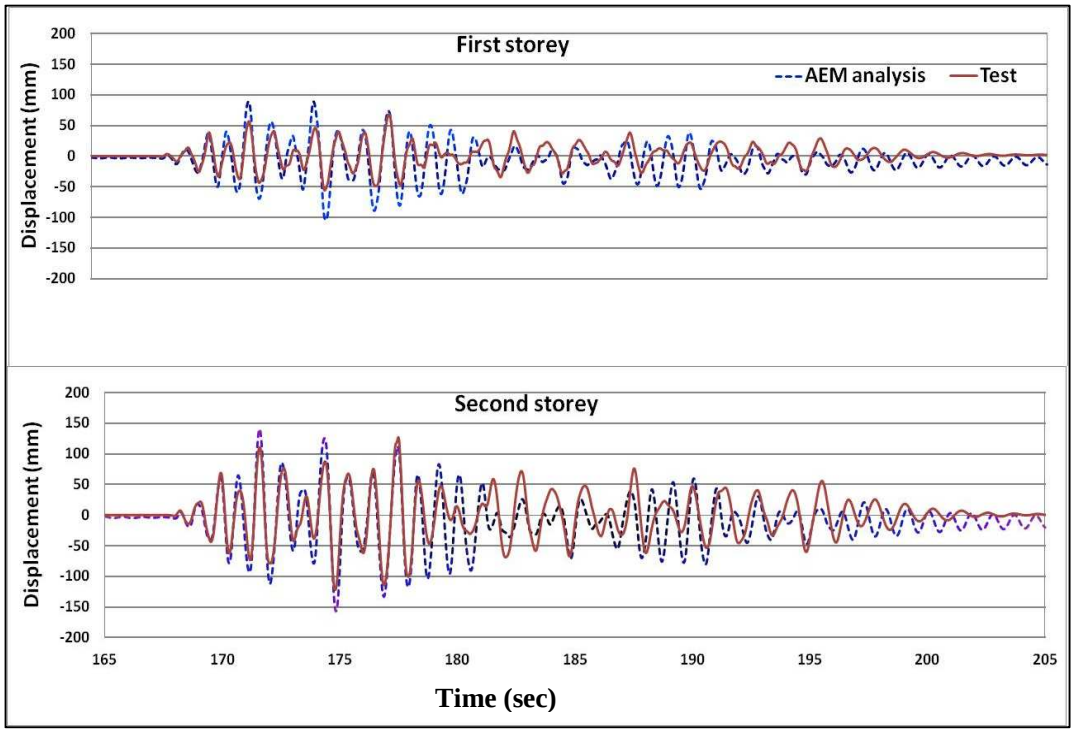

Figure 4-10: Displacement response for 1st and 2nd storeys at a PGA level of 0.3 g

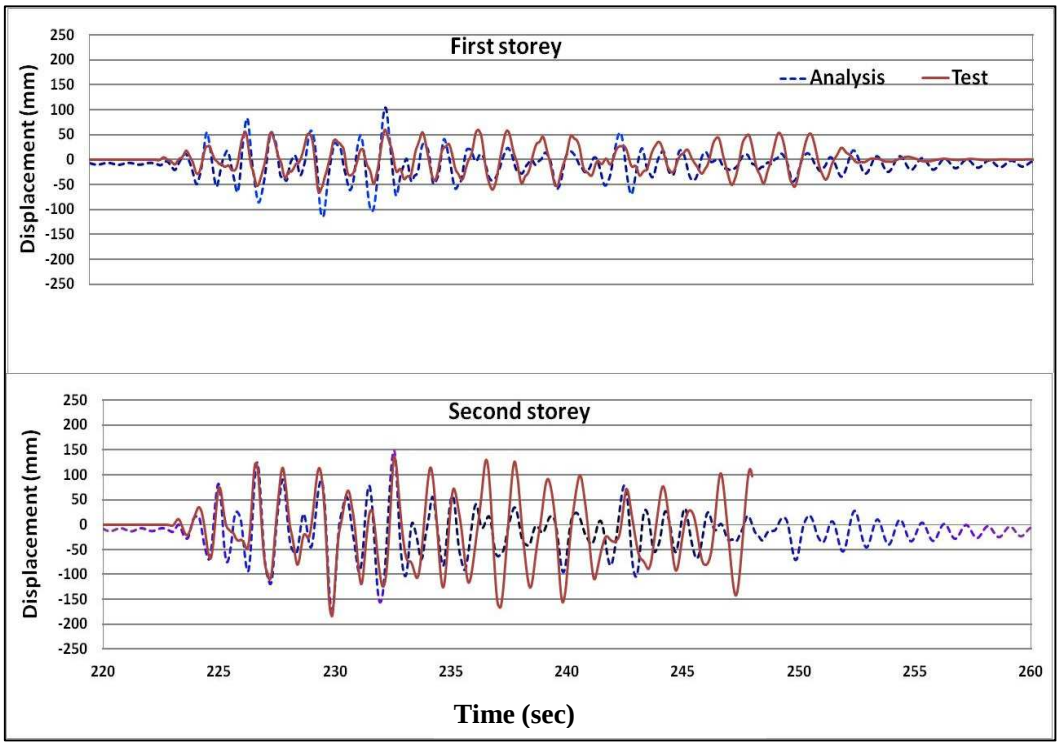

Figure 4-11: Displacement response for 1st and 2nd storeys at a PGA level of 0.4 g

Thus, the occurrence of first soft-storey mechanism may be postponed due to the redistribution of the inter-storey drift demand between the two storeys adjacent to the damaged joints (Calvi et al., 2002a, Calvi et al., 2002b).

It should be mentioned that the procedure for modelling joint damage due to shear failure are very complex. A simple technique for modelling cracks was adopted in the AEM. The internal failure of an element is representing by the failure of the surrounding springs (Tagel-Din and Meguro, 2000c). Also, cracks in the joints cannot be simulated with accuracy as the fracture plane and element edges are not parallel (Tagel-Din and Meguro, 2000c).

4.2.3.2 Inter-storey drift ratios

A comparison between the maximum experimental and the corresponding analytical inter-storey drift ratios of the frame for the different PGA levels is shown in Table 4-3. It was found that the inter-storey drift ratios measured for both storeys are almost the same for low and medium excitation levels. The results therefore, indicate that the analytical model generally tends to overestimate the inter-storey drift of the first storey at high excitation

levels, 0.3 and 0.4 g, while the inter-storey drift at the second storey is underestimated. The analytical inter-storey drift at the first storey is slightly bigger than that at the second storey. However, on the contrary, the measured inter-storey drift ratios for the second storey increased rapidly during the 0.4 g excitation due to the shear failure of the beam-column joints on the top floor of the frame (Chaudat et al., 2005). These differences could be attributed to the approximations in the modelling of the joint shear failure in the AEM, as discussed earlier. It was confirmed that joint shear damage in RC existing structures can reduce inter-storey drift demand with relatively minimal alterations to the demand for global displacement (Calvi et al., 2002a). Modelling this type of problem, which involves failure in joints, is complex. AEM models cannot accurately predict the effect of joint damage on the seismic behaviour of structures. In addition, the previous response histories of the frame under a number of loading stages, and the effects of multiple loading stages on cracking propagation can make the structure's response more complicated.

Spalling of the concrete cover, as observed during 0.4 g test, cannot be modelled, due to the limitations of this software (Tagel-Din and Meguro, 1999a). This suggests a need for further research to consider the additional effects of shear transfer and shear softening, as well as the spalling of the concrete cover (Tagel-Din and Meguro, 1999a). It is interesting to note that despite all of these aforementioned limitations, a reasonable estimate for the seismic response of the studied structure was obtained using the AEM model.

Table 4-3: Comparisons between the maximum experimental and the corresponding analytical inter-storey drift ratios

PGA level	**The 1st storey**			**The 2nd storey**		
	Experiment	**Analyses**	**Error%**	**Experiment**	**Analyses**	**Error%**
0.05 g	0.0019	0.0019	0	0.0015	0.0016	7
0.1 g	0.0040	0.0045	13	0.0032	0.0033	3
0.2 g	0.0138	0.0160	16	0.0118	0.0106	-10
0.3 g	0.0208	0.0277	33	0.0211	0.0163	-23
0.4 g	0.0203	0.0283	39	0.0390	0.0200	-49

4.2.3.3 The natural frequency

The variation in the dynamic characteristics of the structure, as measured by the fundamental period of vibration, is investigated using AEM models. It has been proven, by comparing experimental and analytical results, that the AEM can accurately trace the changes in the natural frequency of reinforced concrete structures, due to the spread of cracking and damage (Uehan and Meguro, 2004b).

The fundamental period of vibration of the studied frame is shown in Table 4-4. The initial first natural period obtained from the analytical model is 0.48 sec, while the corresponding experimentally measured period is about 0.53 sec. This discrepancy could be attributed to some shrinkage cracks, which may have developed in the specimen prior to the seismic tests. It is clear that the analytical and measured structural periods of this frame are similar at the PGA level of 0.05 g.

In general, the natural periods calculated are slightly shorter than the measured ones. This could be due to the reduction in the structure stiffness following the occurrence of diagonal cracking in the joint region, which cannot be accurately modelled in the AEM. Figure 4-12 and Figure 4-13 illustrate the changes in the smooth simulated fundamental vibration period at four PGA levels, namely 0.05, 0.1, 0.3 and 0.4 g. The moving mean average is used for smoothing these plots with a window size of 0.2 (MATLAB, 2008).

Table 4-4: Fundamental period of the frame

PGA level	**1st natural period**		
	Analyses		**Experiment**
	At the end of the analysis	**Maximum value during the loading stage**	**At the end of the test**
own weight and dead load	0.48		0.53
0.05 g	0.58	0.60	0.60
0.1 g	0.615	0.70	0.73
0.2 g	0.75	0.92	0.93
0.3 g	0.87	1.22	1.14
0.4 g	0.9	1.29	1.47

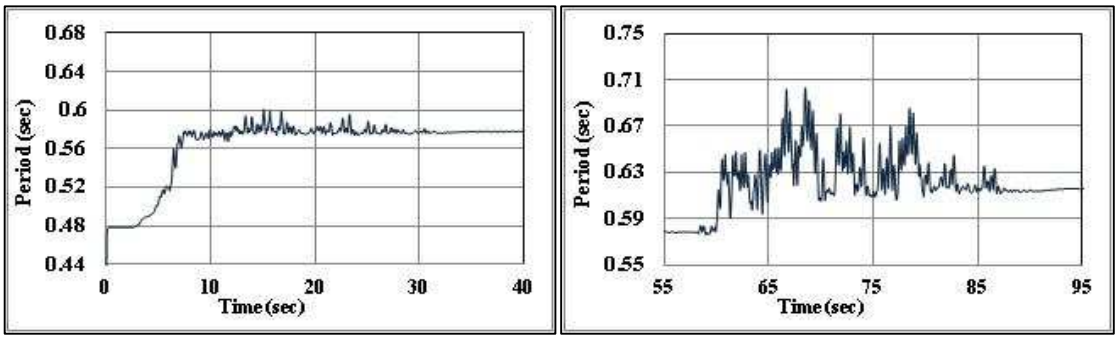

Figure 4-12: Simulated fundamental vibration period at PGA levels of 0.05 and 0.1 g

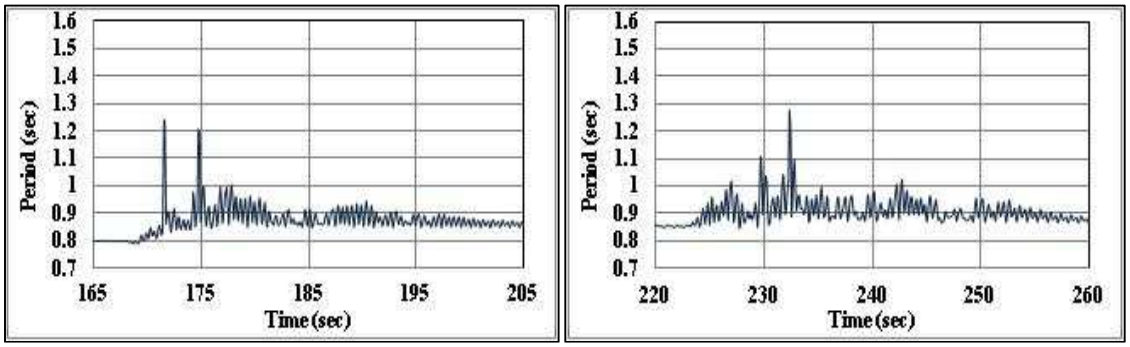

Figure 4-13: Simulated fundamental vibration period at PGA levels of 0.3 and 0.4 g

As can be seen, the fundamental period starts to increase in response to the spread of damage and crack propagation. A significant increase in the vibration periods of the frame has been noted during intervals of high seismic amplitude, as a result of the higher deformation experienced by the structural system; while the stability of the first natural period was observed in the time interval involving low-amplitude shaking. Changing the direction of seismic loading, as well as its value, considerably affects the global stiffness of the structure. In general, two different groups of cracks often exist simultaneously during seismic loading, when cracks in the first group open, cracks in the other tend to close (Meguro and Tagel-Din, 1999a). The width of the crack increases as the loading intensity rises, leading to a reduction in structural stiffness (Tagel-Din and Meguro, 1999a). Consequently, the stiffness of a damaged element, such as a corner column, can be immediately increased with the reversal of the load direction, and hence a displacement reversal. Changes in the global stiffness matrix are associated with crack closure and opening throughout the entire structure. Loading, unloading and reloading stiffness depends on the

crack closure mechanism and the previous deformation history (Tagel-Din and Meguro, 1999a).

It can be concluded from comparing the results of the shaking table test with increasing PGA levels with the AEM models that the analytical models adopted can provide a reasonable estimate of the displacement demands and the natural frequency under different seismic excitations, as confirmed by other studies (Tagel-Din and Meguro, 2000c, Uehan and Meguro, 2004b).

4.2.4 Collapse analysis under high intensity ground motion

In order to investigate the collapse behaviour of the frame, the analysis has been extended. The damaged frame has been next subjected to an additional excitation of 0.8 g as shown in Figure 4-6.

Large displacement effects, element separation and contact, as well as rigid body motion have been considered in the AEM models. The separation of elements has been assumed to occur when the strain of the matrix springs connecting the elements reaches a value of 0.1. The detection of a contact between elements, as well as collision effects are automatically included. The failure criteria parameters related to concrete crushing and ultimate failure of the reinforcement bars are listed in Table 4-2. When elements collide, energy is transferred between them through contact springs, which are generated automatically at the contact location. Normal and two shear springs are generated at each contact point. The recommended value of the contact spring parameters, which depends on the type of the selected materials, are adopted since no actual values are available (Applied Science International (LLC), 2010). Normal and shear contact stiffness factors adopted are 10^{-2} and 10^{-3}, respectively. The normal contact stiffness is higher than the shear contact stiffness. This is because the normal force, which is transmitted during contact, is always higher than the corresponding shear forces (Applied Science International (LLC), 2010). The adopted value of contact spring unloading stiffness factor is set as equal to 10, which means that 90% of the impact energy is dissipated during contact (Applied Science International (LLC), 2010). A value of 0.8 is used as the friction coefficient. Energy resulting from element impact is dissipated during contact throughout due to the internal friction. In addition, the unloading stiffness factor, which represents the ratio between loading and

unloading stiffness of a contact spring, also controls the dissipated energy during contact, as previously explained in Section 3.6.3.

Figure 4-14 provides an insight into the progression of damage and the collapse mechanism. The structure starts to free-fall at 288 sec. The entire structural collapse takes place at about 290 sec, while the first element separation occurs at 278 sec in the column-beam joint of the first storey. It should be noted that the collapse duration is very small because the structure has been severely damaged from the previously applied seismic excitations and it collapses in a side-sway mechanism, a soft-storey mechanism, which takes place during the interval of maximum amplitude of shaking. In addition, the time required for the fracture process is neglected in the AEM, as the residual forces in the failed springs prior to separation are redistributed in the next time increment (Tagel-Din and Meguro, 1999a, Tagel-Din and Meguro, 2000c).

As can be seen from Figure 4-14, a first-storey collapse mode occurs. Although the structure fails with a first-storey mechanism, plastic hinges also form at the top and bottom of the columns of the second storey and some of the element separation occurs in the joint region of the first storey, as illustrated in Figure 4-15. Following the collapse of the columns of the first storey, the top part of the structure moves as a rigid body, colliding with the ground. The impact forces, resulting from the collision between the first storey and the ground, cause considerable damage to the members of the second storey leading to total collapse. The horizontal and vertical displacements of both storeys during the collapse process as well as the fundamental period of vibration are shown in Figure 4-16.

Regarding the seismic test, significant damage was anticipated to occur in the column-beam joints, in addition to flexural failure in most columns, while the transverse reinforcement in the columns and beams was sufficient to avoid shear failure. The analytical results were similar to some extent to the experimental damage pattern, in which the beams experienced slight damage and the plastic hinges, element separation, formed in the columns rather than the beams. The slab system affects the frame's capacity to resist collapse by contributing to the strength and stiffness of the beams. However, the columns of the first storey suffered severe damage and failed before the column capacity at the second storey was completely utilised, contrary to the experimental results.

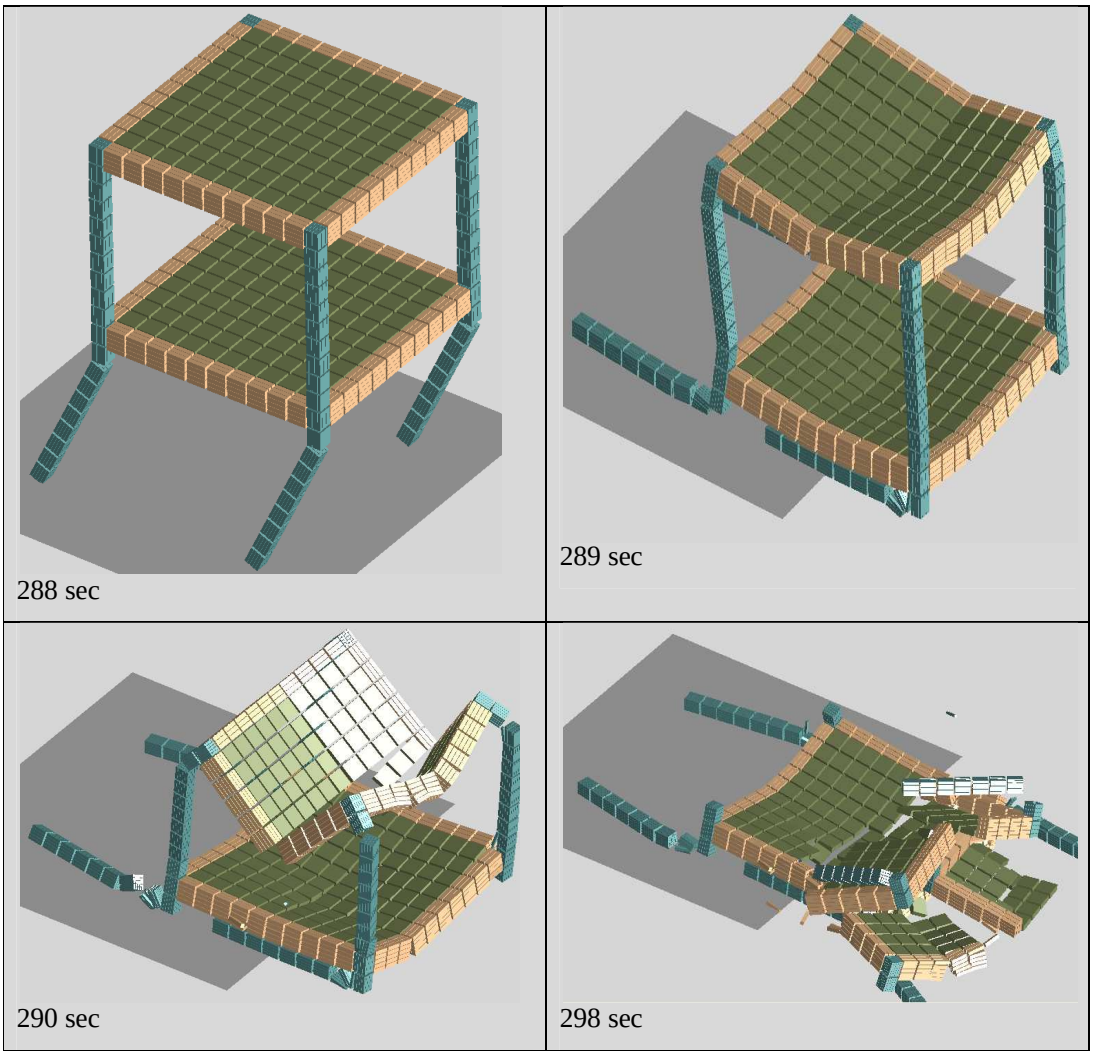

Figure 4-14: Simulation of collapse process

Based on these comparisons, it was found that the seismic structural response can be followed reliably from initial cracking until total collapse using the AEM. One advantage of the analysis is that it does not require any previous knowledge of the failure process. The progression of failure cannot be predicted without a detailed analysis involving element removal, redistribution of gravity and seismic loading and impact forces, as well as the rigid body motion of the falling element. The AEM can reliably account for these important aspects of the collapse phenomenon. It is interesting to mention that the failure mechanism obtained is consistent, to some extent, with the experimentally observed damage.

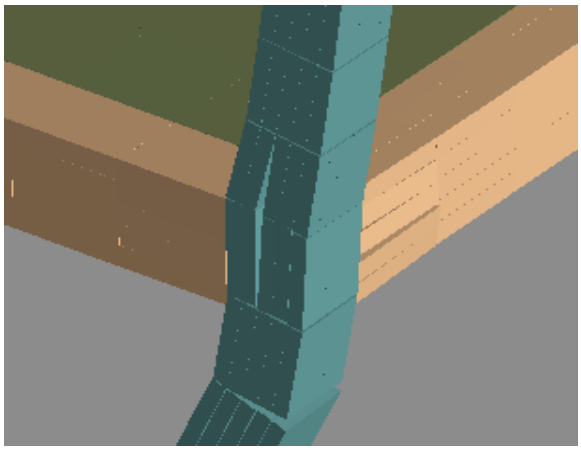

Figure 4-15: Damage in the column-beam joint at the first storey, scaled by 5

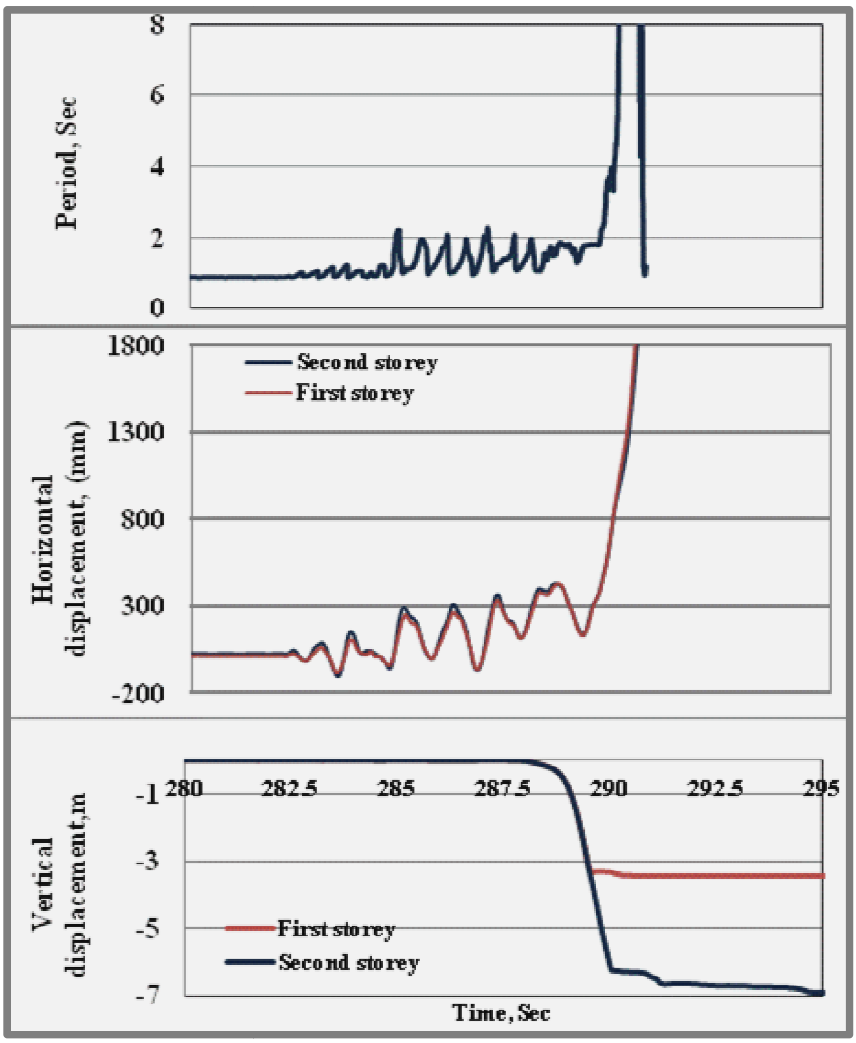

Figure 4-16: Displacement histories and the fundamental period of vibration

4.2.5 Failure criteria

As previously described, adjacent elements in AEM can be connected by sets of three springs distributed on the element faces. There are two groups of springs, matrix springs, representing concrete and reinforcement springs representing steel bars. Separation between two connected elements is assumed to occur when all the springs connecting the neighbouring faces of both elements are removed. If elements are in contact following separation, they behave as rigid bodies and a different type of springs, collision springs are generated between them. Collision springs, comprised of one normal and two shear springs, can also be removed leading to element separation.

Matrix and reinforcement bar springs connecting two adjacent faces can be totally ruptured causing element separation when the value of the average strain of all the matrix springs connected to these two faces reaches a predefined value, known as the separation strain of concrete. The average strain between connected faces is determined as the mean of the absolute strain values of all normal springs. Reinforcement bar springs in compression or tension are cut when the matrix springs rupture. However, only reinforcement bar springs in tension are cut if their normal stress reaches the ultimate specified stress (Applied Science International (LLC), 2010). It has been recommended, in the theory manual for ELS (Applied Science International (LLC), 2010), to use a value between 0.1 and 0.2 for separation strain of the concrete. The value adopted should be higher than the ultimate tensile strain of the steel, in order to avoid unreasonable failure, because this value is used as the failure criterion for simultaneously removing springs representing both materials.

The sensitivity of the seismic collapse process to the failure criterion, the separation strain of concrete, is investigated with a full correlation assumption, which means that the same failure criteria are used for all elements in the structure. The same value for the separation strain is adopted for all concrete elements. The aim of this parametric study is to explore the extent to which the collapse process will be affected by the chosen value of the concrete separation strain, rather than studying the effect of uncertainty in an element's removal criteria on the collapse progression, which is highlighted by a study conducted by Talaat and Mosalam. Changing the failure criteria of structural components within a

structural system according to different ratios has a considerable effect on failure modes (Talaat and Mosalam, 2008).

Three different values for the concrete separation strain, 0.1, 0.15 and 0.2, are adopted. The collapse mechanism and time at incipient collapse for the aforementioned frame structure using these three different separation strain values were investigated. The amplitude of the seismic shaking at the time of separation onset was found to significantly affect the progression of collapse. The effect of the separation strain on the collapse process was thus investigated employing four different PGA levels. By selecting four PGA levels and three values for separation strain, twelve cases were put forward for examination.

The aforementioned analytical model is adopted with some modifications, related to the loading scenario and the damping ratio. Two loading stages are considered here, namely the gravity loading, the self-weight stage, and earthquake loading. The shape of the seismic loads considered is similar to those used in the test but with a different amplitude. The GPA levels for the four considered seismic inputs are 0.65 g, 0.7 g, 0.75 g and 0.8 g. An external damping value of zero is utilised. This is because the dynamic response of the structure under high seismic excitation is highly nonlinear, resulting in sufficient damping forces due to internal damping.

4.2.5.1 Results and discussion

Structure collapse occurs at all PGA levels except for 0.65 g. Figure 4-17 shows the time history of the mean horizontal displacements of the first storey in non-collapse cases. Figure 4-18 illustrates the time history of the mean vertical and mean horizontal displacements of the first and second storeys in the collapse cases. The time history of mean displacement of all elements at the top of each column is almost the same; this means that all the first-storey columns collapse simultaneously in a side-sway collapse mode.

In all cases, the structure behaviour is the same prior to reaching the collapse criteria for the first element. Following the onset of element separation, the redistribution of vertical and seismic loads and changes in the structure dynamic properties contributes to some differences in the seismic response of the frame in selected cases. For a PGA level of 0.65 g,

using a threshold value of 0.2 results in a higher storey displacement than in cases where threshold values of 0.1 and 0.15 are utilised.

In all the collapse cases, a similar collapse mode is obtained, but the time at the onset of collapse differs. The effect of strain separation on the collapse process is not significant in some cases for the following reasons. Firstly, the sequences of failure for structural members are almost the same in all collapse cases, in which a first story collapse mode is developed. The damage spread and propagation throughout the frame is almost always the same in all cases. If the structure can collapse in more than one collapse mode, the effect of strain separation is expected to be more significant, as it strongly depends on the damage spread. Secondly, the same threshold value for element separation is used for all members in the structure, so the progression of damage during the collapse process is not considerably altered. The time at the onset of collapse is based on potential failure mode, the amplitude of the seismic excitation and the threshold values for the element separation criteria. The times at the beginning of the unrestrained free-fall of the structure and the times corresponding to collision with the ground can be seen in Figure 4-18.

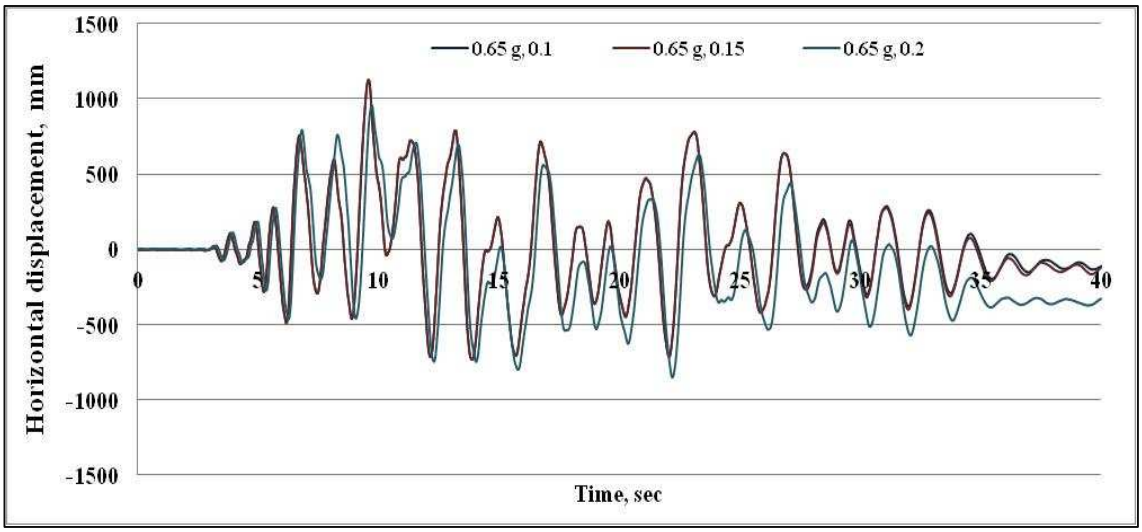

Figure 4-17: Time history of vertical displacements for the non-collapse cases

It should be noted that for the case of a PGA level of 0.8, the effect of separation strain on the time at incipient collapse was small. This could be attributed to the high shaking amplitude, which causes the values of the spring strains to exceed the value of 0.2 in all

cases. Hence, the failure criteria for all these cases was exceeded. The effect of the failure threshold value is more pronounced at a lower PGA level. Increasing the failure threshold value does not always delay the occurrence of collapse. For a PGA level of 0.75, the times at the onset of collapse for the separation strain values of 0.1, 0.15 and 0.2 were 15.5, 14 and 18.5 sec, respectively. This could be because collapse time is governed by more than one factor; such as both load direction and intensity.

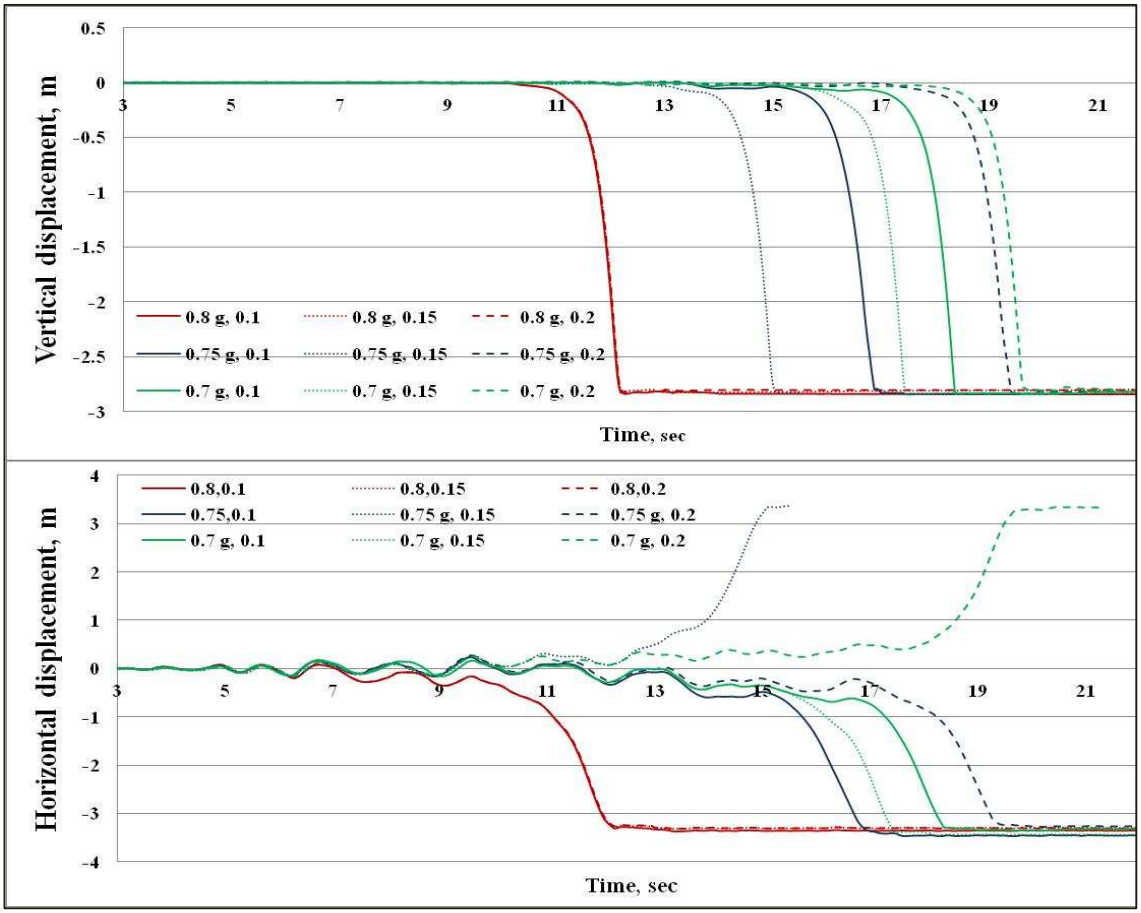

Figure 4-18: Vertical and horizontal displacement time history for the collapse cases

In all collapse cases, the structural system experienced global collapse, as a result of a soft-storey mechanism formed at the first storey. It is clear that several elements separate simultaneously at the top of all first storey columns leading to a side-sway collapse. Collision of the rest of the structure, which is slightly damaged, with the ground leads to complete failure of the structural system. Minor damage is observed in the beams prior to the occurrence of a collision between the first storey slab and the ground. Most of the debris is

spread outside the structure parallel to the seismic shaking direction. It has been noted that the top slab folds, and the resulting debris falls on the damaged slab of the first storey, which is located outside the footprint of the frame. Predicting the spread of debris is important because it can affect surrounding structures and lead to failure arising from impact forces.

Although the effect of strain separation on the collapse process is not considerable in this case study, which is governed by a single collapse mode, probabilistic assessment of seismic collapse considering uncertainly in failure criteria is required.

4.3 Description of shaking table tests 2 and 3

A number of tests on reduced-scale models of six-storey, three-bay reinforced concrete plane frames with different structural systems were performed at the National Technical University of Athens. The aim of these tests was to validate the EC8 seismic provisions with regard to multi-storey structures with different irregularities, and to understand the seismic behaviour of different structural configurations based on experimental comparisons. Only two seismically designed frames, namely a regular frame with a tall first storey, BF1, and an irregular frame with a discontinuous column at the first storey, DCF, were selected from these studies.

These two frames were designed according to EC8 seismic provisions for medium ductility class, PGA of 0.3 g and soil category A (Lu, 1996, Lu, 2002, Lu et al., 1999). The experimental results for the 1:5.5 scaled models were reported in (Lu, 1996, Lu, 2002, Lu et al., 1999). The details of the frames, as well as the shaking table models are described below.

4.3.1 Details of the designed frames, BF1 and DCF

4.3.1.1 Geometry and reinforcement details

The geometry and elevation of the selected frames was shown in Figure 4-19. The total height of the prototype frames is 20 m. The height of all storeys except the first storey is 3 m while the first storey height is 5 m. The cross-section dimensions and the corresponding reinforcement details for the BF1 and DCF frames are given in Table 4-5 and 4-6, respectively. The slab thickness is 140 mm with two layers of Ø15/250 mm. The slab

contribution is taken into account by considering the effective slab width as well as the slab reinforcements within this width.

Capacity design provisions were considered in designing the frame. Consequently, EC8 seismic requirements for medium ductility class were satisfied. Also, the transverse reinforcement satisfied the code requirement, so shear failure could be avoided, particularly in the joints where transverse reinforcement is applied in two directions (Zhang, 1995). The adopted behaviour factor values were 3.5 and 2.7 for BF1 and DCF, respectively. For more details about the design of the frames, reference is made to (Zhang, 1995).

Concrete class C20/25 was adopted in the design of the frames, while the steel grades used were S400 and S220 for flexural and transverse reinforcement, respectively. The vertical loads considered in addition to the structure self weight were 6 and 8 kN/m for dead and live loads, calculated from the three dimensional model of the structure, assuming a span length of 4 m in a perpendicular direction. The vertical loads consisted of the dead plus 30% of the live loads and were combined with seismic loads. The mass for each storey was calculated based on the aforementioned loads is listed in Table 4-7.

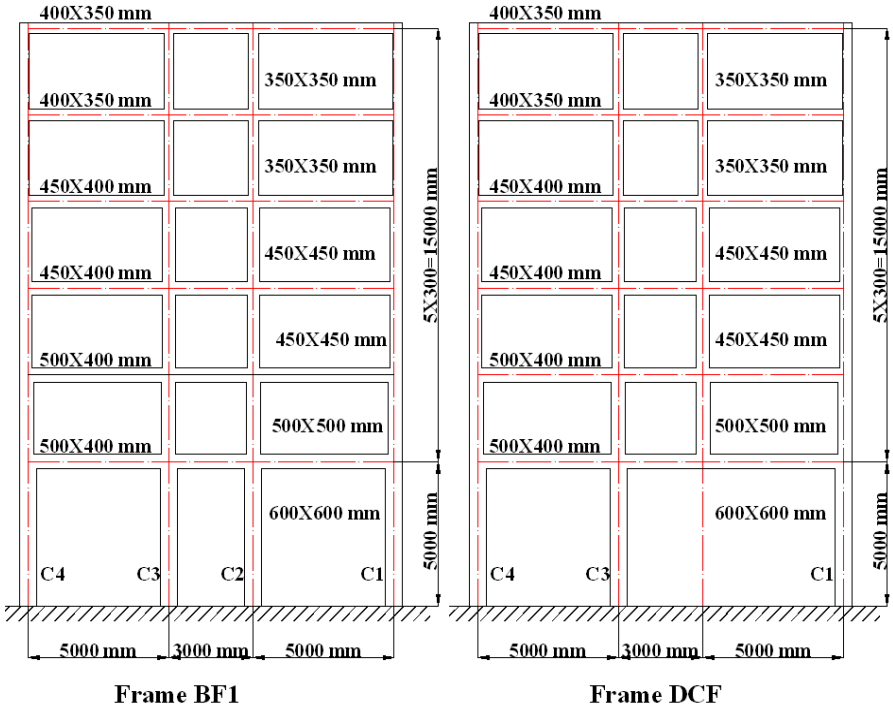

Figure 4-19: Geometry and dimensions of both selected frames (Lu et al., 1999)

Table 4-5: Reinforcement details for the BF1 frame (Zhang, 1995)

Model	Storey level	Column			Beam		
		Cross-section dimensions	**Longitudinal steel**	**Lateral steel**	**Cross-section dimensions**	**Longitudinal steel**	**Lateral steel**
BF1	6	350X350	4Ø32	2Ø15/110	350X400	2Ø32	2Ø15/100
	5	350X350	4Ø32	2Ø15/110	350X400	2Ø32	2Ø15/100
	4	450X450	4Ø32	2Ø15/110	400X450	2Ø32	2Ø15/110
	3	450X450	4Ø32	2Ø15/120	400X450	2Ø32	2Ø15/110
	2	500X500	4Ø32	2Ø15/100	400X500	2Ø32	2Ø15/125
	1 (top)	600X600	4Ø32	2Ø15/100			
	1 (bottom)	600X600	8Ø32	3Ø15/125	400X500	2Ø32	2Ø15/125

Table 4-6: Reinforcement details for the DCF frame (Zhang, 1995)

Model	Storey level	Column			Beam		
		Cross-section dimensions	**Longitudinal steel**	**Lateral steel**	**Cross-section dimensions**	**Longitudinal steel**	**Lateral steel**
DCF	6	350X350	4Ø32	2Ø15/110	350X400	2Ø32	2Ø15/100
	5	350X350	4Ø32	2Ø15/110	350X400	2Ø32	2Ø15/100
	4	450X450	4Ø32	2Ø15/110	400X450	2Ø32	2Ø15/110
	3	450X450	4Ø32	2Ø15/120	400X450	2Ø32	2Ø15/110
	2 (top)	500X500	4Ø32	2Ø15/100			
	2 (bottom)	500X500	4Ø32 (c1,3,4) 12Ø32 (c2)	2Ø15/100 3Ø15/100	400X500	2Ø32-3Ø32	2Ø15/125
	1 (top)	600X600	4Ø32	2Ø15/100			
	1 (bottom)	600X600	8Ø32 (c1,3) 12Ø32 (c4)	3Ø15/125 4Ø15/125	400X500	2Ø32-3Ø32	2Ø15/125

Table 4-7: Mass of each storey of the designed frames (Lu, 1996)

Model	Storey level	Total masses, Kg	Model	Storey level	Total masses, Kg
BF1	6	35120	DCF	6	35120
	5	36920		5	36920
	4	39220		4	39220
	3	40420		3	40420
	2	42520		2	42520
	1	47820		1	45520

4.3.2 Details of test 2 and 3

The seismic tests were constructed as $1/5.5^{th}$- scale replicas of the aforementioned designed frames using materials with similar properties to those expected in the prototype frames; however the gravity loads were augmented with additional masses in order to have similar gravity stresses as in the prototype frames (Lu et al., 1999). The additional masses, calculated based on the similitude laws were 6913 and 6854 Kg for the BF1 and DCF frames, respectively. The mass of each storey of the model is listed in Table 4-8. More details about reactive mass similitude can be found in (Lu, 1996). Figure 4-20 shows the geometry and dimensions of the models. The slab contribution was accounted for by providing a 300-mm wide flange of 30 mm thickness on both sides of the beams. The slab reinforcement was a single mesh of 3 mm-bar at 50 mm spacing in two orthogonal directions (Lu, 2002). The reinforcement of the models was deduced from the prototype frames on a one-to-one basis. Consequently, the reinforcing bars used in the scale models were deformed 6-mm and smooth 3-mm bars for flexural and transverse reinforcement, with mean yield strength of 448 and 195 MPa, respectively. The approximation of the reinforcing bar diameter resulted in an increase in the reinforcement amounts utilised. The mean compressive and tensile concrete strengths were equal to 30 and 3 MPa, respectively. The strengths of the scale models were expected to be more than those of the prototype frames due to the increase in the reinforcement amounts and the strength of the materials used.

Regarding the seismic loads, the N-S component of El Centro 1940 was used as a base acceleration, with gradually increasing intensity from 0.1 g to 0.9 g for the BF1 frame and

from 0.1 g to 1.2 g for the DCF frame. A time scale factor equal to the square root of the test scale factor, 5.5, was adopted to adjust the time of the input ground motion (Lu, 2002).

Table 4-8: Mass of each storey of the models (Lu, 1996)

Model	Storey level	Total masses, Kg	Model	Storey level	Total masses, Kg
BF1	6	1156	DCF	6	1161
	5	1216		5	1221
	4	1298		4	1296
	3	1331		3	1335
	2	1394		2	1404
	1	1580		1	1519

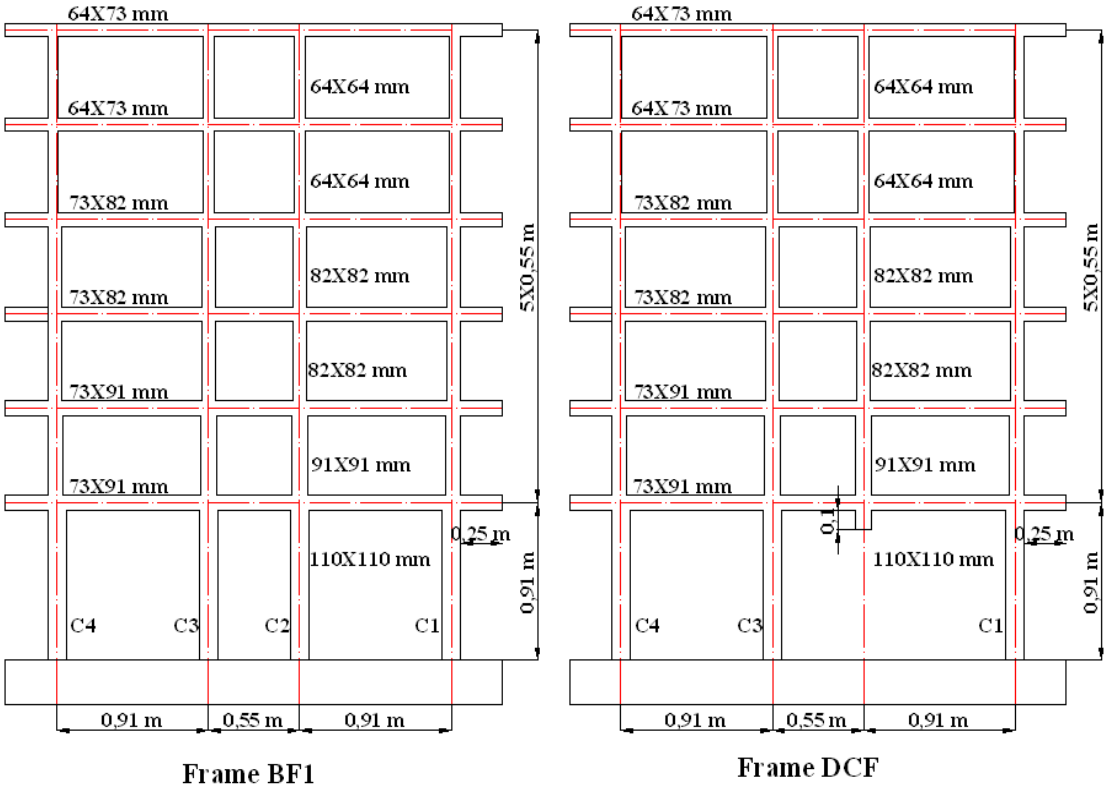

Figure 4-20: Geometry and dimensions of the BF1and DCF frames

A side support system was connected to the test model on the first and third floors. In the BF1 frame test, no firm support was available for the upper two levels, because of the short height of the steel reaction frame. The side-support system was improved for the DCF frame test and resulted in a decrease in the out-of-plane motion. More details about the support system can be found in (Lu, 1996). The BF1 frame could not be tested for 1.2 g, due to the out of plane instability observed in the 0.9 g test. The 1.2 g test was performed for the DCF frame.

4.3.3 AEM models of test 2 and 3

Nonlinear analyses for the scaled models were carried out using Extreme Loading for Structure software. Scaled models were used instead of prototype frames, in order to directly compare the analytical and measured results and to avoid any differences, which may result from the similitude design. Material nonlinearity, large deformations, element separation and contact were all considered in the analyses.

The same material models were used for concrete and steel material, as in test 1, Section 4.2.2. The BF1 frame was modelled by utilising 1716 elements and 126602 springs. The total number of elements was 2258 in the DCF frame model. The material properties for both models are listed in Table 4-9.

Table 4-9: Material parameters used in the AEM models

Material properties	**Concrete**	**Steel (longitudinal-transverse)**
Young's modulus (MPa)	29700	200000
Shear modulus (MPa)	12375	76923.10
Tensile strength (MPa)	3	448-195
Compressive strength (MPa)	30	
Ultimate strain		0.08
Ultimate strength /Tensile yield stress		1.15
Post yield stiffness ratio		0.01

All the reinforcement details for the structures have been explicitly modelled. Splicing of beam reinforcement was avoided using continuous bars along each beam and increasing the length of the bars at both beam edges to provide sufficient straight anchorage for the

reinforcement, similar to the test. Stirrups were applied in two directions in the joints. Springs representing the reinforcement bars were automatically assigned to the element faces at the exact location of the steel bars. Figure 4-21 shows the AEM models and the mesh discretisation.

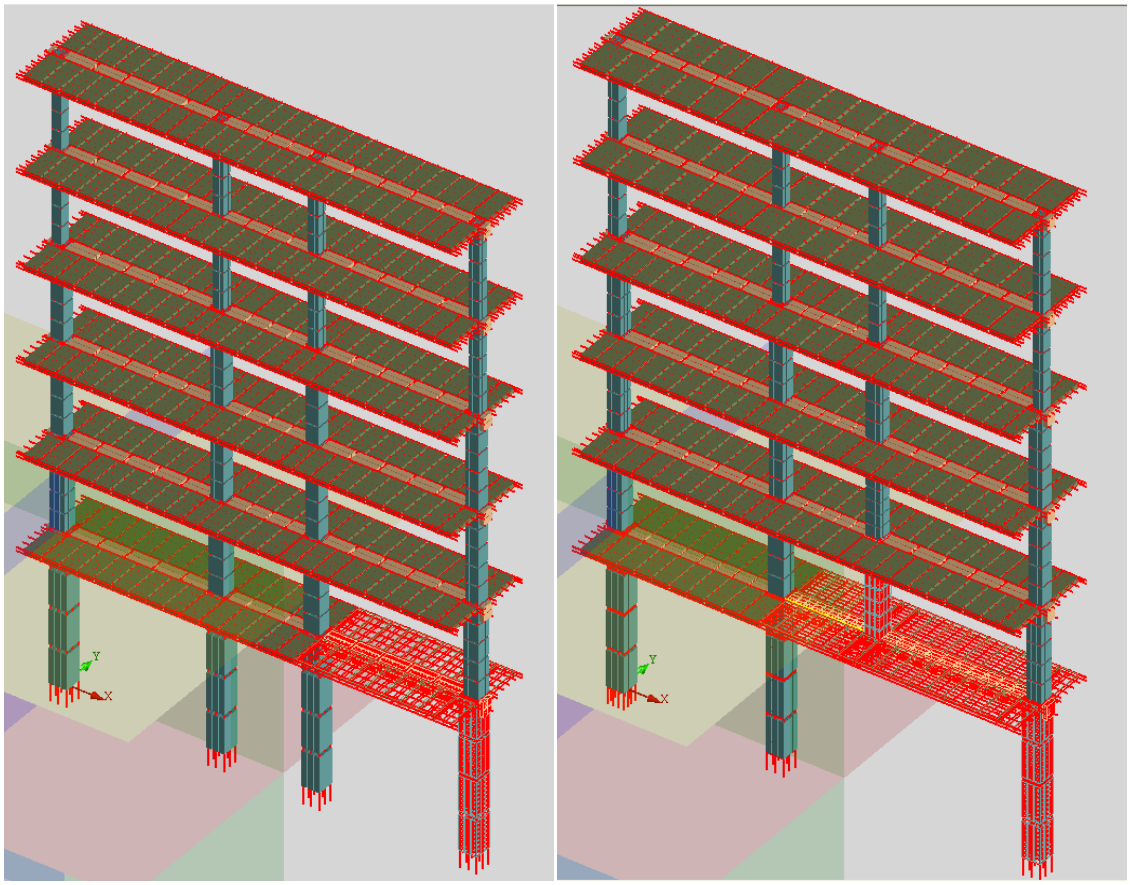

(A) Frame BF1 (b) Frame DCF

Figure 4-21: AEM models for both frames

To prevent the out-of-plane response in a similar way to the test, where a side-support system was provided, the frame displacement restraints in the y direction were fixed at all storeys. A fixed support was applied at the base of the first-storey columns. Hence, the model boundary conditions were consistent with those on the shaking table test.

In order to compare the analytical results with the experimental results, the distribution of gravity stress should be similar in the analytical models and the test models. A uniform

mass distribution was adopted in the modelling. Masses were uniformly distributed on the slabs and beams by increasing the weight of the slabs and beams to account for the loads.

Due to the limited amount of data available, the input ground motion used in the analyses was based on scaling the shaking table acceleration of 0.3 g to obtain the remaining required levels of intensity. Therefore, the response of the analytical models was expected to be less than those obtained from the experiment, as the peak acceleration of the adopted input motion was often smaller than the shaking table acceleration. The out-of-plane motion in the test causes some differences between the shaking table accelerations and the input accelerations (Zhang, 1995). Moreover, some of the details and the accuracy of the experimental displacement records were lost in the digitising process, which aimed to convert the displacement diagrams into numbers, and was carried out using Engauge software (Mitchell, 1991). This is because the results, the displacements measures in the experiments, were available only in paper format.

The loading stages involve both static and dynamic loading. Firstly, the gravity loads were applied to allow the structure to deform under static loads and then the scaled ground motion records are applied in sequence. The seismic loading scenarios for both frames are shown in Figure 4-22. Because of this loading scenario, the damage sustained by the elements during the previous loading stage could be used as the initial condition following the loading stage. The elastic damping ratio was taken as 0.05. Approximately 5 sec of zero acceleration was added between each adjacent dynamic loading stage to allow the structural response to dampen at the end of each stage. The time step utilised for the analyses was 0.008528 sec.

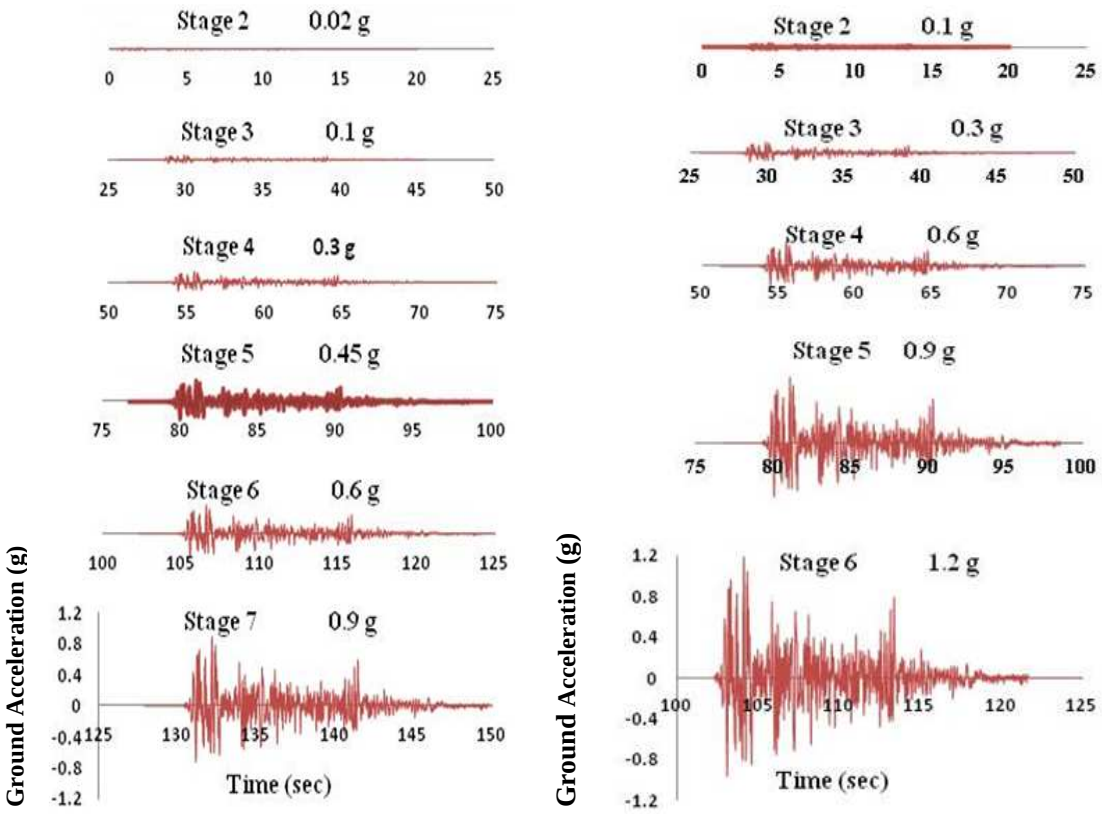

BF1 DCF

Figure 4-22: Seismic loading scenario for the BF1 and DCF frames

4.3.4 Comparison of AEM and experimental results

4.3.4.1 Displacement time history validation

The validation of the AEM models is performed in terms of global response, and the displacement time histories, due to the limited data available. Comparisons between the storey displacements of the AEM and the test models for different peak acceleration levels are shown in Figures 4-23, 4-24 and 4-25.

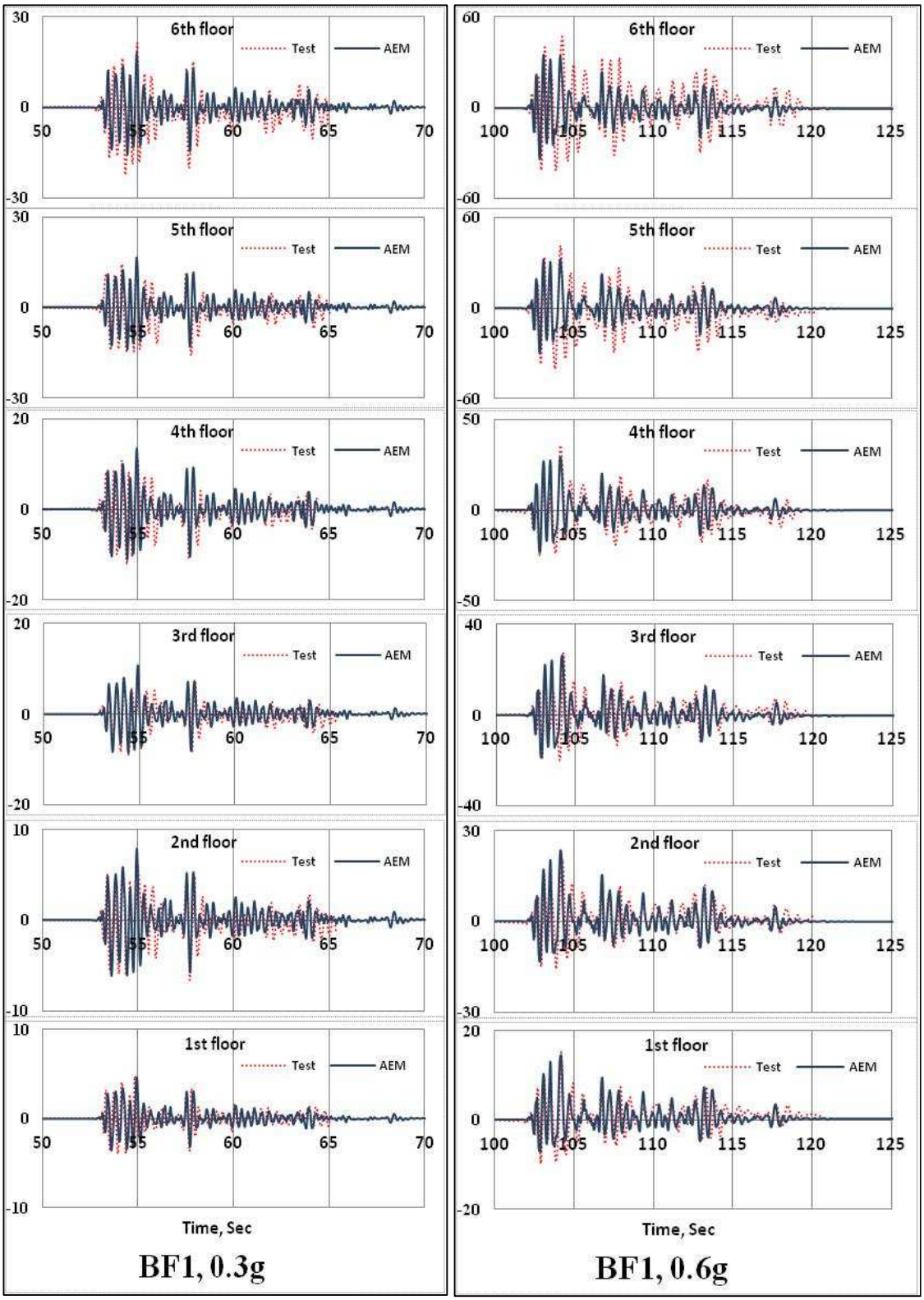

Figure 4-23: Comparison between analytical and experimental storey-displacement histories for the BF1 frame for PGA of 0.3 and 0.6 g

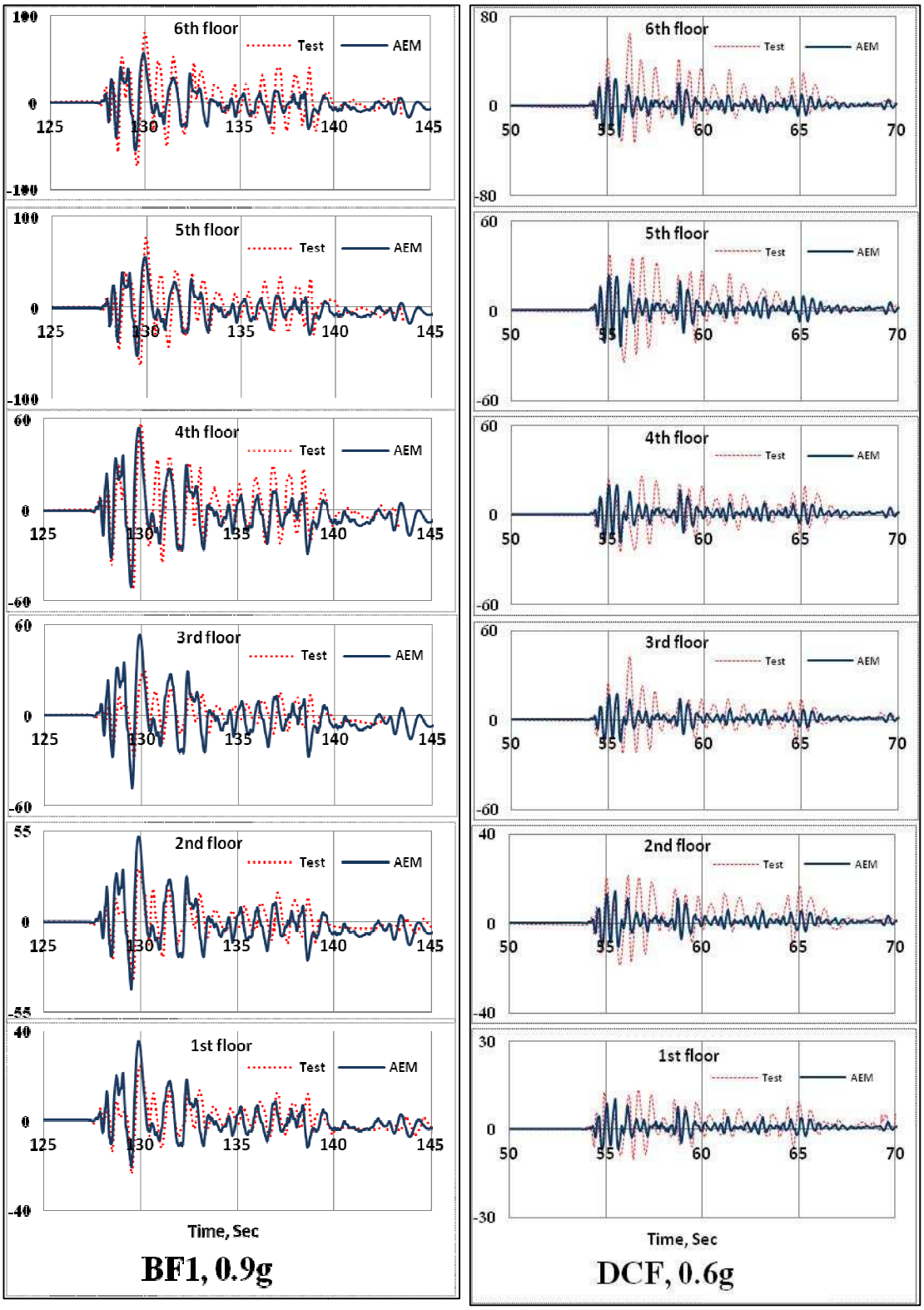

Figure 4-24: Comparison between analytical and experimental storey-displacement histories for the BF1 and DCF frames

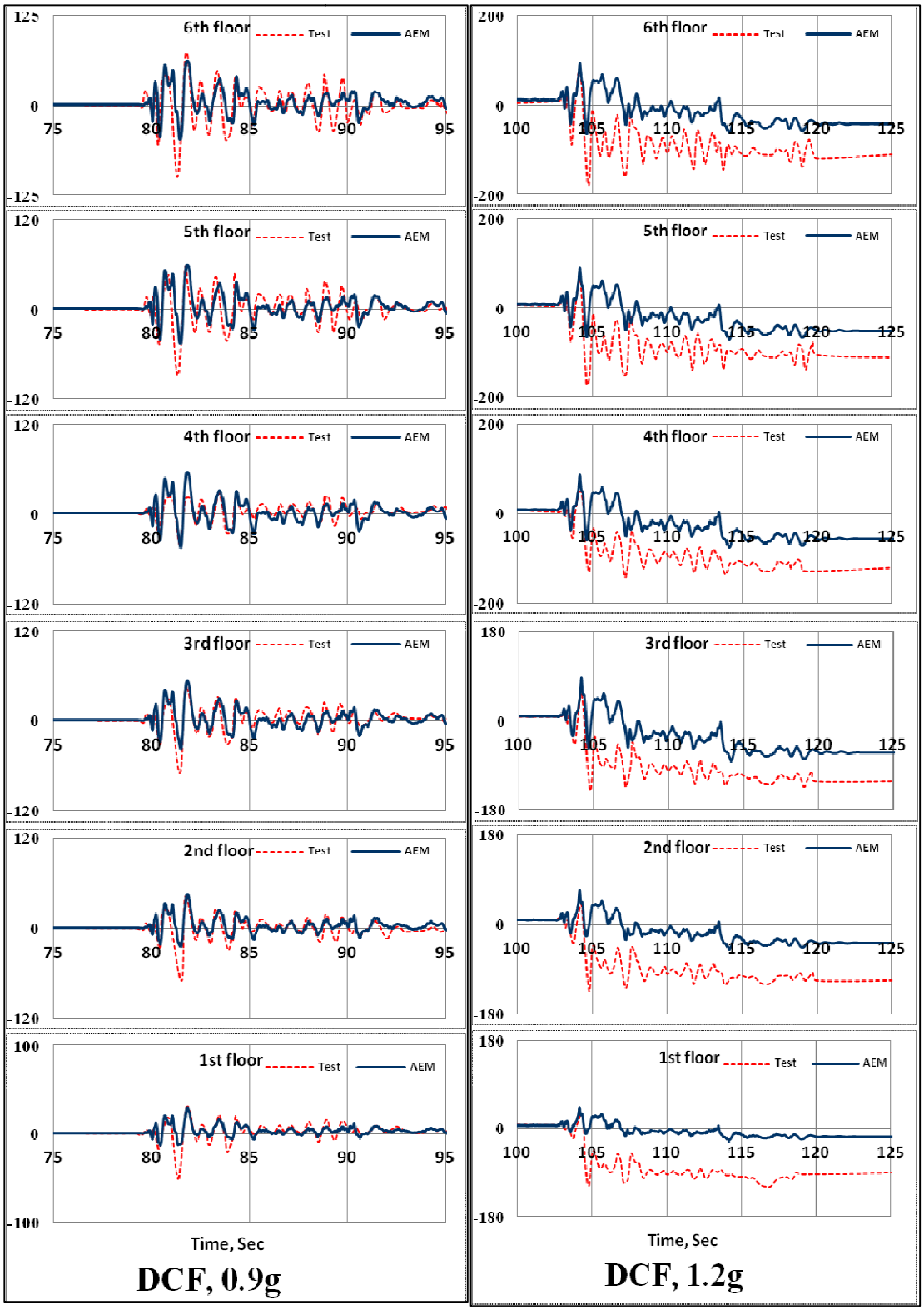

Figure 4-25: Comparison between analytical and experimental storey-displacement histories for the DCF frame for PGA of 0.9 and 1.2 g

In the majority of cases, the AEM models slightly underestimated the storey displacements measured, particularly at high PGA levels. This could be due to two reasons. Firstly, the ground excitations used in the analyses were slightly less than the shaking table accelerations, especially for low ground excitations. Secondly, using a constant value for the elastic damping ratio in all of the analyses led to a reduction in the structure response in the case of high PGA levels. During the small amplitude ground excitation, this damping ratio was appropriate, while for moderate and severe ground motions, the damping forces were increased due to concrete cracking and other nonlinear phenomena, which were automatically included in the analyses. It should be pointed out that using a smaller value for the elastic damping ratio will result in error accumulation. Also, initial cracks in the scale specimen due to curing may decrease the specimen's stiffness, resulting in higher storey displacement in the experiment.

Contrary to the experimental results, no significant amplification of the storey displacements of the fifth and sixth storeys was observed. This could be because of the prevention of the out-of-plane motion in the AEM. The abrupt decrease in the dimensions of the columns at the third and fifth storeys could have contributed to the severe damage at these storeys. However, the out of plane acceleration of the top floor beam is around 0.1 g during the test at 0.9 g for BF1 frame and 0.025 g for the DCF frame (Lu, 1996). The damage to the upper storeys may be intensified, because of a combination of the out-of-plane motion and the P-Delta effects, leading to the acceleration of damage to these storeys. In addition, the out-of-plane motion could be attributed to a discrepancy between the scaled input and the signals of the excitation measured. The peak acceleration of the measured signals is often larger than those of the target input, especially for the BF1 frame (Lu, 1996).

Despite these small differences, good agreement between the analytical and experimental results was obtained, especially for the lower storeys. It is worth noting, based on the comparisons above, that the AEM is a reliable tool for predicting the highly nonlinear response of RC structures.

In both frames, seismic response was predicted using the mean values of all random variables, the structure's dimensions, reinforcement detailing and amounts, and material properties. Thus, treating all random variables as deterministic in the analytical models and using their mean values may explain the differences between the experimental and analytical

results, since there was scatter in some of these values observed during the seismic tests. The results of the sensitivity study of these frames, as carried out in Chapter 5, show that a fifth storey mechanism is one of the most common collapse modes. For more information about the effects of uncertainties in the material properties on the seismic response of these frames, see Chapter 5.

4.4 Summary

This chapter has presented a detailed description of applied element modelling for three different reinforced concrete structures that were previously shaking-table tested. The experimental tests were also summarised. The analytical results were compared with those obtained from the tests in terms of the first two fundamental periods and the inter-storey displacement histories. Good agreement between the AEM results and the experimental results indicated reliability of using the AEM to simulate the seismic structure response from initial damage until total collapse. The effect of using the recommended value of failure criteria, separation strain, on the collapse process has been discussed. The time at incipient collapse can be strongly affected by the failure criteria.

Chapter 5 Effects of modelling uncertainties on the collapse process

5.1 Introduction

In general, the assessment of structural collapse using nonlinear time history analyses is highly uncertain due to a number of sources. These can be categorised as either aleatoric or epistemic uncertainties. The former is inherently random and irreducible, while the latter results from limited databases and lack of knowledge. Thus, epistemic uncertainty can be decreased throughout by additional information and knowledge obtained from more comprehensive analyses and tests.

There are many random variables affecting collapse, such as the uncertainty in material properties, design variables, structural modelling, simulation and analysis methods and the defined limit states. Human errors and uncertainty in the construction phase are also important sources of uncertainty (Haselton et al., 2008b). In addition, the ground motion input in terms of frequency content, characteristics (known as a record to record variability) and intensity, given by the hazard curve for a specific site, can cause a significant variability in the structure response. Record to record variability can be directly investigated by applying an incremental dynamic analysis using a representative set of ground motions with a sufficiently large number of records. All the aforementioned sources of uncertainty are categorised as epistemic uncertainty with the exception of record-to-record variability, which is treated as an aleatoric uncertainty.

Deterministic methods for collapse assessment are not sufficient for evaluating structural safety under seismic loading, due to these uncertainties. Using a complete probabilistic approach to account for all random variables is computationally very expensive and time consuming. Thus, sources of uncertainty that are most influential on the structure response should be determined, and their effects subsequently quantified.

This study cannot address all the random variables. Record to record variability and modelling uncertainty, which have been the focus of many previous research studies (Haselton and Deierlein, 2008), are beyond the scope of this study. The emphasis here is regards the effects of uncertainties in material properties on the collapse process. Collapse is the only limit state of concern here. The reason for this is related to the capacity of the analytical tool utilised, Extreme Loading for Structures, which is based on the AEM. AEM modelling does not require a definition of element stiffness, strength or deformation capacity in contrast with the analytical tools generally used, Drain-2DX software and OpenSees platform (OpenSees, 2005), in which lumped plasticity models are often adopted. The focus of the majority of sensitivity studies have been on the parameters utilised for defining lumped plasticity models. AEM modelling depends on the constitutive relationship used for representing concrete and steel. Thus, the aforementioned effects of element stiffness, strength and deformation capacity are inherent to the model due to the corresponding material properties. In addition, AEM analysis is relatively time consuming and several days normally are required to complete a simple sensitivity analysis using a single record. Therefore, record-to-record variability will not be considered here.

Furthermore, the focus of attention of this sensitivity study is on the time at the onset of collapse, rather than on the capacity of the collapse, which requires around a hundred analyses using the AEM, with a set of 14 records and only one set of material properties. In order to identify the most influential random parameters and to rank these according to their relative importance to global structural response, a deterministic sensitivity analysis, generally utilised for decision analysis (Porter et al., 2002), was conducted for its simplicity and efficiency. A number of uncertain parameters was investigated. Then the most important parameters, obtained from a tornado diagram, will be selected to investigate the effect of the correlation between variables at different storey levels, while the remainder will be excluded. The reason for this is that understanding the effect of correlation between random variables is limited and more investigations are required.

5.2 Previous studies

The methods commonly used to investigate the effect of uncertainty on the dynamic response of structural systems are a deterministic sensitivity analysis called a tornado diagram (Porter

et al., 2002), the first-order second-moment, FOSM, method (Lee and Mosalam, 2005) and Monte Carlo simulation (Esteva and Ruiz, 1989). Although the Monte Carlo method is the most comprehensive method for propagating uncertainty, it is computationally demanding. This is because an excessively large number of simulations are required to reliably estimate the full distribution of the structural performance. Thus, this method is not used in this research as AEM models consist of a large number of elements and springs resulting in a time-consuming simulation, as each AEM analysis requires around three hours to run short ground motion records.

Previous studies have indicated that the impact of uncertainties on the structural modelling and on the material properties affecting the seismic performance of structures is limited (Esteva and Ruiz, 1989, Lee and Mosalam, 2005, Lee and Mosalam, 2006, Ellingwood and Kinali, 2009, Celik and Ellingwood, 2009). This is due to the fact that the focus of these studies has been on the pre-collapse response of structures. Esteva and Ruiz mentioned that further investigations are required in order to determine the importance of the randomness in structural properties on the collapse response (Esteva and Ruiz, 1989). Recent studies have concluded that structural modelling uncertainties related to component models are critical and have a significant impact on collapse performance assessment, which is no less important than the impact of record to record variability (Haselton et al., 2008b). The differences between the results of these various investigations are due to the fact that the effects of modelling uncertainty on seismic structural performance depend strongly on the limit states considered and on the structure selected. If the study focuses on pre-collapse limit states, modelling uncertainty will have a limited influence on seismic performance compared to the effects of uncertainty in ground motions, which, in this case, will be a dominant contributor to structural response.

Regarding the collapse response, a large number of studies have considered the effects of several sources of uncertainties on collapse capacity and quantifying these uncertainties by applying FOSM approximation based on Taylor series expansion. The FOSM method is proposed by (Baker and Cornell, 2003, Baker and Cornell, 2008) for use in seismic performance-based engineering, in order to calculate loss estimation. The FOSM approach was also used by (Ibarra and Krawinkler, 2005) for estimating the total uncertainty in the collapse capacity, due to uncertainty in system parameters. The mean and standard deviation

of the structural response, which represents a sensitivity measure, can be computed by the FOSM method without knowing the probability distribution of the performance function (Lee and Mosalam, 2006). However, the FOSM method may be problematic and so can cause inaccurate results if the performance function relating the uncertain parameters to the response of interest is highly nonlinear as in the case of the collapse response (Liel et al., 2009). It is preferable to perform the calculation of the FOSM in the log-domain of the data instead of the linear domain. This is because the linear assumption of the FOSM is more accurate in the log-domain (Ibarra and Krawinkler, 2005). The FOSM method cannot capture the change in the median collapse capacity that may result when modelling uncertainties have a nonlinear effect on collapse capacity (Liel et al., 2009).

Haselton et al. conducted a probabilistic study to assess the seismic performance of a modern designed structure. They employed the Ibarra-Krawinkler lumped-plasticity model for a collapse simulation, whilst considering global side-sway only. The FOSM approach was utilised for integrating modelling uncertainties with record-to-record uncertainty. The results showed that ignoring modelling uncertainties, especially those associated with element deformation-capacity and post-peak negative stiffness, in a collapse assessment can lead to a significant underestimation of the collapse risk. In addition, the degree of correlation between random variables has a considerable impact on the estimation of collapse capacity (Haselton et al., 2008b). Also, the logarithmic standard deviation due to record-to-record variability is in the range $(0.3 - 0.4)$, while that due to modelling uncertainty is $(0.35 - 0.4)$. The correlation between random variables for a single and for multiple members has a significant effect on dispersion. The dispersion due to modelling and design uncertainties can vary from 0.21 when using uncorrelated variables to 0.54 where there is full correlation. The effects of structural modelling uncertainties are more significant than those of uncertainties in the structural design, such as the height and framing layout (Haselton and Deierlein, 2008).

Ibarra and Krawinkler investigated the importance of the effects of modelling parameters on the side-sway collapse capacity of deteriorating single and multi-degree-of-freedom systems, SDOF and MDOF. The parameters considered in their study were those associated with defining concentrated plasticity models, the modified Ibarra-Krawinkler model, which incorporates stiffness and strength deteriorations, and based on calibration with experimental data. Three different values were used for each selected parameter and all

possible combinations of these parameters are considered in the analyses. It was concluded from the parametric studies that the two most critical parameters for estimating the collapse capacity of ductile systems are post-capping stiffness in the backbone curve and ductility capacity (Ibarra and Krawinkler, 2005, Ibarra and Krawinkler, 2004, Ibarra et al., 2005). It was also found that strength deterioration is an extremely important parameter when astructure is on the verge of collapse, as in the case when a structure is represented by a single-degree-of-freedom system with a period of 0.9 sec, and a damping ratio of 5% (Ibarra et al., 2005). Cyclic deterioration, λ, is not a governing parameter but it is still important in the collapse limit state (Ibarra and Krawinkler, 2005).

The dispersion of collapse capacity due to uncertainties that affect the three parameters of the hysteretic model, namely post-capping stiffness, ductility capacity and cyclic deterioration for SDOF and MDOF systems, was quantified by employing the FOSM method. For SDOF systems, with only one uncertain parameter, namely the post-capping stiffness, the results of the simplified FOSM method were verified using the Monte Carlo method, and a combination of response surface and the Monte Carlo method (Ibarra and Krawinkler, 2005). It was concluded that the dispersion due to uncertainties in the modelling parameters is not less than that due to record-to-record variability and its value depends on the variance of the post capping stiffness and that of ductility capacity, as well as the correlation among parameters (Ibarra and Krawinkler, 2005). The SDOF system is more sensitive to uncertainties in these parameters than the MDOF system.

(Lignos and Krawinkler, 2009, Zareian and Krawinkler, 2009) found that the most important component parameters on the collapse capacity are the post-capping rotation capacity and plastic-rotation capacity.

A study by Liel et al. emphasised quantifying the effect of uncertainties in modelling parameters for a lumped plasticity model when assessing the collapse capacity of a number of ductile and non-ductile frame structures (Liel et al., 2009). The quadratic response surface for each structure represents the relationship between median collapse capacity and random parameters; and accounts for the nonlinearities and asymmetric effects of the random variables. The structure response surface is obtained based on a regression analysis of the data obtained from sensitivity analyses, corresponding to each structure. In order to incorporate the effects of different uncertainty sources, the response surface was combined

with the Monte Carlo method for sampling. Thus, the median collapse capacity was computed for each realisation set, utilising the response surface instead of performing an incremental dynamic analysis. The effects of correlation between random variables were investigated using a response surface method, where by three correlation assumptions were made. In the first case, each of the strength and ductility variables was assumed to be correlated for the beams and columns. Secondly, the beam or column strength variables were assumed to be correlated with the corresponding ductility variables. In the third case, the beam strength for each of the second and third storeys was assumed to be uncorrelated with the beam strengths of the other storeys. It was shown in this study that ignoring the effects of uncertainties in these parameters can lead to un-conservative predictions, especially if the random parameters of concern are highly uncertain and have a highly nonlinear relationship with the response of interest. Modelling uncertainties can lead to a reduction in the median collapse capacity by up to 20% and to an increase in the dispersion. However, these effects depend on the structural system, the random variable selected, the correlation between them, the asymmetric effects of the random variables and the number of possible failure modes in the studied structure. In addition, it was found that the effects of random variables in increasing median collapse capacity is small when a structure has different collapse mechanisms, since changing a given variable may shift the collapse mode from a storey to another. Moreover, in the first case of correlation, the median collapse capacity was higher by 6.4% compared to the case of zero correlation, while it was 10%less in the third type of correlation. This means that the relative differences in strength, as well as the ductility of the beams and columns are more important than the absolute values.

Liel et al. indicated that the FOSM method cannot capture the shift in the median collapse capacity. To solve this problem, they proposed a novel simplified approach called the approximate second order second moment method, ASOSM. Not only does this new method, which is based on the FOSM method, not require large numbers of sensitivity analyses as in the response surface method, but it can also predict the shift in the median collapse capacity (Liel et al., 2009). Its drawback, however, is that it ignores the effect of interactions between random variables; which was proven to have a significant impact.

Several researchers studied the effects of modelling uncertainties on the seismic structural performance using a tornado diagram analysis to identify and rank the parameters

according to their significant effects on the structural response under seismic loading. For example: (Porter et al., 2002, Esteva and Ruiz, 1989, Yin and Li, 2010, Haselton et al., 2008b, Binici and Mosalam, 2007, Lee and Mosalam, 2005).

The results of the tornado diagram analysis using $(\mu_{RV} \mp \sqrt{3}\,\sigma_{RV})$ instead of $(\mu_{RV} \mp \sigma_{RV})$, as recommended by (Ibarra and Krawinkler, 2005), showed that a component plastic-rotation capacity is the most critical variable affecting mean collapse capacity followed by cyclic deterioration capacity, λ, and then the strong-column weak-beam ratio (Haselton et al., 2008b). The difference between the Haselton results and those obtained by Ibarra regarding the importance of cyclic deterioration capacity results from the use of different lower and upper bounds. However, λ is not as important, as predicted by Haselton.

Sensitivity analyses were carried out by (Liel et al., 2009, Liel and Deierlein, 2008) to quantify the effect of modelling uncertainties on the collapse limit state of ductile and non-ductile frame structures by means of the response surface method as mentioned above. Four random variables were considered in both structures, namely column strength, column ductility, beam strength and ductility. Two additional parameters related to the joints, joint strength and ductility, were also considered in the non-ductile frames. All random parameters were assumed to have log-normal distributions. For each random variable, $(\mu_{RV} \mp 1.7\sigma_{RV})$ was employed if the individual parameter changes and $(\mu_{RV} \mp \sigma_{RV})$ was used in the case of combination with other parameters. Thus, 33 and 93 sensitivity analyses were performed for each ductile and non-ductile structure, respectively. For each realisation of uncertain variables, an incremental dynamic analysis of the corresponding modified model was carried using a set of 20 ground motion records. It was concluded that the random variables with the most significant impact on collapse capacity are column strength, represented by $(\mathrm{M_y}, \mathrm{K_e})$, and column ductility, represented by $(\theta_{\mathrm{cap}}, \theta_{\mathrm{pc}}, \lambda)$, respectively. The beam strength and ductility are the least important random parameters. The beam strength adversely affects collapse capacity. This means that an increase in the beam strength can cause a reduction in the median collapse capacity, due to the formation of plastic hinges in the columns rather than in the beams. The asymmetric effects of random variables on seismic response of structures were noted in this study. Decreasing member ductility has a larger effect on the collapse capacity than increasing it.

Talaat and Mosalam investigated the effect of different random variables on the time at incipient collapse of a reinforced concrete frame structure, with infill walls using the tornado diagram analysis, in which the upper and lower bounds were estimated for a confidence interval of 0.997. The collapse simulation was performed using a novel element removal algorithm they developed. They identified an earthquake intensity as the most important parameter was the, followed by infill wall stiffness and live load factor, while the ratio of the viscous damping was the least important factor (Talaat and Mosalam, 2008, Talaat and Mosalam, 2009).

5.2.1 The First-Order Second-Moment Method, FOSM

The FOSM procedures in the non-ln-domain for estimating the uncertainty in collapse capacity can be summarised as follows (Haselton et al., 2008b):

The mean collapse capacity, $\mu_{sa_{collapse}}$, and the variance due to record-to-record variability, $\sigma^2[X_{RTR}]$, can be determined from an incremental dynamic analysis using the mean values of all random variables, RV.

$$\mu_{sa_{collapse}} \cong g(\mu_X) \qquad \text{Equation 5-1}$$

The total variance in collapse capacity can be calculated using the standard deviations and correlation coefficients of each random variable as in Equation 5-2.

$$\sigma^2[Sa_{collpase}] \cong \left[\sum_{i=1}^{n}\sum_{j=1}^{n}\left[\frac{\partial g_{(X)}}{\partial x_i}.\frac{\partial g_{(X)}}{\partial x_j}\right]_{X=\mu_X}\rho_{ij}\sigma_i\sigma_j\right] + \sigma^2[X_{RTR}] \qquad \text{Equation 5-2}$$

$$\frac{\partial g(X)}{\partial x_i} = \frac{g(\mu_i+\Delta x_i)-g(\mu_i-\Delta x_i)}{2\Delta x_i}, i = 1,2,\ldots,n \qquad \text{Equation 5-3}$$

$\frac{\partial g(X)}{\partial x_i}$ is the gradient of $Sa_{collapse}$ related to RV_i, and can be determined from a series of sensitivity studies using the finite differences method. See Equation 5-3, where ρ_{ij} is the correlation coefficient between RV_i and RV_j, σ_i is the standard deviation of RV_i, μ_X is the vector of mean values of RVs, and g is a function that relates the RVs to the collapse capacity.

5.2.2 The Approximate Second Order Second Moment method, ASOSM

In this method, the dispersion due to modelling uncertainties is predicted in a similar way to the FOSM method. The shift in the median collapse capacity of reinforced concrete structures can be determined by multiplying the median collapse capacity, as obtained from an incremental dynamic analysis by the factor $\frac{\hat{m}_{mod}}{\hat{m}}$ (Liel et al., 2009, Liel and Deierlein, 2008). This factor is determined from Equations 5-4 and 5-5.

$$\frac{\hat{m}_{mod}}{\hat{m}} = 0.64(\Delta^{+}/\Delta^{-}) + 0.36 \qquad \text{Equation 5-4}$$

$$\Delta^{+}/\Delta^{-} = \frac{\hat{m}^{+}/\hat{m}}{\hat{m}\ /\hat{m}^{-}}\ ,\ \hat{m}^{+} = \frac{1}{n}\sum_{i=1}^{n} m_{x_i + x\sigma_i}\ ,\ \hat{m}^{-} = \frac{1}{n}\sum_{i=1}^{n} m_{x_i - x\sigma_i} \qquad \text{Equation 5-5}$$

Δ^{+}/Δ^{-} is a parameter related to the response asymmetry, $\hat{m}$ is the median collapse capacity calculated using the mean values of random variables, $m_{x_i + x\sigma_i}$ is the median collapse capacity when the i random variable scaled by $+1.7\sigma_i$, $m_{x_i - x\sigma_i}$ is the median collapse capacity when the i random variable scaled by $-1.7\sigma_i$, and n is the number of considered random variables.

5.2.3 Tornado diagram analysis

Tornado diagram analysis is a simplified method of sensitivity analysis and is used in this study. Even though this method does not provide any statistical information on engineering demand parameters, such as the mean and standard deviation, it can provide useful results regarding the degree of importance of the random variables considered.

The tornado analysis provides considerable insight into the relative importance of the random variables of interest. The probability distribution of each uncertain variable is selected. Each input variable varies between two extreme values, defining the values of the upper-bound and lower-bound of the input probability distribution; e.g. the 90th percentile and the 10th percentile. Figure 5-1 shows the procedures for performing a tornado diagram analysis (Binici and Mosalam, 2007).

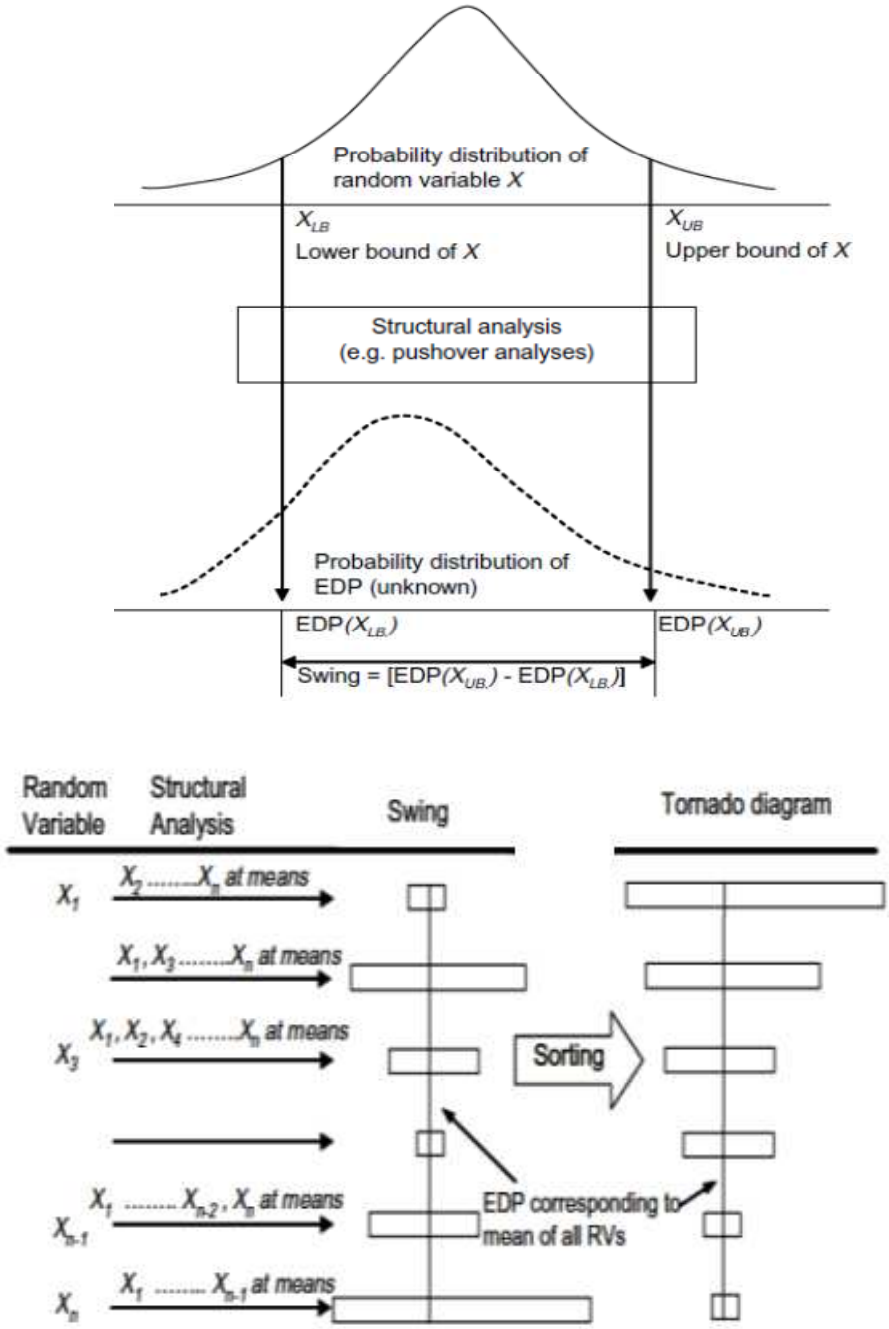

Figure 5-1: Procedures for developing the tornado diagram (Binici and Mosalam, 2007)

For developing the tornado diagram, firstly all random variables are set to their best estimated values, such as their mean or median values. Then, a deterministic analysis is performed using best estimated values, in order to establish a baseline output, e.g. the time at incipient collapse. The measured output of interest is considered as a deterministic function based on

the analytical model. The analysis is repeated for each random variable for both of the extreme values retaining the remaining variables at their best estimate values. The output of interest is measured and plotted as a horizontal bar, associated with each random variable, which is called the swing. The length of the swing represents the sensitivity of the output to the variation in the corresponding random variable. The random input variables are arranged with regard to their swings.

As mentioned previously in Section 5.1, the tornado diagram will be used in this work. This is because the aim of this study to identify and then to rank the most important parameters on the collapse process, rather than quantify the effect of a limited number of random parameters. More than 70 random variables will be studied. The FOSM and ASOSM are generally utilised to calculate the variance in collapse capacity, due to modelling uncertainty. The FOSM and ASOSM often involve conducting a series of sensitivity studies using tornado diagrams, see Section 5.2.1. The time at collapse onset is of interest in this work rather than collapse capacity, due to the computational expense of the analyses and the large number of analyses required to determine collapse capacity.

5.3 Selected random modelling variables

As mentioned earlier in Section 5.1, the seismic collapse performance of structures is highly uncertain, due to the numerous sources of uncertainties. Apart from the uncertainties in characterising ground motions, there are uncertainties associated with analytical models adopted, including input modelling parameters, masses, and geometrical data. Variability in the depth of concrete cover and the location of reinforcement bars generally has little influence on strength and ductility of the RC member, comparing to the effect of concrete and steel strength (Grant et al., 1978). Consequently, its effect on the overall response of structures is less significant when compared to the randomness in the material properties. Therefore, the structure dimensions can be treated as deterministic values.

In this study, only the effect of uncertainties in the input modelling parameters, material properties used in the AEM model, and the uncertainties in the structure mass and its corresponding gravity loads will be investigated, while the remaining parameters will be assumed to be deterministic.

5.3.1 Uncertainty in the structure properties

In general, the stiffness and strength of structural members represent the most important random variables; these have been investigated in many probabilistic studies, as mentioned above.

In the AEM method, the stiffness, strength and deformation capacity depend on the material parameters used in the adopted constitutive model of the ELS, member dimensions and the amount as well as the detailing of reinforcements. The stress-strain relationship at the element level in the AEM is deterministic. The member dimensions and the details and amounts of both of the longitudinal and transverse reinforcements will be treated as deterministic. Only the effect of uncertainties in the concrete, the longitudinal and transverse reinforcing steel are of significant interest to this research, because they are the only input parameters required to define the analytical model. The material parameters considered as random variables are the concrete compressive and tensile strengths, the modulus of elasticity, the steel yield and ultimate strengths and ultimate strain.

5.3.1.1 Properties of concrete

A normal distribution is assumed for each of the three aforementioned concrete properties. The focus here is on the concrete grade C20/25, which is used in the aforementioned seismic tests 2 and 3.

The code design strength for the (C20/25) class concrete $f_{ck,5\%}$ is 20 MPa, with a standard deviation of 5 MPa. The mean value of the concrete compressive strength is assumed to be larger than the design strength by 8 MPa and the coefficient of variation, COV, representing the ratio between the standard deviation and the mean, is 18% (Kappos et al., 1999).

The mean tensile strength of concrete, f_{ctm} is 2.2 MPa obtained from the characteristic concrete compressive strength based on $f_{ctm} = 0.3 f_{ck}^{\frac{2}{3}}$ in MPa unit according to (CEB, 1993). The coefficient of variation of the tensile strength is assumed to be 1.2 times larger than that of the concrete compressive strength. The parameters of the probability distribution

of the concrete tensile strength are defined in similar way to the study detailed in (Vasconcellos Real et al., 2003).

The mean initial tangent modulus of elasticity of concrete, E_c, can be calculated from the following relationship ($E_c = 21500\sqrt[3]{\frac{f_{ck}+8}{10}}$ in MPa unit) according to (CEB, 1993). The coefficient of variation for this variable is assumed to be 8%, as suggested by (Mirza et al., 1979, Lee and Mosalam, 2006). Mirza et al. noted, based on regression analyses, that there was a strong correlation between the compressive strength and the initial modulus of elasticity, and a coefficient of correlation in a range of 0.88 to 0.91 was recommended. Poisson's ratio is assumed to be deterministic with a mean value of 0.2 (Kartal et al., 2011).

5.3.1.2 Properties of the steel used in reinforcement

The reinforcing steel properties of major interest were the yield strength f_y, the ultimate strength f_u, the modulus of elasticity E_s, and the ultimate strain ε_u. A normal distribution assumption was adopted for these four variables. The steel grades of interest were S400 and S220, as these were used for the flexural and transverse reinforcement in the structures selected, respectively.

With regard to the variability in the flexural steel, the characteristic value of the yield strength of S400 steel, $f_{yk,5\%}$, is 400MPa. The mean value is assumed to be 440 MPa with a COV of 6%, accounting for both producer-to-producer and within-producer variations, similar to the study by (Kappos et al., 1999). The mean value of the ultimate strength of reinforcing steel is 502 MPa with a COV of 6%, based on the assumption that the ratio of f_y to f_u is fixed and consistent with requirement of the Eurocode 8 for the Medium Ductility class. The mean value of 9% is considered for the ultimate strain (Dymiotis, 1999). A COV of 9% is assumed for the ultimate strain, as suggested by (JCSS, 1995, Lee and Mosalam, 2006, Kappos et al., 1999, Dymiotis, 1999). The mean value of Poisson's ratio for reinforcing steel is assumed equal to 0.3, which is treated as deterministic.

In reference to the variability in the transverse steel, zero correlation between the longitudinal and transverse steel properties was assumed, due to the fact usage of different types of reinforcement. However, the aforementioned statistics for reinforcing steel properties

can be assumed valid for bars of different types. Hence, the same distributions can be used for both longitudinal and transverse reinforcing steel. It was concluded by Dymiotis et al. that the effect of variability of transverse reinforcement properties on structural member response is small (Dymiotis, 1999, Kappos et al., 1999). In this study, a zero correlation is assumed among all random variables. Two additional variables were also studied, in which full correlation was assumed between the yield and ultimate strength of both the longitudinal and transverse reinforcing steel. The statistical properties of the selected random variables are listed in Table 5-1.

5.3.1.3 Mass

The mass of each storey and the corresponding gravity loads are treated as random variables in similar way to the study conducted by Talaat and Mosalam (Talaat and Mosalam, 2008). The storey-mass is calculated based on the 3 D structure gravity loads, and the dead and live loads. The dead load is assumed constant, while three cases of the live load are considered. These cases are as the following:

1. Full live load (full occupancy with a live load factor of one, LL=1).
2. No live load (no occupancy with a live load factor of zero, LL=0).
3. The live load corresponding to the expected occupancy adopted in the EC 8 design code, LL=30%.

The reference mass is calculated using the full dead load plus 30% of the live load. Perfect correlation is assumed between the masses and loads of all storeys. It should be mentioned that the same live load factor is used when calculating the vertical and corresponding seismic loads. In addition to the structure self weight, the vertical loads considered were 6 and 8 kN/m for the dead and live load, respectively.

Table 5-1: Statistical properties of the basic random variables

Random Variable	**Mean , μ**	**COV %, SD = COV × μ**
Concrete		
Compressive strength, f_c (MPa)	28	18
Tensile strength, f_t (MPa)	2.2	21.6
Initial modulus of elasticity, E_c (MPa)	30305	8
Steel used in longitudinal reinforcement		
Yield strength, f_y (MPa)	440	6
Ultimate strength, f_u (MPa)	506	6
Ultimate strain, u	9%	9
Steel used in transverse reinforcement		
Yield strength, f_{ys} (MPa)	195	6
Ultimate strength, f_{us} (MPa)	225	6
Ultimate strain, u_s	9%	9

5.3.2 The upper and lower bounds of the tornado diagram

The 90th and 10th percentiles of the random variable distribution define the upper and lower bounds in the tornado diagram. Regarding the normal distribution, the 10th percentile of a normal distribution is less than its mean by approximately 1.28 standard deviations, while the 90th percentile is above by 1.28 standard deviations. The reference, minimum and maximum values for each parameter in the tornado diagram analysis are summarised in Table 5-2.

Table 5-2: Range of the random variables in tornado diagram analysis

Parameter		**Reference**	**Minimum**	**Maximum**
Concrete	Compressive strength, f_c (MPa)	28	21.55	34.45
	Tensile strength, f_t (MPa)	2.2	1.6	2.80
	Initial modulus of elasticity, E_c (MPa)	30305	27200	33410
Longitudinal reinforcing steel	Yield strength (f_y), $f_u = 506$ Mpa	440	406	474
	Ultimate strength (f_u), $f_y = 440$ Mpa	506	467	545
	Yield strength ($f_{y.u}$), with $\frac{f_u}{f_y} = 1.15$	440	406	474
	Ultimate strain, u	9%	8%	10%
Transverse reinforcing steel	Yield strength (f_{ys}), $f_{us} = 225$ Mpa	195	180	210
	Ultimate strength (f_{us}), $f_{ys} = 195$ Mpa	225	208	242
	Yield strength ($f_{ys.us}$), with $\frac{f_{us}}{f_{ys}} = 1.15$	195	180	210
	Ultimate strain, u_s	9%	8%	10%
Mass	Life load factor, LL	0.3	0	1

5.3.3 Correlations between variables

Correlations between the variables have not been extensively investigated. Several simplifying assumptions regarding the correlations between variables are made in this study to reduce the problem size and complexity. There are three types of correlation between the selected variables as follows:

1. Correlation between random parameters for a single member, type 1.
2. Correlation between random parameters for different members, type 2.
3. Correlation between random parameters for different storeys, type 3.

5.3.3.1 Correlation between random parameters of material properties for a single structural member

In general, zero correlation is assumed between the material properties of each member, a beam and a column.

5.3.3.2 Correlation between random parameters of material properties for different structural members

Using unique random variables for each member is a prohibitive task, as results in 462 random variables for 42 structural members with 11 parameters for each. Therefore, two cases of correlation between the parameters for the different types of structural members are investigated. In the first case, type 1, similar material parameters are used in all of the structure members, both beams and columns leading to 11 random variables, e.g. $f_c, f_t, E_c, f_y, f_u, f_{y.u}, u, f_{ys}, f_{us}, f_{ys.us}$ and u_s. While in the second case, type 2, the beams and columns are treated separately resulting in 22 random variables, e.g. $f_{c,c}$, $f_{t,c}, E_{c,c}, f_{y,c}$, $f_{u,c}, f_{y.u,c}, u_c, f_{ys,c}, f_{us,c}, f_{ys.us,c}, u_c, f_{c,b}, f_{t,b}, E_{c,b}, f_{y,b}, f_{u,b}, f_{y.u,b}, u_b, f_{ys,b}, f_{us,b}, f_{ys.us,b}, u_b$.

5.3.3.3 Correlation between random parameters of material properties of structural members for different storeys

Two cases will be considered here. Firstly, full correlation is assumed between random parameters for all storey levels; and secondly, partial correlation between structural members at different storey levels will be considered for the most important random variables. Here, the detailed analyses will be limited to a subset of the previously studied input parameters, which are selected based on the results of sensitivity analyses of the first case. The first ten most important random variables selected from the 33 studied uncertain parameters are $E_{c,c}, f_c, f_u, f_{y.u}, f_{c,c}, f_{u,c}, f_{y.u,c}, f_{c,b}$, $f_{y,b}$ and $f_{y.u,b}$. Other parameters with minor contributions to structural collapse are treated deterministically.

Each frame is divided into four sets of storey levels associated with the changes in the member dimensions and reinforcement details as the following: the first storey level, the second storey level, the third and fourth storey levels and the fifth and sixth storey levels. The selected random variables differ from a storey-set to another. Due to variation in the collapse

modes of both frames, which has been observed from the analytical results of the first case, both frames are more likely to collapse in a first storey or a fifth storey collapse mode, while the BF1 frame is also likely to collapse in three additional failure modes associated with the stepping size of the member. Hence, the impact of correlation between the member parameters for different storeys are expected to be significant. Using separate random variables for each subset of storey results in 40 random variables as follows:

$E_{c,c1}, f_{c1}, f_{u1}, f_{y.u1}, f_{c,c1}, f_{u,c1}, f_{y.u,c1}, f_{c,b1}$, $f_{y,b1}, f_{y.u,b1}, E_{c,c2}, f_{c2}, f_{u2}, f_{y.u2}, f_{c,c2}, f_{u,c2}, f_{y.u,c2}, f_{c,b2}$,

$f_{y,b2}, f_{y.u,b2}, E_{c,c3.4}, f_{c3.4}, f_{u3.4}, f_{y.u3.4}, f_{c,c3.4}, f_{u,c3.4}, f_{y.u,c3.4}, f_{c,b3.4}$, $f_{y,b3.4}, f_{y.u,b3.4}, E_{c,c5.6}, f_{c5.6}, f_{u5.6}$,

$f_{y.u5.6}, f_{c,c5.6}, f_{u,c5.6}, f_{y.u,c5.6}, f_{c,b5.6}$, $f_{y,b5.6}$ and $f_{y.u,b5.6}$.

The investigation of the effects of these variables, as related to the correlation between storeys, is very important. This is because decreasing the strength of a single or two storeys can result in weaker storeys compared to the neighbouring storeys, leading to damage concentration in these weaker storeys and earlier collapse. Table 5-3 lists the random variables selected for each type of correlation to use in the sensitivity studies.

Table 5-3: Selected random variables for each type of correlation

Correlation type	**Random variables**
Type 1	$f_c, f_t, E_c, f_y, f_u, f_{y.u}, u, f_{ys}, f_{us}, f_{ys.us}$, u_s
Type 2	$f_{c,c}, f_{t,c}, E_{c,c}, f_{y,c}, f_{u,c}, f_{y.u,c}, u_c, f_{ys,c}, f_{us,c}, f_{ys.us,c}, u_c$, $f_{c,b}, f_{t,b}, E_{c,b}, f_{y,b}, f_{u,b}, f_{y.u,b}, u_b, f_{ys,b}, f_{us,b}, f_{ys.us,b}, u_b$
Type 3	$E_{c,c1}, f_{c1}, f_{u1}, f_{y.u1}, f_{c,c1}, f_{u,c1}, f_{y.u,c1}, f_{c,b1}$, $f_{y,b1}$, $f_{y.u,b1}, E_{c,c2}, f_{c2}, f_{u2}, f_{y.u2}, f_{c,c2}, f_{u,c2}, f_{y.u,c2}, f_{c,b2}$, $f_{y,b2}, f_{y.u,b2}$, $E_{c,c3.4}, f_{c3.4}, f_{u3.4}, f_{y.u3.4}, f_{c,c3.4}, f_{u,c3.4}, f_{y.u,c3.4}, f_{c,b3.4}$, $f_{y,b3.4}, f_{y.u,b3.4}$, $E_{c,c5.6}, f_{c5.6}, f_{u5.6}, f_{y.u5.6}, f_{c,c5.6}, f_{u,c5.6}, f_{y.u,c5.6}, f_{c,b5.6}, f_{y,b5.6}$, $f_{y.u,b5.6}$

5.4 Selected response parameters

The response parameter that will be investigated is the time at incipient collapse, rather than the maximum inter-storey drift prior to the collapse onset, as recommended by Talaat and Mosalam (Talaat and Mosalam, 2008).

Defining the collapse limit state quantitatively is crucial. A structure generally does not collapse due to the loss of a single or several members. Typically, a structure can sustain large deformations exceeding the acceptable drift limit defined by seismic codes, without failure due to the damage redistribution and the resistance of adjacent members. Collapse occurs when the structure or a large portion of it becomes unstable. An important point, then, is to distinguish between partial collapse at which a portion or a single storey of the structure collapses and total collapse due to the extent of the possible local collapse or global collapse. The time at incipient collapse is defined as the onset of an unrestrained increase in either vertical or horizontal displacements at one or more storey levels. The average vertical and horizontal storey displacements, calculated at the top ends of all columns at the considered storey, are used to define the collapse criteria of the vertical and side-sway collapse modes, respectively.

5.5 Ground motion selection and scaling

The collapse process is very sensitive to the input ground motion in terms of its intensity and ground motion profile. Several factors have been taken into account to select the seismic input for this sensitivity study, focusing on the collapse limit state only. An artificial accelerogram generated using SIMQKE-1 (Gasparini and Vanmarcke, 1976) is adopted in this study. Figure 5-2 and Figure 5-3 show the un-scaled accelerogram and the corresponding elastic response spectrum, respectively.

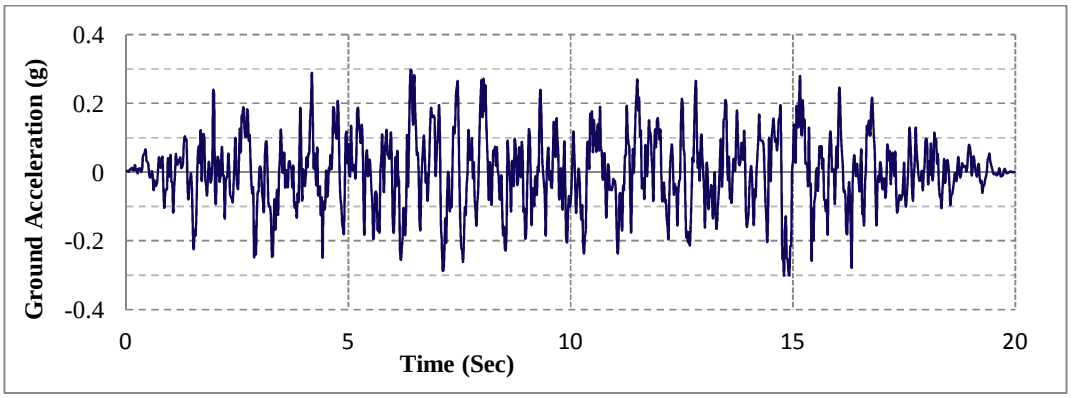

Figure 5-2: Reference ground accelerogram

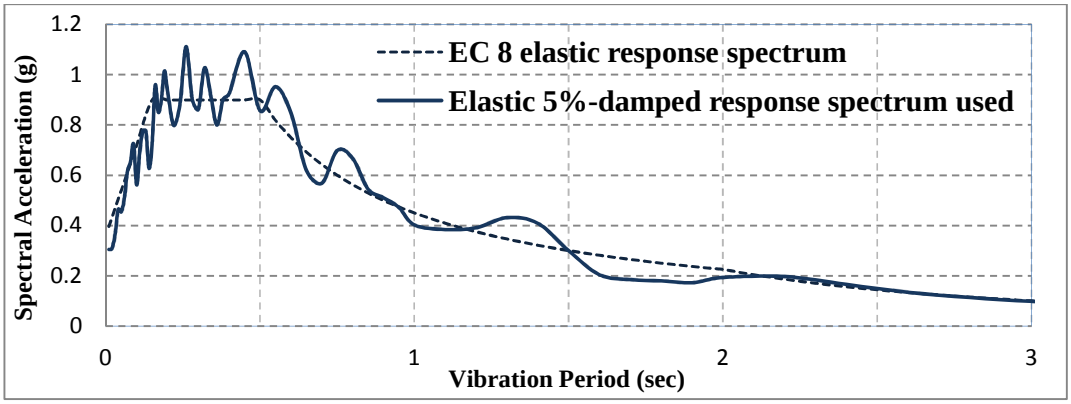

Figure 5-3: Corresponding elastic response spectrum

Although using real records is often desirable, as discussed in Section 6.1.1, using an artificial accelerogram can be more appropriate in this work for the following reasons. Firstly, due to the computational expense of the analyses, only one record will be used in this sensitivity study, which involves around 70 random variables. Moreover, this study focuses on the time at collapse onset, rather than on the collapse capacity, which requires a large set of natural records to be determined. The time at incipient collapse is more sensitive to the selected accelerogram than the collapse capacity. The time at onset collapse depends strongly on the characteristic of the record selected, and the results cannot be generalised for other records with different spectral shape. Secondly, real records are generally scaled, based on the spectral acceleration at the first mode period of vibration, which can significantly change, due to stiffness and strength degradation during the damage propagation. An accelerogram, which matches the EC8 elastic response spectrum, can capture the changes in the dynamic

characteristics. Finally the distribution of the intensity of the selected time history record should be nearly uniform so the structure will be subjected to strong ground shaking during a long duration and will not be governed by the arrival of strong shaking amplitude of real records.

Seismic intensity level should be large enough to cause element separation resulting in progressive collapse. In addition, the seismic demand on the structure needs to be limited. The record intensity should not be very high otherwise it will control the collapse process and will cause instantaneous side-sway collapse, regardless of the structure properties. The tornado diagram analysis will be performed at two intensity levels that satisfy all these requirements. The two desired intensity levels, which are sufficient to cause the structure collapse, are obtained by scaling the accelerogram by factors of 2.85 and 2.35.

5.6 Selection of reference structures for sensitivity analysis

In order to investigate the progressive collapse behaviour of multi-storey structures, two full-scale six-storey RC frames, designed according to EC8, the BF1 and DCF frames, were selected as a test-bed for the sensitivity study. The dimensions and reinforcement details of both structures used are identical to those in Chapter 4, Section 4.3.1. However, the material properties used here differ from those given in Chapter 4. The mean values of the material properties, which are given in Table 5-2, are slightly larger than the mean experimental values, are used in the analytical models.

5.7 Collapse modes

Two different collapse mechanisms were predicted for multi-storey structures, namely side-sway collapse and vertical collapse modes. Deierlein and Haselton summarised the possible side-sway and vertical collapse scenarios for reinforced concrete frame structures, as listed in Table 5-4 (Deierlein and Haselton, 2005). Emphasis will be on the collapse scenarios that occur in the two six-storey frames adopted in this study. It is worth noting that reinforcing bar pull-out failure and the failure of reinforcement lap splices are not possible due to reinforcement details used. Continuous bars are used and the extra bar length then added at the member edges to provide sufficient straight anchorage for reinforcement. The three possible collapse modes are side-sway collapse, pancake collapse and the soft-storey

mechanism. These can each be explicitly considered in the AEM models. Moreover, local failure modes as well as global collapse mechanisms can be captured directly. The likelihood of these collapse scenarios in a specific structure depends on the extent to which seismic design requirements and ductile detailing are used in the design process.

Table 5-4: Possible failure scenarios for RC structures (Deierlein and Haselton, 2005)

Scenario	**Side-sway collapse scenario**	**Scenario**	**Vertical collapse scenario**
	Description		**Description**
FS1	Beam and column flexural hinging, forming side-sway mechanism	FV1	Column shear failure leading to column axial collapse
FS2	Column hinging, forming soft-storey mechanism; a combination soft-storey and side-sway mechanism is also possible	FV2	column flexural-shear failure leading to column axial collapse
		FV3	Punching shear failure leading to slab collapse
FS3	Beam or column flexural-shear failure, forming side-sway mechanism	FV4	Failure of floor diaphragm leading to column instability
FS4	Joint shear failure, possibly with beam and/or column hinging	FV5	Crushing of column leading to column axial collapse; possibly from overturning effects
FS5	Reinforcing bar pull-out or splice failure in columns or beams, leading to side-sway mechanism	FV6	Foundation failure due to uplift or overturning

5.7.1 Concept of mechanism control

Nagae et al. proposed the concept of mechanism control to localise damage in a limited number of storeys by reducing the number of structural members contributing to energy dissipation throughout by strengthening the upper part of structure, without decreasing the collapse capacity (Nagae et al., 2005). They investigated the effects of the extent of the partial collapse mechanism on the collapse capacity of twelve-storey RC frame structures designed to collapse in a complete failure mode involving almost all of the structure storeys. Column strengths are usually designed to be significantly larger than the adjacent beam strengths. Four sizes of collapse mechanism have been examined as follows, a first-storey mechanism, a storey mechanism extending from the first to the fourth storey, a storey mechanism involving all of the first seven storeys and a storey mechanism involving all of the first ten storeys. In each of these mechanisms, plastic hinges are allowed to form only at the beam-ends of the storeys, within the extent of the partial mechanism, in addition to the top column ends in the highest storey in the partial mechanism extents and the bottom ends of the first-storey columns. In the analytical models, only the elements ends that are allowed to inelasticity deform are modelled using inelastic springs. Other members are modelled as elastic elements.

It was concluded that the sum of the maximum plastic rotations of all hinges formed at a specific hazard level and the cumulative hysteretic energies of the entire members are almost the same, regardless of the size of the collapse mechanism (Nagae et al., 2005). At a specific hazard level, a structure consumes approximately a constant amount of energy, regardless of the damage spread. Furthermore, the collapse probability at a given intensity level increases as the partial mechanism size decreases as shown in Figure 5-4. Generally, the energy dissipation is concentred in the lower storeys. Thus, increasing the partial mechanism extent beyond a certain number of storeys (four storeys), will be not be effective as the amount of energy consumed by the upper storeys is small (Nagae et al., 2005).

It was observed that the number of storeys involved in the collapse mechanism of reinforced concrete frame buildings of more than seven storeys is around 25% of the total storey number (Haselton et al., 2011b).

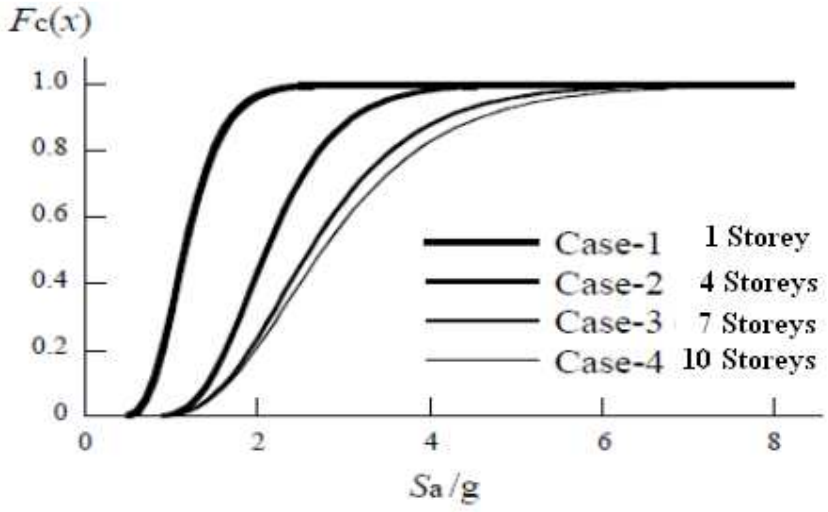

Figure 5-4: Collapse capacity fragility curves (Nagae et al., 2005)

Investigation of the effects of the variation of strength over 8-storey and 12-storey buildings height was performed by Haselton et al. (Haselton and Deierlein, 2008, Haselton et al., 2011b). The strength of the upper storeys of structures was increased, while the strength of the first or both the first and second storeys was held constant in order to have strength ratios of 80% and 65%. The results showed that the collapse margin slightly decreased in the case of weak first and second storey, due to the fact that the predominant collapse mode of the unmodified structures was already a first-second storey mode. Therefore, weakening the lower storeys only resulted in a small amount of localised damage. On the contrary, collapse capacity increased in the case of weak first storey even though the predominant collapse mode was a first storey mode and the strength modification did not change the failure mode. This could be attributed to the fact that the design process caused a slight rise in the inelastic deformation capacity of the first-storey columns, which allowed the energy to dissipate in more storeys and resulted in better seismic collapse resistance.

5.7.2 Beam to column strength ratio

Haselton et al. carried out a study to assess the seismic performance of 30 reinforced concrete structures with ductile special moment-resisting frame systems designed according to modern seismic codes, such as: ICC 2003, ASCE 2005 and ACI 318 (ACI, 2002, ASCE, 2002, ASCE, 2005). Only the side-sway collapse mechanism was considered in this assessment.

They concluded that seismic design provisions can delay the formation of column plastic hinges but do not prevent the occurrence of soft storey mechanisms (Haselton et al., 2008b, Haselton and Deierlein, 2008, Haselton et al., 2011b). Furthermore, it was found that there is often a storey collapse mechanism, in which severe damage is concentrated over a few storeys.

In order to limit the formation of plastic hinges in columns, two methods can be employed, either increasing the strengths of the column with respect to those of beams or decreasing the beam strengths. Haselton et al. investigated the effect of beam strength on the collapse capacity by keeping the column strengths constant and changing the beam strength to vary from 20 to 180% of the design strength. The collapse capacity was found to be relatively higher for beam strength ratios in the range of 60–100%, while the collapse capacity decreased in other cases, where the beam strength ratio was greater than 100% or less than 60% (Haselton et al., 2008b).

Based on the investigation of the influence of the ACI 318 strong-column weak–beam ratio on the seismic collapse resistance of moment resisting frame structures with varying heights, the seismic performance was enhanced by increasing this ratio by up to 1.2 for low-rise frame structures, and to more than 3 for mid- and high-rise buildings, respectively. The number of storeys engaged in the failure mode increased in the latter case due to increase in the plastic deformation capacities of all storeys, while no effects has been noted in the former (Haselton and Deierlein, 2008, Haselton et al., 2011b).

Ibarra and Krawinkler found that code requirements did not prevent the formation of column hinging and that the collapse capacity of generic frames decreased by up to 75% if the strong-column weak-beam factor was 2.4 when compared with the case of using columns with infinite strength (Ibarra and Krawinkler, 2005).

A study of the seismic evaluation of the strength demands of a set of regular moment-resistance frames with various number of storeys illustrated that even though these frames were designed, according to the recent seismic codes, and satisfied the strong-column weak-beam requirements, the possibility of column hinging was relatively high (Medina and Krawinkler, 2005).

Haselton and Deierlein reported that collapse capacity decreases as the strong-column weak-beam ratio reduces, and that increasing this ratio shows no clear trend in increasing the collapse capacity, as shown in Figure 5-5 (Haselton and Deierlein, 2008). This is due to the fact that this study was conducted using a 4-story reinforced concrete frame building and the low-rise building is less sensitive to the changes in this value as mentioned above.

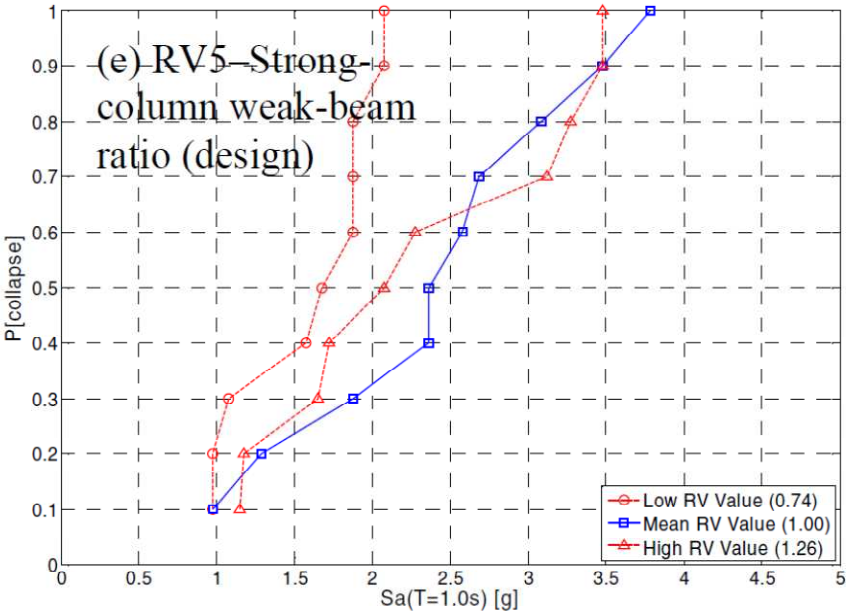

Figure 5-5: Variation in collapse fragility function with strong-column weak-beam ratio varied to ($\mu_{RV} \mp \sqrt{3}\,\sigma_{RV}$) (Haselton and Deierlein, 2008)

The column to beam strength ratio plays an important role in determining seismic collapse behaviour (Zareian and Krawinkler, 2009). Dooley and Bracci suggested utilising a ratio of 2.0 or more to avoid a soft storey mechanism (Dooley and Bracci, 2001).

5.8 Results of sensitivity study

The effect of modelling uncertainties on the seismic collapse process of the BF1 and DCF frames investigated in this study is presented below. The collapse performance will be assessed using an artificial earthquake record with two intensity levels. The concern of this study is on the time at incipient collapse and the corresponding collapse mechanism.

5.8.1 Sensitivity of the time at incipient collapse to each random variable

The variability of the time at incipient collapse, due to uncertainties in the modelling input parameters, is presented in the tornado diagram analyses; the random variables are ordered according to their relative importance. Figures 5-6 and 5-7 show how the random variables, type 1 and 2 correlation, affect the time of collapse onset for the BF1 and DCF frames, respectively. The effects of uncertainties in the correlated random variables of type 3 on the time of collapse onset are depicted in Figures 5-8 and 5-9 for the BF1 and DCF frames, respectively.

The reference values for the tornado diagram analysis for the BF1 frame are 15 and 4.2 sec for PGA level of 0.7 g and 0.86 g, respectively. Similarly, the reference values for the DCF frame are 10 and 4.1 sec for PGA level of 0.7 g and 0.86 g, respectively. A relatively small increase in the seismic intensity results in significantly earlier collapse in both frames. Moreover, the frame BF1 collapses in different failure modes due to an increase of 0.16 g in the seismic intensity. Changing the intensity level alters the order of the importance of the random parameters for correlation of type 1, 2 and 3. The most important random variables for the DCF frame are: f_u, $Mass$, $f_{u,b}$, $f_{u,c}$, $f_{c,b}$, $f_{y.u,c}$ and $E_{c,c}$ at 0.86 g and $f_{y.u,c}$, $f_{y.u}$, $f_{u,c}$, $E_{c,c}$, $Mass$, $f_{c,c}$ and f_u at 0.7 g. For the BF1 frame, the most critical random variables are $E_{c,c}$, $f_{y.u,b}$, $f_{y.u}$, $f_{c,b}$, $Mass$, $f_{c,c}$ and f_u at 0.86 g and $Mass$, $f_{u,c}$, f_u, $f_{u,b}$, $f_{y.u,c}$, $f_{y.u}$ and f_c at 0.7 g. Thus, seismic intensity is one of the most important factors controlling the collapse process. It is worth noting that the effects of scaling random variables on the time at incipient collapse increase in response to a decrease in the seismic intensity level.

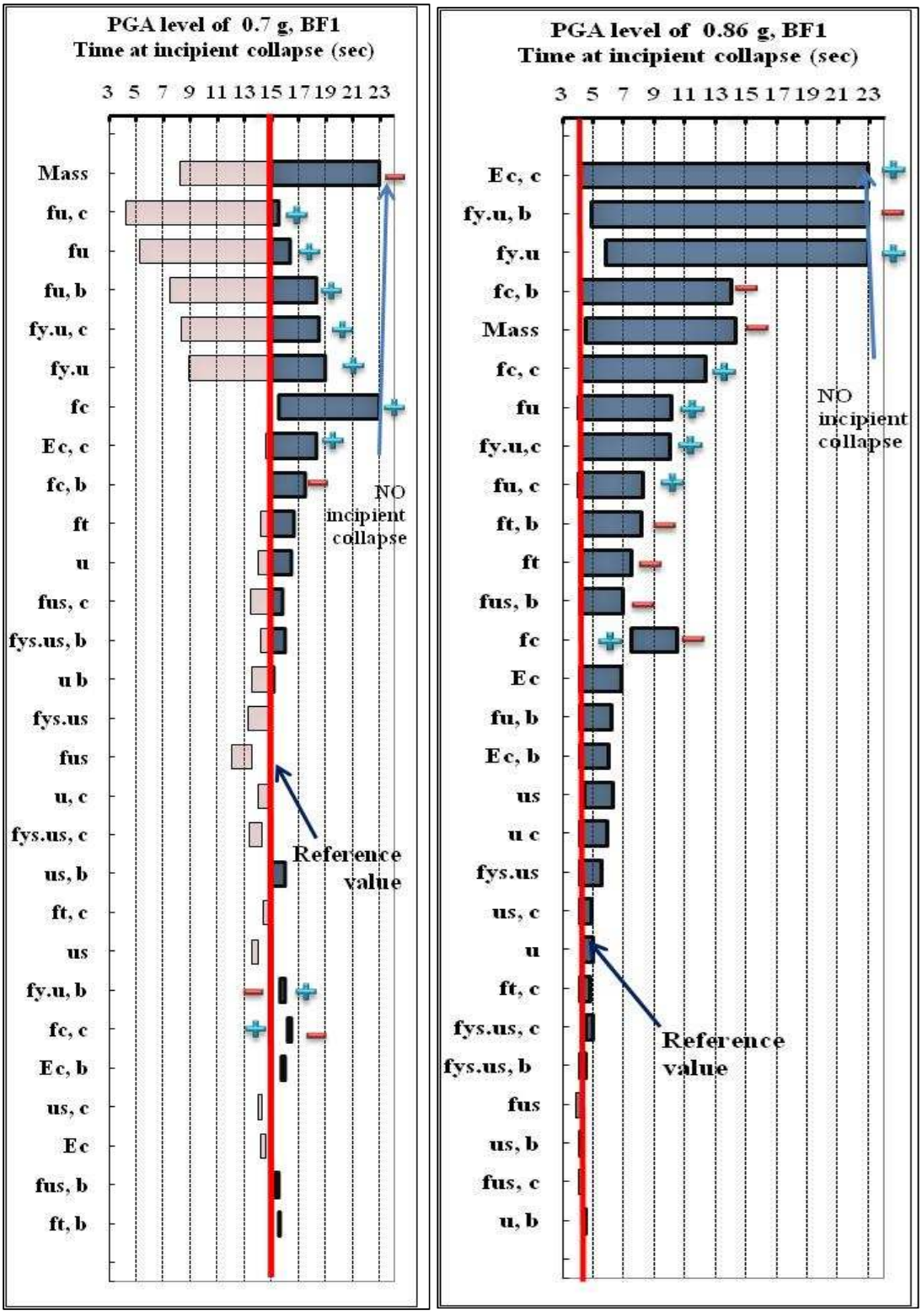

Figure 5-6: Tornado diagram analysis for sensitivity of the time at incipient collapse for the BF1 frame, type 1 and 2

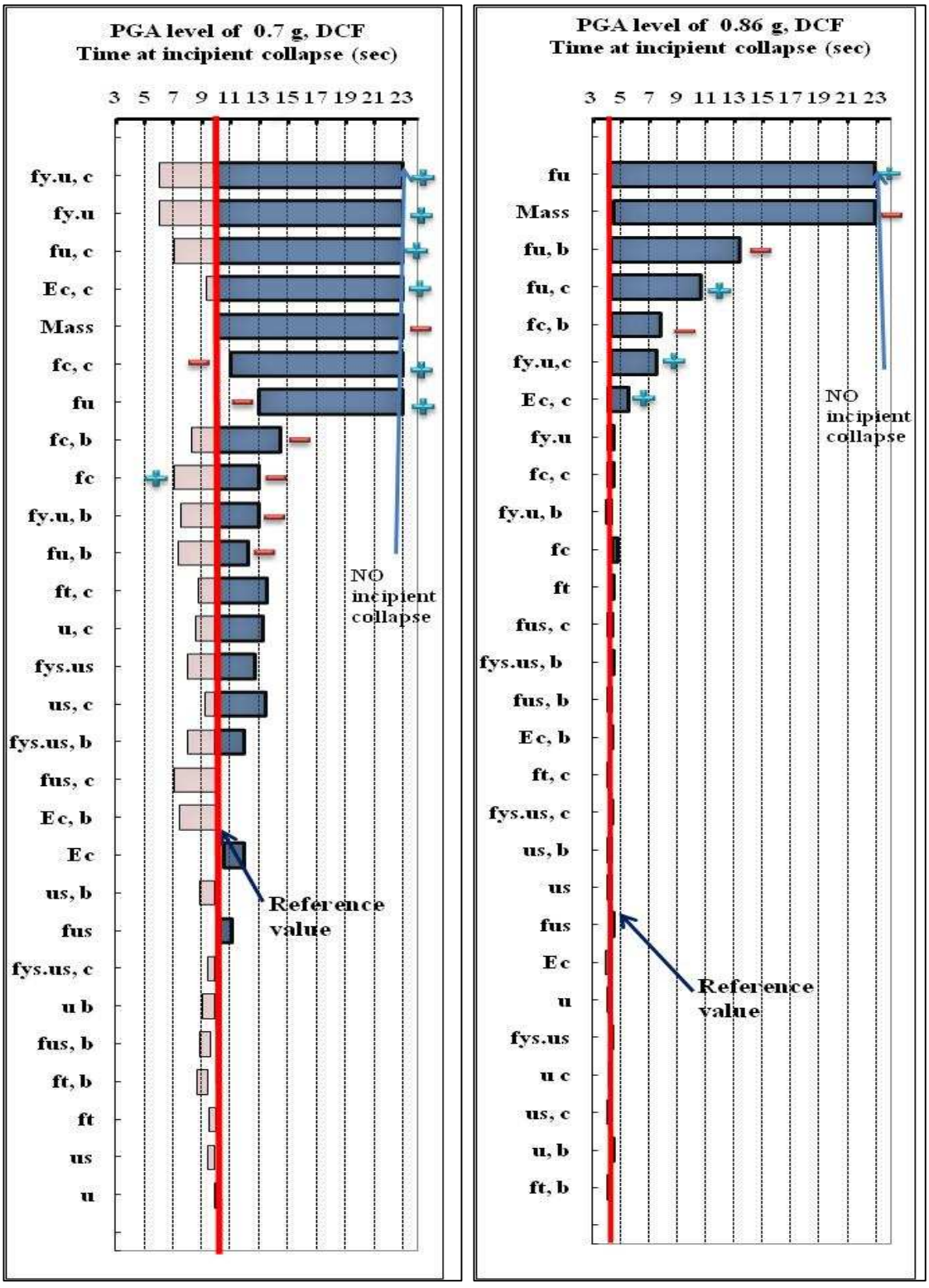

Figure 5-7: Tornado diagram analysis for sensitivity of the time at incipient collapse for the DCF frame, type 1 and 2

In general, it has been found that the effects of the selected parameters are governed by collapse mode, the damage localisation and the secondary effects during the collapse process, such as the impact between different elements and force redistribution following the element separation. As previously mentioned, the energy dissipated in structures at a given intensity levels is constant, regardless of the damage pattern (Nagae et al., 2005). Thus, the effects of changing the input modelling parameters can either lead to a concentration of damage in a single or two storeys resulting in earlier collapse, or to distributing the structural damage throughout the whole structure. Hence, the collapse of the structure will be avoided, or the time at the collapse onset will be delayed.

The order of the importance of the random variables varies according to the structural system, the correlation type and the seismic intensity.

5.8.1.1 Sensitivity of the time at incipient collapse to each random variable (Type 1 and 2 correlation)

Observations from Figures 5-6 and 5-7 regarding how scaling the random variables to $\mp 1.28\sigma$ influences the collapse process of the BF1 and DCF frames are as follows:

Concerning the material properties, the time at collapse onset is often most sensitive to the longitudinal reinforcing steel strength, $f_u, f_{y.u}$, followed by the concrete compressive strength, f_c. Increasing the strength of the longitudinal reinforcing steel in the entire structure, or in all of its columns, leads to a considerable increase in the strength of the corresponding structure, resulting in a stronger structure capable of resisting the seismic loadings.

Regarding the member type, it has been found that increasing the column strength is more effective in delaying the collapse onset than reducing the beam strength at the lower intensity level, 0.7 g. On the contrary, decreasing the strengths of the structure beams is better than enhancing the column strength of the entire frame, when delaying or preventing the collapse occurrence of both frames at higher intensity level. This is due to the fact that the increase in column strength is insufficient to prevent the column hinging at high PGA levels. Increasing the values associated with the column strength, e.g. $f_{y.u,c}$, $f_{u,c}$ and $f_{c,c}$, generally postpones the time at incipient collapse, or avoiding structural collapse.

One of the most important variables is the gravity load in terms of the live load applied, and hence the corresponding distributed masses. In the case of full occupancy, seismic forces and the gravity loads are higher, leading to a decrease in column capacities and resulting in earlier soft-storey mechanisms. On the contrary, the seismic demands on a structure and the gravity-induced axial loads on the columns are less in the case of no occupancy. Utilising a zero live load factor results in avoiding or delaying the occurrence of collapse, e.g. the time at collapse incipient of the BF1 frame is postponed by 10 sec at 0.8 g. The DCF frame survives seismic forces without collapse at both PGA levels in the case of zero live load factor, but the BF1 frame experiences no collapse at the low seismic intensity only.

It is worth noting that changing most of the parameters related to the strength of the beams and the structure mass have an inverse effect on the time at incipient collapse. Thus, decreasing their values often results in delaying the time of the collapse onset and vice versa. The random variable associated with the column stiffness, $E_{c,c}$, has a considerable impact on the collapse process, and increasing the value of this parameter may delay the collapse occurrence, while no effects has been noted when its value reduces. The sensitivity of the time of the collapse onset to the random variable related to the beam stiffness, the initial modulus of elasticity of concrete in the beams, is insignificant. In addition, the concrete tensile strength is not an important variable to the collapse process. The least important parameters are the parameters related to the transverse reinforcing steel. Changing these parameters has a slight effect on the time of incipient collapse, less than 1.8 sec as observed from the sensitivity analyses.

To understand why there is some differences in the effects of the random variables on the collapse process of both frames at the two PGA levels, a closer look at the most important variables has been undertaken in the next section.

As previously mentioned, the formation of column hinging can be delayed or limited by either decreasing the beam strengths and keeping the column strength constant, or by increasing the strengths of the columns without changing the beam strength. The results show that reducing the beam strength has a larger impact on delaying the collapse onset than increasing the column strength at the high intensity level, whilst the opposite occurs at the lower intensity levels. The explanation for this maybe that both frames collapse in a soft first-storey mechanism, controlled by the strength of the members of the first storey at high

intensity level. Delaying the first-storey collapse onset can be achieved by increasing the strength of the first storey column or reducing the strength of the members in the upper storeys or the beams of the first storey. As a full correlation has been assumed between all similar structural members located at all storey-levels, increasing the strength of the first-storey columns accompanies a relatively smaller increase in the column strengths of other storeys according to their dimensions and reinforcement amounts. However, the increase in the column strength is not enough to considerably change the damage distribution; and thus affecting the corresponding failure mode, the soft first-storey mode. While reducing the beam strength of the entire frame leads to better damage distribution over the structure height, there is more damage localisation in the beams rather than in the columns, resulting in a different damage pattern. For example, the BF1 frame collapses in a pancake mode due to the impact between the falling beams, the beams in the fifth storey, and the structural beams below as a result of scaling $f_{c,b}$ to -1.28σ, and this frame does not experience collapse as a result of scaling $f_{y.u,b}$ to -1.28σ.

It is worth noting that the effect of uncertain parameters is not symmetric. At high seismic intensity, both frames are governed by a first-storey mechanism, which occurs approximately at 4 sec. The arrival of strong motions starts around 2.5 sec. Hence, only the effects of uncertainties in random variables on enhancing the seismic performance of structures can be investigated at this intensity level, as the structures are not expected to collapse earlier. At a lower PGA level, the focus is more on selecting the random variables that can lead to earlier failure, less than 15 or 10 sec, since both frames are subjected to a long duration of a shaking motion and are on the verge of collapse.

In certain cases, decreasing the column strength or increasing the beam strength may prompt the opposite trend leading to a delay in the collapse onset, instead of causing earlier collapse. This could also be attributed to the variation in the collapse mode and the significant changes in member strength, which are sufficient for causing a structure to collapse in a different mechanism, e.g. $f_{u,b}$ in the BF1 frame at 0.7 g. Surprisingly, it has been found that scaling $f_{u,b}$ of the BF1 frame results in the opposite trend. Reducing the value of $f_{u,b}$ modifies the collapse mode from a multi-storey mechanism to a fifth soft-storey mechanism, which takes place 8 sec earlier at 0.7 g, and increasing it leads to extending the partial collapse mechanism over three storeys and to 3.5 sec delay to the collapse onset.

Moreover, decreasing and increasing the value of some random variables may show a similar trend, especially at low seismic intensity, e.g. $f_{c,c}, f_{y.u,b}, f_c$ in the BF1 frame and $f_{c,c}, f_u$ in the DCF frame at 0.7 g. This could be also due to the variation in the possible collapse modes and the corresponding damage distribution throughout the entire structures. Based on the sensitivity study results, it has been observed that the frame BF1 collapses in various failure modes, varying from a single soft storey to different multi-storey mechanisms at the PGA of 0.7 g. Furthermore, a combination of vertical and side-sway collapse modes has been noted in several cases. Asymmetric effects have often been observed when scaling random variables switches the failure mode. More information about the potential collapse modes of both frames are presented in the next section.

For instance, scaling the $f_{y.u,b}$ to $\mp 1.28\sigma$ delays the collapse onset of the BF1, due to the formation of two different failure mechanisms. Increasing the $f_{y.u,b}$ leads to a vertical collapse mode, involving the third and fourth storeys. Reducing the value of this variable results in a side-sway collapse over three storeys, from the third to the fifth-storey. A reduction in the value of f_c changes the collapse mode of the BF1 from a first-storey mechanism to a third soft-storey mechanism, which postpones the time at incipient collapse by 6.5 sec at a PGA level of 0.86 g.

The asymmetric effects in the response of the DCF frame are less because this frame generally collapses in a first-storey mechanism with slight damage concentration in the third or the fifth-storey. At a PGA level of 0.7 g, changing the value of f_c of the entire DCF frame adversely influences the collapse onset. This could be due to changes in the ratio of the strong-column weak-beam as a result of the relative changes between the strength of the columns and those of the beams, which depends on the member dimensions. Further investigation of some of these counterintuitive effects is still required.

Increasing the value of f_y while keeping the value of f_u constant shows an opposite trend in all cases, $f_y, f_{y,c}, f_{y,b}$. This is due to the fact that for a large value of f_y, the value of the corresponding ratio of f_u/f_y is relatively small. Seismic collapse is more sensitive to changes in the value of this ratio. Reducing this ratio in columns often leads to earlier collapse despite the increase in the value of f_y. For example, when $f_{y,c}$ decreases without changing the value of f_u, the frame DCF does not collapse at both intensity levels, and the

collapse of the BF1 frame delay by 7 sec at an intensity level of 0.86 g. The swings representing the effects of these random variables have been omitted from the tornado diagram.

Correlation between random variables for different members could considerably affect the results of the sensitivity studies. A comparison between two cases, namely type 1 and type 2, shows that the order of the importance of the random variables does change dramatically as well as the swing of these parameters around the reference value. For instance, the effect of increasing the concrete modulus of elasticity in both beams and columns has insignificant effect contrary to the effect of raising only that of the columns, which may postpone the collapse onset. Furthermore, altering the strength of the beams or columns has more effect than changing the strength of both. This is due to the fact that the strong-column weak-beam ratio plays an important role in governing failure modes and distributing the damage throughout the structures, as mentioned above.

Capturing the effects of uncertainty in correlated parameters is complex. It necessitates taking appropriate correlations between the structure random variables into account when quantifying the uncertainty in the structure performance at the collapse stage. Haselton et al. stated that the uncertainty in collapse capacity is significantly affected by the degree of correlations between random parameters (Haselton et al., 2008b). To understand the effects of correlations between random variables for different storeys, type 3 correlation, a second sensitivity study has been carried out using the most important random variables, based on the results of the first sensitivity study. The dominant contributors to the time at incipient collapse of both frames are: $E_{c,c}$, f_c, f_u, $f_{y.u}$, $f_{c,c}$, $f_{u.c}$, $f_{y.u,c}$, $f_{c,b}$, $f_{u,b}$, $f_{y.u,b}$.

5.8.1.2 Sensitivity of the time at incipient collapse to each random variable for different storeys (Type 3 correlation)

Figures 5-8 and 5-9 show how changing the random variables for different storeys affects the time at incipient collapse. Comparing the results of the first and second sensitivity studies shows that the swing lengths in tornado diagrams are larger in the case of type 3 correlation, indicating the significant impact of the correlation between storey strength on the collapse process. Changing the strength of a single or two storeys without modifying the strength of

the other storeys may result in a single or two weak storeys. Hence, the damage will be localised in a weak area leading to unexpected collapse modes.

The dominant failure mode of the DCF frame is a first-storey mechanism combined with damage localisation in the fifth storey at 0.86 g, and with damage concentration in the third storey at 0.7 g. The collapse of this frame can be delayed or prevented using two strategies as follows: Firstly, significantly increasing the strength of the first-storey member, especially those of the columns. Secondly, weakening the strength of the fifth or of the third storey compared to that of adjacent storeys, in order to allow more energy to dissipate in the weak storey and to reduce the cumulative sum of column plastic rotations in the first storey. The latter can be achieved by either reducing the column strength of the storey or increasing the strength of those of the adjacent storey. The results of sensitivity analyses provide insight into the effectiveness of the modification of the parameters governing the strength or stiffness of a single or couple of storeys.

The most influential random variables for the DCF frame are those related to the strength of the first-storey columns, followed by those affecting the column strength in the upper storeys. The most important random variables are: $f_{y.u,c1}, f_{u,c1}, f_{y.u,c3.4}, f_{u,c3.4}, f_{c,c1}, f_{u,1}$ at 0.86 g; and $f_{c,c1}, f_{u,c5.6}, f_{u,5.6}, f_{y.u,c1}, f_{u,c1}, f_{y.u,1}, f_{u,1}$ at 0.7 g.

The collapse can be avoided by significantly increasing the column strength at the first storey or at the upper storeys due to increasing the value of ($f_{y.u,c1}, f_{u,c1}, f_{c,c1}, f_{y.u,c3.4}, f_{u,c3.4}, f_{u,c5.6}, f_{u,5.6}$). It is interesting to note that increasing as well as reducing the strength of columns at the third and fourth storeys, C3 and C4, can lead to delay or prevent the collapse occurrence at both intensity levels. However, reducing the strength of these columns is less effective. This may be because weakening the strength of the C3 and C4 allows collapse to be triggered in these storeys.

Modification of the strength of the third and fourth storeys has a larger impact than modifying that at the fifth and six storeys at high PGA levels; while the effects of changing the fifth storey's strength are more significant at the lower PGA level. This could be because the collapse mode migrates to the upper storeys, the third, fourth storeys, and the fifth storey, under lower PGA levels. Thus, the contribution of strength of the third and fourth storeys in damage redistribution becomes larger.

Altering the strength of a single or two storeys has a larger influence than changing the strength of the entire structure. At the lower storeys, weakening the strength of any structural member, excluding that of the first storey columns, can delay the time of the collapse onset. This is due to the formation of plastic hinges in these members.

Weakening the strength of any of the four upper storeys will not cause earlier collapse, unless the predicted collapse mode of the structure is changed to another failure mode. Therefore, the predicted time of collapse onset does not increase with decreases in $(f_{u,c5.6}, f_{u,5.6}, f_{u,c3.4})$ at the PGA level of 0.7 g. The alteration of the damage pattern due to scaling some random variables is the main reason for asymmetric effects.

For the BF1 frame, the most critical random variables are $(f_{c,c1}, f_{u,c2}, f_{y.u,c1}, f_{u,2}, f_{u,b1}, E_{c,c1}, f_{u,b2}, f_{u,c1})$ and $(f_{u,c3.4}, f_{u,c5.6}, f_{y.u,c3.4}, f_{u,3.4}, f_{u,1}, f_{u,c1}, f_{y.u,c5.6}, f_{y.u,1})$ at 0.86 g and 0.7 g, respectively. It has been found that the effect of the second storey strength on the time at incipient collapse at the PGA of 0.86g is larger in the BF1 frame than in the DCF frame. This could be due to the dominant first storey mechanism, in which slight damage is predicted in the upper storeys at the higher PGA level. Thus, the strength of the first storey and the surrounding storey are the most important when compared with those of the remaining storeys.

Improving the strength of the first storey by enhancing the column strength or reducing the beam strength can delay the occurrence of collapse while the strength of the second storey column has inverse effects on the time at incipient collapse. The reason could be that strengthening the second storey columns or weakening its beams forces the energy to dissipate in the first storey members, particularly in the columns.

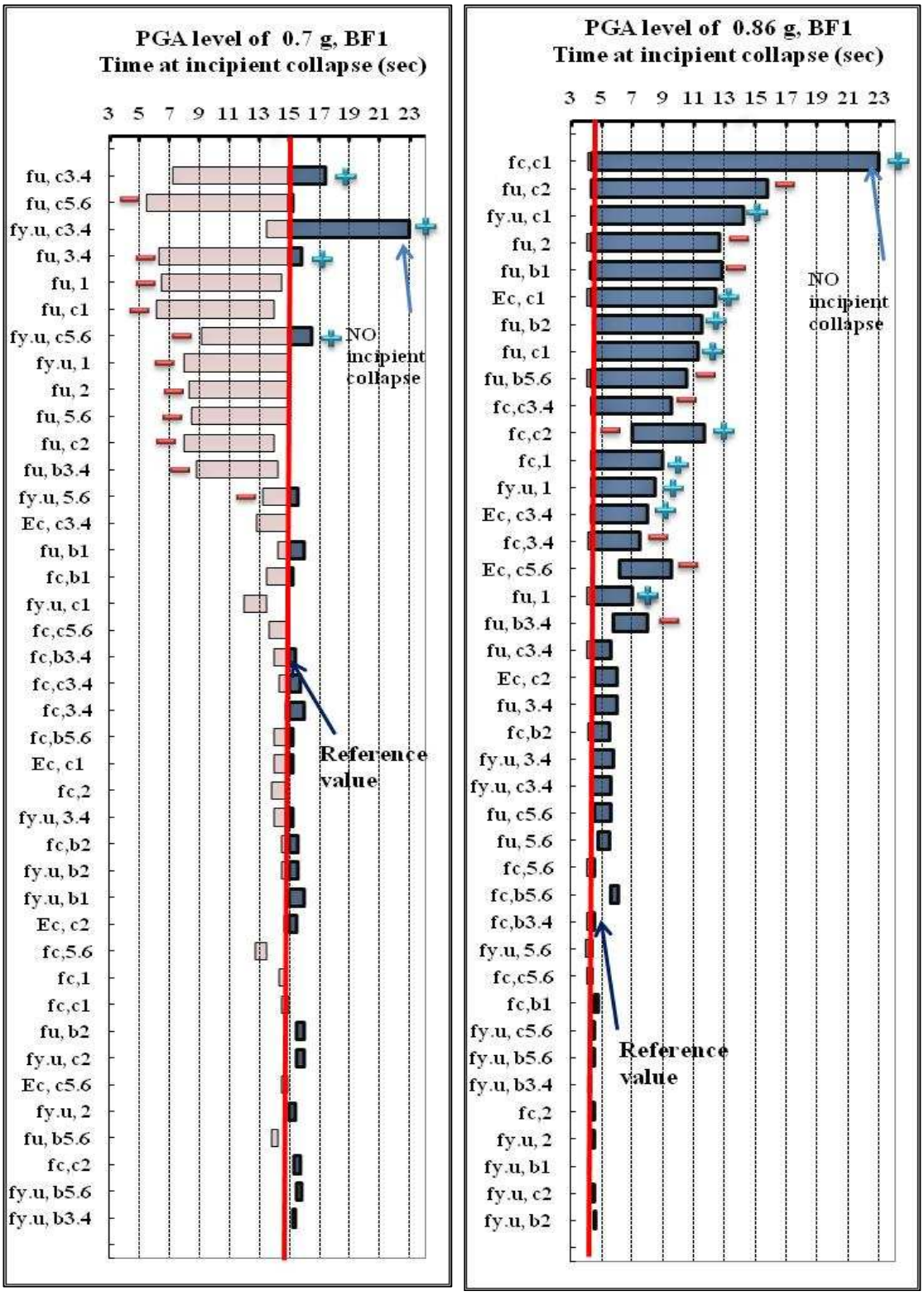

Figure 5-8: Tornado diagram analysis for sensitivity of the time at incipient collapse for the BF1 frame, type 3

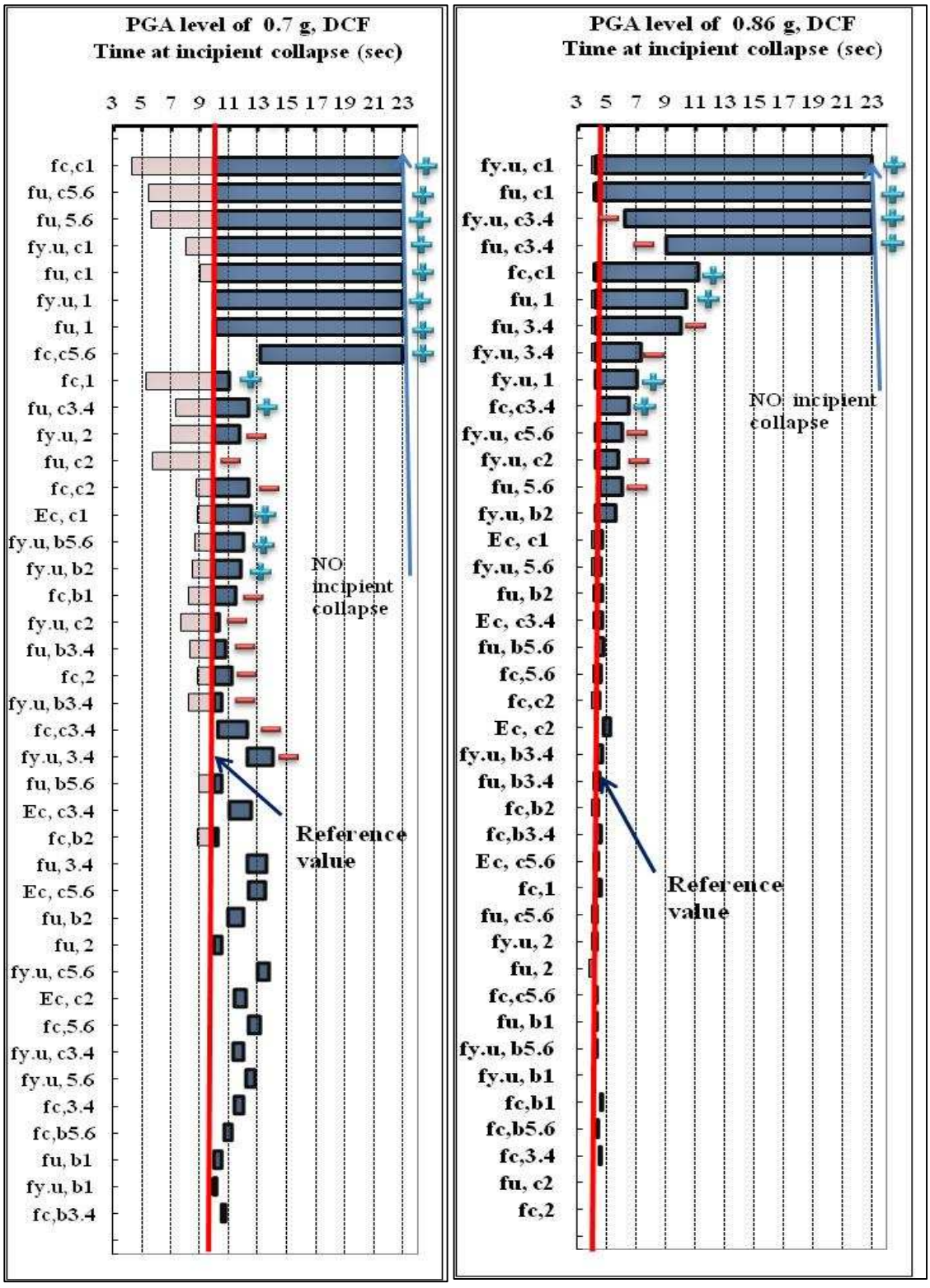

Figure 5-9: Tornado diagram analysis for sensitivity of the time at incipient collapse for the DCF frame, type 3

The strength of the upper storeys has a considerable effect provided the collapse mode is modified. For example, the first storey collapse mode can be altered to a fourth and fifth storey failure mode by weakening the beam strength of the two upper storeys, as a result of reducing $f_{u,b5.6}$. Similarly, a decrease in $f_{u,b3.4}$ causes a pancake collapse, due the impact between the falling beams of the fourth storey and the lower structural members.

At the lower intensity level, the structure can experience several failure modes. Most of these possible collapse modes involve several storeys at the upper part of the structure. Therefore, the structure is more sensitive to the strength of the columns in the four upper storeys and decreasing the steel strength in these columns often results in earlier failure. The effects of enhancing the strength of a couple of storeys at the upper part on the onset of collapse are not significant as the failure mode moves to the neighbouring storeys. Thus, the possible collapse modes are the dominant factor in determining the order of the selected random variables.

Generally, the steel strength of all the columns in the different storeys has larger effects as decreasing this value leads to failure modes concentrated in the corresponding storey to the scaled random variables. For instance, scaling all the following random variables ($f_{u,c3.4}$, $f_{u,c5.6}, f_{y.u,c3.4}, f_{u,3.4}, f_{u,1}, f_{u,c1}$, $f_{y.u,c5.6}, f_{y.u,1}$) to -1.28σ causes the damage to localise in the corresponding storeys and switch the failure mechanism. Only enhancing the columns located at the middle storeys, 3 and 4, leads to a delay in the time at incipient collapse. This could be due to the fact that the damage, which is expected to occur in these two storeys without the scaling, has been redistributed between the upper as well as the lower storeys of the 3 and 4 storeys.

It has been found that maximum storey drift ratio and the maximum horizontal displacement prior to the start of the unrestrained increase of displacements are ineffective measures for assessing the importance of each uncertain parameter on progressive collapse behaviour, especially in the case of vertical collapse, similar to the conclusion of Talaat and Mosalam (Talaat and Mosalam, 2008). A vertical failure mode often results in a smaller storey drift ratio than those of side-sway collapse. With respect to the side-sway collapse mechanism, the earlier a single-storey mechanism forms, the smaller values of both the maximum storey drift ratio and horizontal displacement prior to the onset of collapse are

obtained. This is due the concentration of damage in a single storey instead of the formation of uniformly distributed plastic hinges throughout the structure. Thus, these observations concur well with the results of a study on mechanism control performed by Nagae et al. (Nagae et al., 2005). Furthermore, no clear trend in these measures has been mentioned in such cases without collapse.

The collapse mechanisms obtained from the analyses will be discussed in more detail in the following section.

5.8.2 Results of sensitivity study on the collapse mechanism

The potential collapse modes predicted by the nonlinear dynamic analyses are listed in Tables 5-5 and 5-6, which summarise the primary modes of all collapse cases of both selected frames. In order to clarify the failure modes, the mechanisms are depicted for the point after the collapse onset after the separation of the structure members takes place. Nonlinear time history analyses revealed that modelling uncertainties could lead the BF1 frame to collapse in at least five different collapse mechanisms at both PGA levels for the three correlation types. However, the DCF frame has only one common failure collapse mode, a first-storey collapse mode, for the correlation type 1 and 2. It is interesting to note that only the type 3 correlation results in three additional collapse mechanisms at both intensity levels. These potential failure modes are associated with the stepping of columns sizes throughout the structure.

The predominant collapse mode of the BF1 frame at a PGA level of 0.86 g is a global collapse mode, due to a single first-storey mechanism, while a multi-storey mechanism at upper storeys takes place at a PGA level of 0.7 g. It is noted that the soft storey mechanism often migrates from the lower to the upper storeys as a result of decreasing the seismic intensity for specific accelerograms, and is consistent with the findings of (Zareian et al., 2010, Aslani and Miranda, 2005).

It has been observed that most members in the upper part of the structure exhibit severe damage before the onset of collapse at a lower intensity, generally vertical or multi-storey collapse modes. Side-sway collapse is more likely to occur at high intensity levels.

Even though the collapse behaviour of the BF1 frame structure is governed by two predominant failure modes associated with the PGA level, different collapse mechanisms, such as: side-sway referred to as 'S', and the vertical collapse mechanism noted as 'V', may occur due to uncertainties in the input parameters.

As can be seen in Tables 5-5 and 5-6, common collapse modes are either a single soft storey mechanism, which takes place at one of the fifth bottom storeys, or a multi-storey mechanism extending over more than a single storey.

The predicted single-storey side-sway collapse mechanisms are as the following: a first-storey collapse mode, S1; a second-storey failure mode, S2; a third-storey collapse mechanism, S3; a fourth storey collapse mode, S4; and a fifth-storey failure mode, S5. Two additional side-sway collapse modes were predicted, namely: S3+4 and S4+5. The former is a soft storey mechanism over the third and fourth storey together, and the latter is a side-sway mode over the fourth storey and fifth storey together. Side-sway collapse mechanisms occur due to hinging of the beams and columns in the storey, where the soft-storey is happened.

As regards the vertical collapse mode; four vertical failure modes have been predicted V3, V4, V5 and pancake collapse, due to the impact of the falling beams on the lower parts of the structure. The first three vertical collapse modes occur due to flexure-shear failure of the middle columns of the storeys.

The correlation type between random variables has a significant effect on potential collapse modes. In particular, the correlation of type 3 results in additional different failure modes in both frames compared to the cases of correlation type 1 and 2. Only one failure mode has been predicted in the DCF frame using correlation type 1 and 2, and correlation type 3 can considerably switch the collapse mode. Thus, the collapse of structures can be prevented by altering the strength of the columns located at a single storey rather than changing the entire structure strength.

Table 5-5: Potential collapse mechanisms and the number of occurrence of each failure mode for the BF1 frame

Collapse mode		**0.87 g**	**0.7 g**
S1	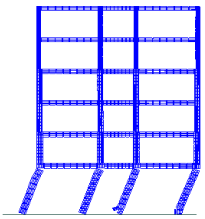	45 51	$+f_t$ $+f_{us,c}$ $-f_{u,1}, -f_{u,c1}, -f_{y.u,1}, -f_{y.u,c1}$
S2	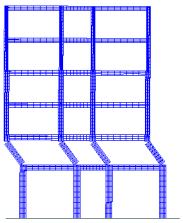	- - $-f_{u,c2}, +f_{u,c1}, -f_{u,2}, +f_{u,1}$	- - $-f_{u,c2}, -f_{u,2}$
S3	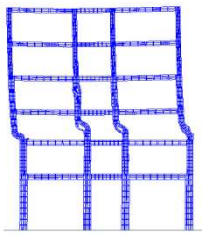	$+f_u, -f_c$ - -	$+f_{y.u}$ $+f_{us,b}$ $-E_{c,c2}, +f_{u,c1}, +f_{u,c5.6}$
S4	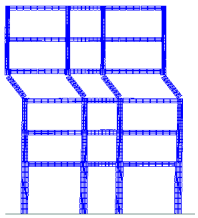	- - -	- - $-f_{u,c3.4}$
S3+4	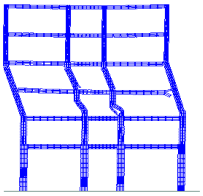	- - $-f_{c,c2}$	- - $-f_{y.u,c3.4}, +f_{y.u,c1}, +f_{c,c3.4}, +E_{c,c3.4},$ $-f_{u,b2}, -f_{u,b}, -f_{c,1}, -f_{c,c1}, +f_{c,2}$
S4+5	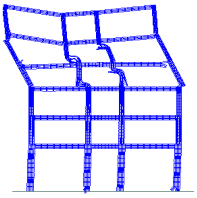	- $-f_{us,b}$ $-f_{u,b5.6}$	- - -

S5	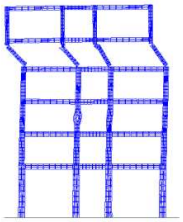	$+f_c$, $-f_u$, $+f_{u,c}$, $-f_{u,5.6}$ $-f_{u,c5.6}$, $+E_{c,c3.4}$, $-f_{c,3.4}$ $+f_{y.u,c1}$, $+f_{c,c2}$	$-f_u$, $-f_{y.u}$, $-f_{u,c}$, $-f_{u,b}$, $-f_{y.u,c}$ $-f_{y.u,2}$, $-f_{y.u,5.6}$, $-E_{c,c3.4}$, $-f_{u,5.6}$ $-f_{c,c5.6}$, $-f_{u,c5.6}$, $-f_{y.u,c5.6}$
V3	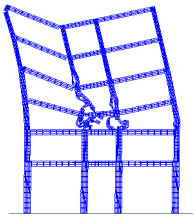	$-$ $-$ $+E_{c,c1}$, $-E_{c,c5.6}$, $-f_{c,c3.4}$	$+f_u$, $+f_{us}$, $+u_b$ $+f_{u,c2}$, $+f_{c,c2}$, $+f_{c,c1}$, $+f_{y.u,c5.6}$ $+f_{c,3.4}$, $-f_{y.u,b3.4}$, $-E_{c,c1}$ $+f_{y.u,b5.6}$, $+f_{c,1}$, $+f_{y.u,b1}$, $-E_{c,c5.6}$ $+f_{u,1}$, $+f_{u,c5.6}$, $-f_{y.u,b1}$, $+f_{u,2}$
V4	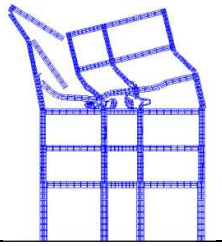	- - -	- - $+f_{y.u,5.6}$, $-f_{c,c2}$, $+f_{c,5.6}$, $-f_{y.u,3.4}$, $+f_{c,b2}$
V5	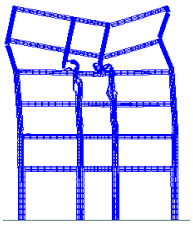	- - -	- - $+f_{y.u,3.4,}+f_{c,c5.6}$
Multi-storey	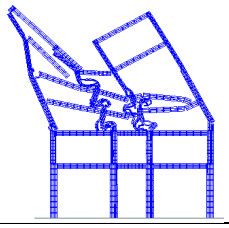	- - -	42 30
Beam impact	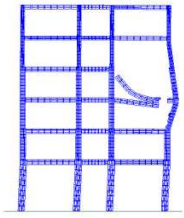	$-u_s$ $-f_{c,b}$, $+f_{y.u,c}$ $-f_{u,c3.4}$, $-f_{u,3.4}$, $-f_{u,b3.4}$	$-f_{us}$ - $-f_{u,3.4}$
Non collapse		$+f_{y.u}$ $+E_{c,c}$, $-f_{y.u,b}$, $+f_{c,c1}$	$-$Mass, $+f_c$ $+f_{y.u,c3.4}$

Table 5-6: Potential collapse mechanisms and the number of occurrence of each failure mode for the DCF frame

Collapse mode		**0.87 g**	**0.7 g**
S1	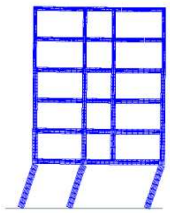	55 71	50 58
S3+4	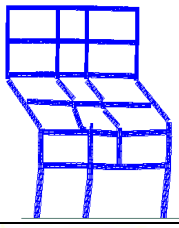	- - -	- - $-f_{u,c3.4}$
S4+5	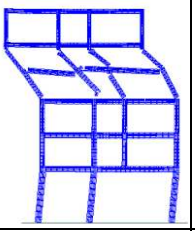	- - $-f_{u,c3.4}$	- - -
S5	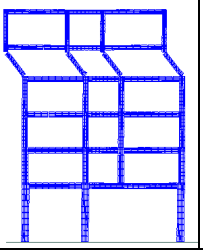	- - $+f_{y.u,1}, -f_{u,5.6}, -f_{u,c5.6}$	- - $-f_{u,5.6}, -f_{u,c5.6}$
Beam impact	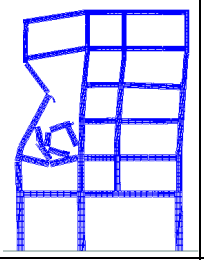	- - $-f_{u,3.4}$	- - $-f_{u,b3.4}$
Non collapse		$+f_u$, $-$Mass - $+f_{y.u,c1}, +f_{u,c1}, +f_{u,c3.4}, +f_{y.u,c3.4}$	$+f_u, +f_{y.u}, -$Mass $+f_{y.u,c}, +E_{c,c}, +f_{c,c}$ $+f_{y.u,c1}, +f_{c,c1}$, $+f_{c,c5.6}$, $+f_{u,1}$ $+f_{u,5.6}$, $+f_{u,c1}, +f_{u,c5.6}$, $+f_{y.u,1}$

The propagation of failure is strongly affected by several factors. These factors are the type of the structural elements that initiate the collapse process, e.g. a beam or a column, the location of this element, e.g. a beam at an exterior or an interior bay, an exterior or an interior column at lower or upper stories, the number of the damaged elements and the capacity of the neighbouring members.

Moreover, the collapse scenarios may change dramatically, due to secondary effects, such as impact between elements and force redistribution. Ignoring these effects may lead to inaccurate predictions of the collapse modes or un-conservative estimation of the collapse probabilities, due to the exclusion of some possible collapse mechanisms. For example, the impact of falling beams on the structural members located at the lower storeys is the main cause of collapse in several cases, as seen in Tables 5-5 and 5-6. Furthermore, failure of the majority of beams at a single storey level can result in a formation of tall columns and consequently a collapse mechanism. In all collapse cases, complete collapse occurs due to the impact forces resulting from collision between the falling elements and the severely damaged members at lower storeys.

Although the design of the structure satisfies the strong-column weak-beam principle and a complete ductile collapse mode is anticipated to occur under the earthquake forces, plastic hinges form in columns in most cases of collapse. These results are consistent with the findings of other researchers, which are mentioned in Section 5.7.2 (Haselton et al., 2011b, Zareian and Krawinkler, 2009). As the same amount of energy is dissipated at a given seismic intensity, the desirable failure mode can be obtained provided the severe damage is uniformly distributed throughout the structure beams and column hinging is limited. Avoiding soft storey mechanism can contribute towards delaying the onset of collapse or preventing it. Therefore, a control mechanism where energy dissipates in the hinging of many beams located in predefined area of a certain number of storeys has been suggested. However, controlling the failure modes can improve the structure performance and its collapse capacity to a certain degree as previously mentioned by (Nagae et al., 2005).

The conclusions of this study provide an insight into the importance of uncertain modelling parameters on the collapse modes. The secondary effects are a primary contributor to the collapse of both frames in several cases and play an important role in determining the next the structural members to progressively separate in all of the collapse cases.

5.9 Conclusions

The effect of uncertainty in material properties on the collapse process has been investigated. The conclusions here are subjected to the assumptions and limitation of the modelling approach. The major findings regarding the effects of a selected set of uncertain parameters with different correlations, on the time at incipient collapse and the corresponding failure mechanism, are summarised below:

- The order of the importance of the random variables depends upon the structural system, the correlation between the random variables and the seismic intensity level.
- Seismic intensity is one of the key factors that governs the collapse process.
- The most important variables are those in which variations can change the collapse process and lead either to a more uniform damage distribution with a larger number of structural members involved in the collapse mechanism or to more damage localisation and a single storey mechanism.
- The longitudinal reinforcing steel strength, $f_u, f_{y.u}$, followed by the concrete compressive strength, f_c, are the most important factors.
- The least important parameters are those related to the transverse reinforcing steel, the concrete tensile strength and the initial modulus of elasticity of concrete in the beams.
- The mass and the random variables that affect the beam's strength often have an inverse effect on the time at incipient collapse.
- The effect of uncertain parameters is not symmetric. Scaling of some random variable can show the opposite trend due to the variation in the possible collapse modes. Therefore, further sensitivity studies of this issue are critical.
- Modification of the strength of all beams in the structure has a greater impact on the collapse process than altering the strength of all the beams in a single or two storeys. Conversely, the effects of scaling the strength or stiffness of the columns of a single or two storeys are more significant than modifying those of the entire structure. Similarly, altering the strength of a single of two storeys has larger influences than changing the strength of the entire structure.

- The uncertainties in the material properties change the damage pattern and thus affect both the collapse modes and the structural collapse capacity (the occurrence of collapse). The time of collapse onset and the collapse mode are highly sensitive to structural modelling uncertainties and to the correlation between these random variables. The order of the importance of the random variables alters dramatically in addition to the swing length of theses parameters in the case of random variables with type 3 correlation, which are the most influential case.
- Different failure modes involving vertical, side-sway and pancake collapse modes have been predicted due to variations in the selected variables with different correlation types.
- The maximum storey drift ratio prior to the onset of collapse is an ineffective measure in determining the importance of random variables on the structure collapse behaviour.
- The most influential random variables for a given structure are those related to the strength of the members that trigger the structure collapse. The structural members that are expected to separate first.
- The soft-storey mechanism often migrates from the lower to the upper storeys as the seismic intensity level of given accelerograms reduces.
- Ignoring the secondary effects, the impact between different elements and force redistribution following element separation, can lead to unsafe collapse predictions, due to neglect of some possible failure modes.
- Even though the structural system in both frames satisfies the seismic code design rules regarding the strong-column weak-beam provision, column hinging often occurs leading the structure to collapse in a soft-storey mechanism.

Chapter 6 Assessment of RC frame structures considering vertical ground motions

6.1 Introduction

Buildings are usually subjected to three-dimensional seismic loadings. Seismic collapse assessment of reinforced concrete, RC, structures under horizontal ground motions has been extensively studied. However, researchers have tended to neglect the effect of vertical ground motion on the collapse process. The collapse probability and failure modes under combined horizontal and vertical earthquakes need to be studied in order to mitigate seismic risk.

This Chapter focuses on assessing the effects of vertical ground motions on the structural collapse response of two RC frame structures, designed according to a modern seismic code, Eurocode 8 (Eurocode 8 (EC8), 1988 (draft); 1994). The importance of considering vertical ground motions on assessing the structure collapse behaviour is investigated by comparing collapse potential and failure modes under earthquake induced collapse, with and without vertical ground motions. Five levels of ground motion intensity, including median collapse capacity, the collapse resistance, have been considered. The median collapse capacity represents the ground motion intensity measure, the spectral intensity, which induces the structural collapse of a building for 50% of seismic records (Liel and Tuwair, 2010).

In this Chapter, a number of studies concerning the effect of the vertical ground motion component on RC buildings are briefly reviewed. Also, the characteristics of the vertical component are described. The EC8 current state of practice in regards to vertical ground motions is summarised. Selection and scaling procedures for ground motion records are presented. A set of seven three-dimensional ground motion records satisfying the EC8 provisions is selected. In order to avoid a special case, where the effects of vertical component are dominant and to provide realistic conclusions, far-field records with different vertical to horizontal ratios, V/H, are selected instead of near-field records. Conclusions are drawn with regard to the progressive collapse response for two different types of RC frame

structures at different ground motion intensity levels. The main focus of this Chapter is on the effect of vertical component on collapse probability and failure modes.

6.2 Previous studies

Damage investigations and failure modes observed during past earthquakes have indicated that the vertical components of strong motions may be the cause of collapse in some structures, especially those located near to a fault during devastating earthquakes (Broderick and Elnashai, 1995, Papazoglou and Elnashai, 1996). The collapse of RC structures observed was attributed to reductions in the column capacity, due to the fluctuation of their axial forces resulting from vertical excitation.

There are a limited number of studies concerning the effect of vertical motion on the inelastic response of RC structures, and most research has focused on the near-field motions, where the intensity of the vertical component is likely to be significantly high. The intensity of vertical excitation decreases more rapidly than that of the horizontal excitation in response to an increase in the source-site distance. Some previous studies, which add weight to the importance of considering vertical ground motions in investigating the seismic performance of RC structures, are reviewed below.

Munshi and Ghosh investigated the inelastic response of a 12-storey reinforced concrete structure subjected to different earthquake records. The analytical results showed that the inclusion of a vertical component in the case of the Northridge earthquake caused a small rise in the maximum deformations to the frame system with a slight difference in the hinge formation pattern and the magnitude of the hinge rotations. Whereas frame-wall system performance was less sensitive to the inclusion of vertical motion (Munshi and Ghosh, 1998).

Collier and Elnashai suggested simple procedures for combining vertical and horizontal earthquake components (Collier and Elnashai, 2001). Their study focused on investigating the effects of the time interval between peaks and the V/H ratios, on the vertical period of a four-storey RC structure. Their results showd that the time interval varies according to source distance. Furthermore, they concluded that the interaction effects of vertical motions are important, especially when the time interval between the horizontal and vertical peaks is not

greater than 2 sec. In addition, the amplitude of both vertical and horizontal accelerations can strongly affect the vertical period of vibration.

Mwafy and Elnashai assessed the seismic response of twelve RC buildings, designed according to Eurocodes 2 and 8, using an incremental dynamic analysis. Three types of structural systems, irregular, regular frames and frame-wall system, with different design levels were investigated (Mwafy and Elnashai, 2006, Mwafy, 2001). They found, by comparing the response of these structures when subjected to only horizontal component with those under combined vertical and horizontal components, that the effect of the vertical component depends on the characteristics of the building and on the ground motions. The effect of the vertical component increases at high ground motion intensity due to $P-\Delta$ effects. These are more pronounced in structural members that are subjected to a relatively low contribution of the lateral action; for example, the interior columns located in the higher storeys of taller structures and the columns of irregular structures. The effect of vertical ground motions on global response differs according to the ground motion intensity and up to a 12% increase in the top storey lateral displacement has been observed in some cases. In addition, the contribution of the vertical component frequently decreased the intensity level, corresponding to the attainment of the collapse limit state at an inter-storey drift of 3%. The effect of the vertical component on the member response, and thus on the failure mode was more obvious. Local failure was observed under a PGA, as less by approximately 23%. Inclusion of the vertical component can lead to a 45% increase in the column axial compressive forces and a 6% decrease in shear strength. Moreover, tensile forces were developed in some columns under combined vertical and horizontal components (Mwafy, 2001, Mwafy and Elnashai, 2006).

Another study of the effect of vertical ground motions on the seismic response of reinforced concrete buildings was conducted by Kadid et al. (Kadid et al., 2010). Three different structures (rigid, semi-rigid and flexible) were nonlinearly analysed utilising distributed and lumped mass models. They concluded that the effect of a vertical component on the inter-storey drift was small, while its effect on column axial forces, which was more pronounced in the case of distributed mass. Tensile forces were induced in some columns. Compression axial forces in columns, especially interior columns could increase by up to 84%.

Kim et al. conducted several studies on the effects of vertical components on RC structures and bridges (Kim et al., 2011b, Kim et al., 2011a, Kim and Elnashai, 2008, Kim and Elnashai, 2009). Kim and Elnashai studied the seismic performance of 15 RC structures, subjected to a suite of records representing the Kashmir earthquake characteristics (Kim and Elnashai, 2009). The seismic response of non-seismically and seismically designed buildings with different ductility levels was investigated at both the global and local levels. Similar conclusions to those detailed in the previous studies by (Mwafy, 2001, Mwafy and Elnashai, 2006) were obtained. It was found that considering the vertical component causes a variation in column axial forces, leading to a strong decrease in the shear capacity of columns, of up to nearly 25%. Thus, local failure was detected in several cases where structures were designed for gravity loads only or for low seismic intensity. Also, no clear trend in variation in the inter-storey ratios was observed. This ratio decreased by up to 50% in some cases and increased by more than 50% in other cases.

An experimental investigation was conducted by Kim et al. utilising a hybrid simulation (Kim et al., 2011b). Four RC bridge piers were tested under different loading scenarios; for example, multi-axial excitation, only horizontal excitation and cyclic loading, with different levels of axial load. The results showed that the vertical excitation, which significantly altered the axial forces, could marginally affect the pier response and collapse modes. Furthermore, the reduction of shear capacity, due to the contribution of vertical motions was proven experimentally.

Another study concerned two key parameters affecting the inelastic response of RC bridges, namely the effect of various H/V ratios and the influence of time intervals between the arrivals of the horizontal and vertical peaks (Kim et al., 2011a). Comparisons were made between two cases; with combined horizontal and vertical components, and with only horizontal excitation. It was found that the effect of the V/H ratio is more significant than the time lag between the peaks. Similar, to previously mentioned findings, experimental and analytical results confirmed that accounting for a vertical component does not show a clear trend toward either decreasing or increasing the inter-storey drift or the lateral displacement. However, the vertical excitation marginally affects inelastic periods and causes a significant decrease in shear capacity of the bridge piers. In addition, axial tension forces were observed only when vertical excitation was considered. Thus, ignoring the vertical earthquake

component may underestimate the shear demand, and significantly over-estimate shear capacity.

Analytical results based on the ASI-Gauss technique for seismic collapse simulation showed that the effect of vertical ground motions on the seismic collapse of a frame structure cannot be neglected as it increases the deformations and may trigger progressive collapse. In particularly, when the amplitude is significantly high (Katahira et al., 2008).

Most studies concerning the effects of vertical ground motions have focused on the response of structures at limit states prior to the occurrence of collapse. However, the majority of such studies predicting structural collapse have ignored the vertical component. This is due to the fact that the method for applying an incremental dynamic analysis to assess structural collapse is not able to account for the effect of vertical motions. Only side-sway collapse modes can be directly simulated, because structural collapse is identified as the intensity that results in excessive inter-storey drifts, dynamic instability (Vamvatsikos and Cornell, 2002).

With regard to the simulation models used in incremental dynamic analysis, IDA, the critical aspects of strength and stiffness deterioration should be captured as accurately as possible. The lumped plasticity model is generally used for seismic performance assessment. This model cannot explicitly consider the axial force-bending moment interaction. This is because at each member end, the model utilises a nonlinear moment-rotation spring based on predefined moment-curvature rules, developed for a constant level of the member's axial force, the level due to the gravity loads. The fiber-based model depends on the stress-strain relationship of each material and can explicitly account for interactions between axial force and bending moments, as well as representing the spread of plasticity along the member and within the cross section. However, it is considered less accurate for simulating structural collapse, because it is not fully validated to capture the strain softening due to the buckling and fracture of the main reinforcements (Haselton et al., 2009).

Although simulation tools for predicting collapse should simulate all possible failure modes, side-sway and vertical progressive collapse; directly incorporating shear failure or flexure-shear failure in column is difficult (Elwood, 2004). Thus, most studies are based on direct collapse simulations with emphasis on side-sway collapse adopting a conservative

post-processing method for detecting non-simulated collapse modes, such as the shear and axial failure modes of non-ductile RC columns (Liel et al., 2011, Aslani and Miranda, 2005). The post-processing method ignores force redistributions and redundancy effects. Drift-based fragility functions are used as component limit state functions to assess whether shear failure, followed by the loss of the vertical-load carrying capacity, occurs in columns (Elwood, 2004, Aslani and Miranda, 2005). Aslani and Miranda developed fragility functions for different structural components in non-ductile RC structures based on experimental data (Aslani and Miranda, 2005).

Axial failure in columns may trigger the progressive collapse of structures, especially non-ductile RC frame structures. A study by Liel et al. was conducted on non-ductile RC frame structures incorporating the vertical collapse limit state for assessing structural collapse using a post-processing approach (Liel et al., 2011). The analytical results indicated that the predicted median structural collapse capacity could be reduced by 2% to 30% when compared to a study by (Liel and Deierlein, 2008) on the same structures considering the side-sway collapse only without this check.

6.3 Characteristics of vertical ground motions

6.3.1 Frequency content

The vertical ground motion component is primarily related to the arrival of vertically propagating P-waves; whereas, the horizontal component is mainly caused by S-waves (Elnashai et al., 2005). Thus, the frequency content of both vertical and horizontal ground motion components differs. The vertical component displays an early arriving high-frequency content even if its energy content over all the frequency range is lower (Kim and Elnashai, 2008). This energy concentration can coincide with the vertical period of the RC buildings. It can cause considerable dynamic amplifications in response of structures in a short period range. The vertical period of conventional RC structures is generally less than 0.2 sec (Mwafy, 2001).

6.3.2 Time interval between the peak vertical and horizontal ground motion

The peak of vertical ground motion acceleration sometimes occurs earlier than the peak of the corresponding horizontal motion, while the time between vertical and horizontal peaks is very small in other records. The relative phasing between peaks is related to the source-distance and the magnitude. The time interval is almost proportional to the source distance and it is often assumed to be equal to zero for distances less than 5 Km (Collier and Elnashai, 2001). The earlier arrival of a high vertical acceleration can cause early shakedown of the structure, while the structural members may be exposed to a high demand if the peaks of both components are coincident (Kim and Elnashai, 2008).

6.3.3 Peak accelerations ratio (V/H)

Recent studies have shown that V/H ratios strongly depend on local soil conditions and on the source to site distance, while other parameters, such as the earthquake magnitude and faulting type are less important (Bozorgnia et al., 1999). Most design codes suggest scaling the horizontal spectral shape by an average V/H ratio of 2/3. However, assuming the V/H ratio equal to 2/3 is over conservative at far-field and seriously unconservative at near-source (Ambraseys and Simpson, 1996, Elnashai et al., 2004). The response spectrum of vertical motions of near-field differs from that in the far-field. A study by Elnashai showed that the peak response at near-field of vertical motions at 2% damping occurs earlier, by almost 0.05 sec, than that at the far-field. It has also been indicated that the peak acceleration of the near-field response spectrum is less by 0.17, as shown in Figure 6-1.

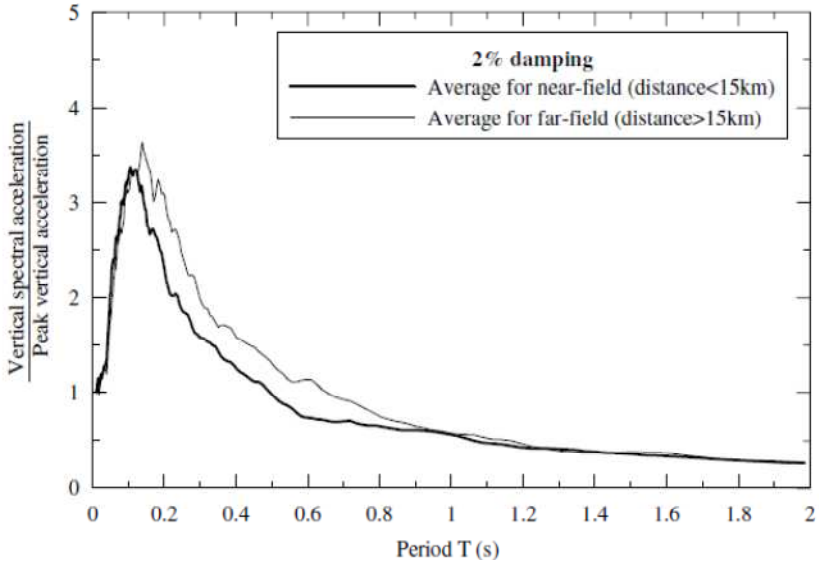

Figure 6-1: Comparison of near and far-field average vertical response spectra (Elnashai et al., 2004)

The peak amplification of the near-field average response spectrum with a damping ratio of 2% is 3.48 and the corner periods are 0.05 and 0.15 sec, as proposed by (Elnashai and Papazoglou, 1997) and recommended by (Elgamal and He, 2004). For alternative damping ratios, Elnashai and Papazoglou suggested altering the design spectra using an amplification correction factor without changing the corner periods (Elnashai and Papazoglou, 1997). Figure 6-1 shows the average near and far-field vertical response spectra at a damping ratio of 2% (Elnashai et al., 2004).

6.3.4 Ground motion duration

The duration of ground motions can affect nonlinear response, energy dissipation and the potential damage to buildings, since it controls the amount of accumulated plastic deformation. A number of studies have focused on defining the strong ground motion duration and 30 definitions have been suggested. A summary of these definitions can be found in a study by Bommer and Martines-Pereira (Bommer and Martinez-Pereira, 1999). These definitions were divided into four groups: bracketed, uniform, significant and effective durations. Bracketed durations, D_b, are defined as the intervals between the first and last excursions beyond specified threshold amplitudes. Uniform durations, D_u, are the sum of all of the time intervals exceeding a particular threshold amplitude. Significant durations, D_s,

are defined as the intervals over which a particular portion of the energy is dissipated. The energy is determined by the integral of the square of the ground motion displacement, velocity, or acceleration. The integral of the square of the acceleration is associated with the Arias intensity, I_A, defined as in Equation 6-1 (Arias, 1970).

$$I_A = \frac{\pi}{2g}\int_0^T a^2(t)dt \qquad \text{Equation 6-1}$$

$a(t)$ represents the acceleration time-history, g is the gravitational acceleration, and T is the entire duration of the record.

Trifunac and Brady defined the significant duration as the time interval between 5% and 95% of the total integral of the square of the acceleration, velocity or displacement (Trifunac and Brady, 1975). The Husid diagram illustrates this significant duration and its limit, since it represents the build up of I_A in time (Husid, 1969). The significant duration based on this definition is denoted as D_{a5-95}. Bracketed and significant durations are the most widely used measures. Figure 6-2 shows an example of the bracketed and significant durations of the Kocaeli earthquake, Sakarya record (Ansal, 2004).

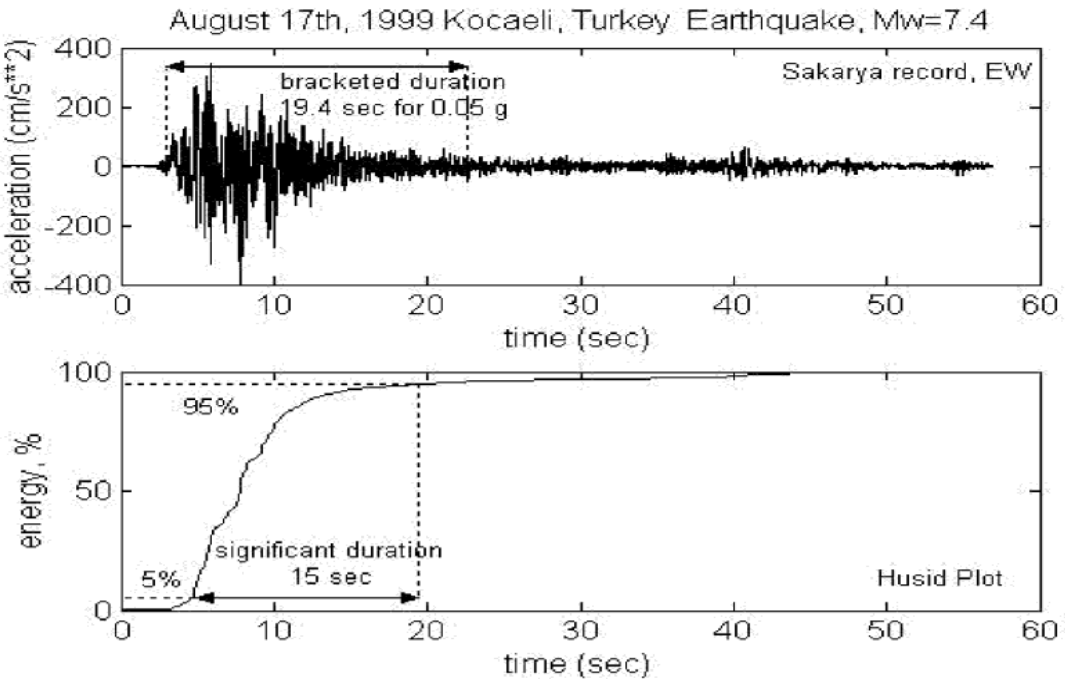

Figure 6-2: Bracketed and significant duration of Kocaeli earthquake (Ansal, 2004)

(Kwon and Elnashai, 2006) altered the lower bound of significant duration and utilised the total time elapsed as between 0.5% and 95% of I_A instead of D_{a5-95}, to avoid subjecting the structure to any unrealistic pulse if the acceleration of the ground motion starts at larger values.

6.4 Approach of Eurocode 8

Vertical spectra have been derived from their horizontal counterparts in many seismic codes, such as UBC 97 (UBC, 1997). The response spectral ratio of the vertical to the horizontal ground motion components is often assumed to be in the range of 1/2 to 2/3 in the seismic codes as suggested earlier by (Newmark and Hall, 1978). Hence, the frequency content will be the same for both the vertical and horizontal components of motion, which is not consistent with the observed characteristics of strong earthquakes. Furthermore, it has been observed that the vertical component exceeded the horizontal component in the vicinity of the causative fault during strong earthquakes (Collier and Elnashai, 2001, Ambraseys and Simpson, 1996, Elnashai and Papazoglou, 1997).

Eurocode 8, EC8, deals with the vertical ground motion in a better way compared to other seismic codes, since it suggests using a vertical response spectrum with a different frequency content and magnitude from the horizontal response spectrum (EC8-1, 2004). The EC8 vertical elastic response spectrum is shown in Figure 6-3. Two types of response vertical spectra are recommended in this code as listed in Table 6-1.

Table 6-1: Parameters recommended for describing both types of vertical spectra

Spectrum	av/ah	T_B	T_C	T_D
Type 1	0.9	0.05	0.15	1
Type 2	0.45	0.05	0.15	1

Using the spectrum of type 2 with V/H ratio of 0.45 is recommended if the surface-wave magnitude of the earthquake contributing most to the seismic hazard defined for the site, for the purpose of probabilistic hazard assessment, is less than 5.5. The spectrum of type 1 with a V/H ratio of 0.9 is recommended for use in the other cases. The corner periods of both vertical spectrum types are the same and unrelated to the corner periods for the

corresponding horizontal spectrum. Thus, the corner periods reflect the observed characteristics of vertical ground motion. The vertical elastic response spectrum is defined as in Equations 6-2 to 6-5 (EC8-1, 2004):

$$0 \le T \le T_B : S_{ve}(T) = a_{vg}.\left[1 + \frac{T}{T_B}(\eta.3 - 1)\right] \quad \text{Equation 6-2}$$

$$T_B \le T \le T_C : S_{ve}(T) = a_{vg}.\eta.3 \quad \text{Equation 6-3}$$

$$T_C \le T \le T_D : S_{ve}(T) = a_{vg}.\eta.3.\left[\frac{T_C}{T}\right] \quad \text{Equation 6-4}$$

$$T_D \le T \le 4s : S_{ve}(T) = a_{vg}.\eta.3.\left[\frac{T_C.T_D}{T^2}\right] \quad \text{Equation 6-5}$$

$S_{ve}(T)$ is the elastic vertical response spectrum, T is the vibration period of a linear single degree of freedom system, a_{vg} is the design vertical ground acceleration for the reference return period, T_B and T_C are the lower and upper limits of the constant spectral acceleration branch, T_D is the value defining the beginning of the constant range of the displacement response of the spectrum, ξ is viscous damping ratio of the structure, and η is the damping correction factor, $\eta = \frac{10}{5+\xi} \ge 0.55$.

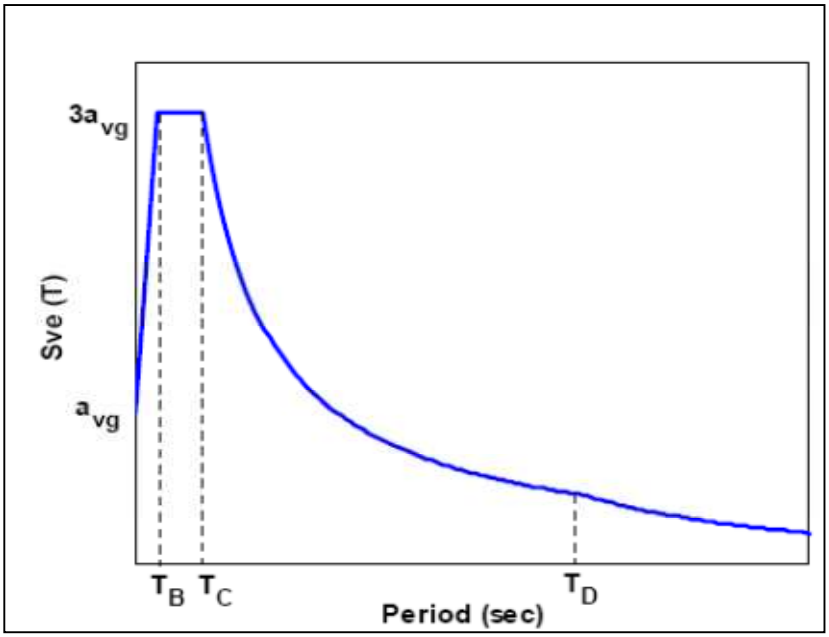

Figure 6-3: Vertical response spectrum of EC8 (EC8-1, 2004)

EC8 recommends considering the effect of the vertical components only when designing certain structures, such as base-isolated structures, pre-stressed components, long cantilevers, beams with spans over 20 m and beam supported planted columns, but no considerations are adopted for sites in the near-field of strong ground motions.

6.5 Selection of reference structures

This study focuses on an investigation for collapse process of the two six-storey RC frames: the BF1 and DCF frames. Validation of the AEM models of the 1/5.5 scale models of both frames were performed in Chapter 4, where good agreement between the analytical and the experimental results was observed. The full-scale models for both frames were developed using ELS software. The dimensions and reinforcement details of both structures were given in Chapter 4, however the reinforcement details slightly differ from the structures, given in Tables 4-5 and 4-6. The same amount of reinforcement is used along the entire member, resulting in stronger columns and beams at the first and second storeys. The intention of this modification was to delay the formation of the first-storey mechanism and to improve structural performance. The material properties, given in Table 4-9, are used in the analytical models. The slab contribution to both the strength and stiffness of the beams is taken into account. The effective flange width is modelled by adding a 452 mm flange to each side of the beams.

The AEM models that represent both of these six-storey RC frames are similar to those discussed in Chapter 4. The AEM models are subjected to a set of fourteen scaled ground motion records with and without their corresponding vertical components. These three-dimensional records are scaled to five different ground motion intensity levels. The AEM models are then subjected to each of these scaled sets of ground motion records and the effects of the inclusion of vertical ground motions investigated at various levels of seismic intensity.

6.6 Ground motion record selection and scaling

6.6.1 Introduction

Three types of seismic input can be utilised in dynamic analysis, namely artificial, synthetic accelerograms or real records.

Using artificial accelerograms compatible with the EC8 spectrum is not recommended in seismic assessment for two reasons. Firstly, they often have an excessive number of cycles in motion with large amplitude and different phasing from the real records. Thus, they may possess an insufficient or unrealistically high energy-content in the frequency range of interest (Buratti et al., 2007). In addition, artificial accelerograms are generated by matching the entire elastic design spectrum, while the elastic design spectrum, which is often a uniform hazard spectrum, is obtained by enveloping the ground motion spectra from a large number of seismic sources. It is not possible to match the entire spectrum to a single accelerogram (Buratti et al., 2007). A study by Carballo and Cornell found that utilising compatible accelerograms could result in an unconservative estimate of the nonlinear demands (Carballo and Cornell, 2000).

Appropriate synthetic accelerograms via modelling the seismological source and taking into account the effects of site and path are difficult to obtain. This is because many input parameters are required to define a specific earthquake scenario; for example, geological conditions, the location and characteristics of the site, source, and path, in addition to the magnitude and rupture mechanism (Bommer et al., 2003).

Moreover, manipulating real records to be perfectly compatible with a target spectrum via modification functions in the time or frequency domain can yield unconservative estimations of the seismic demands (Carballo and Cornell, 2000, Bazzurro and Cornell, 1999). Therefore, real records will be utilised in the following analyses to avoid any biased estimation of seismic assessment.

6.6.2 Selection and scaling ground motion records

Selection and scaling ground motions for nonlinear dynamic analysis are crucial, since this type of analysis is highly sensitive to ground motion input (Kwon and Elnashai, 2006). The method for selection and scaling ground motion depends on the purpose of the nonlinear dynamic analysis, as well as the structural system. There are many possible methods for selecting and scaling records. A summary of these approaches can be found in (Haselton, 2009). Scaling ground motion methods are reviewed in Chapter 7. In this study, relatively simple methods for selecting and scaling real records will be adopted. This is because the aim of this study is to investigate the effect of the inclusion of vertical ground motions on collapse capacity, rather than determining the probability of structural collapse.

With regard to the code procedures for record selection, Eurocode 8 requires that a set of records be chosen in which the average of the 5% damping elastic spectrum of these records exceeds 90% of the corresponding value of the EC8 5%-damped elastic spectrum over a broad range of periods between $0.2T_1$ and $2T_1$. T_1 is the first-mode period of the structure in the same direction as that of the applied record. The limits to this range accounts for both the contribution of higher modes, as well as the period of elongation, as the structure experiences damage.

With regard to the number of records required, Eurocode 8 allows the use of at least three records if the maximum response is of interest, whereas not less than seven records should be utilised in order to consider the average structural response.

It is worth noting that the code approach for selecting spectrum compatible records is not recommended for use in collapse assessments, since the probability of exceeding a range of spectral values is unknown, and utilising this method is expected to over-estimate the structure's response (Haselton, 2009).

6.6.2.1 Selecting ground motion records

6.6.2.1.1 REXEL 2.31 beta software

Recently, databanks of real records and appropriate tools for selecting record sets satisfying the EC8 provisions and the new Italian Building Code requirements have become available. REXEL 2.31 beta software (Iervolino et al., 2010, Iervolino et al., 2009, Iervolino and Galasso, 2009) is freely available on the website of the Italian network of earthquake engineering laboratories (http://www.reluis.it/index_eng.html). This software can be used for selecting real records that are compatible on average with a target spectrum derived from the European Strong-Motion Database (Ambraseys et al., 2002) based on epicentral distance, R, and moment magnitude criteria, M. These records are available at http://www.isesd.cv.ic.ac.uk.

A set of un-scaled natural records compatible in the average with EC8 elastic response spectra, (Type 1, with an anchoring value of 0.3 g and ground type A), is selected using the REXEL 2.31 beta software. Selecting a set of scaled real records instead of un-scaled records yields smaller individual variability (Iervolino et al., 2010). This is because the individual record selected within the set closely matches the non-dimensional reference spectra. However, amplitude scaling in the time domain may result in large scaling factors (Iervolino et al., 2010). Furthermore, different scaling factors for the records, representing the three components of ground motion are employed. Real records scaled using the REXEL 2.31 are avoided in this study, because using a set of such scaled records is inconsistent with the scaling approach adopted in this study. The same scale factor for the components acting simultaneously will be utilised.

Two additional parameters are considered when selecting the combination of the un-scaled records in the REXEL 2.31 beta software, in order to reduce the average and individual spectra variability with regard to the target code spectrum. These parameters are the average spectra deviation, σ, and the maximum deviation in a single record within a set in regard to the code spectrum, σ_{max}. The definition of these additional constraints can be found in (Iervolino et al., 2008, Iervolino et al., 2006a).

6.6.2.1.2 Characteristics of selected ground motion records

Ground motion records with different V/H ratios are obtained from the European Strong-motion Database (ESD). The ground motion records are selected from relatively large magnitude earthquakes (Mw $\geq$ 6), with source distance greater than 5 Km, in order to avoid directivity effects. All these ground motions are for similar soil conditions (soil type A). In the selected record set, no more than two records from a single earthquake event are selected to minimise the correlation because of event commonality (Iervolino and Cornell, 2005). A set of seven records is selected. The minimum set size for considering the mean response. Each record of ground motion has three components.

The average of fourteen records, two horizontal components recorded at the same station, has to match the horizontal target spectrum. The horizontal component of the reference spectrum has to be closely matched in the period range between 0.1 and 1.5 sec. This period range is consistent with structures that have their horizontal fundamental period in the range of 0.5 to 0.75 sec. The horizontal fundamental vibration period of the AEM models of the reference frames are 0.53 and 0.56 sec, respectively. The lower and upper limits for the underestimation and overestimation of the horizontal EC8 spectrum are set to 10%, as recommended by EC8, and 30%, respectively. EC8 does not provide any indication for the upper bound tolerance in spectral matching. However, in order to reduce the spectrum of overestimation, the upper limit is set to 30%.

The ratio of the horizontal to vertical fundamental periods of RC frame structures with a number of storeys varying between 1 and 8 is in the range of 2.5 to 7 (Papazoglou and Elnashai, 1996). The upper limit of the vertical period of RC buildings is 0.2 sec, based on a study by (Mwafy, 2001). The vertical period of both structures, calculated from a relatively simple equation proposed by (Elnashai and Papazoglou, 1997), is about 0.1 sec. Thus, the range of vertical periods is set to a range of 0.01 to 0.5 sec. By adopting the aforementioned tolerance limits to select the corresponding vertical components, no set of records with horizontal and vertical components was found that is compatible with both the horizontal and vertical EC8 spectrum within the allowable tolerances. To solve this problem, a decision was made to obtain a set of records for which only their horizontal components are compatible on average with the horizontal component of the EC8 response spectrum. This was achieved by setting different tolerances for the vertical components. A tolerance value of 40% is used for

both the lower and upper limits of the vertical components in the period range of 0.01 to 0.5 sec. The lower bound tolerance is higher than the 10% specified by EC8, and thus does not satisfy the code requirement, but the minimum tolerance limit can be used.

A set of seven records with three components, where only the horizontal components match on average the code horizontal spectrum, has been selected. Tables 6-2 and 6-3 list the data for the three components of the selected combination, as given by REXEL. Figure 6-4 Figure 6-5 show the elastic 5%-damped response spectra of the horizontal and vertical components of the seven selected records, respectively.

Table 6-2: Record data obtained from REXEL

Record ID	**Earthquake ID**	**Station ID**	**Earthquake Name**	**Date**	**Mw**	**Fault Mechanism**	**R [km]**
000055	34	ST20	Friuli	06/05/1976	6.5	thrust	23
000182	87	ST54	Tabas	16/09/1978	7.3	oblique	12
000198	93	ST64	Montenegro	15/04/1979	6.9	thrust	21
001231	472	ST575	Izmit	17/08/1999	7.6	strike slip	9
004674	1635	ST2486	South Iceland	17/06/2000	6.5	strike slip	5
007142	2309	ST539	Bingol	01/05/2003	6.3	strike slip	14
006349	2142	ST2558	South Iceland	21/06/2000	6.4	strike slip	5

Table 6-3: Record data obtained from REXEL

Record ID	**PGA_X [m/s^2]**	**PGA_Y [m/s^2]**	**PGA_Z [m/s^2]**	**PGV_X [m/s]**	**PGV_Y [m/s]**	**PGV_Z [m/s]**	**Site class**
000055	3.4985	3.0968	2.6227	0.2061	0.3262	0.1048	A
000182	3.316	3.7789	1.7085	0.1768	0.2457	0.1078	A
000198	1.7743	2.1985	2.0758	0.1705	0.2591	0.1169	A
001231	1.5764	2.1922	1.3923	0.1901	0.2664	0.1095	A
004674	3.1176	3.3109	2.6815	0.6122	0.2377	0.1432	A
007142	5.0514	2.9178	4.427	0.336	0.2097	0.1324	A
006349	7.2947	8.218	4.1405	0.4557	0.9202	0.2385	A

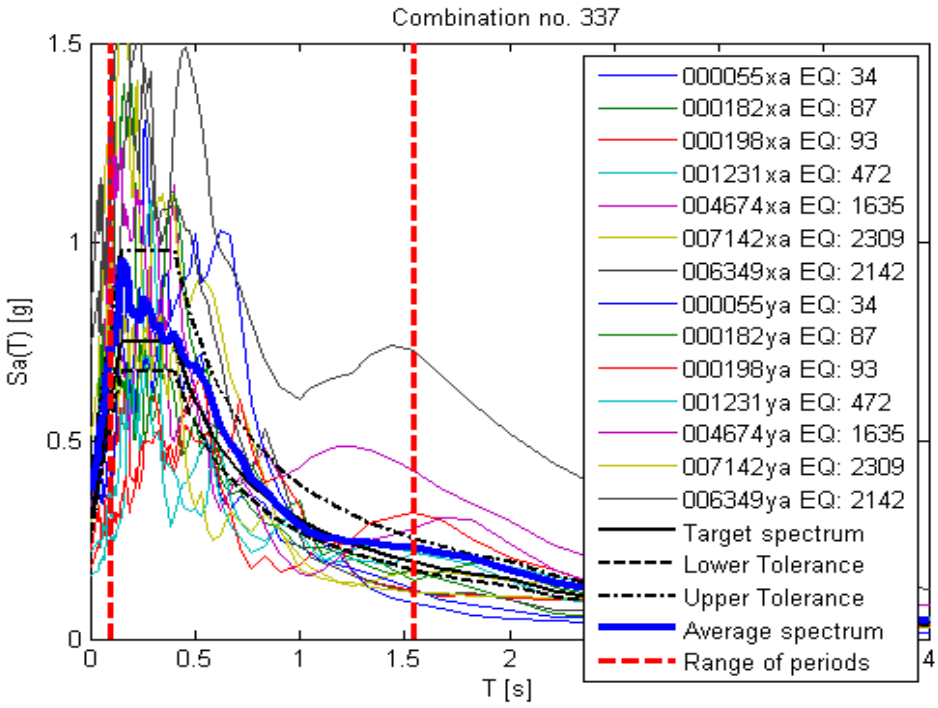

Figure 6-4: Elastic response spectra of un-scaled horizontal components matching on average the EC8 response spectrum

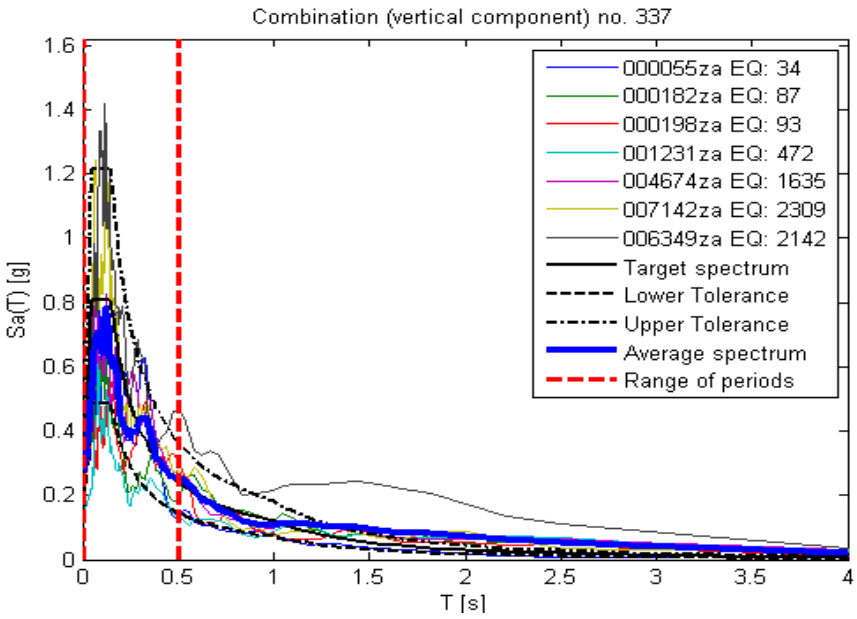

Figure 6-5: Elastic response spectra of un-scaled vertical components corresponding to the horizontal components

6.6.2.1.3 Ground motion duration

This study involves a large number of simulations, which are time consuming. Therefore, instead of employing the total duration of ground motions in these analyses, the duration of ground motions was reduced based on the definition of ground motion durations.

Since the selected records will be used for studying the effect of vertical components on the collapse process, the definition of the ground motion duration, which relates to its destructive potential and accumulated energy, will be employed. Therefore, the significant duration measure, $D_{a0.5-95}$, is utilised for defining the duration of ground motion records.

The Seismosignal software (SeismoSoft, 2011) is used to calculate the significant duration of the selected set based on $D_{a0.5-95}$. Table 6-4 lists the significant duration, the time of the strong shaking phase of each of the three components of the seven ground motion records. The significant duration of each record is altered slightly in order to avoid changing the time interval between the peaks of vertical and horizontal ground motions. Thus, the same significant duration and start times are used for all the three components of each record.

It was found that the duration of both 000182 and 001231 records is 38 sec, because there is more than one arrival of high amplitude. For example, in the 000182xa_record, there were a second and a third arrival point at around 26 and 36 sec, as shown in Figure 6-6. On the other hand, the durations of the other records ranged between 8 and 15 sec. Both records with a longer duration are expected to be more destructive. Figure 6-6 shows 000055xa_record and 000182xa_record accelerograms and their corresponding Husid plots, in which the significant duration is represented by a solid blue line.

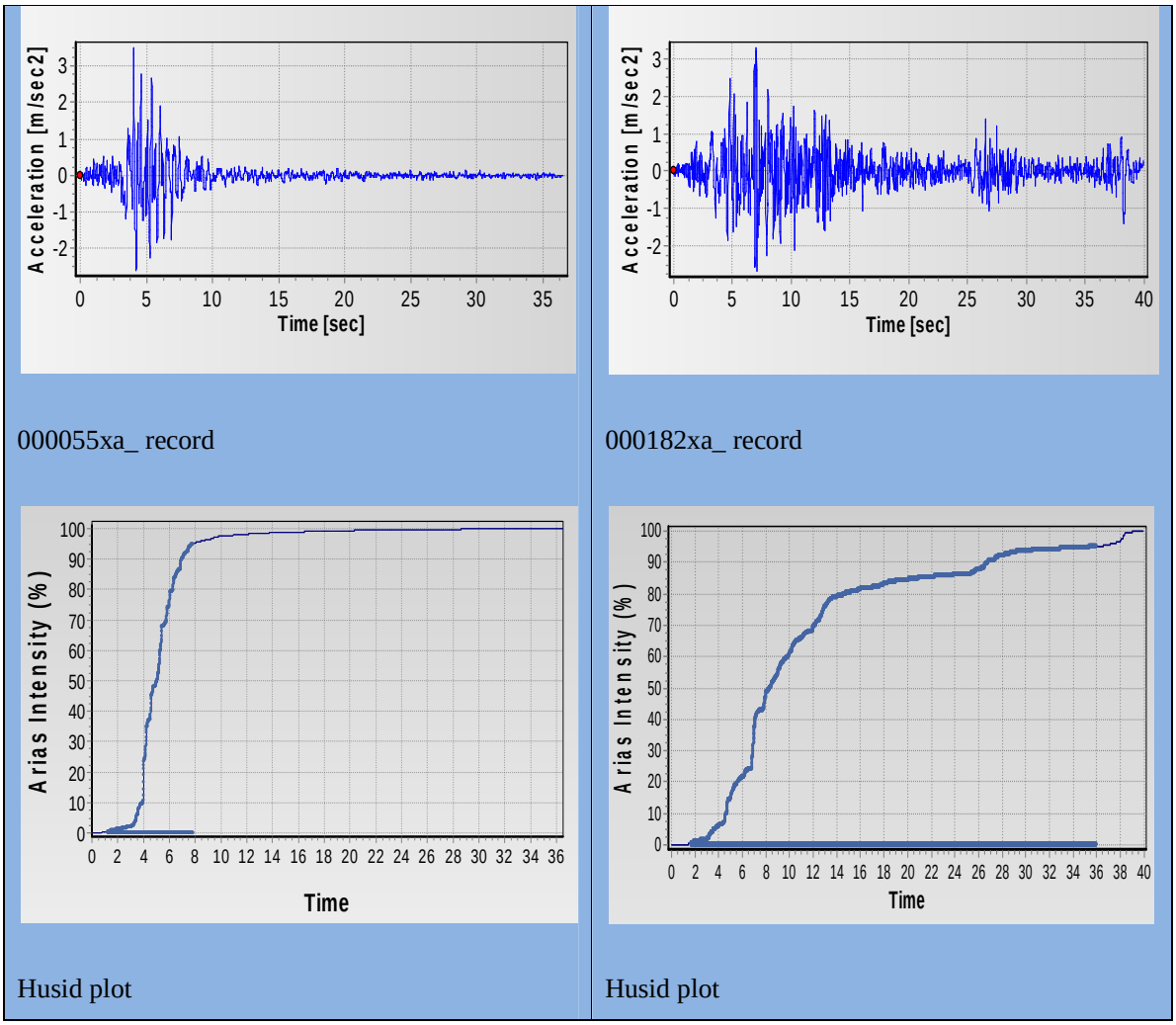

Figure 6-6: Accelerograms of 000055xa and 000182xa records and their corresponding Husid plots

Table 6-4: Significant duration and time at the start of the strong motion phase of the ground motion records

Record ID	Component	Total Duration, sec	The start time, sec	The significant duration, sec	The start time, sec	The adopted significant duration, sec
000055	x	35.41	1.26	6.54	0	10
	y		3.05	6.09		
	z		0.65	6.33		
000182	x	39.96	0.87	34.33	0	38
	y		1.65	35.25		
	z		1.05	28.6		
000198	x	40.37	2	12.84	0	15
	y		2.14	12.71		
	z		1.64	11.74		
001231	x	51.94	1.2	35.67	0	38
	y		1.71	35.58		
	z		064	34.66		
004674	x	76.78	11.89	5.02	10	8
	y		11.64	5.59		
	z		11.22	5.59		
006349	x	55.99	11.4	5.85	10	8
	y		11.34	4.25		
	z		11	5		
007142	x	64.71	21.27	5.86	20	10
	y		21.17	8		
	z		20.29	6.95		

6.6.2.1.4 Ground motion scaling

The response of the reference structures will be studied for a given magnitude and distance from the source. In addition, the spectral acceleration at the structure's fundamental period will be used as an intensity measure. The EC8 states that only the average spectra for all records should match the design spectrum, however, the selected records will be scaled in order to check that their individual spectra approximate the design response spectrum; in particular, the elastic spectral acceleration response at the period of the first-mode of the structure. A slight adjustment may be needed following these procedures to ensure that the average spectrum does not underestimate the design spectrum.

Following the selection of a set of seven records, amplitude scaling of the selected ground motion records was adopted by multiplying all the values of the record acceleration by a scaling factor. The geometric mean of the spectral acceleration for both horizontal components of the record at the fundamental period of the structure, $S_a(T_1, 5\%)$, was used as the intensity measure, in order to avoid using inconsistent intensity measures. Seismologists generally use the geometric mean of both components in computing the ground motion prediction equations (Baker and Cornell, 2006c). Therefore, the scale factor utilised for each record was set as equal to the ratio between the elastic spectral acceleration of the EC8 spectrum and the geometric mean value of $S_a(T_1, 5\%)$ of the both horizontal components of each unscaled record. Figure 6-7 shows the mean spectra of the both horizontal components of each record, which is scaled at $S_a(T_1, 5\%)$. Figure 6-8 depicts the mean horizontal spectrum of these scaled records, together with the EC8 spectrum and the corresponding upper and lower tolerances.

For each record, the scale factor used for the horizontal components of the record was employed for normalising its vertical component, in order to avoid changing the ratio of the vertical to horizontal peak accelerations (Mwafy and Elnashai, 2006). Table 6-5 lists the ratio of vertical to horizontal peak accelerations within the selected set and the scaling factor of each earthquake record. As can be noted from Table 6-5, the values of the scaling factor varied between 0.554 and 1.336.

Each horizontal component of the selected and scaled records in the previous section is treated as an independent record so considering the two horizontal components of the record

set yields fourteen records. Figures 6-8 and 6-10 depict the horizontal and vertical spectra of the scaled records with their corresponding mean spectrum. Figure 6-11 shows the accelerograms of the three components of each record following scaling to $S_a(0.53 - 0.56, 5\%) \cong 5.5 m/Sec^2$.

Table 6-5: Ratio of the vertical to horizontal peak accelerations and corresponding scaling factors

Record ID	**PGA_Z / PGA_X**	**PGA_Z / PGA_Y**	**Scaling factor**
000055	0.75	0.85	0.753
000182	0.52	0.45	0.939
000198	1.17	0.94	1.017
001231	0.88	0.64	1.336
004674	0.86	0.81	1.081
007142	0.88	1.52	0.554
006349	0.57	0.50	0.967

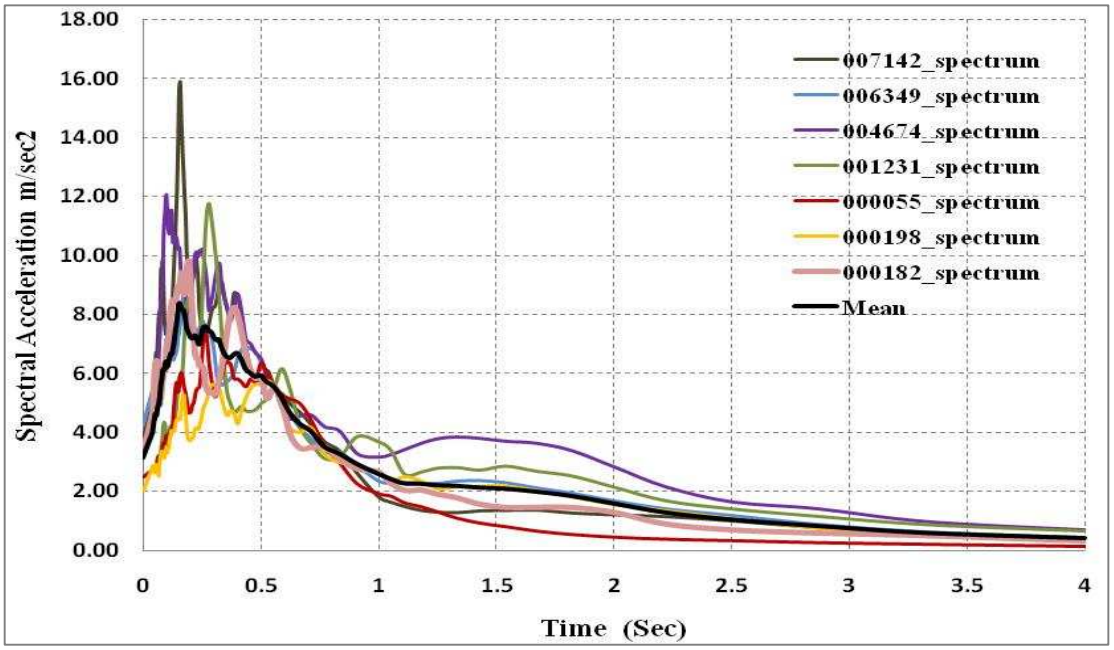

Figure 6-7: Mean spectra of both horizontal components of each scaled record together with the mean of the total fourteen horizontal records

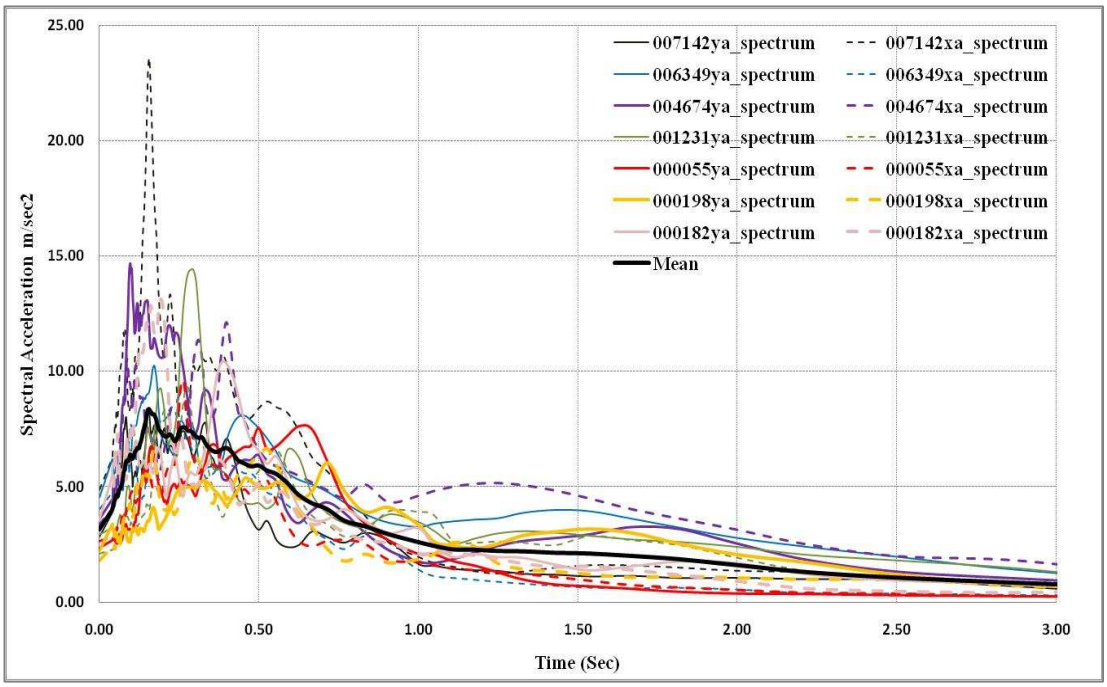

Figure 6-8: Horizontal spectrum of the scaled records together with their corresponding mean spectrum

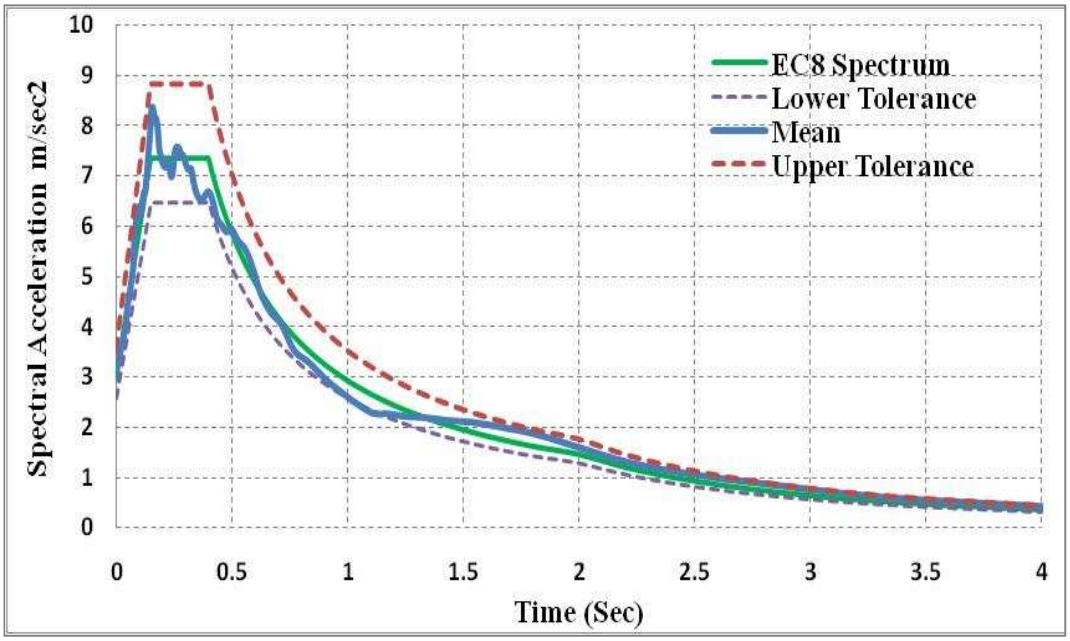

Figure 6-9: Mean horizontal spectrum of the scaled records together with the EC8 spectrum and the corresponding upper and lower tolerances

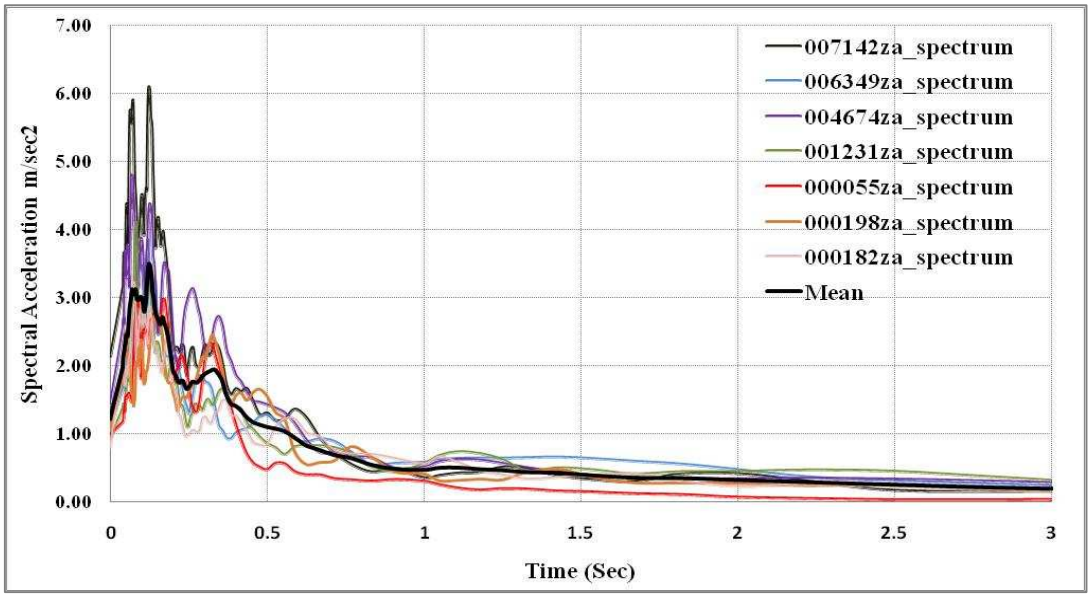

Figure 6-10: Vertical spectrum of the scaled records together with their corresponding mean spectrum

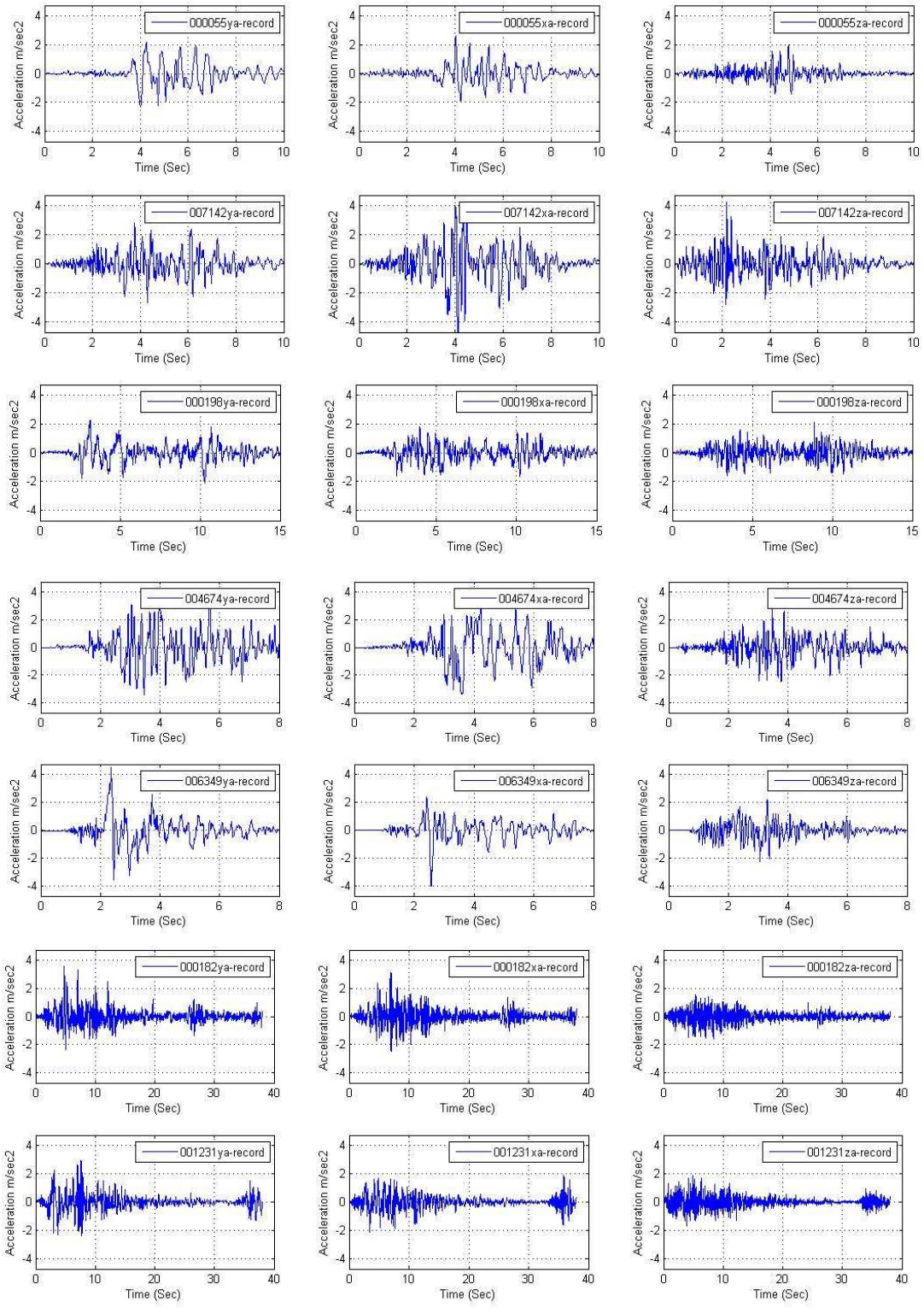

Figure 6-11: Accelerograms of the three components of each record

6.7 Defining the collapse limit state

Collapse occurs when the structural system, or a part of it, cannot sustain the gravity loads under seismic loading. Local or global failure may occur. The collapse limit state is identified in this work as following:

1. Partial collapse of the structure is defined by the failure and collapse of at least two RC columns at the same floor. This collapse limit state is associated with developing a storey mechanism, such as a soft storey mechanism or a vertical collapse mode, which can result from shear failure of both of the internal columns of a single storey.
2. Complete collapse of the structure is described by the collapse of the entire first storey columns or the collapse of most of the structural members.

Probability of collapse at a given intensity measure level, IM, is determined according to the ratio of the number of records, in which the pre-defined limit state (the collapse limit state) is reached, to the total number of records scaled to that given intensity level.

6.8 Determination of seismic intensity levels

The effects of vertical ground motions on structural collapse response are estimated at five and six different intensity levels for the DCF and BF1 frames, respectively. These values are selected as follows:

1. The spectral intensity level corresponding to the collapse resistance, the intensity level where 50% of the horizontal records excluding the effect of the vertical component induced the structure to collapse.
2. Two spectral intensity levels smaller than that associated with the collapse resistance. These two intensity levels correspond approximately to a 15% and to a 40% probability of collapse.
3. Two or three spectral intensity levels higher than that related to the mean collapse probability. These intensity levels should correspond to values of collapse with a probability less than 80%.

The intention of selecting lower and higher spectral intensity levels than the collapse resistance is to study the effect of the vertical component on the collapse response, as governed by different loading scenarios. In addition, having knowledge about the intensity levels corresponding to different collapse probabilities can be effective when checking the effect of the inclusion of the vertical components on the median collapse capacity. For example, if there is a significant increase in the collapse probability for a small change in the intensity level, then the effect of considering a vertical ground motion is expected to be large and vice versa. The collapse probability of the DCF and BF1 frames is assessed with and without inclusion of vertical ground motions at these pre-defined intensity levels. The collapse response of the BF1 frame is investigated under six, instead of five, intensity levels in order to check the trend toward the effect of vertical ground component on the collapse probability and increase the confidence in the analytical results.

6.9 Evaluation of the collapse capacity of the selected frames

6.9.1 Introduction

The collapse resistance represents the spectral intensity level, which causes the collapse of a structure for 50% of the seismic records (Liel and Tuwair, 2010). Instead of using the incremental dynamic analysis technique (Vamvatsikos and Cornell, 2002), which is computationally intensive, a practical approach developed by Liel and Tuwair for assessing the structural resistance to seismic collapse will be used (Liel and Tuwair, 2010). It should be mentioned that preliminary estimated value and step size do not affect the accuracy of this method. However, the computational efficiency of the approach is affected by the step size used, and a small step size may marginally increase the analysis time (Liel and Tuwair, 2010).

Furthermore, in order to reduce the number of records to run in each analysis which is computationally expensive, a similar assumption to (Liel and Tuwair, 2010) is made and the list of ground motion records to run is updated following each analysis. It is assumed that if a record results in structural collapse at $s_a = y$, it will cause collapse at all higher spectral values $s_a > y$, and if a record does not result in structural collapse at $s_a = y$, it will not lead to collapse at lower spectral values $s_a < y$. Following determination of the collapse capacity

utilising this approach, this assumption is checked by running the analysis using the total number of ground motion records at the spectral intensity corresponding to the median collapse capacity. Sometimes a ground motion record can lead to the structural collapse at a spectral intensity $s_a = y$, but may not cause collapse at higher intensities. This record is known as a resurrecting record. This could be due to the possibility of developing different failure modes. This step is important because more than three different collapse modes can take place in both the selected frames at different intensity levels.

6.9.2 Evaluation of the collapse capacity of the DCF frame

The initial estimate for the ground motion intensity measure, $s_{a1}(T_1 = 0.56\,\text{sec})$, is set as equal to 1.68 g, three times the spectral acceleration of the design earthquake. This value is adopted, based on the results of aforementioned studies by (Lu, 1996, Lu, 2002, Lu et al., 1999), in which the base shear over strength factor and displacement ductility demands were found to be approximately in the range of 3 to 4. It is worth noting that the strength of both frames in this study was increased due to the modification of reinforcement details, as mentioned earlier. Then, the ground motion records scaled to this value, the computed collapse probability, $P[\text{collapse}/s_{a1} = 1.68\,\text{g}]$, is equal to 14.2%. The collapse resistance is higher than $s_{a1} = 1.68\,\text{g}$. Since the collapse probability is significantly lower than 50%, a new estimate for the collapse capacity is selected. A value of 2.24 g for spectral acceleration at the fundamental period of the structure is adopted. The collapse probability at the revised estimate was 43%, $P[\text{collapse}/s_{a2} = 2.24\,\text{g}] = \frac{6}{14} = 43\%$. All the horizontal ground motion records are utilised in the first two analyses. A step size of 0.42 g is used for the next run. Only 8 ground motion records, which have not caused collapse at the previous intensity levels, are scaled to $s_{a3} = 2.66\,\text{g}$ and utilised in the analysis. The collapse probability is found to be 71%, $P[\text{collapse}/s_{a3} = 2.66\,\text{g}] = \frac{4+6}{14} = 71\%$. At this point, it is clear that the structural collapse resistance should be in a range between s_{a2} and s_{a3}. Therefore, a spectral intensity value near to the mean of these two spectral intensity levels, $s_{a4} = 2.47\,\text{g}$, is selected. The ground motion list to run is updated and only four ground motion records are scaled to this intensity level. It was found that more than 50% of the records caused collapse and $P[\text{collapse}/s_{a4}] = \frac{6+2}{14} = 57\%$. The collapse probability at s_{a4} is still larger than 50%, so the spectral intensity value is reduced to a smaller value and set as equal to $2.38\,\text{g}$.

Subsequently, the number of records to run is reduced to two. At $s_{a5} = 2.38$ g, the probability of collapse is equal to $P[\text{collapse}/s_{a5}] = 57\%$. This process is then repeated. The two following analyses, which correspond to $s_{a6} = 2.32$ g and $s_{a7} = 2.34$ g, are run with only two records, namely 001231ya and 00198ya. The collapse probability at the intensity level of 2.32 g is similar to that corresponding to s_{a2}. This generates the results that the probability of collapse at an intensity level of 2.34 g is equal to 50%. The collapse resistance, the lowest spectral intensity level at which 50% of the records cause structural collapse, is equal to 2.33 g. At this intensity level, corresponding to the collapse resistance, the analysis is run with the entire horizontal ground motion records, 14 records, in order to ensure that there is no resurrecting record.

The time required to obtain the median collapse of DCF frame was around 200 hours with 60 runs. Figure 6-13 shows the process used for determining collapse resistance. Figure 6-12 depicts the lower spectral intensity level that causes structural collapse for each record.

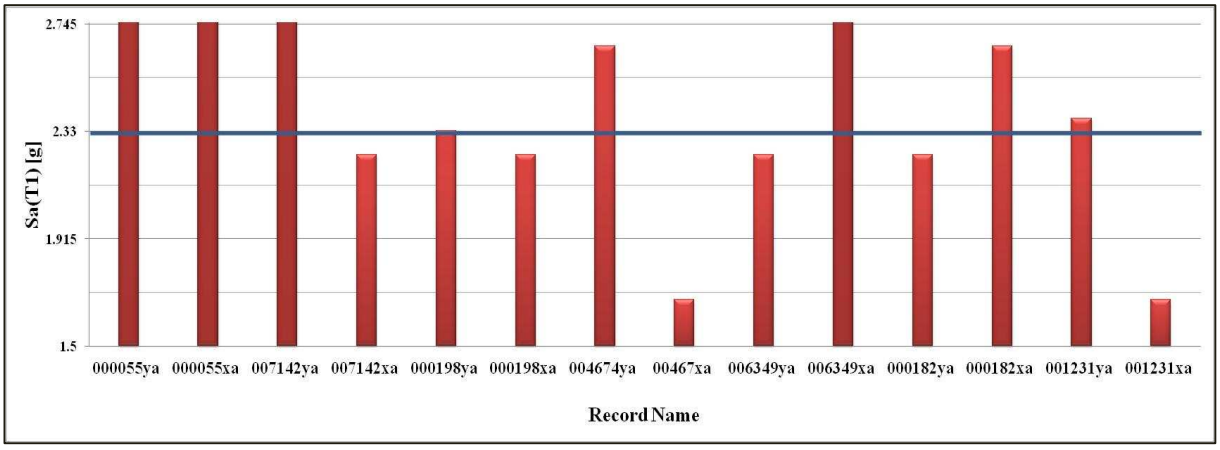

Figure 6-12: Lower spectral intensity level that causes the structural collapse for each record

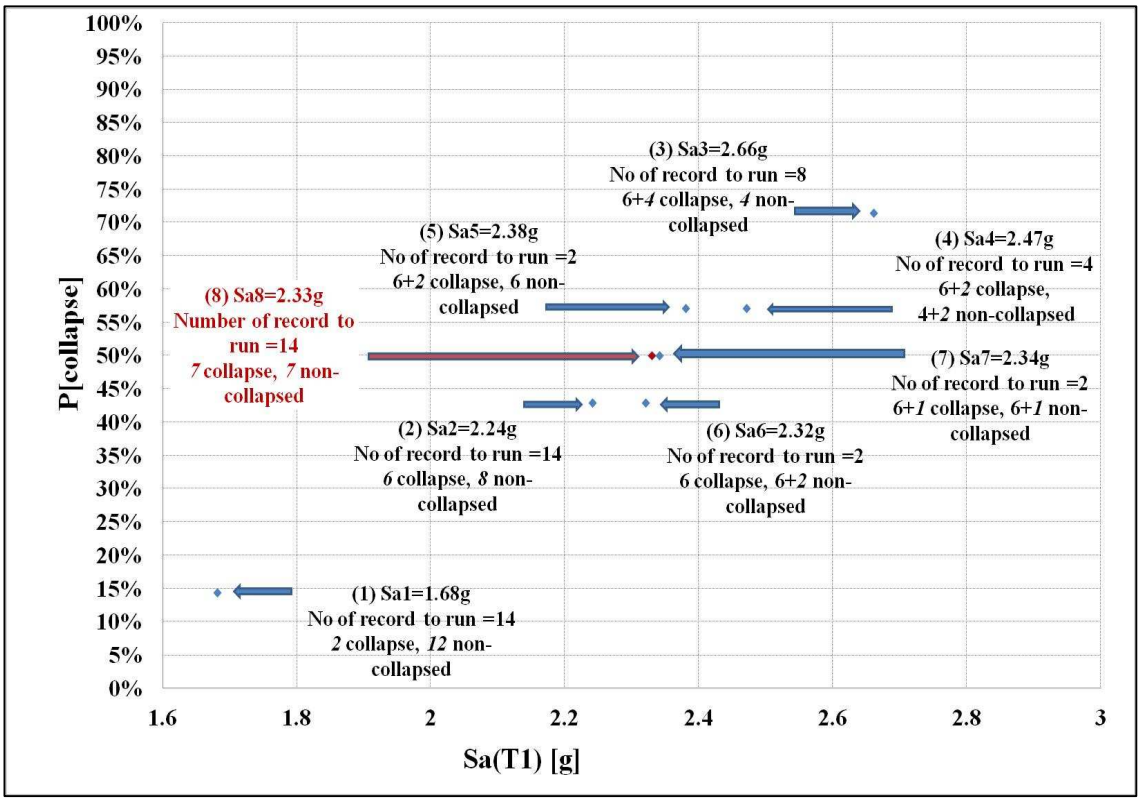

Figure 6-13: Process used for determining the structural collapse resistance of the DCF frame

6.9.3 Evaluation of the collapse capacity of the frame BF1

The collapse resistance for the BF1 frame is determined in a way that is similar to the collapse resistance of the DCF frame with an initial intensity estimate, $s_{a1}(T_1 = 0.53 \text{ sec})$, equal to 2.24 g, four times the spectral acceleration of the design earthquake. The process used for determining collapse resistance is shown in Figure 6-14. As can be seen, the collapse resistance of this frame is 2.07 g. The collapse resistance of the DCF frame is approximately 1.125 times greater than the mean collapse of the BF1 frame.

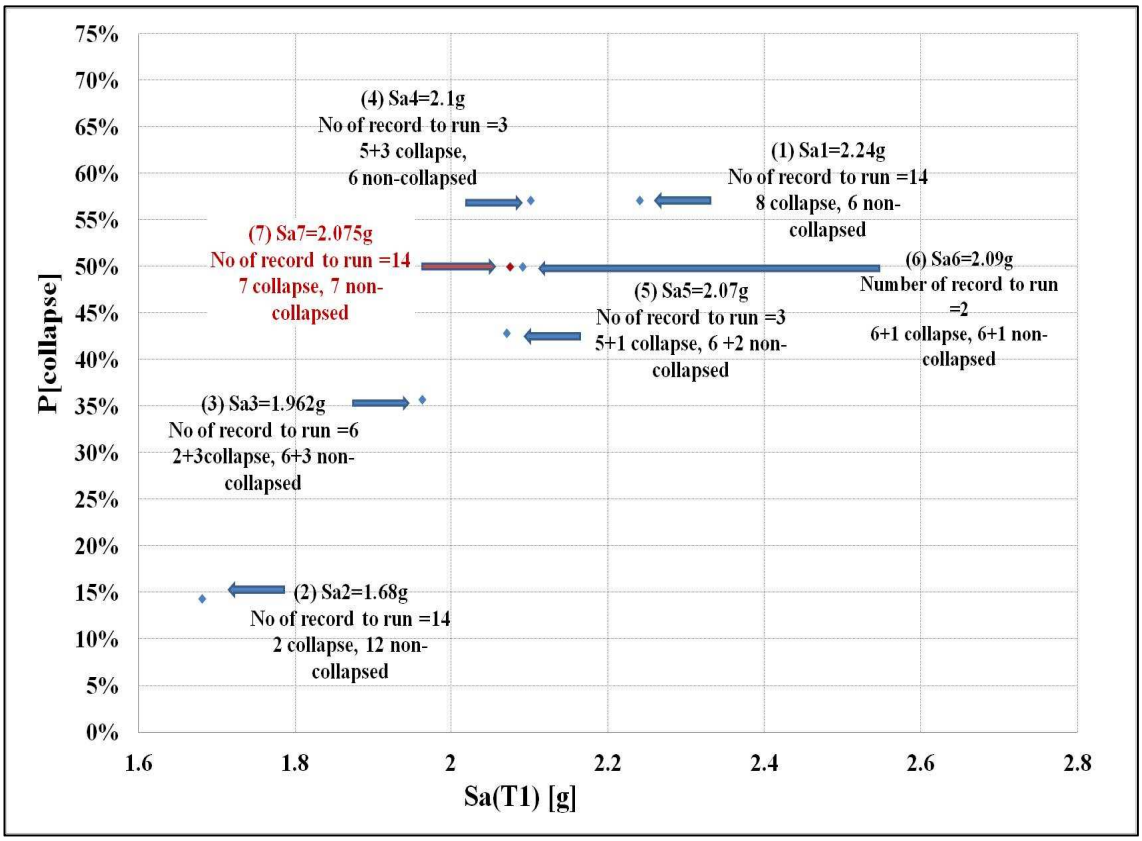

Figure 6-14: Process used for determining the structural collapse resistance of the BF1 frame

6.10 Effects of the vertical ground motion on the collapse response of the DCF and BF1 frames

The two prototype structures selected, the DCF and BF1 frames, were subjected to combined vertical and horizontal ground motions and only to horizontal components at five and six ground motion intensity levels, respectively. The collapse response of the DCF frame was investigated at five intensity levels, namely 1.682, 2, 2.324, 2.663 and 2.812 g. The collapse response of the BF1 frame was investigated at six different levels of seismic intensity, namely 1.682, 1.692, 2.032, 2.075, 2.243 and 2.523 g.

6.10.1 Effect of vertical ground motions on the structural collapse probability of the DCF and BF1 frames

The results at various intensities are listed in Table 6-6 and Table 6-7 with and without the effect of the vertical ground motion component, where H represents the case where only the horizontal component is applied and H+V represents the case utilising the vertical and horizontal components together. The computed collapse probability is compared in these Tables. It is clear that the effect of the vertical component on collapse probability depends on the geometric irregularities of the structural systems and on the characteristics of the combined components. Figures 6-15 and 6-16 show the effect of vertical ground motions on structural collapse probability. The effect of the vertical component on the collapse probability varies according to the intensity level and the structural system.

The results indicate that the collapse probability of the irregular frame, the DCF frame, increased by up to 21.5% due to the inclusion of vertical ground motions, except for the intensity level of 1.682 g. The percentage of increase is not constant but varies according to the intensity level. It is worth noting that the failure modes observed confirm the significant effect of vertical ground motions.

Conversely, considering the effect of vertical excitation on the collapse response of the BF1 frame shows a different trend when compared to that of the DCF frame. The effect of the vertical component varies according to the seismic intensity levels. Considering vertical ground motions surprisingly causes a significant reduction in the collapse probability of the BF1 frame at intensity levels that are higher than the collapse resistance. However, the collapse resistance does not change when vertical motions are taken into account. While an increase in the collapse probability of up to 21.43% is observed at the lowest intensity levels. These differences in the collapse response under combined ground motions could be justified by the significant change in the potential of collapse in a small intensity level range, as depicted in Figure 6-14, illustrating that the intensity levels corresponding to collapse probability of 35.7% and 57.14% are 1.962 and 2.1 g, respectively. The collapse potential for the BF1 frame was raised by 21.44% due to a 0.14 g increase in the intensity level, indicating that a small change in the intensity level causes a marginal change in the collapse probability of the BF1 frame. Thus, in this range of intensity, the structure is expected to be very

sensitive to any variation in the loading scenario. It can be inferred that the contribution of vertical ground motions could dramatically alter the collapse potential if the structure were very sensitive to the seismic intensity level.

The irregular frame, the DCF frame, with a discontinuous column at the first storey was more sensitive to the inclusion of vertical motion than the regular frame, BF1, although the collapse resistance of the DCF frame was higher. Although both frames were adequately designed according to EC8 and satisfied the shear capacity design rules, the effect of vertical ground motions on the shear strength of the columns in both these frames was considerable.

Regarding BF1, shear failure was avoided and flexural-shear or flexural failure was developed in this frame. The increase in vertical seismic forces resulted in variations in the axial forces in the columns and an increase in shear demand. Despite the reduction in shear strength as a result of vertical ground motions, the capacity design rules helped to spread the damage among a larger number of columns in a number of storeys, leading to a delay in the development of the side-sway mechanism or sometimes preventing it, especially at higher intensity levels. In terms of the collapse response of the DCF frame, the missing column was often the main cause of structural collapse. It controlled the failure modes, leading to vertical rather than side-sway collapse in most cases. The collapse mechanisms for both frames will be discussed in more detail in section 6.10.2.

It can be concluded that ignoring the vertical components in a seismic collapse assessment may either lead to an underestimation or an overestimation of the collapse probability, depending on the structure's configuration and the seismic intensity level. Neglecting the contribution of vertical ground motions to irregular RC frame structures, especially those susceptible to shear failure, could lead to unsafe predictions. These results are generally consistent with previously mentioned studies. The differences are due to the fact that previously mentioned studies have often employed collapse criteria that relate to the global response and have assessed the effect of vertical motions at lower levels of deformation; while this study has adopted collapse criteria at the element level and focused on the collapse limit state. In addition, most previous studies have confirmed that the shear capacity of RC columns or piers often deteriorates due to the inclusion of the vertical component, so that when column shear failure is considered in assessment studies, the

contribution of the vertical component will then be apparent (Mwafy, 2001, Mwafy and Elnashai, 2006).

The analytical results of this study indicate that the effect of vertical motions on the displacements and inter-storey drifts prior to collapse show no clear trend. The total number of collapsed cases for each record at the pre-defined intensity levels for both frames with and without the vertical component is illustrated in Figure 6-18.

As can be seen in Figures 6-15 and 6-16, the effect of the vertical component often increases as the intensity level increases, due to P-Delta effects, even though the ratio of vertical to horizontal components is the same. The reason for this could be that the effect of the vertical component strongly depends on both the intensity of the vertical excitation and the V/H rather than on the ratio of the vertical to horizontal components only. In addition, the effect of combined components on the overall performance of a structure varies according to the intensity level and dynamic characteristics of the structure, which is also affected by the ground motion characteristics. The damage level and the spread of cracking increase at higher intensity levels. Therefore, the horizontal and vertical vibration periods of a structure can increase, leading to a different response depending on the shape of the response spectra of each record. For example, the vertical component of 007142ya-record, 007142za-record with V/H=1.52, has the strongest impact on the response of the DCF frame, followed by the vertical component of 001231ya-record, 001231za-record with V/H=0.64. The 007142za-record does not have any impact on the collapse probability of the BF1 frame, while the contribution of the vertical component of 00182ya-record with V/H=0.45 is most significant for the BF1 frame. Although the V/H of the 00198xa-record is 1.17, no effects have been observed on the collapse probability of the DCF frame, due to the inclusion of this component. Furthermore, the characteristics of the horizontal and vertical components have a considerable impact on the structure's response. A different trend in the collapse response of the studied frames is observed for each record. Also, the contribution of vertical ground motions on the collapse response of the two frames is completely different. These findings are consistent with the conclusions of other studies (Mwafy, 2001, Mwafy and Elnashai, 2006), which found that considering the effect of vertical motions is more significant at higher intensity levels than that at lower intensity levels, due to P-Delta effects.

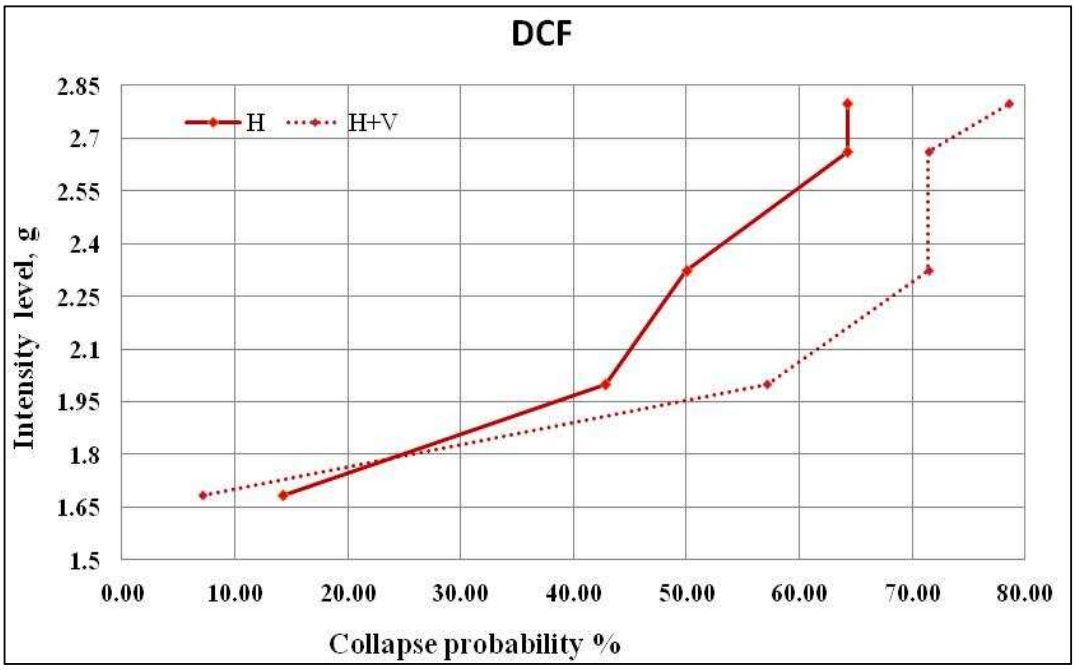

Figure 6-15: Structural collapse probability for the DCF frame

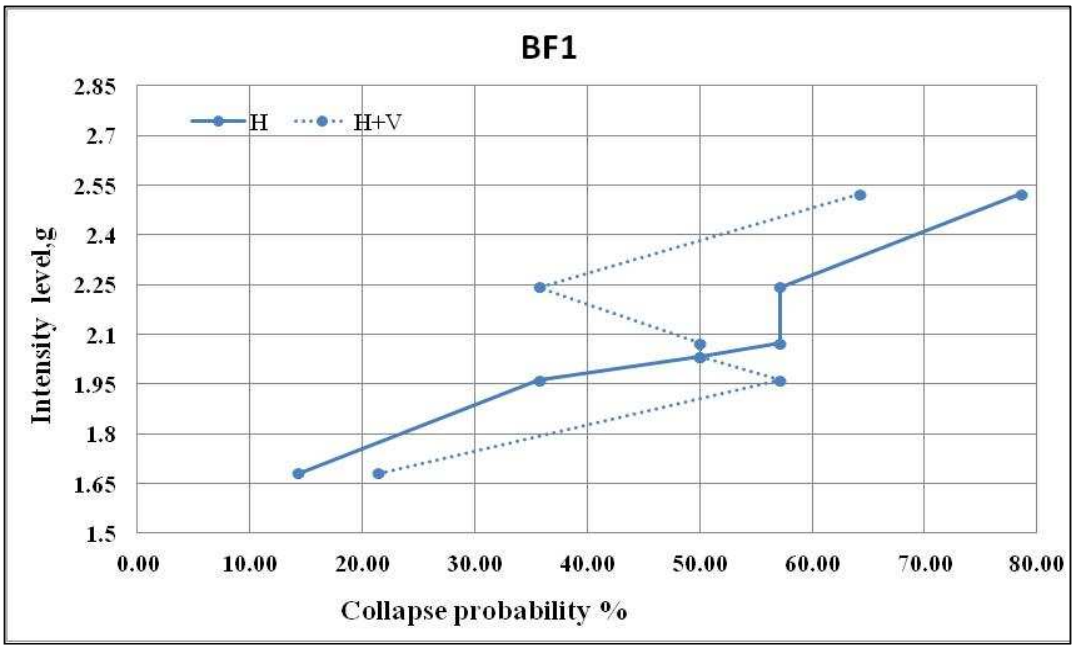

Figure 6-16: Structural collapse probability for the BF1 frame

The most demanding horizontal records are 001231xa and 004674xa for both frames, as they cause the structure to collapse at almost all intensity levels, see Tables 6-10 and 6-11.

The least demanding records are 000055xa, 000055ya and 006349xa. The effect of accounting for a vertical component is insignificant for some records. For example, 000055xa with V/H =0.75, 000055ya with V/H =0.85, 007142xa with V/H =0.88 and 004674xa with V/H =0.86 have minimal effect on the collapse response of both structures. While a considerable effect is observed for other records.

With regard to the DCF frame, 007142ya with V/H =1.52 is the most demanding record when it is utilised with its corresponding vertical component. These combined components trigger the vertical collapse of the DCF frame in most cases, where the collapse mechanism is dominated by the planted column, while no collapse case is observed when this frame is subjected to only the horizontal component of the record.

Regarding the BF1 frame, the combined vertical and horizontal components of 000182ya record with V/H =0.45 are the most demanding records. These cause the structure to collapse in five cases, compared to three cases when utilising only the horizontal component. On the other hand, utilising the 001231ya record plus its vertical component prevents the failure of the BF1 frame in three cases, compared to the cases where only a horizontal record is employed, as shown in Table 6-7. This could be due to the dissipation of the energy throughout a larger number of structural members because of variations in their axial forces.

The record-to-record variability is clear. A different collapse response is often detected for the seven records. Some unexpected cases are found; for example, the 006349ya record does not cause the DCF frame to collapse at the highest intensity level, even though it results in the collapse of this frame at all lower intensity levels. At an intensity level of 2.8 g, a first storey mechanism almost develops at 3 sec, as shown in Figure 6-17, but the following two strong shakings in the opposite direction help to return the frame to a stable position, leading to prevention of the side-sway collapse. This frame is severely damaged and on the verge of collapse.

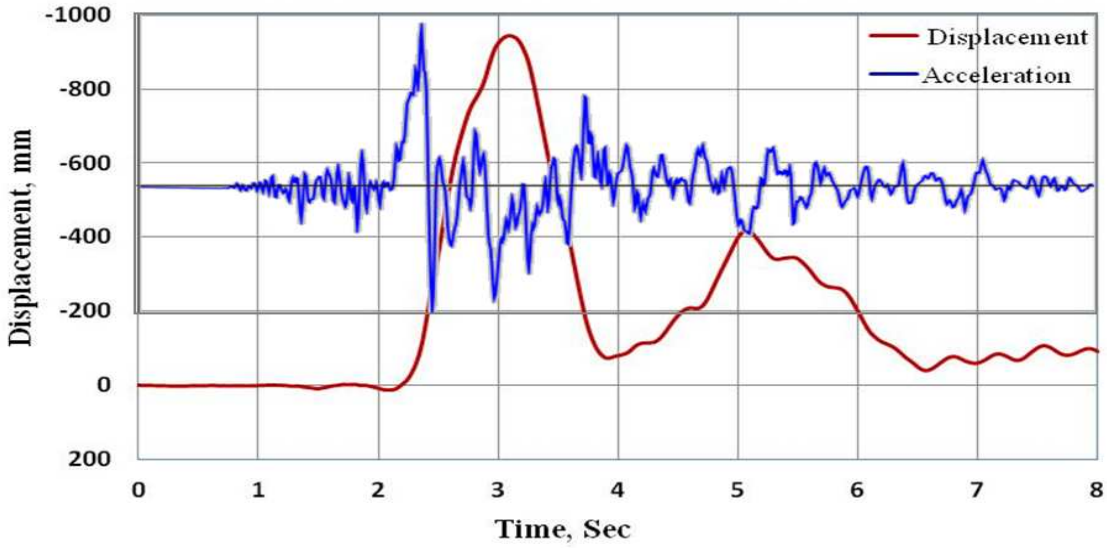

Figure 6-17: Lateral displacement of the first storey of the DCF frame under the 006349ya record

Table 6-6: Effect of the vertical component on the collapse probability of the DCF frame

	Record name	Intensity level / Case	1.682 g	2 g	2.324 g	2.663 g	2.8 g
DCF	000055ya	H					
		H+V					
	000055xa	H					
		H+V					
	007142ya	H					
		H+V		Partial collapse	Collapse	Collapse	Collapse
	007142xa	H		Collapse	Collapse	Collapse	Collapse
		H+V		Partial collapse	Collapse	Collapse	Collapse
	000198ya	H			Collapse	Collapse	Collapse
		H+V			Collapse	Collapse	Collapse
	000198xa	H		Collapse	Collapse	Collapse	Collapse
		H+V		Collapse	Collapse	Collapse	Collapse
	004674ya	H				Collapse	Collapse
		H+V			Collapse	Collapse	Collapse
	004674xa	H	Collapse	Collapse	Collapse	Collapse	Collapse
		H+V	Collapse	Collapse	Collapse	Collapse	Collapse
	006349ya	H		Collapse	Collapse	Collapse	Near collapse

		H+V		Collapse	Collapse	Collapse	Collapse
	006349xa	H					
		H+V					
	000182ya	H		Collapse	Collapse	Collapse	Collapse
		H+V		Collapse	Collapse	Collapse	Collapse
	000182xa	H					Collapse
		H+V					Collapse
	001231ya	H				Collapse	Collapse
		H+V		Collapse	Collapse	Collapse	Collapse
	001231xa	H	Collapse	Collapse	Collapse	Collapse	Collapse
		H+V		Collapse	Collapse	Collapse	Collapse
	Collapse probability %	H	14.29	42.86	50.00	64.29	64.29
		H+V	7.14	57.14	71.43	71.43	78.57

Table 6-7: Effect of the vertical component on the collapse probability of the BF1 frame

	Record name	Intensity level / Case	1.682 g	1.962 g	2.033 g	2.075 g	2.243 g	2.523 g
BF1	000055ya	H						Collapse
		H+V				Collapse		
	000055xa	H						
		H+V						
	007142ya	H						
		H+V						
	007142xa	H		Collapse	Collapse	Collapse	Collapse	Collapse
		H+V		Collapse	Collapse	Collapse	Collapse	Collapse
	000198ya	H		Collapse	Collapse	Collapse	Collapse	Collapse
		H+V		Collapse	Collapse	Collapse		Collapse
	000198xa	H				Collapse	Collapse	Collapse
		H+V		Collapse				Collapse
	004674ya	H						Collapse
		H+V						Collapse
	004674xa	H		Collapse	Collapse	Collapse	Collapse	Collapse
		H+V	Collapse	Collapse	Collapse	Collapse	Collapse	Collapse
	006349ya	H			Collapse	Collapse	Collapse	Collapse

		H+V		Collapse	Collapse	Collapse	Collapse	Collapse
	006349xa	H						
		H+V						
	000182ya	H			Collapse	Collapse	Collapse	Collapse
		H+V	Collapse	Collapse	Collapse	Collapse	Collapse	Collapse
	000182xa	H						Collapse
		H+V						
	001231ya	H	Collapse	Collapse	Collapse	Collapse	Collapse	Collapse
		H+V		Collapse	Collapse			Collapse
	001231xa	H	Collapse	Collapse	Collapse	Collapse	Collapse	Collapse
		H+V	Collapse	Collapse	Collapse	Collapse	Collapse	Collapse
	Collapse probability %	H	14.29	35.71	50.00	57.14	57.14	78.57
		H+V	21.43	57.14	50.00	50.00	35.71	64.29

6.10.1.1 Results at the collapse resistance of the DCF and BF1 frames

The collapse probabilities of the DCF frame at the intensity level of 2.324 g with and without a vertical ground motion component are approximately 71% and 50%, respectively. Ten ground motion records resulted in structural collapse for the former case, while only seven records led to collapse in the latter case. It is clear that the inclusion of a vertical component increases the probability of structural collapse by 21%. Table 6-6 illustrates which ground motion records caused the structural collapse in the two cases, with and without the inclusion of a vertical ground motion component.

It is interesting to note that inclusion of vertical components of 007142ya, 001231ya and 004674ya cause the structure to collapse at a lower intensity. This could be due to the fact that the spectral values of the 007142za and 004674za records in the range of the vertical period of the structure are the highest among all the records in the selected list, as shown in Figure 6-10. Thus, the effect of the vertical component of these records is more noticeable. The combinations of 007142za and 004674za records with their corresponding horizontal records, 007142xa, 007142ya, 004674xa and 004674ya records cause structural collapse in all four cases. The V/H ratios for these records vary between 0.81 and 1.52. Thus, it is clear that the contribution of the vertical component does not depend only on the V/H ratio, but also on spectral acceleration at the horizontal and vertical periods of the structure, the characteristics of the structure and of the vertical and horizontal components of the record utilised.

With regard to the BF1 frame, the collapse resistance was not affected by the inclusion of the vertical ground motion component. The same number of records caused the structural collapse of this frame in both the cases with and without the vertical component. The collapse mechanism with and without the inclusion of a vertical ground motion component will be discussed in more detail in the following section.

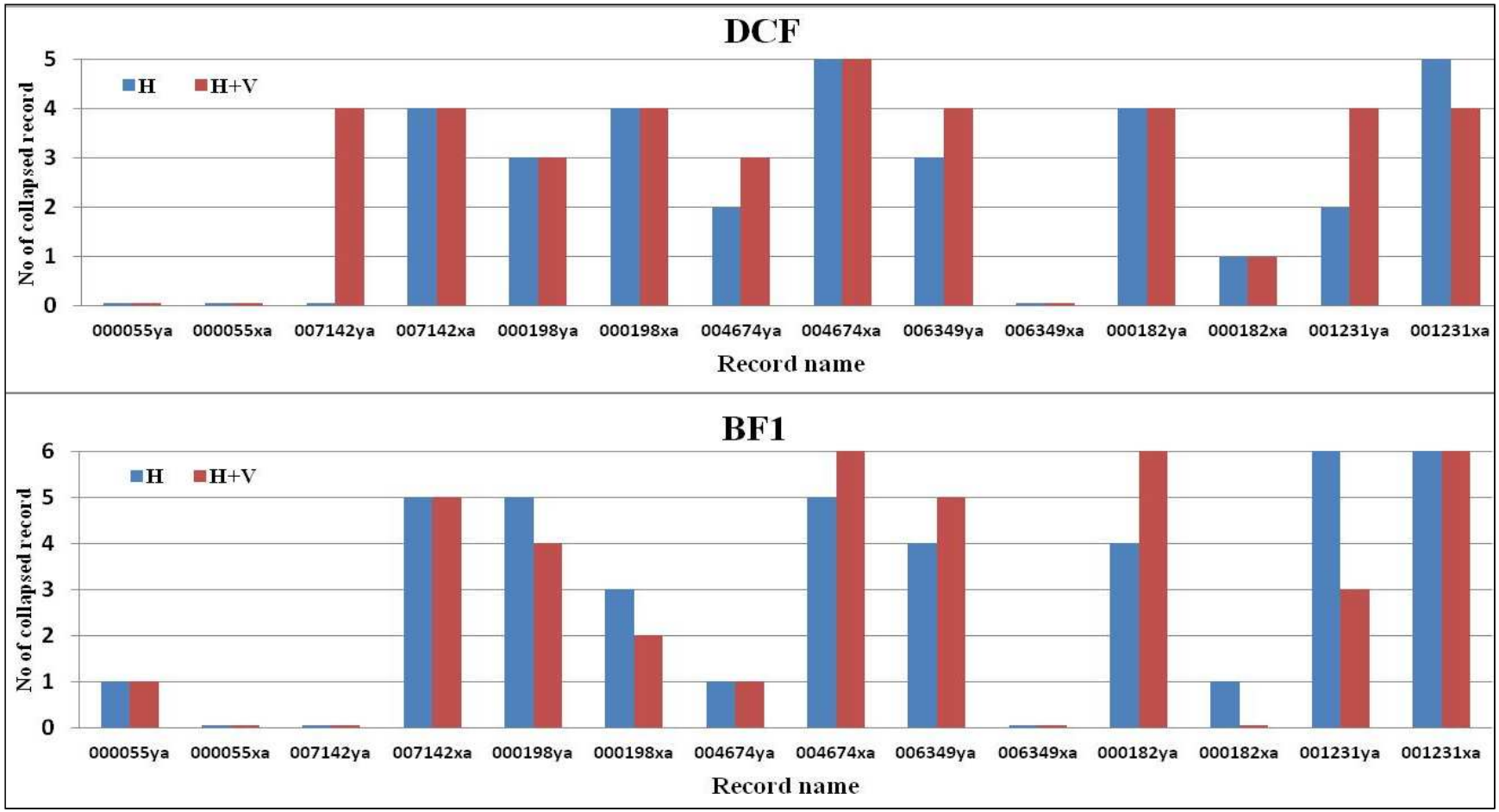

Figure 6-18: Number of collapsed records for the DCF and BF1 frames

6.10.2 Effect of vertical ground motions on the structural collapse modes of the DCF and BF1 frame

The collapse simulation based on the AEM allows for both side-sway and vertical collapse modes. Vertical collapse can occur due to axial or flexural-shear failure in columns, especially intermediate columns. Dynamic instability collapse, side-sway collapse, may occur due to large lateral displacements intensified by $P-\Delta$ effects in a single storey or more. The spread of initial damage to neighbouring elements and the impact from falling elements on surrounding members may lead to progressive collapse (Liu et al., 2003). In this study, the AEM permits element separation and the following dynamic redistribution of forces, accounting for the effect of additional loads resulting from impact due to falling debris.

Tables 6-8 and 6-9 illustrate failure modes, predicted by dynamic analyses with and without vertical ground motions, for the DCF and BF1 frames, respectively. Collapse mechanisms for the DCF and BF1 frames are also listed in Tables 6-10 and 6-11, respectively. The failure modes presented in Tables 6-10 and 6-11 are the collapse mechanism prior to the impact of elements falling with the surrounding structural members. For each RC frame, there are 12 distinct collapse mechanisms, all of which depend on the intensity level, the ground motion record and the contribution of a vertical component. In general, soft-storey mechanisms lead to a partial rather than total structural collapse, except in the case of a first-storey mechanism. When a soft-storey mechanism occurs at an upper storey, the lower part of the structure may still sustain the gravity loads and the additional debris loads. Impact forces increase the damage to both frames because the elements, which are subjected to impact forces, are already severely damaged prior to collision. The analytical results show that impact loading due to falling debris can lead to a progressive collapse (Liu et al., 2003).

In cases where the effect of vertical ground motions is not considered, various side-sway collapse modes are noted in both RC frames. This is due to the fact that the dimensions of the column cross-sections in the selected frames are different throughout the height of the structures. Soft-storey mechanisms are likely to develop on intermediate storeys, because of varying column cross-sections. Plastic hinges in the columns often developed on those

storeys containing smaller column cross-sections. In addition, it was found that a first-storey mechanism is very common in the DCF frame, which has tall columns in the first storey.

Considering the effect of the vertical component often causes vertical collapse in the DCF frame. 22 vertical collapse cases were observed under the combined ground motion components compared to two cases obtained under horizontal only motions. Both structures were most susceptible to side-sway collapse when only horizontal components were modelled. The DCF frame collapses in 30 side-sway collapse modes out of 32 collapse cases under only horizontal motions. Similarly, the BF1 frame collapses in 35 side-sway collapse modes out of 41 collapse cases under horizontal motions. The irregular RC frame is more vulnerable to vertical collapse, compared to the regular RC frame, where shear failure in the planted column and the support beam is detected in most cases, leading to a local rather than a global instability collapse, see the collapse cases described as V and S1+2 vertical in Table 6-8. The DCF frame collapses in the vertical mode, V, for more than ten cases, due to the inclusion of a vertical component. At higher intensity levels, the collapse mechanisms of the DCF frame are governed by the contribution of a vertical motion leading to vertical collapse for most records due to the higher axial forces in the structure columns. For example, the DCF frame vertically collapses in 9 cases out of 11 under combined components at an intensity level of 2.8 g.

Table 6-8: Potential collapse mechanisms for the DCF frame

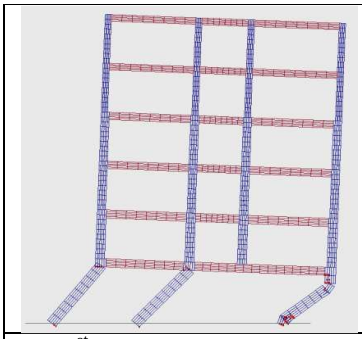	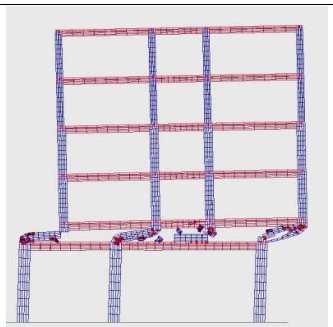	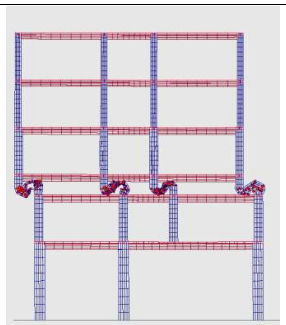
S1 (1st-storey mechanism)	S2 (2nd-storey mechanism)	S3 (3rd-storey mechanism)
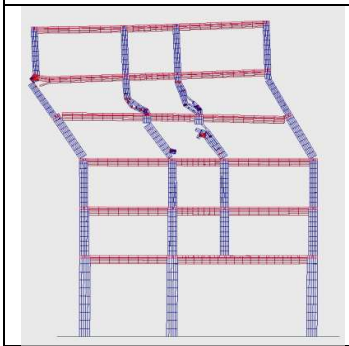	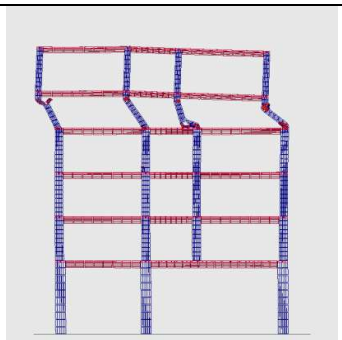	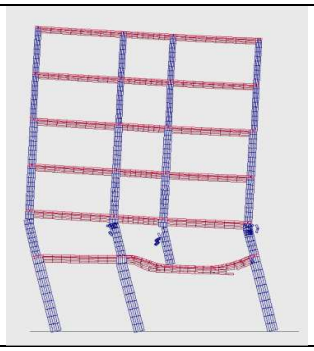
S4+5(4+5th-storey mechanism)	S5 (5th-storey mechanism)	S1+2 vertical
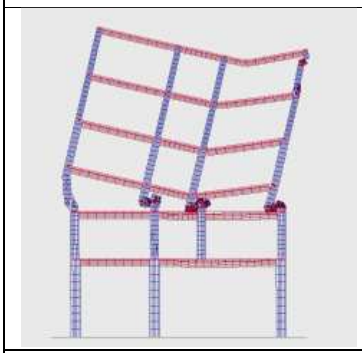	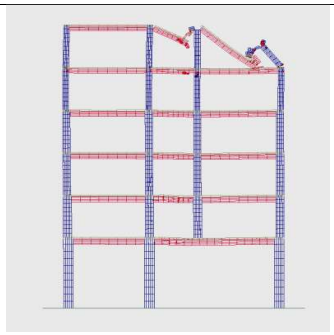	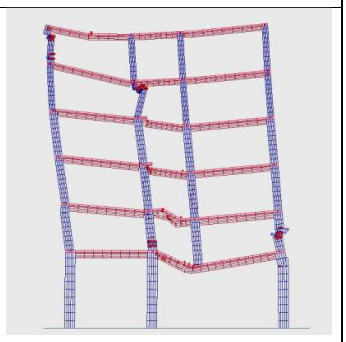
V3	Vp	V
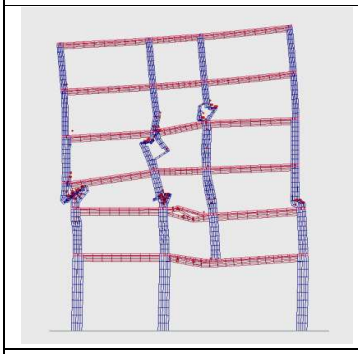	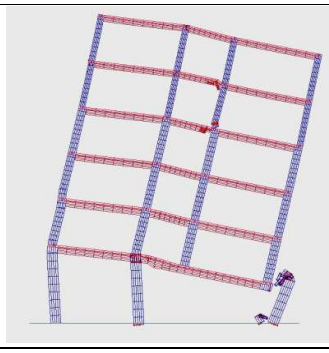	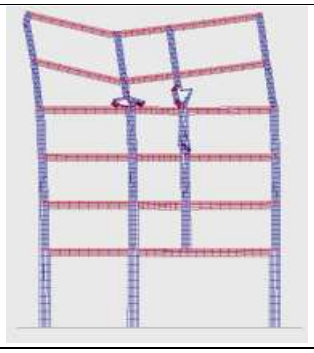
V2-5	R1	V5

Table 6-9: Potential collapse mechanisms for the BF1 frame

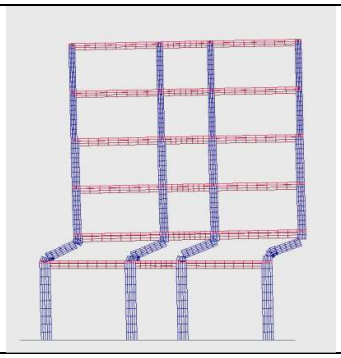	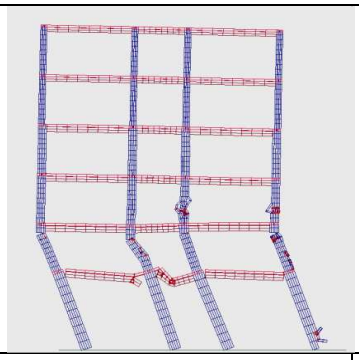	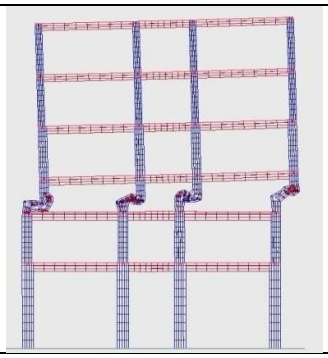
S2	S1+2	S3
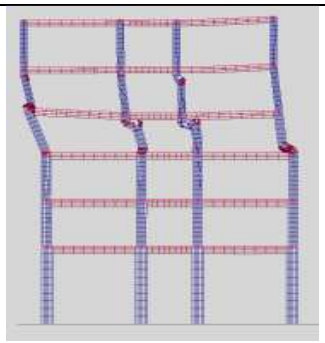	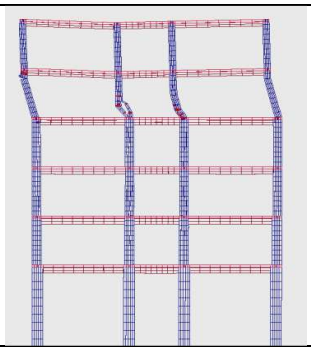	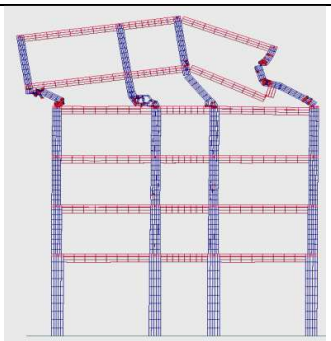
S4+5	S5	S5+top
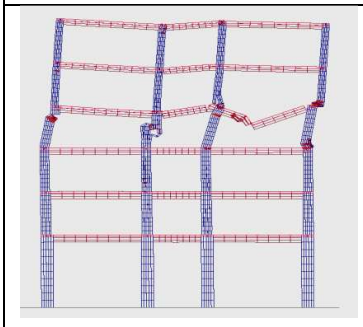	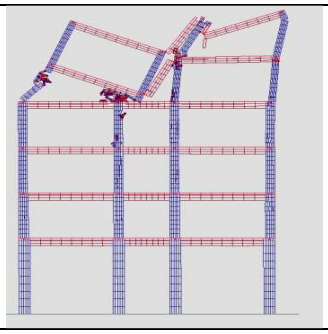	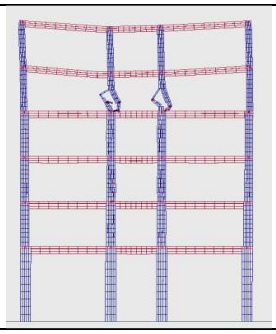
V4	p	V5
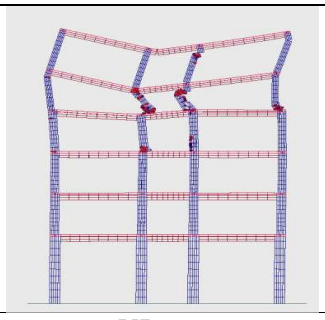	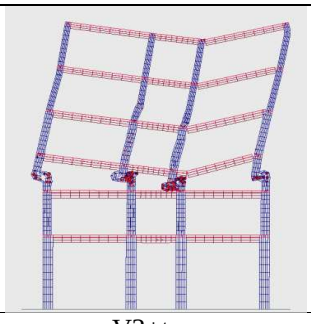	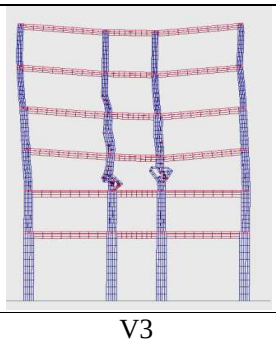
V5+top	V3+top	V3

Table 6-10: Effect of the vertical component on the collapse mechanisms of the DCF frame

	Record name	**Intensity level** / **Case**	**1.682 g**	**2 g**	**2.324 g**	**2.663 g**	**2.8 g**
DCF	000055ya	H					
		H+V					
	000055xa	H					
		H+V					
	007142ya	H					
		H+V		Vp	V	V	V
	007142xa	H		S5	S5	S5	S5
		H+V		Vp	V	V	V
	000198ya	H			S1	S1	S1
		H+V			S1	S1	S1
	000198xa	H		S3	S3	V3	S3
		H+V		S3	V3	V5	S3
	004674ya	H				V3	S5
		H+V			V	V	V
	004674xa	H	S1	S1	S1	S1	S1
		H+V	V3	S2	S1	S1+2v	V
	006349ya	H		S1	S1	S1	
		H+V		S1	S1	S1	R1
	006349xa	H					
		H+V					
	000182ya	H		S5	S5	S4+5	S5
		H+V		S5	S5	V5	V2-5
	000182xa	H					S3
		H+V					V3
	001231ya	H				S1	S1
		H+V		S3	S2	S1	R1
	001231xa	H	V3	S3	S3	S3	S1
		H+V		S3	S3	S3	V

Table 6-11: Effect of the vertical component on the collapse mechanisms of the BF1 frame

	Record name	Intensity level / Case	1.682 g	1.962 g	2.033 g	2.075 g	2.243 g	2.523 g
BF1	000055ya	H						S5
		H+V				S5+top		
	000055xa	H						
		H+V						
	007142ya	H						
		H+V						
	007142xa	H		S5	S5	S4+5	S4+5	S5
		H+V		V5+top	S5	p	S5	S5
	000198ya	H		S3	S3	S3	S2	S1+2
		H+V		S3	S3	S3		S2
	000198xa	H				V3	V3	V3
		H+V		V3				V3+top
	004674ya	H						S3
		H+V						V4
	004674xa	H		S1+2	S1+2	S1+2	S2	S2
		H+V	S2	S2	S2	S2	S2	S2
	006349ya	H			S2	S2	S2	S1+2
		H+V		S2	S2	S2	S2	S2
	006349xa	H						
		H+V						
	000182ya	H			S5	S5	S5	S5
		H+V	V4	S5	V3	S5+top	V3	S5
	000182xa	H						V5
		H+V						
	001231ya	H	S3	S3	S3	S3	S3	S2
		H+V		V3	V3+top			S2
	001231xa	H	S3	S3	S3	V3	V3	S3
		H+V	S3	V3	V3+top	S3	V3+top	S3

As a result of the capacity design requirements, no direct shear failure is observed. The columns of both frames yield first in flexure, followed by shear failure. The BF1 frame typically fails at the 2nd, 3rd and 5th storeys. Vertical ground motions often influence collapse modes. The vertical collapse cases for this frame have been increased from 6 to 15 cases, due to vertical ground motion effects. The BF1 frame experiences more distributed yielding when the effect of the vertical component on the collapse response is considered. More cracking and severe damage to a larger number of storeys leads to delay structural collapse. In general, the columns of both frames are more damaged when vertical ground motions are included.

As can be seen from Tables 6-8 and 6-9, the contribution of a vertical component is more pronounced on the top storey columns and intermediate columns, especially in the intermediate and higher storeys; for example, the failure modes called Vp and V for the DCF frame and P, S5+top and V3+top for the BF1 frame. The most frequent vertical failure modes occured in the 3rd, 4th and 5th storeys, the failure modes are called V3 and V5 and V2-5. This is because the axial loads in these columns are often low, and the axial forces resulting from flexural forces due to lateral loads are also low. This is consistent with the findings of (Mwafy, 2001, Mwafy and Elnashai, 2006).

It is worth noting that the effect when considering vertical motions on the collapse behaviour differs between records. The DCF frame fails in a 1st-storey mechanism under the 000198ya record both when the vertical component is considered, and when it is not. No effect from the vertical ground motion is found on the collapse modes under this record. On the other hand, including the 007142za vertical record in the analysis leads to local vertical failure governed by the missing column.

It is interesting to note that collapse assessment reflects that failure modes are not only associated with overall system ductility, but also with the loading scenario, as described by the intensity level and shape of the spectra of each component of the record. Vertical ground motion effects can accelerate the collapse of irregular systems but may delay the collapse of ductile structural systems.

RC frame structures, designed according to EC8, are capable of withstanding higher seismic intensity levels than the level they were designed for and of experiencing significant deformations prior to collapse. It was found that modern RC frames, which satisfy the

capacity design provisions including ductile reinforcement detailing and more stringent requirements on transverse reinforcements, are not vulnerable to unfavourable collapse modes, such as beam-column joint failure or column shear failure. However, soft-storey or multi-storey mechanisms cannot be completely prevented using modern seismic code provisions.

The failure modes reflect how important it is to simulate those aspects associated with the collapse process, such as element separation, force redistribution and impact forces; all of which can play an important role in determining the collapse behaviour of RC structures. Dynamic redistribution of gravity and seismic loads following the removal of a column can significantly change the collapse response. As discussed previously, in Chapter 5, the type and location of a first separated member are one of the key parameters that can affect failure mechanisms. As shown in Table 6-9, separation of corner columns and the discontinuities in framing can result in failure in the middle span of a neighbouring beam, which is generally not considered in FEM models. The AEM does not require any previous knowledge of crack and failure locations, as these cannot be predicted prior to analysis (Tagel-Din and Meguro, 1999a). Ignoring these effects may result in inaccurate predictions regarding failure modes. This study, which is based on the AEM, also highlights key aspects that affect the collapse behaviour. In order to assess the collapse response of RC structures with reliable accuracy, it is essential to model the structural response not only up to failure, but also until complete collapse, and to account for the key aspects that affect failure mode.

6.11 Conclusions

Based on the analytical investigations, some conclusions, which are subjected to the assumptions and limitation of the modelling approach, have been drawn as follows:

- The inclusion of vertical ground motion often influences the collapse probability and failure modes of RC frame structures, which are designed according to EC8. The collapse probability may increase or decrease according to overall structural system ductility, the characteristics of both vertical and horizontal components of each record and the intensity level of both components.

- The effect of the inclusion of vertical motions on collapse probability is not consistent at a given intensity level. Irregular frame structures are more likely to be sensitive to the inclusion of vertical ground motions.
- The ratio of vertical to horizontal accelerations does not reflect the contribution of the vertical component on the collapse process. The effect of vertical ground motion also increases in response to an increase in its intensity level.
- The effects of vertical ground motion can modify failure modes of modern frame structures, leading to vertical rather than side-sway collapse modes.
- Ignoring the effect of vertical ground motions in a collapse assessment of a modern RC frame structure can lead to unsafe predictions, especially for an irregular frame structure.
- A reliable simulation of the important aspects of collapse is required in a collapse assessment, especially for predicting failure mode and the extent of damage throughout a structural system. Ignoring the effect of element separation, contact and collision and any following force redistribution can lead to inaccurate predictions regarding the collapse process. The AEM can track the complete seismic behaviour of RC frame structures, and thereby account for the most important aspects of the collapse process.

Chapter 7 Scaling ground motions for seismic assessment of structures

7.1 Introduction

In order to evaluate the seismic response of structures using nonlinear dynamic analysis with acceptable accuracy, appropriate criteria for selecting and scaling ground motions should be used. Uncertainties in ground motions can significantly influence a structure's response. Although several approaches for selecting and scaling ground motions for seismic assessment and for code-based design have been developed recently, there is no consensus yet on the most appropriate selection and scaling criteria for use in a nonlinear time history analysis, especially when a structure is on the verge of collapse (NIST, 2011). Furthermore, most of the selection and scaling methods developed to date have not been used in engineering practice up to now, because the application of these approaches is complicated and may have not been considered in seismic codes. Scaling ground motion using a carefully selected intensity measure, IM, can result in accurate seismic assessments without any need to perform a detailed ground motion selection, as required by probabilistic seismic hazard analysis.

Determination of the mean annual frequency of exceeding a pre-defined limit state, such as the collapse limit state, for a specific structure at a given site presumes that the selected set of ground motions for nonlinear dynamic analyses is a good representative of the earthquake scenario for the given site. Furthermore, two key elements required to perform probabilistic seismic assessment are the ground motion intensity measure that describes the damaging effects of ground motions and the engineering demand parameters, EDPs, which describe structural damage. Maximum inter-storey drift ratios, maximum roof displacement ratios, peak floor accelerations, plastic hinge rotations, member forces, and damage indices are examples of commonly used EDPs. The IM provides a link between seismic hazard curves and structural analyses. The better is the correlation between these two elements, the more accurate is the evaluation of the structure response. A good correlation depends not

only on selecting a suitable IM but also on choosing an appropriate engineering demand parameter to represent the structural damage.

The intensity measure should be practical, efficient, sufficient and scaling robustness. The requirement that it should be practical is related to the feasibility when computing the seismic hazard map and hazard curves at a given site in terms of IM, as well as to the availability of attenuation relationships for the IM (Mehanny, 2009). Efficiency means that dispersion in the structural response of interest is relatively small so that the number of records to be used can be reduced without loss of accuracy. The number of records required to gain the same level of confidence in demand estimates is reduced by a factor of four when the dispersion is reduced by a factor of two (Vamvatsikos and Cornell, 2005). Meanwhile, sufficiency requires that the measures of the structural response given an IM are conditionally independent of magnitude, distance and other parameters of ground motion (Luco, 2002). The latter refers to the fact that linearly scaling the ground motions to different levels of seismic intensity does not introduce a bias in demand estimates and so no strong correlation exists between the scaling factor and the structural response (Tothong, 2007). It is worth nothing that these features depend on the characteristics of ground motions, e.g. near-field or ordinary motions, structure type and the structural response parameters of concern.

Several scaling methods have been developed for use in scaling records in a ground motion set to have the same seismic intensity, as expected at the site of concern. The scatter when estimating the seismic demands can be increased or decreased based on the scaling method selected. It has been found that the scatter depends on the type of structure and is increased as the seismic intensity level increases when structures experience highly nonlinear response (Cantagallo et al., 2012).

Ductile RC frame structures tend to experience much period elongation prior to collapse. Thus, the effects of spectral shape on these structures are expected to be important. Ductile frame structures tend to collapse at high seismic intensity corresponding to rare ground motions.

It has been stated that ground motion frequency content is associated with the hazard level. For example, ground motions corresponding to rare events with a small annual frequency of exceedance have different spectral shapes in the region of the structure's

fundamental period, than is the case for ground motions associated with frequent events (Baker and Cornell, 2006a).

The main aim of this study is not to provide an answer about which approach is the best method for selecting and scaling ground motions, but rather to examine the impact when using different intensity measures for scaling natural ground motion records on the prediction of the structural damage. Moreover, focus is on investigating a correlation between intensity measures and engineering demand parameters in terms of the peak roof drift, the peak inter-storey drift ratios and damage indices, determined based on changes to the first natural period of a structure for different levels of nonlinear response.

A review of the current approaches for selecting and scaling real ground motion records has been presented.

7.2 Earthquake scenarios

Earthquake scenarios can be defined using seismic hazard analysis, SHA, using either deterministic or probabilistic methods (Gupta, 2002). Deterministic seismic hazard analysis, DSHA produces earthquake parameters, e.g. a combination of magnitude and distance, as related to the maximum credible earthquake, MCE, which corresponds to the largest amplitude at a given site, and accounts for the seismic history and tectonic characteristics in the zone of interest. However, the likelihood of the occurrence of the maximum earthquake is not considered in a DSHA. Seismic hazard is computed using probabilistic seismic hazard analysis, PSHA, in order to calculate the mean annual frequency of exceeding various levels of an intensity measure, such as the peak ground acceleration or a spectral response value at a period of concern (Baker and Cornell, 2006a). PSHA accounts for the contributions from all the expected seismic sources, thus it can provide information about which earthquake scenarios are most likely to occur. The seismic hazard curve plots the annual probability of exceedance versus spectral accelerations. After which, the combination of seismic parameters that strongly contribute to the desired seismic hazard can be calculated through disaggregation of the probabilistic hazards, such as M, R and ε (Iervolino and Manfredi, 2008).

The attenuation relationship is a function of an intensity measure and different earthquake parameters, e.g. magnitude, site to source distance and soil conditions, and it is derived using regression analyses of recorded ground motion data.

The uniform hazard spectrum, UHS, developed by PSHA at a given site is a response spectrum for one probability level of exceeding of each ordinate. This spectrum is obtained based on the PSHA of a specific site by enveloping elastic spectral acceleration with a specified probability of exceedance for 50 years at all periods. It was concluded that using UHS as a target response spectra for record selection was not suitable. This is due to that fact that UHS is conservative and cannot represent the response spectra of any individual ground motion. This is because it is based on enveloping spectral values computed by the PSHA for each period. Thus, it does not consider the probability of a joint occurrence of spectral acceleration values at different periods (Baker, 2011). An alternative to the USH is the conditional mean spectrum including epsilon, CMS-ε.

The Conditional Mean Spectrum including epsilon is illustrated in Figure 7-1. The CMS-ε provides an expected mean response spectrum that is conditional on a target spectral acceleration at a single period, as obtained from PSHA. Disaggregation information about mean magnitude, distance and ε values is utilised to compute the conditional distribution of spectral acceleration values at other periods (Baker and Cornell, 2006a). In addition, correlations between ε values at different periods are required when calculating CMS-ε. CMS-ε depends on both target S_a and the period of interest. Epsilon, ε, is defined by seismologists as the number of standard deviations between the spectral acceleration of the selected un-scaled ground motion at a given period and the median spectral acceleration at the same period, as calculated according to attenuation function (Baker and Cornell, 2005). $\varepsilon(T)$ can be calculated using Equation 7-1 (Baker, 2011).

$$\varepsilon(T) = \frac{\ln S_a(T) - \mu_{\ln S_a}(M,R,T)}{\sigma_{\ln S_a(T)}} \qquad \text{Equation 7-1}$$

$\mu_{\ln S_a}$ and $\sigma_{\ln S_a(T)}$ are the mean logarithmic and the logarithmic standard deviation of $S_a(T)$. These two parameters can be determined from attenuation ground motion models.

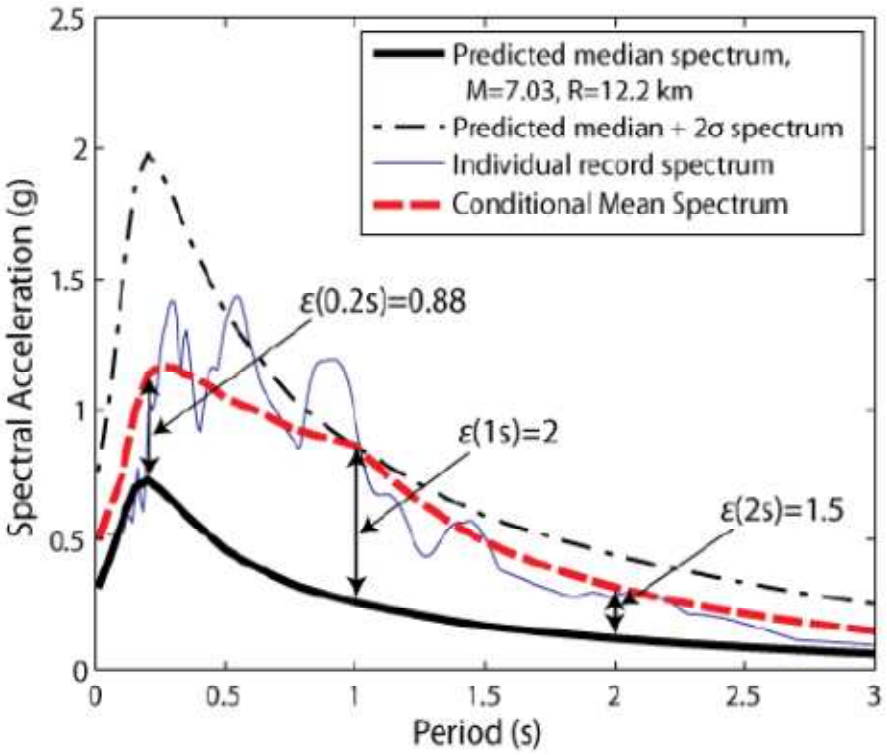

Figure 7-1: Conditional mean values of spectral acceleration at all periods, given $S_a(1S)$ (Baker, 2011)

7.3 Review of selection methods for nonlinear dynamic analysis

(Katsanos et al., 2010, Iervolino and Manfredi, 2008) have summarised the available criteria for ground motion selection as the follows:

7.3.1 Selecting record based on magnitude and distance

Earthquake magnitude, M, and source to site distance, R, in Km, are the two most common earthquake parameters used for record selection, as they are generally associated with earthquake scenarios. However, a number of studies have found that earthquake magnitude has a slight effect on various structural response, whereas the structure's response, particularly structural displacements or inter-storey drift ratios, are almost independent of the distance (Carballo and Cornell, 2000, Baker and Cornell, 2005, Luco, 2002, Bommer and Acevedo, 2004, Stewart et al., 2001). Therefore, M can be considered as an initial criterion for the selection of real records.

(Iervolino and Cornell, 2005) examined the importance of accounting for M and R in record selection on the nonlinear response in terms of the maximum drift. A large number of case studies were investigated, including SDOF systems with different periods, hysteresis relationships and levels of ductility, as well as MDOF systems representing RC and steel structures. Two groups of record sets were considered. The first group consisted of six sets of ten records corresponding to a specific scenario, M and R. The second group consisted of ten randomly chosen sets. The conclusions that were drawn based on this study indicated that the effects of M and R on the nonlinear structural response are minor. Nevertheless, the best practice for record selection, e.g. ASCE 2005, is currently based on an earthquake scenario, M and R, as determined by disaggregating the PSHA on the $S_a(T_1)$ value corresponding to a specified probability (Cornell, 2005).

7.3.2 Soil Profile at the site of interest, S

Another important selection criterion is soil type. The amplitude and the response spectra of ground motions are affected by soil type (Bommer and Acevedo, 2004). Soil profiles can be classified based on shear–wave velocity at the upper 30 m or according to the provisions of seismic codes, e.g. EC8 soil site classification. However, the number of specific (M, R and S) records may be limited, and not enough for nonlinear dynamic analyses. Therefore, the constraints when selecting M and R should be relaxed within an interval of $\mp\Delta M$ and $\mp\ \Delta R$, respectively.

7.3.3 Strong motion duration

A strong motion duration can be used as an additional selection criterion to M, R and S. Several studies concluded that strong motion duration affects some damage indices, relative to the hysteretic energy, while the indices based on peak displacement are insensitive to this criterion (Shome et al., 1998, Iervolino et al., 2006b).

7.3.4 Seismotectonic environment

The influence of seismotectonic environment on real ground motions has been highlighted in a number of studies. An example of the seismotectonic features are source path and environment, as well as the fault mechanism, e.g. normal, normal-oblique, reverse normal,

reverse oblique and strike slip. (Kappos and Kyriakakis, 2000) investigated the effect of using different seismotectonic environments and soil conditions on elastic and inelastic spectra. By examining reports it can be seen that the frequency content of records varied according to tectonic regime, whether American or Greek. In addition, the response of Greek records decays more rapidly.

7.4 Review of scaling methods for nonlinear dynamic analysis

In these methods, the ground motion non-stationary content is not modified, as opposed to the amplitude. These scaling methods can be classified into spectral matching-based methods that are generally adopted by seismic codes and intensity-based methods. The focus of this study will be on the latter.

7.4.1 Intensity-based scaling ground motion methods

The choice of appropriate scalar measures is a concern for most studies in this field.

The earliest scaling method is based on using the peak value of the ground motion acceleration, PGA, as a scalar intensity measure. PGA is only an efficient IM for low period structures. Using PGA as an IM can produce inaccurate response estimation and large dispersion, especially if the structure responds inelastically (Shome et al., 1998).

Other scaling measures are Arias intensity, AI; effective peak acceleration, EPA; effective peak velocity, EPV (Kurama and Farrow, 2003); Housner intensity, HI (Housner, 1952); velocity spectrum intensity, VSI; and acceleration spectrum intensity, ASI (Von-Thun et al., 1988). EPA is calculated by dividing the mean value of spectral acceleration in a period range from 0.1 to 0.5 sec by a factor of 2.5. Similarly, EPV is determined by dividing the mean value of spectral velocity in a period range between 0.8 and 1.2 sec by a factor of 2.5. EPA and EPV control the short-period range of the response spectra of the ground motion so that they are not suitable for structures with periods larger than 0.5 sec (Kurama and Farrow, 2003). HI is defined as the area under the pseudo-velocity response spectrum in a period range 0.1 to 2.5 sec. VSI is obtained in a similar way to HI but employs an absolute velocity spectrum. ASI is the area under the pseudo-acceleration response spectrum in a period range between 0.1 and 0.5 sec.

Cumulative absolute velocity, CAV, is the integral of the absolute value of the acceleration time history. A good correlation has been reported between CAV and structural damage (Kramer and Mitchell, 2006). Characteristic intensity, I_c, which accounts for ground motion amplitude and duration, can be used as a structural damage indicator. Another index for ground motion damage potential, denoted I_F, has been introduced by (Fajfar et al., 1990). I_F takes into consideration two ground motion parameters PGV and significant duration.

Yang et al. suggested using new non-structure intensity measures, improved effective peak acceleration, IEPA, and improved effective peak velocity, IEPV, for near-fault pulse-like ground motions (Yang et al., 2009). These two parameters can be determined in a similar way to the previous parameters, but utilise a different period range. The period range for IEPA is equal to $(T_{PA} - 0.2, T_{PA} + 0.2)$, while the IEPV period range is equal to $(T_{PV} - 0.2, T_{PV} + 0.2)$ sec. T_{PA} and T_{PV} are the periods corresponding to the maximum value of pseudo spectral acceleration and that of spectral velocity, respectively.

All of the previously mentioned IMs are independent of the structure's dynamic characteristics. Thus, they may produce large scatter in the estimated demands. Considering the structural vibration properties, when defining the intensity measure, can result in improved IM with less dispersion for estimating EDPs.

It has Also been found that the 5% damped spectral acceleration at the structure first period, $S_a(T_1)$, is an efficient and sufficient intensity measure (Shome et al., 1998). $S_a(T_1)$ is convenient as an intensity measure for estimating the drift response of structures, governed by the first mode of vibration and almost elastically response. When the structural system experiences strong degradation, its first mode period elongates due to the damage progression. This means that its response can be affected by all spectral values in the period range, from the initial fundamental period to the maximum elongated period. $S_a(T_1)$ does not provide adequate information regarding the spectral shape of the ground motion records. Thus, the elastic spectral acceleration or displacement is not a good intensity measure for prediction of highly nonlinear response. Furthermore, recent investigations have shown that scaling ground motion based only on $S_a(T_1)$ can lead to a larger scatter in the seismic demand estimates for near fault ground motions (Yahyaabadi and Tehranizadeh, 2011, Tothong and Luco, 2007, Luco and Cornell, 2007, Cordova et al., 2001) and for long-period structures, as

the higher-mode contribution is significant (Shome, 1999, Luco, 2002). $S_a(T_1)$ can be obtained from a code design spectrum or the uniform hazard spectrum, as determined from PSHA for the site of concern. This intensity measure is widely used, due to the fact that most hazard maps and hazard curves quantify seismic threat in terms of this parameter.

A scaling method based on the arithmetic mean of the 5% damped spectral accelerations over a range of periods $(T_0 \rightarrow T_\mu)$ has been introduced in order to allow for consideration of nonlinear response by accounting for period elongation (Kennedy et al., 1984, Kurama and Farrow, 2003, Martinez-Rueda, 1998). T_μ is the elongation period related to the secant stiffness associated with the peak displacement demand.

Shome has stated that scatter in the predicted deformation demands can be decreased by spectral averaging over a narrow frequency range, with the structure fundamental frequency located in the range centre, and by employing higher damping ratios for computing the acceleration spectra, as recommended by Kennedy et al. (Shome, 1999, Kennedy et al., 1984).

It has been noted that the response prediction of structures can be improved provided advance intensity measures considering the structure type, the spectral shape and the expected level of nonlinear response are used (Mehanny, 2009). A review of advanced intensity measures, which have been developed based on the information obtained from modal vibration analyses, pushover analyses, elastic spectral displacements or inelastic spectral displacements, can be summarised as follows:

Cordova and Mehanny developed a new two-parameter intensity measure accounting for period elongation corresponding to damage accumulation and nonlinear response as in Equation 7-2 (Mehanny, 1999, Cordova et al., 2001).

$$S_{a,cordova} = S_a(T_1)\left(\frac{S_a(c.T_1)}{S_a(T_1)}\right)^{\alpha} \qquad \text{Equation 7-2}$$

Estimation of the parameters α and c is based on an appropriate calibration of the results obtained from four multi-storey frames in order to minimise the variability in the estimated response. It has been suggested that $\alpha = 0.5$ and $c = 2$ be used for general applications. Attenuation functions for this new intensity measure can be obtained easily and directly from

those attenuation relationships corresponding to $S_a(T_1)$ and $S_a(cT_1)$, provided that the correlation coefficients between these two variables, which have determined by (Inoue and Cornell, 1990), are available.

Previous research has introduced several new structure-specific intensity measures for near-source and ordinary ground motions (Luco, 2002, Luco and Cornell, 2007). The peak inter-storey drift angle was the EDP of interest. These six alternative IMs involve an adjustment of $S_a(T_1)$ to reflect the higher-mode contributions or the level of excepted inelasticity or both. Two of the proposed IMs, denoted $IM_{1E\&2E}$ and $IM_{1I\&2E}$, allow for the consideration of the effect of the second mode. The four remaining scalars, involving the properties of the first mode of vibration are $IM_{1I}, IM_{1E}, IM_{1eff}$ and IM_{1eq}, corresponding to inelastic spectral displacement, elastic spectrum at T_1, elastic spectral displacement at an effective period and spectral displacement of an equivalent SDOF elastic oscillator, respectively. Through assessment of the response of three moment-resistance steel structures with different heights under two ground motion sets corresponding to near-source and ordinary records, it has been concluded, using a one-parameter linear regression model, that the most efficient and sufficient IMs for the three structures investigated under both of the ground motion sets is $IM_{1I\&2E}$. This is due to the fact that $IM_{1I\&2E}$ combines both inelastic spectral displacement and higher-mode contributions. The formulation of the best IMs is as in Equations 7-3 and 7-4.

$$IM_{1I\&2E} = \frac{S_d^I(T_1,\xi_1,d_y)}{S_d(T_1,\xi_1)} IM_{1E\&2E} \quad \text{Equation 7-3}$$

$$IM_{1E\&2E} = \sqrt{\left[PF_1^{[2]} S_d(T_1,\xi_1)\right]^2 + \left[PF_2^{[2]} S_d(T_2,\xi_2)\right]^2} \quad \text{Equation 7-4}$$

$PF_1^{[2]}, PF_2^{[2]}$ are the first-mode and second-mode participation factors for the storey related to the SRSS estimate of the first two modes of vibration, respectively, $S_d(T_1,\xi_1)$ is the elastic spectral displacement corresponding to the first-mode, $S_d(T_2,\xi_2)$ is the second-mode elastic spectral displacement, and $S_d^I(T_1,\xi_1,d_y)$ is the first-mode inelastic spectral displacement. $S_d^I(T_1,\xi_1,d_y)$ can be computed from an elastic-perfectly-plastic, a bilinear or a trilinear oscillator, with period of T_1, a damping ratio of ξ_1, and yield displacement of d_y determined with a pushover analysis.

Tothong and Cornell developed a scalar intensity measure based on inelastic spectral displacement, S_{di}, for structures governed by the first-mode of vibration for both ordinary and near-source pulse-like records (Tothong and Cornell., 2007). It was proved that the efficiency and sufficiency of this intensity measure is better than that conventionally used $S_a(T_1)$. $IM_{1I\&2E}$ is recommended for structures with higher-mode contributions. By using this scalar measure, consideration of epsilon can be avoided. The spectral shape at longer periods than T_1 can be captured well by S_{di}. Moreover, this advanced scalar measure can capture the effects of pulse-like ground motion, as opposed to the vector intensity measure consisting of $S_a(T_1)$ and ε, which is deficient for near-source ground motion (Tothong, 2007). The applicability of these intensity measures is relatively limited (Bojórquez et al., 2008). This is due to the fact that there are some difficulties associated with the computation of the seismic hazard curve in terms of S_{di} and $IM_{1I\&2E}$. Although empirical attenuation relations for S_{di} and $IM_{1I\&2E}$ with given properties of ground motions, e.g. M, R, site condition, are estimated by Tothong (Tothong, 2007), this attenuation model is not yet widely known.

(Hutchinson et al., 2004) suggested using the average elastic spectral displacement over a range of periods, Δ_{mean}, as an IM for predicting the inelastic response of bridges subjected to near-fault motions. The lower and upper bounds of the period range correspond to the fundamental period and the period related to the secant stiffness, which corresponds to the maximum displacements.

(Baker and Cornell, 2006a, Bianchini, 2008) proposed a new intensity measure, namely $S_{a,avg}(T_1, \dots, T_n)$, in order to predict nonlinear response of structures. $S_{a,avg}$ is defined as the geometrical mean of the spectral acceleration ordinates in a $(T_1, \dots, T_n)$ set of periods corresponding to periods of interest and related to the structure fundamental period as in Equation 7-5.

$$S_{a,avg}(T_1, \dots, T_n) = \left(\prod_{i=1}^{n} s_a(T_i)\right)^{\frac{1}{n}} \qquad \text{Equation 7-5}$$

A set of ten periods with logarithmic-spacing rather than arithmetic-spacing is recommended for use when computing the scalar as in Equation 7-6 (Bianchini, 2008):

$$S_{a,avg} = \left(\underbrace{s_a(k_1 T) \times \dots \times s_a(k_u T)}_{10 \text{ points log-spaced}}\right)^{\frac{1}{10}} \qquad \text{Equation 7-6}$$

It has been noted that $S_{a,avg}$, which considers effects of both higher modes and structure softening, as a result of employing $k_1$and k_u, is a better intensity measure than both $S_a(T_1)$ and PGA for seismic assessment of SDOF and MDOF systems (Bianchini et al., 2009). The optimal values for k_1 and k_u are structure specific. It has been concluded that using $k_1 = 0.25$ is suitable for structures affected by higher modes, while $k_1 = 1$, should be used for SDOF systems or structures dominated by the fundamental period. Setting k_u as equal to 2 or 3 is suitable for structures with ductility levels of 2 and 4, respectively. Furthermore, computing the seismic hazard in terms of $S_{a,avg}$ is simple and can be performed in a similar way to that corresponding to a single value of S_a, and by using existing attenuation laws.

(Mehanny, 2009) improved the new two-parameter intensity measure developed by (Cordova, 2000). The expected level of structural damage is related to the ground motion intensity, and the structure capacity. Thus, instead of using a constant value for the parameter c for all structures with different strengths, a self-adaptive multiplier for the structure first mode period, $c = f(R)$ is utilised to reflect the period elongation, corresponding to the expected damage level associated with the design assumptions adopted in the structure of interest. R is the nominal relative lateral strength of an equivalent SDOF system. $R = \frac{V_e}{V_y}$ is calculated from a pushover analysis of a MDOF. c is set as equal to $\sqrt{R}$, where equal displacement rules hold true, otherwise $c = \sqrt[3]{R}$ (e.g., for long-period structures). Based on the evaluation of nonlinear response of a large number of first-mode dominant structures represented by SDOF systems with different constitutive models, levels of cyclic degradation and R values under four sets of ground motions corresponding to different scenarios, the efficiency and sufficiency of the proposed IM have been proved. This scalar does not account for the contribution of higher modes. Thus, it is not suitable for use in the seismic assessment of tall and long-period structures. Also, it has been noted that this improved IM is not recommended for use for very short-period structures.

(Weng et al., 2010) proposed a new scaling method for high-rise structures, dominated by higher-mode effects. In this method, the scaling factor was determined by minimising the differences between the spectral parameters of a scaled record and those of the design spectra, for the first few important modes. The modes, which constitute not less than 90% of the total effective mass of the structure, should be considered here.

Alternative scalars based on spectral acceleration at periods different from the first-mode elastic period were introduced. In a seismic assessment, the most important aspects in scaling records incorporating $S_a(T)$ as IM are the reference level for the spectral acceleration and the reference period T. It was suggested that using 1.1 times the structure fundamental period as a reference period is necessary for scaling. The minimum required number of records for use in seismic assessment, in order to obtain reliable results, is about 30 records (Catalan et al., 2010).

(Cantagallo et al., 2012) suggested two values to use for the reference periods, called: T_{crack} and T_*, resulting in two IMs, $S_a(T_{crack})$ and $S_a(T_*)$. T_{crack} and T_* are the cracked and the inelastic periods determined from pushover analyses. The latter can be determined according to Equation 7-7.

$$T_* = 2\pi\sqrt{\frac{m^* \times d_y^*}{F_y^*}} \qquad \text{Equation 7-7}$$

$m^*$is the mass of the equivalent SDOF system, d_y^* is the yield displacement, and F_y^* is the ultimate strength.

A new scalar intensity measure based on the spectral acceleration at the fundamental structure period and the spectral shape, I_{NP}, was proposed by (Bojorquez and Iervolino, 2011) as shown in Equation 7-8.

$$I_{NP} = S_a(T_1)N_P^{\alpha} \qquad \text{Equation 7-8}$$

N_p is a new proxy for spectral shape, introduced by (Ibarra and Krawinkler, 2004); see Equation 7-9.

$$N_p = \frac{S_{a_{avg}}(T_1,\ldots,T_N)}{S_a(T_1)} \qquad \text{Equation 7-9}$$

If the value of N_p of a record is lower than one, this means that the spectra tend to decrease beyond T_1 and vice versa. The optimal value for α is 0.4. T_N can be set as equal to $2T_1$ or to nearly $2.5T_1$ (Bojorquez et al., 2012, Bojorquez and Iervolino, 2011). I_{NP} is a good predictor for ordinary, as well as for near-fault pulse-like ground motions. Computing seismic hazard in terms of I_{NP} can be easily performed using tools currently available.

(Yahyaabadi and Tehranizadeh, 2011) introduced a new displacement-based scalar intensity measure incorporating optimal combinations of elastic spectral displacements and considering the effects of higher modes and period elongation. The EDP of interest was the peak inter-storey drift ratio. The results of the IDA of several generic one-bay frames subjected to 40 pulse-like ground motions showed that optimal combinations of spectral displacements depend on structure type (e.g. short, moderate and long period structures) and seismic intensity level. The contribution of higher modes can be neglected for relatively short-period structures (e.g. structures with up to six storeys), while they dominate the response for long-period structures, in which the effects of the elongation period are insignificant. The contribution of spectral parameters at longer periods than T_1 increase as the seismic intensity increases. Consequently, these effects should be considered in the improved IM, in such a way that it reduces the record-to-record variability at higher intensity levels, provided it does not result in more scatter at lower levels. The improved intensity for collapse assessment additionally involves $S_d(1.6T_1)$. The two general formulations for the improved IM in non-collapse and collapse cases are as shown in Equations 7-10 and 7-11.

$$IM_{Nc} = \left[\Gamma_1^2\left[0.8\, S_d^2(T_1) + 0.2\, S_d^2(1.2T_1)\right] + \Gamma_2^2 S_d^2(T_2)\right]^{0.5} \quad \text{Equation 7-10}$$

$$IM_c = \left[\Gamma_1^2\left[0.4\, S_d^2(T_1) + 0.4\, S_d^2(1.2T_1) + 0.2\, S_d^2(1.6T_1)\right] + \Gamma_2^2 S_d^2(T_2)\right]^{0.5} \quad \text{Equation 7-11}$$

$S_d(T_1)$ and $S_d(T_2)$ are the elastic spectral displacements corresponding to the first two modes. $\Gamma_1 = PF_1 \times ID_1$, PF_1 and ID_1 are the first mode participation factor and the inter-storey drift related to the storey where $\sqrt{[PF_1 ID_1\, S_d(T_1)]^2 + [PF_2 ID_2\, S_d(T_2)]^2}$ is maximised.

Attenuation models for the new IMs can be derived directly from the existing attenuation relationships for S_d and the correlations between S_d at different periods.

(Kadas et al., 2011) developed an intensity measure to account for the period elongation of structures under earthquake loadings. A new IM, called I_a, accounts for the spectral shape along the period softening path by utilising the area under the elastic acceleration spectrum in the period range from the fundamental to the elongated period, normalised by the structure's yield capacity, A_y, and $(T_f - T_1)$. (Kadas et al., 2011) adapted this IM to more accurately reflect the features of descending or ascending spectra, by adding the term $(T - T_1)$. The formulations for these two IMs are as given in Equations 7-12 and 7-13.

$$I_a = \frac{1}{A_y(T_f - T_1)} \int_{T_1}^{T_f} S_a(T, \xi)\, dT \qquad \text{Equation 7-12}$$

$$I_{am} = \frac{1}{A_y(T_f - T_1)} \int_{T_1}^{T_f} S_a(T, \xi)(T - T_1)\, dT \qquad \text{Equation 7-13}$$

T_1 and T_f are the initial and elongated periods and can be determined from a pushover analysis. Also, T_f can be estimated from Equation 7-14 for $S_a(T_1) > A_y$.

$$T_f = 1.07 \times T_1 \times \left[\frac{S_a(T_1)}{A_y}\right]^{0.45} \leq 2T_1 \qquad \text{Equation 7-14}$$

The response of seven RC frames under a set of 100 ground motion records, representing a wide range of ground motion characteristics, has been evaluated using the two proposed IMs and the unnormalised I_a. It was found that the best correlations are obtained between the maximum inter-storey drift ratio and the unnormalised I_a, as well as I_{am}. However, I_{am} is preferable as it accounts for spectral shape and structural capacity.

A scaling method based on modal-pushover analyses was proposed by (Kalkan and Kwong, 2011, Kalkan and Chopra, 2010, Kalkan and Chopra, 2011, Kalkan and Chopra, 2012, Reyes and Chopra, 2012). This method explicitly accounts for the structural strength, estimated according to the pushover curve related to the first mode. Each record in the set is scaled to match the target inelastic deformation value. The scale factor for a single record is determined in such a way that the maximum deformation obtained from the time history analysis of the inelastic SDOF system, with force-deformation associated with the pushover curve under the record of concern, is almost matched to the target value. The target value is the median peak inelastic deformation obtained from a large ground motion set compatible with the seismic hazard at a specific site. This value can be determined by multiplying the value of deformation corresponding to the target spectrum using the inelastic deformation ratio calculated from the empirical equation developed by (Chopra and Chintanapakdee, 2004) based on the yield-strength reduction factor. Moreover, this method allows the user to check the higher-mode compatibility and select a subset with higher-mode consideration. The subset consists of scaled records, in which elastic spectral displacements at the second period approximate to the target value.

7.4.2 Vector-valued ground motion intensity measures

Several vector-valued intensity measures have been proposed to improve the efficiency of the scalar intensity measures. Most vector-valued intensity measures are comprised of two or more parameters. Commonly, the first parameter is the elastic spectral acceleration at the fundamental period of the structure. The latter parameters commonly account for the spectral shape of the ground motion records.

Vector intensity measures accounting for the effect of higher modes have been proposed, such as a vector of $S_a(T_1)$ and $S_a(T_2)$ or of $S_a(T_1)$ and $S_a(T_1)/S_a(T_2)$ (Bazzurro, 1998, Shome, 1999).

Using a vector consisting of $S_a(T_1)$ and the spectral shape parameter, epsilon, ε, is more convenient for predicting highly nonlinear response of structures than a scalar IM (Baker and Cornell, 2005). As previously mentioned, ε is a measure of the difference between the mean predicted and the record spectral acceleration at a given period. The expected epsilon depends on the site of the selected structures and the hazard level of interest. For instant, $\varepsilon = 0$ in the Eastern United States and $\varepsilon = +2$ in coastal California for the 2% in 50 year ground motion (Haselton et al., 2008b). The epsilon value is generally positive for rare ground motions, corresponding to 2% in the 50 years hazard level. While negative epsilon values are expected for frequent ground motions with hazard levels 50% in 50 years (Baker and Cornell, 2006a). Furthermore, the value of ε is also affected by the attenuation relationship used and the period of interest. (Baker and Cornell, 2005) investigated the effects of accounting for the ground motion spectral shape, as represented by ε, on the structural collapse capacity of a reinforced concrete structure and a number of generic frame models. It was found that the collapse capacity increased if records with as large as ε as recommended, based on the results of ground motion hazard disaggregation, were considered. Moreover, the impact of ε on the seismic response of structures is larger than the effects of M and R. This is due to the fact that ε is a better index for spectral shape (Baker and Cornell, 2005, Baker and Cornell, 2006a).

The spectral shape strongly affects the collapse capacity prediction. The effects of spectral shape can be reduced by using a more appropriate IM for collapse analysis. It was concluded that selecting ground motion records with a proper ε at the effective period of the

structure, and then scaling the records to a target spectral acceleration at this effective period, rather than the fundamental period, is better in reducing the structure's sensitivity to the spectral shape, ε (Haselton and Baker, 2006). The optimal effective period for ductile structures is around twice its fundamental period. However, the vector intensity measure $< S_a(T_1), \varepsilon >$ is not efficient for predicting the response of structures under pulse-like ground motions (Tothong and Cornell., 2007).

(Mousavi et al., 2011) introduced a new spectral shape index, namely eta, η. Eta is a linear combination of two epsilons: the previously mentioned epsilon, which is associated with the spectral acceleration, and a new parameter called the peak ground velocity epsilon, ε_{PGV}. An analytical equation was developed based on regression analyses, in order to predict the target ε_{PGV} for a given ε_{Sa}. It was stated that this new spectral shape indicator is more efficient than the convenient ε_{Sa} for predicting the nonlinear response of structures with periods in the range of 0.25 to 3 sec.

A new vector-valued ground motion intensity measure consisting of the spectral acceleration at the fundamental structure period and the spectral shape proxy, N_p, was introduced by (Bojorquez and Iervolino, 2011, Bojórquez et al., 2008). They found that the IM vector <Sa, Np> is not only good in predicting maximum displacement, but also in estimating cumulative damage (Bojórquez et al., 2008). Furthermore, the efficiency of this vector at different intensity levels was explored and proved based on a comparison between $< S_a(T_1), R_{T_1,T_2} >$ and $< S_a(T_1), \varepsilon >$. Moreover, $< S_a(T_1), N_p >$ was shown to be a better candidate for near-source pulse-like ground motion and narrow-band motions (Bojorquez and Iervolino, 2011). Also, $< S_a(T_1), N_p >$ was found to be less sensitive to the value selected for the final period than $< S_a(T_1), R_{T_1,T_2} >$.

There are many difficulties involved in using vector-valued IMs. For example: scaling techniques used, hazard calculations, seismic hazard analyses and attenuation functions for vectors of parameters (Mehanny, 2009).

7.5 Review of investigations on the effect of using different scaling methods on nonlinear dynamic response

A number of studies have been carried out to investigate the correlations between several IMs and EDPs.

Kurama and Farrow studied the effectiveness of seven ground motion intensity measures associated with ground motion characteristics, in decreasing the variability in the peak displacement demands (Kurama and Farrow, 2003). A large number of nonlinear SDOF systems, subjected to four ground motion sets with different characteristics and epicentral distances were studied. In addition, two MDOF systems subjected to a set of 20 records were considered. The selected IMs were the peak ground acceleration, effective peak acceleration, Arias parameter, AI, effective peak velocity, maximum incremental velocity, MIV, spectral acceleration at the fundament period and spectral acceleration over a range of periods, $S_a(T_0 - T_y)$. It was found that the effectiveness of the intensity measure depends on the characteristics of both the soil site and the structures, in terms of structural strength and period of a structure. A good scaling method for stiff soil and far-field may result in large scatter for soft soil and near-field ground motions. Using maximum incremental velocity as an IM for scaling ground motion records can result in less scatter in estimated peak displacements, when compared with results obtained using the other six IMs, for most structural characteristics at sites with different soil characteristics. Although the MIV scaling method depends on ground motion parameters only, and can be easily applied to different structures, implementation of this intensity measure for performance-based assessment requires an estimation of the mean annual frequency of exceeding the MIV at a given site and an attenuation relationship for MIV.

(Luco et al., 2005) examined the efficiency of a number of scalar IMs and vector-valued IMs on the response of three steel moment-resisting frame structures, with different numbers of storeys: 3, 9 and 20, under two sets of 70 ground motions representing near-field and ordinary motion. The parameters for ground motions with available attenuation functions were selected, such as: $S_a(T_1)$, $S_a(T_2)/S_a(T_1)$, $S_a(T_3)/S_a(T_1)$, $S_a^D(T_1, d_y)/S_a(T_1)$ and energy-based parameters. The correlations between several vectors consisting of a different combination of previously mentioned ground motion parameters, and a vector of the

maximum inter-storey drift ratios for all the structure storeys was also studied. The results indicated that the vector accounting for the effects of higher modes and inelasticity is the best predictor of the nonlinear response.

Riddell studied the efficiency of 23 simple ground motion intensity parameters employing SDOF systems with different periods and using three nonlinear models (Riddell, 2007). It was shown that the effectiveness of these parameters was dependent on characteristics of a structure. Some parameters correlated well with structural damage for only short-to-medium period structures, while others had a good correlation for long period structures. None of the investigated intensity parameters was a good damage indicator for the entire period range.

Yakut and Yalmaz examined the correlation between several commonly used intensity measures and the maximum inter-storey drift ratio of 16 reinforced concrete frames subjected to 80 records, with different levels of seismic intensities (Yakut and Yalmaz, 2008). The selected ground motion parameters were PGA, PGV, $S_a(T_1)$, CAV, ASI, VSI, AI, I_c, I_F and EPA. It was noted that the spectrum intensity parameters, such as: HI, VSI, ASI and $S_a(T_1)$, were superior to other intensity parameters, which were calculated using ground motion records for medium period structures.

Bianchini compared the efficiency of $S_{a,avg}$ with other intensity measures, e.g. PGA, PGV, PAD, $S_a(T_1)$, and S_{di}, based on dispersion (Bianchini, 2008). A set of SDOF and MDOF systems with different types, hysteretic models, periods under a set of 40 ordinary records was considered. The results show that $S_{a,avg}$ is the best, out of all the IMs considered, except for S_{di}. S_{di} is better for MDOF systems with short period.

(Lucchini et al., 2011) investigated the correlation between five intensity measures and two EDPs for a complex structure, an irregular three-dimensional structure under bi-directional ground motion, rather than unidirectional ground motions, which had been the primary focus in the most previous studies. The maximum ratio of inter-storey drift and the maximum ratio of roof drift were the two EDPs selected. The IMs of interest were $S_a(T_1)$, $S_{a,cordova}$, $< S_a(T_1), \varepsilon >$, a vector intensity measure including S_a at higher modes and a vector of IMs consisting of a combination of two orthogonal ground motion components. Based on the results of multiple regression analyses, it was noted that the intensity measures

accounting for inelastic period and higher-mode contributions improved the damage prediction.

(Cantagallo et al., 2012) conducted a correlation study between the peak inter-storey drift of nine RC three-dimensional structures and different intensity measures, e.g. PGA, PGV, $S_a(T_1)$, HI and ASI. This study was conducted using two sets of un-scaled records, corresponding to two limit states, ultimate and damage limit states. Two intensity measures related to acceleration response spectra were introduced. The efficiency of $S_a(T_{crack})$ and $S_a(T_*)$, corresponding to the cracked and nonlinear structure period, was proved. The results of the comparison study showed that the dispersion in the deformation demands could be reduced using these new IMs.

Most of the comparative studies previously conducted have focused on simple intensity measures derived directly either from the response spectra or ground motions.

(Bojorquez et al., 2012) compared the accuracy of six vector-valued IMs for predicting the failure probability of four steel structures subjected to narrow-band motions. The first parameter of the vector used in this study was $S_a(T1)$, while six parameters were used alternatively for the second component, namely PGA, PGV, t_D, ID (Cosenza and Manfredi, 1970), $R_{T1,T2}$ and N_p. ID is defined as the normalisation of Arias Intensity, with respect to PGA and PGV. The results indicated that the vectors, which account for the spectral shape, are the most efficient when predicting seismic response in terms of the peak inter-storey drift and energy-based damage index. Furthermore, it was found that the vector $< S_a(T1), N_p >$ provides more information about the spectral shape than the vector $< S_a(T1), R_{T1,T2} >$. Consequently, the vector $< S_a(T1), N_p >$ appears to be superior to the other vectors, not only in predicting the maximum displacement, but also in estimating cumulative damage (Bojorquez et al., 2012).

Fontara et al. studied the correlation between eight advance IMs and three response measures, namely the inter-storey drift ratio, the roof drift ratio and the overall damage index by analysing two multi-storey reinforcement concrete frames, using a set of 33 ground motion records scaled to three levels of seismic intensity (Fontara et al., 2012). The results showed a good correlation between selected structure-specific intensity measures and the

overall damage index, compared with the two EDPs. Thus, the damage index was a proper engineering demand parameter. It was found that the intensity measures accounting for spectral shape strongly correlate well with the damage index for all nonlinearity levels and for both the structures. Meanwhile, intensity measures based on the integration of the velocity spectrum curve were not found to be appropriate for all response ranges.

The Pacific Earthquake Engineering Research, PEER working group, reviewed the current available ground motion selection and modification methods, GMSM, for estimating the median values of response of structures in term of maximum inter-storey drift. Then, they compared the accuracy of 17 methods for predicting nonlinear structural response (Haselton, 2009, Watson-Lamprey et al., 2008). The responses of five reinforced concrete structures were evaluated utilising two earthquake scenarios. The results indicated that the methods accounting for spectral shape, and those incorporating record properties important to nonlinear response resulted in the smallest dispersion when predicting the median response. For example, using methods, based on CMS- ε or on S_{di}, results in an accurate prediction of structural response.

7.6 Models and analysis

7.6.1 Structural models

The structures considered in this Chapter are the BF1 and DCF frames. For further information about the details of these frames, see Chapter 4, Section 4.3.1. The material properties adopted in the analyses are given in Table 5-2. The seismic response of the frames considered was evaluated using 2D nonlinear dynamic analyses using Extreme Loading for Structures software, ELS. The AEM models of these frames were described in Chapter 4, Section 4.3.1. The time history analyses for the AEM models were carried out by employing two sets of 40 ground motions, scaled to different levels of seismic intensity. In addition, two preliminary analyses were carried out in order to obtain the structural parameters required in many of the scaling methods. Firstly, Eigenvalue analyses were carried out to determine the dynamic characteristics of the frames related to the first three modes, such as: the periods of vibration, the modal participation factors, and the modal mass participation ratios. Secondly, pushover analyses were performed to determine the properties of the frames in terms of yield

displacement and ultimate strength. These preliminary analyses were performed using the SAP2000 program (Computers and Structures, 2000).

7.6.2 Eigenvalue analyses

A simple analytical model for each of the planar frames was developed for linear analysis. With regard to EC8, the values for the bending and shear stiffness of the cracked structural members were set as equal to half of the stiffness value of the corresponding uncracked members. Rigid offsets were taken into account in the analytical model, in order to consider the inter-connection between beams and columns. Table 7-1 lists the dynamic characteristics of the frames. The dynamic properties of the frames suggest that both frames are first-mode dominant structures.

Table 7-1: Dynamic characteristics of the frames

Mode	BF1 frame			DCF frame		
	Period	**Modal participation factors**	**Modal mass participation ratios**	**Period**	**Modal participation factors**	**Modal mass participation ratios**
1	0.80	1.38	0.80	0.87	1.36	0.84
2	0.31	-0.52	0.14	0.33	-0.47	0.12
3	0.18	-0.22	0.03	0.18	-0.19	0.02

7.6.3 Nonlinear static analyses

For the DCF frame, a nonlinear static analysis was conducted for both directions of loading contrary to the BF1 frame. This was done because of the irregularity in the investigated frame. The two load patterns considered here were a uniform pattern and a modal pattern, proportional to the first mode shape (Fajfar and M.EERI, 2000). The previously mentioned analytical models were extended for the pushover analyses. The flexural behaviour of the frame beams and columns were modelled by using lumped plasticity hinges at both ends. Initially, each frame was subjected to gravity loads. Then, different horizontal load patterns

were applied. The results of the nonlinear static analyses of each frames, e.g. the equivalent mass of the SDOF system, m^*, the elastic period of the idealised bilinear system, T^*, the yield displacement, d_y, and the yield strength, A_y, are listed in Table 7-2. The reduction factor, R_μ, was determined for three levels of ground motions. Ground motions were represented by elastic response spectra with peak ground acceleration corresponding to 0.3 g, 0.45g and 0.6g. The values of R_μ, according to the three ground motion levels, are 1, 1.1 and 1.3 for the DCF frame and 1, 1.15 and 1.53 for the BF1 frame, respectively.

Table 7-2: Dynamic characteristics of the frames obtained from pushover analyses

Load Pattern	**BF1 frame**				**DCF frame**			
	m^* tons	T^* sec	d_y cm	A_y	m^* tons	T^* sec	d_y cm	A_y
Uniform	14	0.78	5.8	0.38g	15	0.83	6.7	0.38g
Modal	14	0.88	6.5	0.34g	15	0.96	7.7	0.34g

The pushover curves representing the relationship between the base shear force and the roof displacements are shown in Figure 7-2 and 7-3.

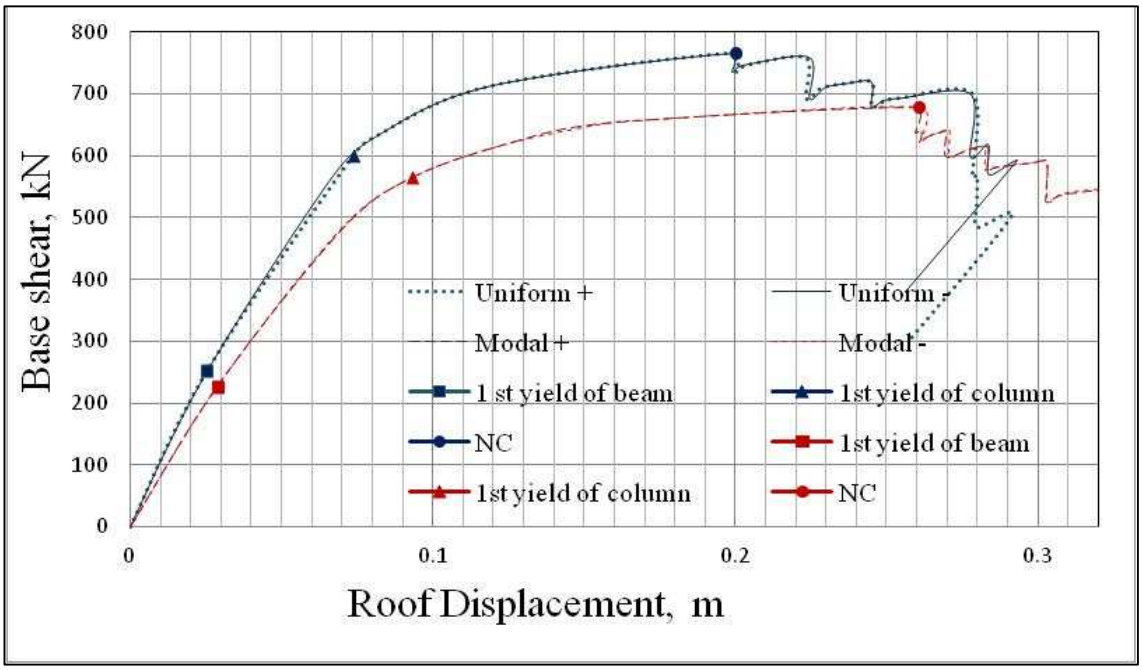

Figure 7-2: Base shear vs. roof displacement relations of the DCF frame under a uniform and a modal pattern

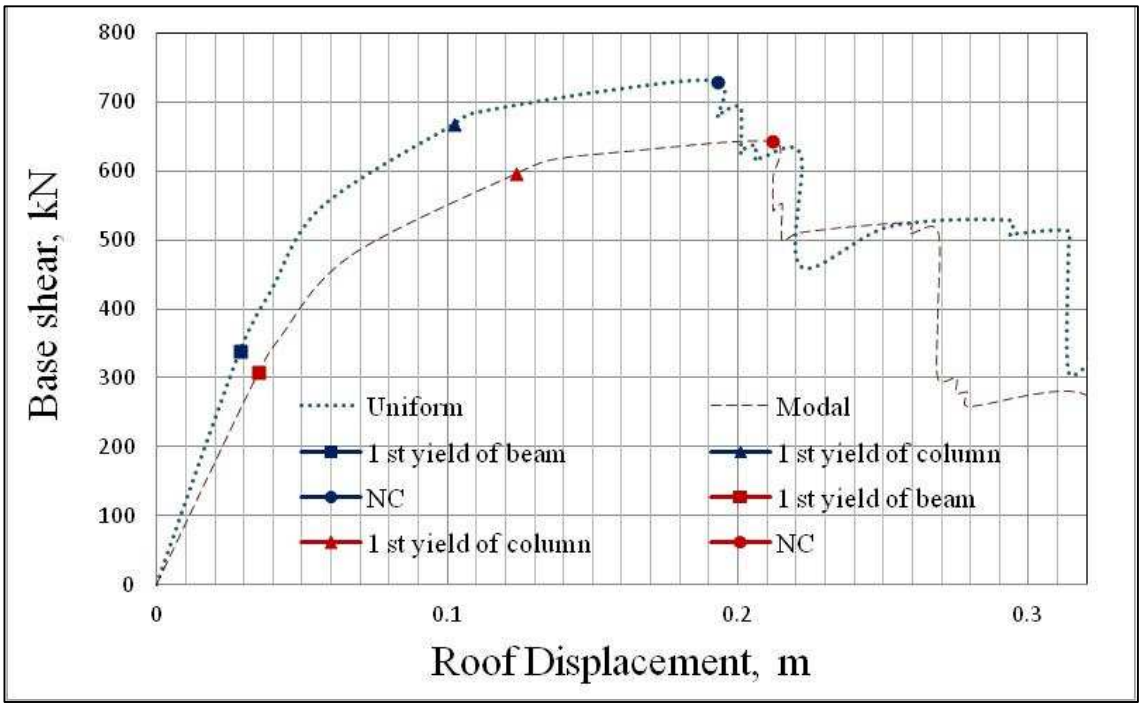

Figure 7-3: Base shear vs. roof displacement relations of the BF1 frame under a uniform and a modal pattern

7.7 Engineering demand parameters

The commonly investigated EDPs are the peak roof drift ratio, PRDR, and the peak inter-storey drift ratio, PIDR. The peak roof drift ratio is determined by dividing the peak roof lateral displacement by the total height of the frame. The peak inter-storey drift ratio is the peak inter-storey drift, normalised by the corresponding storey height. In addition to these common EDPs, global damage indices based on the structural dynamic characteristics, such as the change in the fundamental period, are the main focus of this study. The damage indices of concern are softening indices and the ultimate stiffness degradation index.

Two inelastic periods were required for calculating the damage indices. The inelastic periods are the maximum and damage periods, as be obtained from the nonlinear dynamic analysis. Maximum period, T_{max}, is defined as the peak period during the strong shaking. Damage period, T_{dam}, is that at the transient part of seismic loading.

The ultimate stiffness degradation index, D_G, can be calculated using the initial fundamental period, T_0, and the fundamental period at cycle j as in Equation 7-15 (DiPasquale and Cakmak, 1987).

$$D_G = \frac{T_j - T_0}{T_0} \quad \text{Equation 7-15}$$

Softening indices were developed by Dipasquale and Cakmak using the previously mentioned fundamental periods. These softening indices are the final, plastic and maximum softening and denoted as $D_{G,f}$, $D_{G,pl}$ and $D_{G,m}$, respectively (DiPasquale and Cakmak, 1987, DiPasquale and Cakmak, 1989). $D_{G,f}$ measures the average decrease in the structure stiffness and $D_{G,pl}$ separates the dynamic effects from the stiffness degradation. $D_{G,m}$ is an indicator that accounts for stiffness softening and nonlinear effects. These indices are expressed as in Equations 7-16, 7-17 and 7-18.

$$D_{G,f} = 1 - \left(\frac{T_0}{T_{dam}}\right)^2 \quad \text{Equation 7-16}$$

$$D_{G,pl} = 1 - \left(\frac{T_{dam}}{T_{max}}\right)^2 \quad \text{Equation 7-17}$$

$$D_{G,m} = 1 - \frac{T_0}{T_{max}} \quad \text{Equation 7-18}$$

The change in the fundamental period of a structure can be easily measured experimentally, or determined analytically. $D_{G,m}$ is the best damage index, however it requires input of information about the time history response. The $D_{G,f}$ can be easily used for damage assessment of structures after earthquakes. Damage evolution can be assessed based on period elongation. Period elongation occurs during earthquakes due to damage accumulation. The structure stiffness decreases as the damage increases, leading to period elongation. The period softening results in a structural response that is sensitive to spectral values evaluated at larger periods than the fundamental period. Thus, the response of a structure cannot be governed by a single period. Period elongation is a function of structure's characteristics, the level of nonlinearity and the parameters of the selected ground motions.

7.8 Ground motion intensity measures

The focus of this study is on scalar intensity measures. In particular, ground motion intensity measures derived from acceleration response spectra and dependent on the dynamic characteristics of the selected structure. A number of simple and more complicated scalar intensity measures, which are multiplicative modifications of $S_a(T_1)$, are therefore selected as follows:

1. The spectral acceleration evaluated at the fundamental period of the structure, $S_a(T_1)$.
2. The spectral acceleration evaluated at the effective period of the structure, $\mathrm{S_a}\left(\mathrm{T_{*,uniform}}\right)$, $\mathrm{S_a}\left(\mathrm{T_{*,modal}}\right)$.
3. The two-parameter scalar intensity measure developed by Cordova et al (2005) with $\alpha = 0.5$ and $c = 2$.
4. The two-parameter scalar intensity measure modified by (Mehanny, 2009) with $\alpha = 0.5$ and $c = \sqrt{R}$.
5. The geometric mean of spectral acceleration values over a specific period range, $S_{a,avg}(T_1, \dots, T_n) = \left(\underbrace{s_a(k_1 T) \times \dots \times s_a(k_u T)}_{10\ points\ log-spaced} \right)^{\frac{1}{10}}$ using $(k_1 = 0.25, k_{\mathrm{u}} = 2)$ and $(k_1 = 1, k_{\mathrm{u}} = 2)$.

6. $I_{NP} = S_a(T_1)N_P^{\alpha}$ proposed by (Bojorquez and Iervolino, 2011) with $N_p = \frac{S_{a_{avg}}(T_{1,\ldots,}T_N)}{S_a(T_1)}$.
7. $I_{am} = \frac{1}{A_y(T_f - T_1)} \int_{T_1}^{T_f} S_a(T,\xi)(T - T_1)\, dT$.
8. $I_a = \int_{T_1}^{T_f} S_a(T,\xi)\, dT$.
9. $IM_{Nc} = \left[\Gamma_1^2\left[0.8\, S_d^2(T_1) + 0.2\, S_d^2(1.2T_1)\right] + \Gamma_2^2 S_d^2(T_2)\right]^{0.5}$.
10. $IM_c = \left[\Gamma_1^2\left[0.4\, S_d^2(T_1) + 0.4\, S_d^2(1.2T_1) + 0.2\, S_d^2(1.6T_1)\right] + \Gamma_2^2 S_d^2(T_2)\right]^{0.5}$.

7.9 Selection of ground motion records

Two sets of 40 ground motions as recorded on ground type A were selected from the European strong-motion Database (Ambraseys et al., 2002) and the PEER-NGA (Chiou et al., 2008). These records were taken from more than 27 earthquakes. The ground motion sets used here have a moment magnitude, M, ranging between 5 and 7.5. The site to source distance, R, is in a range of 5 to 20 km for the second set, set 2, and 21 to 50 km for the first set, set 1. The records for the first set represent far-field ground motions, while the second set consists of near-field records with a distance less than 20 Km. Tables 7-2 and 7-3 list the selected ground motion records used in this study.

Table 7-3: Summary of the selected real records for set 1

Waveform ID	**Earthquake ID**	**Station ID**	**Earthquake Name**	**Date**	**Mw**	**R (km)**	**Duration (sec)**	$\mathbf{D_{a0.5-97.5}}$
169	80	ST45	Calabria	1978	5.2	10	22.81	12
193	91	ST64	Montenegro	1979	5.4	15	11.53	8
321	153	ST120	Campano Lucano	1981	5.2	8	42.41	16
359	174	ST136	Umbria	1984	5.6	17	83.72	18
383	176	ST153	Lazio Abruzzo	1984	5.5	14	18.18	17
384	176	ST154	Lazio Abruzzo	1984	5.5	6	59.84	9
385	176	ST155	Lazio Abruzzo	1984	5.5	15	60.46	25
471	227	ST40	Vrancea	1990	6.9	6	24.26	20
473	228	ST40	Vrancea	1990	6.3	7	23.59	20
638	292	ST233	Umbria Marche	1997	5.6	17	28.17	14
646	292	ST234	Umbria Marche	1997	5.6	17	28.35	18
651	291	ST236	Umbria Marche	1997	5.5	5	19.99	10
707	60	ST26	Friuli	1976	5.3	8	16.83	7
765	355	ST266	Umbria Marche	1997	5.2	11	19.63	8
766	292	ST266	Umbria Marche	1997	5.6	12	23.32	9
791	355	ST234	Umbria Marche	1997	5.2	18	11.62	10
798	355	ST233	Umbria Marche	1997	5.2	19	17.36	10
813	350	ST235	Umbria Marche	1997	5.3	8	49.92	11
822	350	ST236	Umbria Marche	1997	5.3	5	45	14
826	355	ST236	Umbria Marche	1997	5.2	14	19.99	15
851	363	ST235	Umbria Marche	1998	5.4	18	23.03	20
852	364	ST235	Umbria Marche	1998	5.1	11	23.03	8
873	364	ST233	Umbria Marche	1998	5.1	17	12.56	10
981	72	ST1043	Friuli	1977	5.4	11	13.05	11
982	72	ST309	Friuli	1977	5.4	9	16.33	9
990	176	ST313	Lazio Abruzzo	1984	5.5	15	55.57	35
1900	658	ST1323	Kalamata	1987	5.3	17	20.20	7
1917	648	ST1328	Ierissos	1983	5.1	15	16.85	7
1960	676	ST1335	Near NE coast of Rodos	1987	5.1	19	19.67	12
3802	1226	ST2368	SE of Tirana	1988	5.9	7	11.97	8
5027	1509	ST2496	Oelfus	1998	5.1	18	22.60	10
5028	1509	ST2552	Oelfus	1998	5.1	9	68	16
5038	1509	ST2495	Oelfus	1998	5.1	11	70.40	30
5078	1464	ST2496	Mt. Hengill Area	1998	5.4	18	19.09	12
5085	1464	ST2497	Mt. Hengill Area	1998	5.4	15	42.23	12
5086	1464	ST2556	Mt. Hengill Area	1998	5.4	15	12.01	12.01
5090	1464	ST2495	Mt. Hengill Area	1998	5.4	18	58.88	20
5655	1825	ST2950	NE of Banja Luka	1981	5.7	10	12.46	7
6115	2029	ST1320	Kozani	1995	6.5	17	29.38	14
6335	2142	ST2557	South Iceland	2000	6.4	15	58	14

Table 7-4: Summary of the selected real records for set 2

Waveform ID	**Earthquake ID**	**Station ID**	**Earthquake Name**	**Date**	**Mw**	**R (km)**	**Duration (sec)**	$\mathbf{D_{a0.5-97.5}}$
1726	561	ST549	Adana	1998	6.3	30	29.21	20
1735	561	ST581	Adana	1998	6.3	39	21.70	21
6144	559	ST1332	Aigion	1995	6.5	42	30	25
6138	559	ST1330	Aigion	1995	6.5	43	38.41	30
6142	559	ST1331	Aigion	1995	6.5	43	39.51	30
335	158	ST121	Alkion	1981	6.3	25	28.61	20
7067	2284	ST608	Altinsac	2000	5.5	38	97.03	50
6154	2028	ST1333	Arnaia	1995	5.3	28	17	6
6087	2028	ST1311	Arnaia	1995	5.3	32	17	10
6037	2028	ST1298	Arnaia	1995	5.3	43	17	10
5892	1932	ST1306	Arnissa	1984	5.2	21	19.79	11
5895	1932	ST1354	Arnissa	1984	5.2	30	20.78	16
1852	628	ST1301	Astakos	1988	5.1	27	13.19	10
1846	628	ST127	Astakos	1988	5.1	34	10.99	10
1905	628	ST126	Astakos	1988	5.1	35	14.87	13
7187	2322	ST3311	Avej	2002	6.5	28	58.88	10
7343	2366	ST87	Azores	2000	5.1	39	84.95	25
352	170	ST131	Biga	1983	6.1	45	19.21	18
6059	646	ST1307	Bitola	1994	6.1	39	21.75	7
4557	1387	ST750	Bovec	1998	5.6	25	119.42	25
4560	1387	ST727	Bovec	1998	5.6	38	36	23
168	80	ST44	Calabria	1978	5.2	33	19.28	15
287	146	ST93	Campano Lucano	1980	6.9	23	72.62	50
292	146	ST98	Campano Lucano	1980	6.9	25	66.50	50
294	146	ST100	Campano Lucano	1980	6.9	26	72.69	60
5488	224	ST2881	Chenoua	1989	5.9	29	12	5
1794	587	ST65	Cubuklu	1988	5.5	34	10.50	10
1720	349	ST543	Dinar	1995	6.4	47	25.26	20
426	201	ST168	Dodecanese	1987	5.3	26	15.72	13
1967	664	ST1339	Drama	1985	5.2	42	13.10	13
429	204	ST169	Etolia	1988	5.4	21	9.43	8
1863	204	ST1303	Etolia	1988	5.4	21	20.50	13
428	203	ST169	Etolia	1988	5.3	23	25.41	20
474	229	ST123	Filippias	1990	5.5	38	16.88	16
1884	229	ST1312	Filippias	1990	5.5	43	9.65	8
1908	229	ST126	Filippias	1990	5.5	44	23.90	22
7156	2313	ST3291	Firuzabad	1994	5.9	21	43.52	14
7157	2313	ST3292	Firuzabad	1994	5.9	22	38.39	15
7158	2313	ST3293	Firuzabad	1994	5.9	39	24.31	20
55	34	ST20	Friuli	1976	6.5	23	36.54	10

7.10 Methodology

The ground motion records are scaled as a set by constant factors, 1, 2, 3.5 and 5. This means that, each record in the set is multiplied by a constant factor in order to allow the frame to experience different levels of nonlinear response.

As can be seen in Tables 7-3 and 7-4, the strong motion duration of each record considered is the significant duration estimated between 0.5 and 97.5 of the Arias intensity denoted as $\mathbf{D_{a0.5-97.5}}$, which is calculated with the Seismosignal software (SeismoSoft, 2011). The records that cause a structure to collapse, or those that lead to only an elastic response in a frame are not considered when examining the correlation between the IMs and EDPs.

A cloud analysis approach is adopted in this study. In this method, raw ground motion records without scaling to a common value of the considered IM are used in nonlinear analyses as described in (Baker and Cornell, 2006b). Then, a regression analysis is performed on the analytical results, described as point data, to estimate the dispersion in the EDP.

The correlation between the selected intensity measures and the three engineering demands parameters has been evaluated employing the coefficient of determination, R^2, and Pearson's correlation coefficient, ρ, based on a linear regression. The value of R^2 is in the range from 0 to 1. The closer this value is to one, the better is the correlation between the considered data. Pearson's correlation coefficient is defined as the square root of the value of R^2. Thus, the values of ρ are in a range between -1 and +1. The value of ρ reveals the extent of the linear relationship between the data. The equations for these two indices are Equations 7-19 and 7-20 (Yakut and Yalmaz, 2008):

$$R^2 = \frac{\sum_i^n (Y_{pi} - Y_m)^2}{\sum_i^n (Y_i - Y_m)^2} \qquad \text{Equation 7-19}$$

$$\rho = \frac{n\sum_i^n X_i Y_i - \sum_i^n X_i \sum_i^n Y_i}{\sqrt{\left[n\sum_i^n X_i^2 - (\sum_i^n X_i)^2\right]\left[n\sum_i^n Y_i^2 - (\sum_i^n Y_i)^2\right]}} \qquad \text{Equation 7-20}$$

Y_{pi} is the value estimated from the linear fitting to the data set, Y_i is the actual value from the data set, Y_m is the mean value, and N is the number of the points in the data set.

7.11 The results of correlation study

The fifteen ground motion intensity measures investigated in this study were computed for each record using MATLAB software (MATLAB, 2008). These intensity measures were computed based on elastic response spectra. Tables 7-5 to 7-20 list the correlation coefficient, R^2, between the engineering demand of concern and the evaluated intensity measures for the BF1 and DCF frames when subjected to two different sets of ground motions, which were scaled to four levels of seismic intensity.

7.11.1 $S_a(T_1)$ as an intensity measure

In regards to using $S_a(T_1)$ as an IM, the following observations have been made:

Tables 7-5 to 7-20 show that the spectral acceleration at the fundamental period of the structure has the strongest correlation with the EDPs, T_{max}, PIDR and PRDR, for both frames at low seismic intensity levels, a scale factor of 1. It can be shown from Figure 7-4 that the R^2 value is around 0.93 and more than 0.96 at this intensity level for the DCF and BF1 frame under the ground motion set 1, respectively. This observation indicates that the structure response is governed by the first-mode period of the structure. This finding is in agreement with the results obtained from the modal analyses. In response to a scale factor value increase from 2 to 3.5, the correlation coefficient value for $S_a(T_1)$ decreases by about 6%. For high seismic intensity, a scale factor of 5, a weak correlation was observed between $S_a(T_1)$ and all the EDPs examined. This is due to the fact that $S_a(T_1)$ cannot account for the effects of inelasticity and period elongation.

The highest R^2 values for $S_a(T_1)$ are in the range from 0.91 to 0.98 for both frames at the intensity factors of 1 and 2. These values have been observed at the two lowest seismic intensity levels for set 1, far-field ground motions. While for set 2, near field pulse-like ground motions, the R^2 values are in the range from 0.81 to 0.86 at the same seismic intensity levels and for both frames, as shown in Tables 7-7, 7-8, 7-11 and 7-12. It was found that $S_a(T_1)$ appears to be a poor indicator for the near-field pulse-like ground motions.

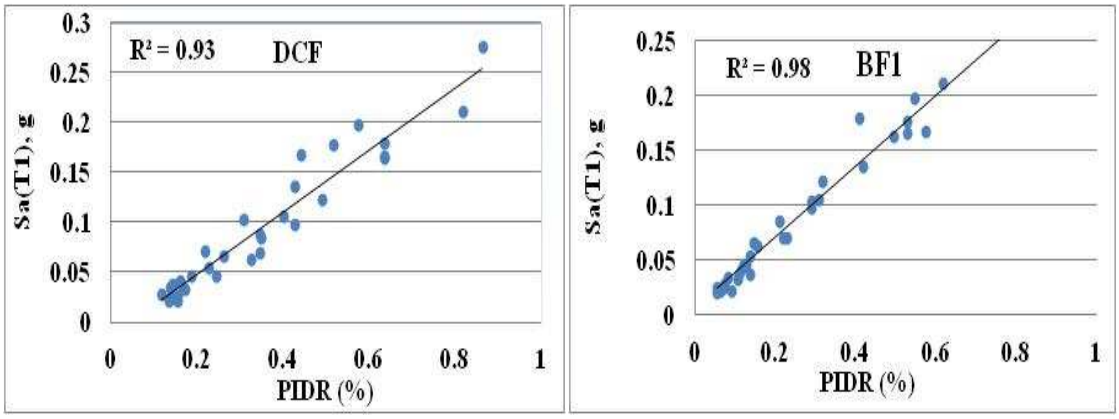

Figure 7-4: Relationship between the selected GMI's and PIDR for the DCF and BF1 frames subjected to the ground motion set 1, scaled by a factor of 1

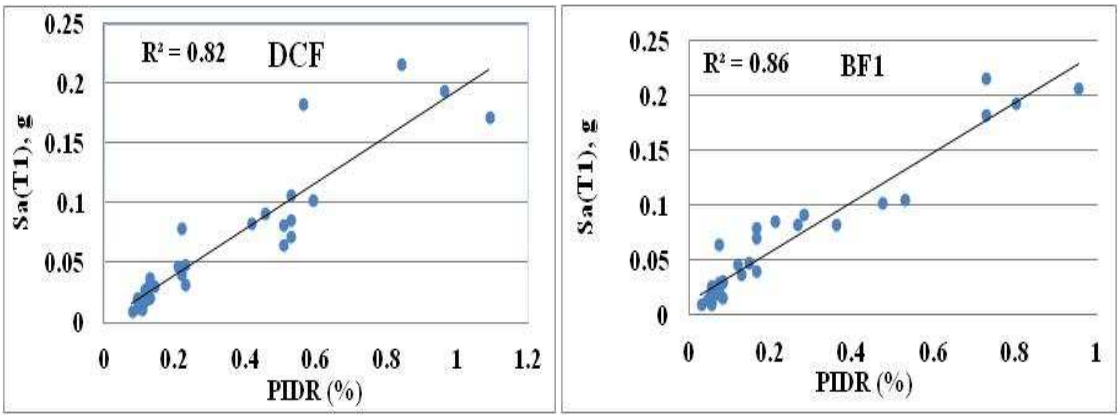

Figure 7-5: Relationship between the selected GMI's and PIDR for the DCF and BF1 frames subjected to the ground motion set 2, scaled by a factor of 1

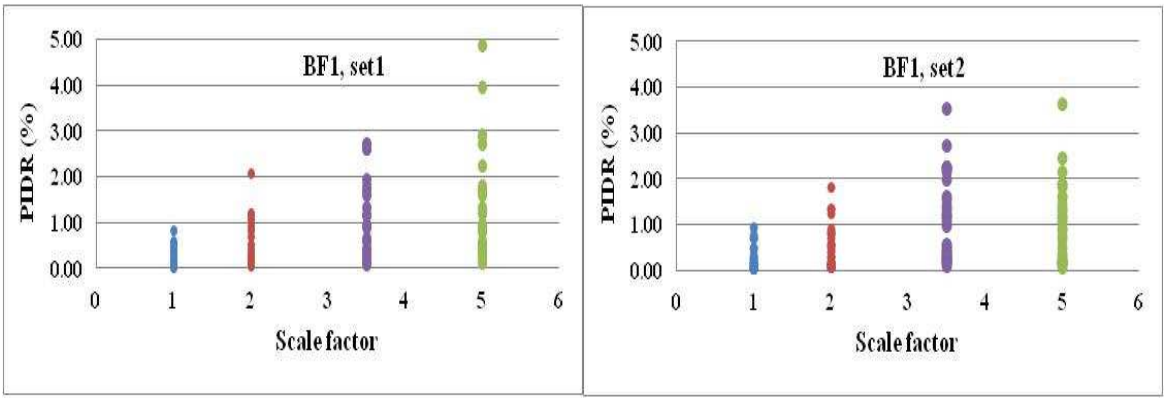

Figure 7-6: PIDR of the BF1 frame for each scale factor

Table 7-5: Correlation coefficients between the selected EDPs of the BF1 frame and the IMs of concern for the ground motion set 1, scaled by a factor of 1

BF1 frame	T_{max}	T_{dam}	PIDR	PRDR	$D_{G,f}$	$D_{G,pl}$	$D_{G,m}$
$S_a(T_1)$	0.94	0.91	0.98	0.96	0.90	0.82	0.95
$S_a(T_{*,uniform})$	0.73	0.72	0.79	0.71	0.71	0.62	0.73
$S_a(T_{*,modal})$	0.62	0.64	0.63	0.58	0.61	0.49	0.62
$S_{a,cordova}$, $\alpha = 0.5$ and $c = 2$	0.87	0.88	0.88	0.85	0.85	0.73	0.88
$S_{a,cordova}$, $\alpha = 0.5$ and $c = \sqrt{R_1}$	0.96	0.91	0.98	0.97	0.89	0.86	0.96
$S_{a,cordova}$, $\alpha = 0.5$ and $c = \sqrt{R_2}$	0.93	0.89	0.97	0.93	0.88	0.84	0.94
$S_{a,avg}(T_1, \dots, T_n)$, $(k_1 = 0.25, k_u = 2)$	0.84	0.86	0.85	0.81	0.84	0.68	0.85
$S_{a,avg}(T_1, \dots, T_n)$, $(k_1 = 1, k_u = 2)$	0.84	0.83	0.86	0.81	0.81	0.72	0.84
I_{NP}, $(k_1 = 0.25, k_u = 2)$	0.92	0.93	0.95	0.93	0.92	0.76	0.94
I_{NP}, $(k_1 = 1, k_u = 2)$	0.93	0.92	0.96	0.93	0.91	0.78	0.94
I_a	0.94	0.85	0.96	0.92	0.82	0.90	0.92
Normalised I_a	0.94	0.91	0.97	0.94	0.90	0.82	0.94
I_{am}	0.94	0.86	0.96	0.91	0.83	0.89	0.92
IM_{Nc}	0.95	0.93	0.98	0.96	0.92	0.82	0.96
IM_c	0.93	0.92	0.95	0.91	0.90	0.79	0.94

Table 7-6: Correlation coefficients between the selected EDPs of the DCF frame and the IMs of concern for the ground motion set 1, scaled by a factor of 1

DCF frame	T_{max}	T_{dam}	PIDR	PRDR	$D_{G,f}$	$D_{G,pl}$	$D_{G,m}$
$S_a(T_1)$	0.92	0.87	0.93	0.93	0.87	0.79	0.91
$S_a(T_{*,uniform})$	0.62	0.52	0.55	0.53	0.53	0.70	0.62
$S_a(T_{*,modal})$	0.49	0.41	0.40	0.39	0.43	0.55	0.50
$S_{a,cordova}$, $\alpha = 0.5$ and $c = 2$	0.82	0.76	0.75	0.76	0.76	0.76	0.81
$S_{a,cordova}$, $\alpha = 0.5$ and $c = \sqrt{R_1}$	0.91	0.86	0.92	0.93	0.86	0.77	0.89
$S_{a,cordova}$, $\alpha = 0.5$ and $c = \sqrt{R_2}$	0.91	0.86	0.91	0.91	0.86	0.79	0.90
$S_{a,avg}(T_1, \dots, T_n)$, $(k_1 = 0.25, k_u = 2)$	0.81	0.72	0.73	0.69	0.74	0.81	0.81
$S_{a,avg}(T_1, \dots, T_n)$, $(k_1 = 1, k_u = 2)$	0.75	0.67	0.69	0.68	0.68	0.75	0.75
I_{NP}, $(k_1 = 0.25, k_u = 2)$	0.93	0.85	0.87	0.85	0.86	0.85	0.92
I_{NP}, $(k_1 = 1, k_u = 2)$	0.91	0.84	0.86	0.85	0.85	0.83	0.90
I_a	0.88	0.82	0.90	0.90	0.81	0.78	0.87
Normalised I_a	0.90	0.84	0.88	0.87	0.86	0.80	0.90
I_{am}	0.89	0.82	0.88	0.87	0.82	0.81	0.88
IM_{Nc}	0.92	0.87	0.92	0.91	0.87	0.80	0.91
IM_c	0.88	0.80	0.84	0.83	0.81	0.82	0.87

Table 7-7: Correlation coefficients between the selected EDPs of the BF1 frame and the IMs of concern for the ground motion set 2, scaled by a factor of 1

BF1 frame	T_{max}	T_{dam}	PIDR	PRDR	$D_{G,f}$	$D_{G,pl}$	$D_{G,m}$
$S_a(T_1)$	0.86	0.81	0.86	0.84	0.82	0.79	0.86
$S_a(T_{*,uniform})$	0.70	0.64	0.73	0.68	0.67	0.68	0.71
$S_a(T_{*,modal})$	0.59	0.52	0.62	0.54	0.55	0.62	0.60
$S_{a,cordova}$, $\alpha = 0.5$ and $c = 2$	0.70	0.64	0.69	0.65	0.66	0.70	0.71
$S_{a,cordova}$, $\alpha = 0.5$ and $c = \sqrt{R_1}$	0.90	0.88	0.90	0.89	0.88	0.78	0.90
$S_{a,cordova}$, $\alpha = 0.5$ and $c = \sqrt{R_2}$	0.90	0.88	0.91	0.90	0.87	0.77	0.90
$S_{a,avg}(T_1, \dots, T_n)$, $(k_1 = 0.25, k_u = 2)$	0.69	0.62	0.74	0.58	0.66	0.71	0.71
$S_{a,avg}(T_1, \dots, T_n)$, $(k_1 = 1, k_u = 2)$	0.73	0.67	0.74	0.69	0.70	0.71	0.74
I_{NP}, $(k_1 = 0.25, k_u = 2)$	0.81	0.76	0.83	0.74	0.79	0.76	0.83
I_{NP}, $(k_1 = 1, k_u = 2)$	0.82	0.77	0.82	0.79	0.80	0.75	0.83
I_a	0.90	0.85	0.92	0.89	0.81	0.79	0.86
Normalised I_a	0.90	0.91	0.90	0.93	0.90	0.72	0.90
I_{am}	0.90	0.86	0.93	0.91	0.82	0.79	0.87
IM_{Nc}	0.89	0.84	0.91	0.86	0.85	0.80	0.89
IM_c	0.83	0.79	0.87	0.82	0.80	0.75	0.84

Table 7-8: Correlation coefficients between the selected EDPs of the DCF frame and the IMs of concern for the ground motion set 2, scaled by a factor of 1

DCF frame	T_{max}	T_{dam}	PIDR	PRDR	$D_{G,f}$	$D_{G,pl}$	$D_{G,m}$
$S_a(T_1)$	0.80	0.81	0.82	0.81	0.78	0.62	0.79
$S_a(T_{*,uniform})$	0.78	0.72	0.78	0.78	0.68	0.71	0.75
$S_a(T_{*,modal})$	0.79	0.72	0.79	0.79	0.68	0.75	0.76
$S_{a,cordova}$, $\alpha = 0.5$ and $c = 2$	0.75	0.75	0.76	0.75	0.72	0.60	0.74
$S_{a,cordova}$, $\alpha = 0.5$ and $c = \sqrt{R_1}$	0.85	0.86	0.85	0.85	0.84	0.64	0.84
$S_{a,cordova}$, $\alpha = 0.5$ and $c = \sqrt{R_2}$	0.87	0.88	0.87	0.87	0.85	0.67	0.86
$S_{a,avg}(T_1, \dots, T_n)$, $(k_1 = 0.25, k_u = 2)$	0.80	0.79	0.84	0.81	0.75	0.64	0.78
$S_{a,avg}(T_1, \dots, T_n)$, $(k_1 = 1, k_u = 2)$	0.83	0.79	0.84	0.83	0.76	0.72	0.81
I_{NP}, $(k_1 = 0.25, k_u = 2)$	0.83	0.84	0.86	0.84	0.81	0.64	0.82
I_{NP}, $(k_1 = 1, k_u = 2)$	0.85	0.84	0.86	0.85	0.82	0.67	0.84
I_a	0.82	0.79	0.84	0.83	0.74	0.68	0.79
Normalised I_a	0.92	0.93	0.91	0.92	0.91	0.72	0.92
I_{am}	0.83	0.79	0.86	0.84	0.75	0.71	0.80
IM_{Nc}	0.84	0.85	0.87	0.85	0.82	0.65	0.83
IM_c	0.87	0.84	0.88	0.87	0.80	0.74	0.85

Table 7-9: Correlation coefficients between the selected EDPs of the BF1 frame and the IMs of concern for the ground motion set 1, scaled by a factor of 2

BF1 frame	T_{max}	T_{dam}	PIDR	PRDR	$D_{G,f}$	$D_{G,pl}$	$D_{G,m}$
$S_a(T_1)$	0.90	0.85	0.90	0.93	0.82	0.86	0.87
$S_a(T_{*,uniform})$	0.76	0.74	0.83	0.79	0.71	0.68	0.73
$S_a(T_{*,modal})$	0.66	0.66	0.75	0.66	0.64	0.58	0.64
$S_{a,cordova}$, $\alpha = 0.5$ and $c = 2$	0.85	0.82	0.91	0.86	0.77	0.78	0.81
$S_{a,cordova}$, $\alpha = 0.5$ and $c = \sqrt{R_1}$	0.89	0.84	0.91	0.94	0.81	0.87	0.86
$S_{a,cordova}$, $\alpha = 0.5$ and $c = \sqrt{R_2}$	0.88	0.82	0.92	0.93	0.79	0.86	0.85
$S_{a,avg}(T_1, \dots, T_n)$, $(k_1 = 0.25, k_u = 2)$	0.84	0.82	0.91	0.84	0.78	0.78	0.82
$S_{a,avg}(T_1, \dots, T_n)$, $(k_1 = 1, k_u = 2)$	0.82	0.79	0.90	0.85	0.76	0.76	0.79
I_{NP}, $(k_1 = 0.25, k_u = 2)$	0.91	0.89	0.93	0.92	0.86	0.86	0.90
I_{NP}, $(k_1 = 1, k_u = 2)$	0.91	0.88	0.93	0.93	0.85	0.85	0.89
I_a	0.86	0.80	0.91	0.93	0.75	0.84	0.81
Normalised I_a	0.90	0.86	0.94	0.94	0.83	0.88	0.88
I_{am}	0.86	0.81	0.92	0.92	0.77	0.84	0.82
IM_{Nc}	0.91	0.86	0.94	0.93	0.83	0.88	0.88
IM_c	0.89	0.85	0.95	0.92	0.82	0.85	0.87

Table 7-10: Correlation coefficients between the selected EDPs of the DCF frame and the IMs of concern for the ground motion set 1, scaled by a factor of 2

DCF frame	T_{max}	T_{dam}	PIDR	PRDR	$D_{G,f}$	$D_{G,pl}$	$D_{G,m}$
$S_a(T_1)$	0.93	0.83	0.90	0.94	0.79	0.89	0.89
$S_a(T_{*,uniform})$	0.76	0.75	0.82	0.71	0.72	0.69	0.76
$S_a(T_{*,modal})$	0.64	0.67	0.72	0.58	0.64	0.54	0.65
$S_{a,cordova}$, $\alpha = 0.5$ and $c = 2$	0.87	0.82	0.92	0.86	0.77	0.79	0.84
$S_{a,cordova}$, $\alpha = 0.5$ and $c = \sqrt{R_1}$	0.93	0.83	0.90	0.95	0.79	0.89	0.89
$S_{a,cordova}$, $\alpha = 0.5$ and $c = \sqrt{R_2}$	0.94	0.85	0.90	0.95	0.81	0.88	0.90
$S_{a,avg}(T_1, \dots, T_n)$, $(k_1 = 0.25, k_u = 2)$	0.84	0.81	0.87	0.80	0.78	0.78	0.84
$S_{a,avg}(T_1, \dots, T_n)$, $(k_1 = 1, k_u = 2)$	0.85	0.82	0.89	0.82	0.78	0.76	0.84
I_{NP}, $(k_1 = 0.25, k_u = 2)$	0.93	0.88	0.91	0.90	0.85	0.86	0.92
I_{NP}, $(k_1 = 1, k_u = 2)$	0.94	0.89	0.93	0.92	0.86	0.86	0.93
I_a	0.92	0.82	0.92	0.94	0.77	0.88	0.87
Normalised I_a	0.92	0.88	0.91	0.91	0.84	0.85	0.91
I_{am}	0.90	0.83	0.91	0.90	0.78	0.84	0.86
IM_{Nc}	0.94	0.85	0.91	0.94	0.81	0.89	0.91
IM_c	0.94	0.88	0.94	0.92	0.84	0.87	0.92

Table 7-11: Correlation coefficients between the selected EDPs of the BF1 frame and the IMs of concern for the ground motion set 2, scaled by a factor of 2

BF1 frame	T_{max}	T_{dam}	PIDR	PRDR	$D_{G,f}$	$D_{G,pl}$	$D_{G,m}$
$S_a(T_1)$	0.79	0.80	0.84	0.86	0.77	0.44	0.76
$S_a(T_{*,uniform})$	0.66	0.73	0.78	0.74	0.68	0.29	0.63
$S_a(T_{*,modal})$	0.73	0.76	0.84	0.84	0.71	0.36	0.69
$S_{a,cordova}$, $\alpha = 0.5$ and $c = 2$	0.80	0.76	0.83	0.82	0.74	0.54	0.78
$S_{a,cordova}$, $\alpha = 0.5$ and $c = \sqrt{R_1}$	0.82	0.79	0.83	0.86	0.78	0.53	0.80
$S_{a,cordova}$, $\alpha = 0.5$ and $c = \sqrt{R_2}$	0.84	0.83	0.87	0.90	0.80	0.50	0.81
$S_{a,avg}(T_1, \dots, T_n)$, $(k_1 = 0.25, k_u = 2)$	0.68	0.77	0.83	0.78	0.70	0.28	0.65
$S_{a,avg}(T_1, \dots, T_n)$, $(k_1 = 1, k_u = 2)$	0.81	0.82	0.89	0.88	0.78	0.44	0.77
I_{NP}, $(k_1 = 0.25, k_u = 2)$	0.81	0.84	0.88	0.85	0.80	0.42	0.78
I_{NP}, $(k_1 = 1, k_u = 2)$	0.85	0.85	0.89	0.89	0.83	0.49	0.83
I_a	0.76	0.79	0.86	0.89	0.74	0.37	0.72
Normalised I_a	0.87	0.86	0.90	0.92	0.84	0.51	0.84
I_{am}	0.74	0.80	0.87	0.89	0.73	0.33	0.69
IM_{Nc}	0.81	0.84	0.89	0.89	0.80	0.43	0.78
IM_c	0.80	0.85	0.91	0.90	0.80	0.39	0.77

Table 7-12: Correlation coefficients between the selected EDPs of the DCF frame and the IMs of concern for the ground motion set 2, scaled by a factor of 2

DCF frame	T_{max}	T_{dam}	PIDR	PRDR	$D_{G,f}$	$D_{G,pl}$	$D_{G,m}$
$S_a(T_1)$	0.86	0.81	0.86	0.84	0.82	0.79	0.86
$S_a(T_{*,uniform})$	0.70	0.64	0.73	0.68	0.67	0.68	0.71
$S_a(T_{*,modal})$	0.59	0.52	0.62	0.54	0.55	0.62	0.60
$S_{a,cordova}$, $\alpha = 0.5$ and $c = 2$	0.70	0.64	0.69	0.65	0.66	0.70	0.71
$S_{a,cordova}$, $\alpha = 0.5$ and $c = \sqrt{R_1}$	0.90	0.88	0.90	0.89	0.88	0.78	0.90
$S_{a,cordova}$, $\alpha = 0.5$ and $c = \sqrt{R_2}$	0.90	0.88	0.91	0.90	0.87	0.77	0.90
$S_{a,avg}(T_1, \dots, T_n)$, $(k_1 = 0.25, k_u = 2)$	0.69	0.62	0.74	0.58	0.66	0.71	0.71
$S_{a,avg}(T_1, \dots, T_n)$, $(k_1 = 1, k_u = 2)$	0.73	0.67	0.74	0.69	0.70	0.71	0.74
I_{NP}, $(k_1 = 0.25, k_u = 2)$	0.81	0.76	0.83	0.74	0.79	0.76	0.83
I_{NP}, $(k_1 = 1, k_u = 2)$	0.82	0.77	0.82	0.79	0.80	0.75	0.83
I_a	0.90	0.85	0.92	0.89	0.81	0.79	0.86
Normalised I_a	0.90	0.91	0.90	0.93	0.90	0.72	0.90
I_{am}	0.90	0.86	0.93	0.91	0.82	0.79	0.87
IM_{Nc}	0.89	0.84	0.91	0.86	0.85	0.80	0.89
IM_c	0.83	0.79	0.87	0.82	0.80	0.75	0.84

Table 7-13: Correlation coefficients between the selected EDPs of the BF1 frame and the IMs of concern for the ground motion set 1, scaled by a factor of 3.5

BF1 frame	T_{max}	T_{dam}	PIDR	PRDR	$D_{G,f}$	$D_{G,pl}$	$D_{G,m}$
$S_a(T_1)$	0.82	0.59	0.85	0.91	0.61	0.21	0.76
$S_a(T_{*,uniform})$	0.71	0.57	0.84	0.83	0.57	0.14	0.65
$S_a(T_{*,modal})$	0.65	0.51	0.81	0.73	0.52	0.13	0.59
$S_{a,cordova}$, $\alpha = 0.5$ and $c = 2$	0.77	0.56	0.93	0.91	0.57	0.19	0.70
$S_{a,cordova}$, $\alpha = 0.5$ and $c = \sqrt{R_1}$	0.83	0.60	0.88	0.93	0.61	0.21	0.76
$S_{a,cordova}$, $\alpha = 0.5$ and $c = \sqrt{R_2}$	0.81	0.60	0.87	0.94	0.61	0.19	0.74
$S_{a,avg}(T_1, \dots, T_n)$, $(k_1 = 0.25, k_u = 2)$	0.77	0.60	0.89	0.89	0.61	0.16	0.71
$S_{a,avg}(T_1, \dots, T_n)$, $(k_1 = 1, k_u = 2)$	0.77	0.58	0.92	0.90	0.59	0.17	0.70
I_{NP}, $(k_1 = 0.25, k_u = 2)$	0.86	0.63	0.89	0.93	0.66	0.21	0.80
I_{NP}, $(k_1 = 1, k_u = 2)$	0.86	0.63	0.91	0.94	0.65	0.21	0.79
I_a	0.80	0.59	0.92	0.95	0.59	0.19	0.72
Normalised I_a	0.84	0.62	0.93	0.94	0.64	0.20	0.77
I_{am}	0.78	0.59	0.92	0.91	0.59	0.18	0.71
IM_{Nc}	0.84	0.61	0.88	0.93	0.63	0.21	0.78
IM_c	0.85	0.63	0.93	0.95	0.64	0.20	0.78

Table 7-14: Correlation coefficients between the selected EDPs of the DCF frame and the IMs of concern for the ground motion set 1, scaled by a factor of 3.5

DCF frame	T_{max}	T_{dam}	PIDR	PRDR	$D_{G,f}$	$D_{G,pl}$	$D_{G,m}$
$S_a(T_1)$	0.84	0.73	0.84	0.85	0.69	0.73	0.78
$S_a(T_{*,uniform})$	0.84	0.74	0.91	0.91	0.70	0.73	0.79
$S_a(T_{*,modal})$	0.73	0.58	0.84	0.84	0.56	0.71	0.69
$S_{a,cordova}$, $\alpha = 0.5$ and $c = 2$	0.85	0.70	0.93	0.92	0.66	0.78	0.79
$S_{a,cordova}$, $\alpha = 0.5$ and $c = \sqrt{R_1}$	0.84	0.73	0.85	0.85	0.68	0.73	0.78
$S_{a,cordova}$, $\alpha = 0.5$ and $c = \sqrt{R_2}$	0.86	0.76	0.86	0.87	0.71	0.74	0.80
$S_{a,avg}(T_1, \dots, T_n)$, $(k_1 = 0.25, k_u = 2)$	0.85	0.74	0.91	0.91	0.70	0.76	0.81
$S_{a,avg}(T_1, \dots, T_n)$, $(k_1 = 1, k_u = 2)$	0.88	0.75	0.95	0.96	0.71	0.79	0.82
I_{NP}, $(k_1 = 0.25, k_u = 2)$	0.90	0.80	0.91	0.91	0.76	0.79	0.86
I_{NP}, $(k_1 = 1, k_u = 2)$	0.92	0.81	0.94	0.94	0.77	0.80	0.87
I_a	0.87	0.76	0.93	0.93	0.70	0.76	0.81
Normalised I_a	0.92	0.82	0.95	0.95	0.78	0.80	0.87
I_{am}	0.88	0.75	0.95	0.94	0.70	0.77	0.81
IM_{Nc}	0.86	0.75	0.87	0.87	0.71	0.76	0.81
IM_c	0.92	0.80	0.95	0.95	0.75	0.81	0.86

Table 7-15: Correlation coefficients between the selected EDPs of the BF1 frame and the IMs of concern for the ground motion set 2, scaled by a factor of 3.5

BF1 frame	T_{max}	T_{dam}	PIDR	PRDR	$D_{G,f}$	$D_{G,pl}$	$D_{G,m}$
$S_a(T_1)$	0.71	0.65	0.82	0.83	0.59	0.56	0.64
$S_a(T_{*,uniform})$	0.74	0.73	0.85	0.87	0.64	0.50	0.66
$S_a(T_{*,modal})$	0.68	0.64	0.82	0.82	0.57	0.48	0.59
$S_{a,cordova}$, $\alpha = 0.5$ and $c = 2$	0.76	0.63	0.89	0.88	0.56	0.61	0.64
$S_{a,cordova}$, $\alpha = 0.5$ and $c = \sqrt{R_1}$	0.73	0.66	0.83	0.85	0.59	0.57	0.64
$S_{a,cordova}$, $\alpha = 0.5$ and $c = \sqrt{R_2}$	0.72	0.68	0.82	0.85	0.62	0.54	0.65
$S_{a,avg}(T_1, \dots, T_n)$, $(k_1 = 0.25, k_u = 2)$	0.61	0.61	0.77	0.75	0.54	0.42	0.55
$S_{a,avg}(T_1, \dots, T_n)$, $(k_1 = 1, k_u = 2)$	0.78	0.72	0.91	0.92	0.64	0.58	0.68
I_{NP}, $(k_1 = 0.25, k_u = 2)$	0.74	0.71	0.85	0.84	0.65	0.55	0.68
I_{NP}, $(k_1 = 1, k_u = 2)$	0.80	0.75	0.90	0.90	0.68	0.62	0.73
I_a	0.61	0.55	0.76	0.80	0.48	0.45	0.52
Normalised I_a	0.75	0.71	0.82	0.86	0.65	0.58	0.69
I_{am}	0.64	0.58	0.79	0.83	0.50	0.47	0.54
IM_{Nc}	0.70	0.67	0.80	0.84	0.61	0.54	0.65
IM_c	0.73	0.70	0.84	0.87	0.63	0.55	0.66

Table 7-16: Correlation coefficients between the selected EDPs of the DCF frame and the IMs of concern for the ground motion set 2, scaled by a factor of 3.5

DCF frame	T_{max}	T_{dam}	PIDR	PRDR	$D_{G,f}$	$D_{G,pl}$	$D_{G,m}$
$S_a(T_1)$	0.87	0.72	0.88	0.85	0.67	0.82	0.80
$S_a(T_{*,uniform})$	0.81	0.72	0.84	0.85	0.66	0.72	0.74
$S_a(T_{*,modal})$	0.83	0.73	0.87	0.87	0.65	0.74	0.75
$S_{a,cordova}$, $\alpha = 0.5$ and $c = 2$	0.83	0.68	0.84	0.83	0.64	0.80	0.77
$S_{a,cordova}$, $\alpha = 0.5$ and $c = \sqrt{R_1}$	0.87	0.74	0.88	0.87	0.70	0.84	0.83
$S_{a,cordova}$, $\alpha = 0.5$ and $c = \sqrt{R_2}$	0.90	0.76	0.90	0.90	0.72	0.85	0.84
$S_{a,avg}(T_1, \dots, T_n)$, $(k_1 = 0.25, k_u = 2)$	0.83	0.77	0.86	0.78	0.68	0.69	0.74
$S_{a,avg}(T_1, \dots, T_n)$, $(k_1 = 1, k_u = 2)$	0.88	0.78	0.90	0.91	0.72	0.81	0.82
I_{NP}, $(k_1 = 0.25, k_u = 2)$	0.89	0.79	0.90	0.85	0.73	0.80	0.82
I_{NP}, $(k_1 = 1, k_u = 2)$	0.90	0.79	0.90	0.90	0.74	0.84	0.85
I_a	0.89	0.73	0.92	0.91	0.66	0.82	0.79
Normalised I_a	0.91	0.84	0.90	0.94	0.79	0.84	0.87
I_{am}	0.89	0.75	0.93	0.92	0.66	0.80	0.79
IM_{Nc}	0.92	0.81	0.93	0.92	0.74	0.84	0.85
IM_c	0.90	0.80	0.93	0.93	0.73	0.81	0.83

Table 7-17: Correlation coefficients between the selected EDPs of the BF1 frame and the IMs of concern for the ground motion set 1, scaled by a factor of 5

BF1 frame	T_{max}	T_{dam}	PIDR	PRDR	$D_{G,f}$	$D_{G,pl}$	$D_{G,m}$
$S_a(T_1)$	0.76	0.67	0.83	0.85	0.60	0.62	0.71
$S_a(T_{*,uniform})$	0.83	0.69	0.82	0.90	0.64	0.64	0.75
$S_a(T_{*,modal})$	0.78	0.67	0.73	0.85	0.61	0.58	0.70
$S_{a,cordova}$, $\alpha = 0.5$ and $c = 2$	0.83	0.70	0.87	0.93	0.63	0.66	0.75
$S_{a,cordova}$, $\alpha = 0.5$ and $c = \sqrt{R_1}$	0.79	0.71	0.86	0.88	0.62	0.61	0.72
$S_{a,cordova}$, $\alpha = 0.5$ and $c = \sqrt{R_2}$	0.80	0.71	0.85	0.89	0.63	0.62	0.73
$S_{a,avg}(T_1, \dots, T_n)$, $(k_1 = 0.25, k_u = 2)$	0.79	0.66	0.82	0.90	0.62	0.64	0.74
$S_{a,avg}(T_1, \dots, T_n)$, $(k_1 = 1, k_u = 2)$	0.86	0.73	0.87	0.95	0.67	0.66	0.78
I_{NP}, $(k_1 = 0.25, k_u = 2)$	0.81	0.70	0.84	0.90	0.66	0.68	0.78
I_{NP}, $(k_1 = 1, k_u = 2)$	0.85	0.74	0.87	0.93	0.68	0.69	0.80
I_a	0.81	0.70	0.88	0.91	0.61	0.63	0.72
Normalised I_a	0.86	0.74	0.87	0.94	0.67	0.69	0.79
I_{am}	0.83	0.68	0.86	0.92	0.61	0.67	0.74
IM_{Nc}	0.80	0.69	0.84	0.88	0.63	0.64	0.74
IM_c	0.85	0.74	0.87	0.94	0.68	0.67	0.79

Table 7-18: Correlation coefficients between the selected EDPs of the DCF frame and the IMs of concern for the ground motion set 1, scaled by a factor of 5

DCF frame	T_{max}	T_{dam}	PIDR	PRDR	$D_{G,f}$	$D_{G,pl}$	$D_{G,m}$
$S_a(T_1)$	0.83	0.78	0.82	0.84	0.73	0.73	0.80
$S_a(T_{*,uniform})$	0.87	0.83	0.92	0.91	0.77	0.73	0.83
$S_a(T_{*,modal})$	0.83	0.77	0.87	0.88	0.70	0.71	0.78
$S_{a,cordova}$, $\alpha = 0.5$ and $c = 2$	0.91	0.83	0.92	0.95	0.76	0.80	0.85
$S_{a,cordova}$, $\alpha = 0.5$ and $c = \sqrt{R_1}$	0.84	0.78	0.82	0.85	0.73	0.73	0.80
$S_{a,cordova}$, $\alpha = 0.5$ and $c = \sqrt{R_2}$	0.85	0.79	0.84	0.87	0.74	0.76	0.82
$S_{a,avg}(T_1, \dots, T_n)$, $(k_1 = 0.25, k_u = 2)$	0.88	0.81	0.91	0.92	0.76	0.78	0.85
$S_{a,avg}(T_1, \dots, T_n)$, $(k_1 = 1, k_u = 2)$	0.93	0.85	0.95	0.96	0.78	0.81	0.88
I_{NP}, $(k_1 = 0.25, k_u = 2)$	0.88	0.84	0.90	0.91	0.80	0.78	0.87
I_{NP}, $(k_1 = 1, k_u = 2)$	0.91	0.86	0.92	0.94	0.82	0.80	0.89
I_a	0.91	0.83	0.93	0.94	0.76	0.78	0.85
Normalised I_a	0.93	0.87	0.95	0.96	0.82	0.81	0.90
I_{am}	0.91	0.84	0.95	0.96	0.77	0.77	0.85
IM_{Nc}	0.86	0.79	0.84	0.87	0.75	0.76	0.82
IM_c	0.92	0.85	0.92	0.94	0.79	0.81	0.88

Table 7-19: Correlation coefficients between the selected EDPs of the BF1 frame and the IMs of concern for the ground motion set 2, scaled by a factor of 5

BF1 frame	T_{max}	T_{dam}	PIDR	PRDR	$D_{G,f}$	$D_{G,pl}$	$D_{G,m}$
$S_a(T_1)$	0.69	0.48	0.78	0.73	0.50	0.19	0.65
$S_a(T_{*,uniform})$	0.70	0.49	0.85	0.86	0.51	0.18	0.64
$S_a(T_{*,modal})$	0.64	0.39	0.71	0.73	0.44	0.20	0.60
$S_{a,cordova}$, $\alpha = 0.5$ and $c = 2$	0.76	0.42	0.80	0.77	0.47	0.26	0.71
$S_{a,cordova}$, $\alpha = 0.5$ and $c = \sqrt{R_1}$	0.66	0.50	0.78	0.75	0.49	0.16	0.61
$S_{a,cordova}$, $\alpha = 0.5$ and $c = \sqrt{R_2}$	0.66	0.51	0.81	0.80	0.50	0.15	0.60
$S_{a,avg}(T_1, \dots, T_n)$, $(k_1 = 0.25, k_u = 2)$	0.71	0.44	0.78	0.64	0.50	0.23	0.68
$S_{a,avg}(T_1, \dots, T_n)$, $(k_1 = 1, k_u = 2)$	0.77	0.50	0.88	0.89	0.53	0.22	0.71
I_{NP}, $(k_1 = 0.25, k_u = 2)$	0.79	0.51	0.85	0.75	0.56	0.25	0.76
I_{NP}, $(k_1 = 1, k_u = 2)$	0.81	0.53	0.88	0.85	0.57	0.23	0.75
I_a	0.64	0.51	0.81	0.80	0.49	0.14	0.57
Normalised I_a	0.76	0.56	0.87	0.89	0.57	0.18	0.69
I_{am}	0.72	0.54	0.88	0.88	0.54	0.17	0.65
IM_{Nc}	0.67	0.51	0.79	0.72	0.51	0.17	0.63
IM_c	0.70	0.53	0.85	0.82	0.53	0.18	0.65

Table 7-20: Correlation coefficients between the selected EDPs of the DCF frame and the IMs of concern for the ground motion set 2, scaled by a factor of 5

DCF frame	T_{max}	T_{dam}	PIDR	PRDR	$D_{G,f}$	$D_{G,pl}$	$D_{G,m}$
$S_a(T_1)$	0.68	0.57	0.84	0.83	0.56	0.24	0.63
$S_a(T_{*,uniform})$	0.60	0.77	0.68	0.74	0.71	0.05	0.57
$S_a(T_{*,modal})$	0.60	0.68	0.70	0.75	0.63	0.08	0.55
$S_{a,cordova}$, $\alpha = 0.5$ and $c = 2$	0.64	0.64	0.77	0.79	0.60	0.14	0.59
$S_{a,cordova}$, $\alpha = 0.5$ and $c = \sqrt{R_1}$	0.66	0.55	0.83	0.83	0.54	0.24	0.62
$S_{a,cordova}$, $\alpha = 0.5$ and $c = \sqrt{R_2}$	0.69	0.59	0.85	0.87	0.59	0.24	0.65
$S_{a,avg}(T_1, \dots, T_n)$, $(k_1 = 0.25, k_u = 2)$	0.70	0.68	0.81	0.71	0.65	0.17	0.65
$S_{a,avg}(T_1, \dots, T_n)$, $(k_1 = 1, k_u = 2)$	0.67	0.72	0.80	0.85	0.67	0.12	0.63
I_{NP}, $(k_1 = 0.25, k_u = 2)$	0.74	0.68	0.88	0.82	0.66	0.22	0.70
I_{NP}, $(k_1 = 1, k_u = 2)$	0.72	0.69	0.86	0.88	0.66	0.19	0.68
I_a	0.68	0.65	0.84	0.88	0.62	0.17	0.62
Normalised I_a	0.71	0.72	0.83	0.89	0.69	0.15	0.67
I_{am}	0.67	0.71	0.82	0.86	0.67	0.12	0.62
IM_{Nc}	0.73	0.61	0.88	0.85	0.60	0.26	0.68
IM_c	0.72	0.72	0.86	0.87	0.69	0.16	0.67

A comparison between the values of the correlation coefficient for $S_a(T_1)$ and the response parameters of each frame, as listed in Tables 7-5 to 7-12, shows that $S_a(T_1)$ for the regular frame has a stronger correlation than $S_a(T_1)$ for the irregular frame at all seismic intensity levels.

In general, it was found that spectral acceleration at the fundamental period of the structure is an efficient intensity measure for mid-rise structures response almost elastically and subjected to far-field ground motions. In addition, $S_a(T_1)$ is often a better intensity measure for regular structures than irregular structures. These findings are in agreement with the findings of (Shome, 1999, Luco and Cornell, 2007).

7.11.2 $S_a(T_{*,uniform})$ and $S_a(T_{*,modal})$ as intensity measures

In regards to using intensity measures based on the spectral acceleration values at periods different from the first-mode elastic period of the structure, the following observations have been made:

These IMs do not correlate better with the PIDR and PRDR than $S_a(T_1)$ in most cases. The strongest correlation between $S_a(T_{*,uniform})$ and the EDPs was observed for the DCF frames under ground motion set 1, scaled by a factor of 3.5 and 5. This could be due to the response of both frames under the different scaled ground motion sets varying within each case. The two selected frames experienced various degree of response, ranging from linear to highly nonlinear in each case. The elastic periods under seismic loads were increased and lengthened depending on the seismic intensity level. For example, for both frames under the two selected sets, the ratio of T_{max} to T_1 is in the range from 1 to 1.4, from 1.05 to 1.5, from 1.1 to 1.7 and from 1.15 to 2 for the seismic scale factor of 1, 2, 3.5 and 5, respectively. If the IM is based on a single period, which is dominant in the range of response, a strong correlation will be found, as shown in Tables 7-14 and 7-18. Otherwise, a weak correlation will be observed between the scalar IM and the EDPs examined.

Based on the results of the study, it can be concluded that using a scalar intensity measure, which is based on a single period value, is not recommended for seismic assessment, because developing fragility curves requires increasingly scaling ground motions and tracing structural response from a linear range to collapse.

7.11.3 $S_{a,cordova}$ and $S_{a,cordova}$ modified by Mehanny as intensity measures

In regards to using the IMs introduced by Cordova et al and those improved by the modification of c as suggested by Mehanny, observations can be summarised as follows:

From Tables 7-5 to 7-20, it was found that using the above mentioned intensity measures accounting for period elongation, $S_{a,cordova}$, can lead to better correlations between the IM evaluated and the selected EDPs, especially when the structure response is in the high nonlinear range. Using $S_{a,cordova}$ with $\alpha = 0.5$ and $c = 2$ as an IM may lead to a slightly weaker correlation for low nonlinearity. For a scale factor of 1, the largest value for T_{max}/T_1 is 1.5. Thus, using a combination of $S_a(T_1)$ and $S_a(2T_1)$ does not result in better correlation between this evaluated IM and the response parameters of concern at the intensity level corresponding to scale factor of 1. It reduces the values of R^2 by a ratio of 0.8-0.9. On contrary, the R^2 values increase by a ratio up to 1.09 when the improved intensity measure is applied, $S_{a,cordova}$ with $\alpha = 0.5$ and $c = \sqrt{R_1}$. The modification for c, which was proposed by Mehanny, enhances the correlation in both the linear and nonlinear ranges for both ground motion sets.

7.11.4 $S_{a,avg}(T_1, \dots, T_n)$ and I_{NP} as intensity measures

As can be observed by comparing the R^2 values for $S_{a,avg}(T_1, \dots, T_n)$ with $(k_1 = 0.25, k_u = 2)$ and $S_{a,avg}(T_1, \dots, T_n)$ with $(k_1 = 1, k_u = 2)$ for all cases, the later IM appears to be relatively better than the former IM. Employing $k_1 = 1$ in computing $S_{a,avg}$ leads to a higher correlation with PIDR and PRDR than when using $k_1 = 0.25$. This means the effect of higher-mode contributions on the structural response is not dominant in both frames under the two sets. Similarly, I_{NP}, computed by utilising $k_1 = 1$, appears to be a better ground motion indictor than that calculated based on $k_1 = 0.25$. This is in agreement with the finding of (Yahyaabadi and Tehranizadeh, 2011). They found, based on a statistical study for determining the optimal combination of the spectral values at different periods of structures, that higher mode contributions can be neglected in short period structures; of up to six storeys. Moreover, it was observed that I_{NP} better correlates with the PIDR and PRDR than

$S_{a,avg}$ computed using the same k_1 value. With regard to the results of the correlation study, presented in Tables 7-5 to 7-20, it was found that I_{NP}, computed by utilising $k_1 = 1$, tends to be better than the first ten IMs, discussed earlier. This intensity measure has a strong correlation at almost all intensity levels for both frames under the two ground motion sets. Even at a very low intensity level, I_{NP} highly correlates with the PIDR and PRDR of the BF1 frame. However, a slight decrease in R^2 values for I_{NP} has only been observed in the DCF frame at the seismic intensity factor of 1.

7.11.5 I_a, I_{am} and the normalised I_a as intensity measures

In regards to the IMs, based on the integration of the curve of the pseudo-acceleration response spectrum in a specific period range between T_0 and T_f, the following observations have been made:

The determination coefficients of I_a, I_{am} and the normalised I_a, summarised in Tables 7-5 to 7-20, show that there is no clear trend to indicate which of the three intensity measures has the strongest correlation with the PIDR and PRDR for both frames subjected to the ground motion set 1 at the four intensity levels. However, it has been observed that the normalised I_a, which accounts for the structure strength, has the strongest correlation with the PIDR and PRDR for both frames under the near-field ground motion set at four intensity levels.

The results of the comparison between the R^2 values for the intensity measures, I_a, I_{am} and the normalised I_a, and those for other intensity measures reveal that these IMs have a strong correlation with the PIDR and PRDR for all cases. One exception is the DCF frame under un-scaled far-field ground motions. In this case, the efficiency of the IMs is less than that of the spectral acceleration at the fundamental period of the structure.

The determination coefficients of I_a, I_{am} and the normalised I_a were recalculated using two different periods, from T_f. The two utilised periods were T_{max} and T_{dam}, which were obtained from the AEM analyses. Tables 7-21 and 7-24 summarise the R^2 values for the three recalculated IMs and the PIDR and PRDR for both frames under two ground motion sets.

Table 7-21: Correlation coefficients between the PIDR and PRDR of the BF1 frame and I_a, I_{am} and the normalised I_a for the ground motion set 1

BF1 frame subjected to ground motion set 1		Scale factor of 1		Scale factor of 2		Scale factor of 3.5		Scale factor of 5	
		PIDR	PRDR	PIDR	PRDR	PIDR	PRDR	PIDR	PRDR
T_f	I_a	0.96	0.92	0.91	0.93	0.92	0.95	0.88	0.91
	Normalised I_a	0.97	0.94	0.94	0.94	0.93	0.94	0.87	0.94
	I_{am}	0.96	0.91	0.92	0.92	0.92	0.91	0.86	0.92
T_{max}	I_a	0.92	0.88	0.93	0.95	0.94	0.97	0.92	0.96
	Normalised I_a	0.96	0.93	0.91	0.90	0.91	0.95	0.81	0.92
	I_{am}	0.93	0.89	0.94	0.94	0.94	0.95	0.85	0.94
T_{dam}	I_a	0.94	0.92	0.92	0.95	0.90	0.95	0.92	0.94
	Normalised I_a	0.98	0.95	0.91	0.92	0.89	0.95	0.80	0.88
	I_{am}	0.95	0.91	0.95	0.92	0.93	0.95	0.87	0.94

Table 7-22: Correlation coefficients between the PIDR and PRDR of the BF1 frame and I_a, I_{am} and the normalised I_a for the ground motion set 2

BF1 frame subjected to ground motion set 2		Scale factor of 1		Scale factor of 2		Scale factor of 3.5		Scale factor of 5	
		PIDR	PRDR	PIDR	PRDR	PIDR	PRDR	PIDR	PRDR
T_f	I_a	0.92	0.89	0.80	0.83	0.76	0.80	0.81	0.80
	Normalised I_a	0.90	0.93	0.87	0.92	0.82	0.86	0.87	0.89
	I_{am}	0.93	0.91	0.83	0.87	0.79	0.83	0.88	0.88
T_{max}	I_a	0.93	0.90	0.90	0.92	0.91	0.94	0.89	0.91
	Normalised I_a	0.90	0.91	0.85	0.89	0.88	0.91	0.87	0.89
	I_{am}	0.95	0.90	0.92	0.93	0.92	0.94	0.92	0.95
T_{dam}	I_a	0.87	0.89	0.87	0.90	0.85	0.89	0.75	0.77
	Normalised I_a	0.90	0.93	0.82	0.88	0.80	0.84	0.84	0.84
	I_{am}	0.86	0.90	0.87	0.91	0.86	0.89	0.82	0.84

Table 7-23: Correlation coefficients between the PIDR and PRDR of the DCF frame and I_a, I_{am} and the normalised I_a for the ground motion set 1

DCF frame subjected to ground motion set 1		Scale factor of 1		Scale factor of 2		Scale factor of 3.5		Scale factor of 5	
		PIDR	PRDR	PIDR	PRDR	PIDR	PRDR	PIDR	PRDR
T_f	I_a	0.90	0.90	0.92	0.94	0.93	0.93	0.93	0.94
	Normalised I_a	0.88	0.87	0.91	0.91	0.95	0.95	0.95	0.96
	I_{am}	0.88	0.87	0.91	0.90	0.95	0.94	0.95	0.96
T_{max}	I_a	0.92	0.93	0.92	0.95	0.95	0.95	0.94	0.96
	Normalised I_a	0.88	0.88	0.89	0.91	0.92	0.94	0.92	0.93
	I_{am}	0.91	0.91	0.92	0.93	0.96	0.96	0.94	0.95
T_{dam}	I_a	0.93	0.95	0.93	0.96	0.88	0.88	0.92	0.93
	Normalised I_a	0.88	0.88	0.90	0.95	0.90	0.91	0.89	0.91
	I_{am}	0.84	0.83	0.94	0.92	0.95	0.95	0.92	0.94

Table 7-24: Correlation coefficients between the PIDR and PRDR of the DCF frame and I_a, I_{am} and the normalised I_a for the ground motion set 2

DCF frame subjected to ground motion set 2		Scale factor of 1		Scale factor of 2		Scale factor of 3.5		Scale factor of 5	
		PIDR	PRDR	PIDR	PRDR	PIDR	PRDR	PIDR	PRDR
T_f	I_a	0.84	0.83	0.86	0.89	0.92	0.91	0.84	0.88
	Normalised I_a	0.91	0.92	0.90	0.92	0.90	0.94	0.83	0.89
	I_{am}	0.86	0.84	0.87	0.89	0.93	0.92	0.82	0.86
T_{max}	I_a	0.93	0.92	0.94	0.96	0.95	0.93	0.89	0.91
	Normalised I_a	0.89	0.90	0.88	0.91	0.89	0.94	0.82	0.88
	I_{am}	0.93	0.92	0.94	0.95	0.94	0.92	0.85	0.89
T_{dam}	I_a	0.93	0.92	0.91	0.92	0.93	0.94	0.83	0.86
	Normalised I_a	0.89	0.89	0.87	0.90	0.89	0.92	0.81	0.87
	I_{am}	0.94	0.94	0.90	0.91	0.91	0.92	0.80	0.84

A comparison between the R^2 values for the intensity measures, namely I_a, I_{am} and the normalised I_a, which have been calculated using three different value for T_f, shows that the three intensity measures are sensitive to the choice of T_f. Employing the maximum period of the structure when determining these three intensity measures results in a better correlation with the EDPs than utilising the estimated T_f. In contrast, weaker correlations were found when the T_{dam} was employed. T_f cannot be determined accurately before analysis. Simplifying methods for predicting the period elongation may lead to inaccurate estimates.

7.11.6 IM_{Nc} and IM_c as intensity measures

Regarding those intensity measures that rely on optimal combinations of spectral displacement values at different structure periods, elastic and inelastic periods, it was found that:

IM_{Nc} appears to correlate well with the PIDR and PRDR for both frames under the far-field ground motions, as scaled by a factor of 1 and 2. The efficiency of this intensity decreases at high intensity levels. IM_c has a stronger correlation with the EDPs than IM_{Nc} in the highly nonlinear range of response.

The results of the investigation study summarised in Tables 7-5 to 7-20 revealed there is no intensity measure to highly correlate with the peak inter-storey drift ratio, the peak roof displacement drift and the maximum structure period for both frames under the two ground motion sets scaled to the four seismic intensity levels, in all sixteen cases studied. It was found that the level of nonlinearity, the type of structure, and the properties of the employed ground motion records are the key parameters affecting the efficiency of the scaling method.

In summary, it can be concluded when comparing the R^2 values for all the investigated ground motion intensity measures that the I_{NP} determined without considering the higher-mode contributions trend to be the best intensity measure for mid-rise structures subjected to far-and near-field ground motions, followed by I_a, calculated utilising the maximum period of the structure and then the intensity measures proposed by (Yahyaabadi and Tehranizadeh, 2011), IM_{Nc} for non-collapse cases and IM_c for near collapse and collapse cases. IM_{Nc} and IM_c reflect the effects of period elongation by considering an optimal combination of

spectral values over elastic and inelastic periods. However, the efficiency of these two intensity measures is not very high for near-field ground motions.

The efficiency of the fifteen IMs investigated is higher for far-field ground motions than that for near-field ground motions.

7.11.7 T_{max} and T_{dam} as EDPs

It is worth noting that the efficiency of the scaling methods may differ according to the response of concern. It has been concluded that the elastic spectral shape and the inelastic spectral displacement have a strong impact on the maximum inter-storey drift. While the peak ground acceleration strongly affects the structure response in terms of peak floor acceleration (Krawinkler, 2005). In general, the results show that the intensity measures, which correlate well with the PIDR and PRDR, have a good correlation with the T_{max}. However, the efficiency of the IMs examined for T_{max} is less than for the PIDR and PRDR of the BF1 frame at high intensity levels. I_a appears to be a better predictor for structural damage in terms of period softening, compared to the other fourteen examined IMs. Thus, it is better to estimate the elongation period of the structure based on I_a rather than on only $S_a(T_1)$.

One of the important observations from this study is that the maximum period, T_{max}, can be a good Engineering Demand Parameter when compared to the common EDPs, the maximum storey drifts and the maximum roof displacement drifts. T_{max} correlates well with ground motion intensity measures for the first three seismic levels. The correlation coefficient for T_{max} is relatively low at high seismic intensities, especially for near-field ground motions. The largest value of R^2 for the BF1 frame under set 2 scaled by a factor of 5 is 0.81.

The results indicate that the correlations between T_{max} and the IMs of concern are often better than those between T_{dam} and the IMs for both frames at the four seismic intensity scale factors and for both ground motion sets. The Damage period, T_{dam}, is not an appropriate EDP, especially in nonlinear range. The results show that it has the weakest correlation with the intensity measures. As the seismic intensity scale factor increases, the R^2 for T_{dam} decreases.

It also has been noted that the global damage indices, $D_{G,f}$, $D_{G,pl}$ and $D_{G,m}$, which are based on T_{max} and/or T_{dam}, often have weak correlations with the IMs for almost all cases.

7.12 Conclusions

The conclusions here are subjected to the assumptions and limitation of the modelling approach. From the correlation studies between different intensity measures and a number of engineering demand parameters, it was found that:

- The spectral acceleration at the fundamental period of the structure is an efficient intensity measure for mid-rise structures subjected to far-field ground motions at low and/or moderate seismic intensity levels.
- $S_a(T_1)$ is a better intensity measure for regular structures than for irregular structures.
- A scalar intensity measure, which is based on a single spectral value, cannot be efficient at all seismic intensity levels due to the period elongation.
- The efficiency of the intensity measures, which are based on a combination of two spectral values, is better than those based on a single period.
- The effect of higher mode contributions can be neglected in mid-rise structures.
- The maximum period of the structure appears to be a good damage predictor prior to near collapse.
- The damage period of the structure does not correlate well with the IMs examined, compared to T_{max}, PIDR and PRDR.
- The damage indices, $D_{G,f}$, $D_{G,pl}$ and $D_{G,m}$, of the structure do not have good correlation with the IMs examined.
- The efficiency of scaling methods may differ according to engineering demand parameters of concern.
- The key factors affecting the efficiency of intensity measures are structure type, ground motion properties and seismic intensity level.
- The intensity measures that consider the spectral shape are the most efficient.
- The most appropriate intensity measures for utilisation in scaling ground motions for the seismic assessment of mid-rise structures tend to be I_{NP}, computed without considering the higher-mode contributions.

- The efficiency of the fifteen investigated IMs is higher for far-field ground motions than for near-field ground motions.
- The efficiency of the intensity measure, namely I_a, I_{am} and the normalised I_a, is sensitive to the accuracy of the estimate for the elongation period, T_f.

Chapter 8 Conclusions and recommendations for future work

8.1 Introduction

This study mainly focused on assessing the behaviour of RC bare multi-storey frame structures, designed according to EC8, when subjected to seismic loads using the Applied Element Method for direct collapse simulation. Emphasis has placed on various aspects of the collapse process; such as the time at incipient collapse, possible failure modes, and collapse probability.

The aim of this research is to lead to a better understanding of the collapse behaviour of RC frame structures and those key factors that affect it. Knowing the most important parameters that should be considered in the seismic collapse analysis can result in more accurate analysis.

The research has involved a literature review, a summary of the AEM, validation of the AEM models, an investigation of the effect of modelling uncertainties on the collapse response, an investigation of the effect of inclusion of the vertical ground motions on the collapse process, an investigation of the correlation between different intensity measures based on spectral values and four engineering demand parameters, particularly the maximum and damage periods.

This chapter summarises the most important conclusions drawn based on the different tasks and also presents recommendations for further studies. All conclusions presented in this chapter are subjected to the assumptions and limitation of the modelling approach.

8.2 Summary of conclusions

From the background study of the AEM and from the validation study, the following conclusions were reached:

1. The storey displacement histories, obtained from the AEM analyses of the full-scale two-storey one-bay RC frame structure previously shaking-table tested were found to be in good agreement with those obtained from experimental results for low and

moderate seismic intensity levels. While a reasonable agreement has found for high seismic intensity levels.

2. The storey displacement histories obtained from the AEM analyses of the two six-storey RC frame structures, designed according to EC8, are in reasonable agreement with those obtained from experimental results for all different seismic intensity levels.
3. The AEM is not a very accurate method for modelling existing structures, which involve joint shear failure, due to the simple techniques adopted for shear modelling.

From the sensitivity studies concerning the effect of randomness in material properties on the time at onset collapse, and the corresponding failure mechanism of the BF1 and DCF frames, it was found that:

1. The order of importance of random variables may change depending on the structural system, the correlation type between random variables, the possible collapse modes and the seismic intensity level.
2. Seismic intensity is one of the key factors governing the collapse process.
3. The most important variables are those that can change the collapse process and lead either to more uniform damage distribution, with a larger number of structural members involved in the collapse mechanism or to more damage localisation and a single storey mechanism.
4. Different failure modes including vertical, side-sway and pancake collapse modes were predicted depending on the uncertainty in the selected variables and the correlation between them.
5. Ignoring the secondary effects, impact between different elements and force redistribution following the element separation, can lead to unsafe collapse predictions, due to neglect of some of the possible failure modes.

The following conclusions were drawn based on study emphases on the effect of considering the ground motion vertical component on the collapse probabilities and possible failure modes:

1. Vertical ground motion often influences both collapse probability and failure modes of RC frame structures, designed according to EC8. Therefore, ignoring the effect of

vertical ground motion in a collapse assessment of modern RC frame structures can lead to unsafe predictions, especially for irregular frame structures.

2. The collapse probability of frame structures subjected to horizontal and vertical ground motion components combined may increase or decrease according to the overall structural system ductility, the characteristics of both vertical and horizontal components of each record and the intensity level of both components.
3. The Irregular Frame structure, with discontinuous column at the first storey, is more likely to be sensitive to the inclusion of vertical ground motion compared to the regular frame structure, BF1.
4. The collapse capacity of the DCF frame decreased by around 0.35g when accounting for the effect of vertical ground motions. However, the collapse capacity of the BF1 frame did not change when the effect of vertical ground motions was considered.
5. The effects of vertical ground motion can modify failure modes of modern frame structures, leading to vertical rather than side-sway collapse.

From the correlation studies, focusing on different intensity measures, it was found that:

1. The key factors that affect the efficiency of intensity measures are the structure type, the ground motion properties and the seismic intensity level.
2. A scalar intensity measure, based on a single spectral value, cannot be efficient at all seismic intensity levels due to the structure period elongation.
3. The efficiency of intensity measures, based on a combination of two spectral values, is better than those based on a single period.
4. The maximum period of a structure appears to be a good damage predictor prior to near collapse. However, the damage period of the structure does not correlate well with the IMs examined.
5. The intensity measures that do consider the spectral shape are the most efficient. Thus, the best intensity measures to be utilised in scaling ground motions for seismic assessment of mid-rise structures tend to be I_{NP} computed, without considering the higher-mode contributions.

8.3 Recommendations for future work

This study mainly focused on 2D bare reinforced concrete multi-storey frame structures designed according to EC8. In particular, the seismic response of the mid-rise frame RC structures up to collapse was investigated and the effects of key factors on the collapse process were examined in the study. For future studies, a number of recommendations can be made as follows:

1. The results obtained from this study need to be expanded on, to cover different types of structures, low- and high-rise structures.
2. The effects of infill walls, slabs and non-structural members may affect the structure's stiffness and hence modify damage progression and the following collapse mode. Thus, these effects should be considered in further studies.
3. Structures with different types of structural systems and/or different materials, e.g. steel, should be studied. For example, structures consist of dual systems or shear-wall systems.
4. Soil-structure interaction effects need to be considered.
5. Three-dimensional models subjected to two or three ground motion components need to be considered in order to account for the torsion effect, and to investigate the effect of the interaction of ground motion components.
6. The effect of the buckling of reinforcement bars needs to be considered in the AEM models.
7. Improvements are needed for modelling the shear failure of column-beam joints.
8. Further studies, using artificial ground motions; such as spectrum compatible or synthetic motions, can be performed.
9. Further investigation on the effect of the correlation between random variables on the collapse process can be conducted.
10. Further sensitivity studies to understand the asymmetric effects of modelling uncertainties need to be conducted.
11. Further investigation into the effect of the uncertainty in the value of failure criterion, separation strain, on the collapse process could usefully be carried out.

References

ACI 2002. Building code requirements for structural concrete and commentary. *ACI 318-02/ACI 318R-02, Farmington Hills, MI*.

AHMADIZADEH, M. & SHAKIB, H. 2004. On the December 26, 2003, southeastern Iran earthquake in Bam region. *Eng Struct,* 26**,** 1055-1070.

AMBRASEYS, N., SMIT, P., SIGBJORNSSON, R., SUHADOLC, P. & MARGARIS, B. 2002. Internet-Site for European Strong-Motion Data. *European Commission, Research-Directorate General, Environment and Climate Programme* <*http://www.isesd.cv.ic.ac.uk/ESD/*>.

AMBRASEYS, N. N. & SIMPSON, K. A. 1996. Prediction of vertical response spectra in Europe. *Earthquake Engineering & Structural Dynamics,* 25**,** 401-412.

ANSAL, A. 2004. *Recent advances in earthquake geotechnical engineering and microzonation,* Kluwer Academic Publishers.

APPLIED SCIENCE INTERNATIONAL (ASI) 2010. Extreme Loading for Structures, Version 3.1.

APPLIED SCIENCE INTERNATIONAL (LLC) 2010. Extreme Loading® for Structures, Theoretical manual.

ARIAS, A. 1970. *A measure of earthquake intensity, in seismic design in nuclear power plants,* MIT Press, Cambridge, MA.

ASCE 1997. FEMA 273: NEHRP Commentary on the Guidelines for the Seismic Rehabilitation of Buildings. *Report No. FEMA 273, ASCE/FEMA.*

ASCE 2000. FEMA 356: Prestandard and Commentary for the Seismic Rehabilitation of Buildings. *Report No. FEMA 356, ASCE/FEMA Agency.*

ASCE 2002. Minimum design loads for buildings and other structures. *ASCE 7-02, Reston, VA.*

ASCE 2005. Minimum design loads for buildings and other structures. *ASCE 7-05, Reston, VA.*

ASLANI, H. & MIRANDA, E. 2005. Probabilitistic earthquake loss estimation and loss disaggregation in buildings. *Blume TR 157, Stanford University.*

ASPRONE, D., NANNI, A., SALEM, H. & TAGEL-DIN, H. 2010. Applied Element Method Analysis of Porous GFRP Barrier Subjected to Blast. *Advances in Structural Engineering,* 13.

ATC 1996. Seismic Evaluation and Retrofit of Concrete Buildings (ATC40), Applied Technology Council, Redwood City, CA.

BAKER, J. & CORNELL, C. A. 2003. Uncertainty Specification and Propagation for Loss Estimation Using FOSM Methods. *PEER Rep. No. 2003/07, Pacific Earthquake Engineering Research Center, Univ. of California, Berkeley*.

BAKER, J. W. 2011. Conditional Mean Spectrum: Tool for ground motion selection. *Journal of Structural Engineering* 137**,** 322-331.

BAKER, J. W. & CORNELL, C. A. 2005. A vector-valued ground motion intensity measure consisting of spectral acceleration and epsilon. *Earthquake Engineering & Structural Dynamics,* 34**,** 1193-1217.

BAKER, J. W. & CORNELL, C. A. 2006a. Spectral shape, epsilon and record selection. *Earthquake Engineering and Structural Dynamics,* 35**,** 1077-95.

BAKER, J. W. & CORNELL, C. A. 2006b. Vector-Valued Ground Motion Intensity Measures for Probabilistic Seismic Demand Analysis. *PEER report 2006/08, Pacific Earthquake Engineering Research Center, University of California, Berkeley*.

BAKER, J. W. & CORNELL, C. A. 2006c. Which spectral acceleration are you using? *Earthquake Spectra,* 22**,** 293-312.

BAKER, J. W. & CORNELL, C. A. 2008. Uncertainty Propagation in Probabilistic Seismic Loss Estimation. *Structural Safety,* 30**,** 236-252.

BAZZURRO, P. 1998. *Probabilistic seismic demand analysis. Ph.D. Dissertation*, Stanford University.

BAZZURRO, P. & CORNELL, C. A. 1999. Disaggregation of seismic hazard. *Bulletin of the Seismological Society of America,* 89**,** 501-520.

BIANCHINI, M. 2008. Improved scalar intensity measures in performance-based earthquake engineering. *Nota Tecnica n. 215, DISTART, Università di Bologna*.

BIANCHINI, M., DIOTALLEVI, P. & BAKER, J. W. 2009. Prediction of inelastic structural response using an average of spectral accelerations. *10th International Conference on Structural Safety and Reliability (ICOSSAR 09).*

BINICI, B. & MOSALAM, K. M. 2007. Analysis of reinforced concrete columns retrofitted with fiber reinforced polymer lamina. *Composites Part B: Engineering,* 38**,** 265-276.

BOJORQUEZ, E. & IERVOLINO, I. 2011. Spectral shape proxies and nonlinear structural response. *Soil Dynamics and Earthquake Engineering,* 31**,** 996-1008.

BOJÓRQUEZ, E., IERVOLINO, I. & MANFREDI, G. 2008. Evaluating a new proxy for spectral shape to be used as an intensity measure. *In: Proceedings of the 2008 seismic*

engineering conference commemorating the 1908 Messina and Reggio Calabria earthquake (MERCEA '08).

BOJORQUEZ, E., IERVOLINO, I., REYES-SALAZAR, A. & RUIZ, S. E. 2012. Comparing vector-valued intensity measures for fragility analysis of steel frames in the case of narrow-band ground motions. *Engineering Structures,* 45**,** 472-480.

BOMMER, J. J. & ACEVEDO, A. B. 2004. The use of real earthquake accelerograms as input to dynamic analysis. *Journal of Earthquake Engineering,* 8**,** 43-92.

BOMMER, J. J., ACEVEDO, A. B. & DOUGLAS, J. 2003. The Selection and Scaling of Real Earthquake Accelerograms for Use in Seismic Design and Assessment. *Proceedings of ACI International Conference on Seismic Bridge Design and Retrofit, American Concrete Institute.*

BOMMER, J. J. & MARTINEZ-PEREIRA, A. 1999. The effective duration of earthquake strong motion. *Journal of earthquake engineering* 3**,** 127-172.

BOZORGNIA, Y., CAMPBELL, K. & NIAZI, M. 1999. Vertical Ground Motion: Characteristics, Relationship with Horizontal Components, and Building Code Implications. *SMIP99 Seminar on Utilization of Strong-Motion Data,* 23 - 50.

BRODERICK, B. M. & ELNASHAI, A. S. 1995. Analysis of the failure of Interstate 10 freeway ramp during the Northridge earthquake of 17 January 1994. *Earthquake Eng. Struct. Dyn,* 24**,** 189-208.

BURATTI, N., FERRACUTI, B. & SAVOIA, M. 2007. Recorded and simulated ground motion time histories for seismic fragility analysis of RC structures. *XII Conference of the Associazione Nazionale Italiana di Ingegneria Sismica, Pisa*.

CALVI, G. M., MAGENES, G. & PAMPANIN, S. 2002a. Experimental Test on a Three Storey R.C. Frame Designed for Gravity Only. *12th European Conference on Earthquake Engineering.* London.

CALVI, G. M., MAGENES, G. & PAMPANIN, S. 2002b. Relevance of Beam-Column Joint Damage and Collapse in RC Frame Assessment. *Journal of Earthquake Engineering,* 6**,** 75-100.

CANTAGALLO, C., CAMATA, G., SPACONE, E. & COROTIS, R. 2012. The variability of deformation demand with ground motion intensity. *Probabilistic Engineering Mechanics,* 28**,** 59-65.

CARBALLO, J. E. & CORNELL, C. A. 2000. Probabilistic seismic demand analysis: spectrum matching and design. *Report No. RMS-41, Reliability of Marine Structures Program.* Stanford, CA: Department of Civil and Environmental Engineering, Stanford University.

CATALAN, A., BENAVENT-CLIMENT, A. & CAHIS, X. 2010. Selection and scaling of earthquake records in assessment of structures in low-to-moderate seismicity zones. *Soil Dynamics and Earthquake Engineering,* 30**,** 40-49.

CEB, C. E.-I. D. B. 1993. CEB-FIP Model Code 1990: Design Code. London: Thomas Telford.

CELIK, O. C. & ELLINGWOOD, B. R. 2009. Seismic fragilities for non-ductile reinforced concrete frames-Role of aleatoric and epistemic uncertainties. *Structural Safety,* 32**,** 1-12.

CHAUDAT, T., GARNIER, C., CVEJIC, S., POUPIN, S., LE CORRE, M. & MAHE, M. 2005. ECOLEADER Project No. 2: Seismic tests on a reinforced concrete bare frame with FRP retrofitting-Tests Report. SEMT/EMSI/RT/05-006/A. . CEA, Saclay (France).

CHIOU, B., DARRAGH, R., GREGOR, N. & SILVA, W. 2008. NGA project strong motion database. *Earthquake Spectra,* 24**,** 23-44.

CHOPRA, A. & CHINTANAPAKDEE, C. 2004. Inelastic Deformation Ratios for Design and Evaluation of Structures: Single-Degree-of-Freedom Bilinear Systems. *Journal of Structural Engineering,* 130**,** 1309-1319.

COLLIER, C. J. & ELNASHAI, A. S. 2001. A procedure for combining vertical and horizontal seismic action effects *Journal of Earthquake Engineering,* 5**,** 521-539.

COMARTIN, C. D. 2001. PBEE needs, buildings perspective: critical needs throughout the performance spectrum. *2001 PEER Annual Meeting, Oakland, California.*

COMPUTERS AND STRUCTURES 2000. SAP 2000 version 8.0, . *Computers and Structures Inc., Berkeley, California, U.S.A.*

CORDOVA, P. 2000. Development of a two-parameter seismic intensity measure and probabilistic seismic assessment procedure. *PEER Report 2000/10. Berkeley: Pacific Earthquake Engineering Research Center, University of California Berkeley.*

CORDOVA, P. P., MEHANNY, S. S. F., DEIERLEIN, G. G. & CORNELL, C. A. Development of a two-parameter seismic intensity measure and probabilistic seismic assessment procedure. Proceedings of the 2nd U.S.-Japan Workshop on Performance-Based Seismic Earthquake Engineering Methodology for Reinforced Concrete Building Structures, 2001 Sapporo, Japan. 195-214.

CORNELL, C., JALAYER, F., HAMBURGER, R. & FOUTCH, D. 2002. Probabilistic Basis for 2000 SAC Federal Emergency Management Agency Steel Moment Frame Guidelines. *Journal of Structural Engineering,* 128**,** 526-533.

CORNELL, C. A. 2005. On earthquake record selection for nonlinear dynamic analysis. *The Esteva Symposium, Mexico.*

COSENZA, E. & MANFREDI, G. 1970. The improvement of the seismic-resistant design for existing and new structures using damage criteria. *In: P. Fajfar and H. Krawinkler, eds. 1997. Seismic Design Methodologies for the Next Generation of Codes. Rotterdam, The Netherlands: A.A Balkema,* 119-130.

CUNDALL, P. A. & STRACK, O. D. L. 1979. Discrete numerical model for granular assemblies. *Geotechnique, Mar 1979, London,* 29**,** 47-65.

DEIERLEIN, G. G. 2004. Overview of a Comprehensive Framework for Earthquake Performance Assessment. *Performance-Based Seismic Design Concepts and Implementation, Proceedings of an International Workshop, PEER Report 2004/05, UC Berkeley, p. 15-26.*

DEIERLEIN, G. G. & HASELTON, C. B. 2005. Developing consensus on provisions to evaluate collapse of reinforced buildings. *Proceedings of the First NEES/E-Defense Workshop on Collapse Simulation of Reinforced Concrete Building Structures, PEER Rep. No. 2005/10, Pacific Earthquake Engineering Research Center, Univ. of California, Berkeley.*

DESSOUKY, A. S., TAGEL-DIN, H. S. & MOURAD, S. A. 2007. Collapse Analysis of Stone-Block Structures under Seismic Excitation using Applied Element Method. *the Twelfth International Colloquium on Structural & Geotechnical Engineering, Ein Shams University, December 2007.*

DIPASQUALE, E. & CAKMAK, A. S. 1987. Detection and assessment of seismic structural damage *NCEER-87-0015, Buffalo, N.Y. : National Center for Earthquake Engineering Research, Technical report, 1v (500 N24 87-15).*

DIPASQUALE, E. & CAKMAK, A. S. 1989. On the relation between local and global damage indices *NCEER-89-0034, Buffalo, N.Y. : National Center for Earthquake Engineering Research, Technical report, 1v (500 N24 89-34).*

DOOLEY, K. L. & BRACCI, J. M. 2001. Seismic Evaluation of Column-to-Beam Strength Ratios in Reinforced Concrete Frames. *ACI Structural Journal,* 98**,** 843-851.

DYMIOTIS, C. 1999. *Probabilistic seismic assessment of reinforced concrete buildings with and without masonry infills.* Doctor of Philosophy in Structural Engineering, Imperial College of Science, Technology and Medicine.

EC8-1 2004. Design of structures for earthquake resistance, part 1: general rules, seismic actions and rules for buildings, European standard EN 1998-1. European Committee for Standardization (CEN), Brussels.

ELGAMAL, A. & HE, L. 2004. Vertical earthquake ground motion records: an overview. *Journal of Earthquake Engineering,* 8**,** 663-697.

ELKHOLY, S. & MEGURO, K. 2004. Numerical Simulation of High-Rise Steel Buildings Using Improved Applied Element Method. *13th World Conference on Earthquake Engineering,Vancouver, B.C., Canada.* Vancouver, B.C., Canada.

ELLINGWOOD, B. R. & KINALI, K. 2009. Quantifying and communicating uncertainty in seismic risk assessment. *Structural Safety,* 31**,** 179-187.

ELNASHAI, A., SPENCER, B., KUCHMA, D., KIM, S. J., BURDETTE, N., HOLUB, C., GONZALES, J., NAKATA, N., YANG, G. & GAN, Q. 2005. Analysis and distributed hybrid simulation of shear-sensitive RC bridges subjected to horizontal and vertical earthquake ground motion. *Proceedings of 36th US-Japan Workshop on Wind and Earthquake.*

ELNASHAI, A. S., HE, L. & ELGAMAL, A. 2004. Spectra for vertical earthquake ground motion. *13th World Conf. on Earthquake Engineering. Vancouver, Canada.*

ELNASHAI, A. S. & PAPAZOGLOU, A. J. 1997. Procedure and spectra for analysis of RC structures subjected to strong vertical earthquake loads. *Journal of Earthquake Engineering,* 1**,** 121-155.

ELWOOD, K. & MOEHLE, J. 2005a. Axial capacity model for shear-damaged columns. *Structural Journal, American Concrete Institute,* 102**,** 578-587.

ELWOOD, K. J. 2004. Modeling failures in existing reinforced concrete columns. *Canadian Journal of Civil Engineering* 31.

ELWOOD, K. J. & MOEHLE, J. P. 2003. Shake table tests and analytical studies on the gravity load collapse of reinforced concrete frames. *PEER Rep. No. 2003/01, Pacific Earthquake Engineering Research Center, Univ. of California, Berkeley.*

ELWOOD, K. J. & MOEHLE, J. P. 2005b. Drift capacity of reinforced concrete columns with light transverse reinforcement. *Earthquake Spectra,* 21**,** 71-89.

ELWOOD, K. J. & MOEHLE, J. P. 2008. Dynamic shear and axial-Load failure of reinforced concrete columns. *Journal of Structural Engineering,* 134**,** 1189-1198.

ESTEVA, L. & RUIZ, S. E. 1989. Seismic Failure Rates of Multistory Frames. *Journal of Structural Engineering,* 115**,** 268-284.

EUROCODE 8 (EC8) 1988 (draft); 1994. Design provisions for earthquake resistance of structures. *CEN (European Commission for Standardization)/TC250/SC8, Brussels, Belgium.*

FAJFAR, P. & M.EERI 2000. A Nonlinear Analysis Method for Performance Based Seismic Design. *Earthquake Spectra,* 16**,** 573-592.

FAJFAR, P., VIDIC, T. & FISCHINGER, M. 1990. A measure of earthquake motion capacity to damage medium-period structures. *Soil Dyn. Earthquake Eng,* 9**,** 236-242.

FARDIS, M. N., KRAWINKLER, H., ZAREIAN, F., LIGNOS, D. & IBARRA, L. 2010a. Significance of Modeling Deterioration in Structural Components for Predicting the Collapse Potential of Structures Under Earthquake Excitations. *Advances in Performance-Based Earthquake Engineering.* Springer Netherlands.

FARDIS, M. N., MOSALAM, K. & GUNAY, M. S. 2010b. Seismic Retrofit of Non-ductile Reinforced Concrete Frames Using Infill Walls as a Rocking Spine. *Advances in Performance-Based Earthquake Engineering.* Springer Netherlands.

FONTARA, I.-K. M., ATHANATOPOULOU, A. M. & AVRAMIDIS, I. E. 2012. Correlation between advanced, structure-specific ground motion intensity measures and damage indices. *15 WCEE, Lisboa*.

GALAL, K. & EL-SAWY, T. 2009. Effect of retrofit strategies on mitigating progressive collapse of steel frame structures. *Journal of Constructional Steel Research,* 66**,** 520-531.

GARCIA, R., HAJIRASOULIHA, I. & PILAKOUTAS, K. 2010. Seismic behaviour of deficient RC frames strengthened with CFRP composites. *Engineering Structures,* 32**,** 3075-3085.

GAREVSKI, M., ANSAL, A. & PINTO, A. 2010. Large scale testing. *In:* ANSAL, A. (ed.) *Earthquake Engineering in Europe.* Springer Netherlands.

GASPARINI, D. & VANMARCKE, E. H. 1976. *SIMQKE -1: A Program for Artificial Motion Generation,* Department of Civil Engineering, Massachusetts Institute of Technology, Cambridge,MA.

GHANNOUM, W. M. & MOEHLE, J. P. 2008a. Experimental collapse of a lightly reinforced concrete frame subjected to high intensity ground motions. *The 14th World Conference on Earthquake Engineering October 12-17, 2008, Beijing, China*.

GHANNOUM, W. M. & MOEHLE, J. P. 2008b. Shear Failure Model for Flexure-Shear Critical Reinforced Concrete Columns. *The 14th World Conference on Earthquake Engineering October 12-17, 2008, Beijing, China.*

GHANNOUM, W. M., MOEHLE, J. P. & BOZORGNIA, Y. 2008. Analytical collapse study of lightly confined reinforced concrete frames subjected to Northridge earthquake ground motions. *Journal of Earthquake Engineering,* 12**,** 1105-1119.

GRANT, L. H., MIRZA, S. A. & MACGREGOR, J. G. 1978. Monte Carlo study of strength of concrete columns. *ACI Struct J,* 75**,** 348-357.

GUPTA, I. D. 2002. The State of The Art in Seismic Hazard Analysis. *ISET Journal of Earthquake Technology,* 39**,** 311-346.

GURAGAIN, R., WORAKANCHANA, K., MAYORCA, A. & MEGURO, K. 2006. Simulation of Brick Masonry Wall Behavior Under Cyclic Loading Using Applied Element Method. *SEISAN KENKYU,* 58**,** 531-534.

GURLEY, C. 2008. Progressive collapse and earthquake resistance. *Practice Periodical on Structural Design and Construction ASCE,* 13**,** 19-23.

HAKUNO, M. & MEGURO, K. 1993. Simulation of concrete-frame collapse due to dynamic loading. *J. Eng. Mech., ASCE,,* 119**,** 1709-1723.

HALLQUIST, J. 2006. LS-DYNA keyword user's manual, Version 971, Livermore Software Technology, Livermore, CA.

HAMED, S. 2011. Computer-Aided Design of Framed Reinforced Concrete Structures Subjected to Flood Scouring. *Journal of American Science,* 7**,** 191-200.

HASELTON, C., LIEL, A., DEAN, B., CHOU, J. & DEIERLEIN, G. 2007. Seismic collapse safety and behavior of modern reinforced concrete moment frame buildings. *Structural Engineering Research Frontiers,* 1.

HASELTON, C., LIEL, A., TAYLOR LANGE, S. & DEIERLEIN, G. G. 2008a. Beam-column element model calibrated for predicting flexural response leading to global collapse of RC frame buildings. *PEER Rep. 2007/03, Pacific Earthquake Engineering Research Center (PEER), Univ. of California at Berkeley, Berkeley, CA.*

HASELTON, C. B. 2009. Evaluation of ground motion selection and modification methods: predicting median interstory drift response of buildings. *PEER Rep. No. 2009/01, Pacific Earthquake Engineering Research Center, Univ. of California, Berkeley*.

HASELTON, C. B. & BAKER, J. W. 2006. Ground motion intensity measures for collapse capacity prediction: Choice of optimal spectral period and effect of spectral shape. *8th National Conference on Earthquake Engineering.* San Francisco, California.

HASELTON, C. B., BAKER, J. W., LIEL, A. B. & DEIERLEIN, G. G. 2011a. Accounting for Ground-Motion Spectral Shape Characteristics in Structural Collapse Assessment through an Adjustment for Epsilon. *Journal of Structural Engineering,* 137**,** 332-344.

HASELTON, C. B. & DEIERLEIN, G. G. 2008. Assessing Seismic Collapse Safety of Modern Reinforced Concrete Moment-Frame Buildings. *Report No. PEER 2007/08, Pacific Earthquake Engineering Research Center, University of California, Berkeley*.

HASELTON, C. B., GOULET, C. A., MITRANI-REISER, J., BECK, J. L., DEIERLEIN, G. G., PORTER, K. A., STEWART, J. P. & TACIROGLU, E. 2008b. An assessment to benchmark the seismic performance of a code-conforming reinforced concrete moment-frame building. *PEER Rep. No. 2007/12, Pacific Earthquake Engineering Research Center, Univ. of California, Berkeley*.

HASELTON, C. B., LIEL, A. B. & DEIERLEIN, G. G. 2009. Simulating structural collapse due to earthquakes: model idealization, model calibration, and numerical solution algorithms. *Computational Methods in Structural Dynamics and Earthquake Engineering (COMPDYN).* Rhodes, Greece.

HASELTON, C. B., LIEL, A. B., DEIERLEIN, G. G., DEAN, B. S. & CHOU, J. H. 2011b. Seismic Collapse Safety of Reinforced Concrete Buildings. I: Assessment of Ductile Moment Frames. *Journal of Structural Engineering. April 2011: American Society of Civil Engineers***,** 481-491.

HASHEMI, A. & MOSALAM, K. M. 2006. Shake-table experiment on reinforced concrete structure containing masonry infill wall. *Earthquake Engineering & Structural Dynamics*, 35**,** 1827-1852.

HOUSNER, G. W. 1952. Spectrum Intensities of Strong-Motion Earthquakes. *Proc. Symp. Eathquake and Blast Effects on Structures, Engineering Research Institute, Los Angeles.*

HUTCHINSON, T. C., CHAI, Y. H., BOULANGER, R. W. & IDRISS, I. M. 2004. Inelastic Seismic Response of Extended Pile-Shaft-Supported Bridge Structures. *Earthquake Spectra*, 20**,** 1057-1080.

IBARRA, L. F. & KRAWINKLER, H. 2004. Global collapse of deteriorating MDOF systems. *The 13th World Conference on Earthquake Engineering, Vancouver, B.C., Canada*.

IBARRA, L. F. & KRAWINKLER, H. 2005. Global collapse of frame structures under seismic excitations. *PEER Rep. No. 2005/06, Pacific Earthquake Engineering Research Center, Univ. of California, Berkeley*.

IBARRA, L. F., MEDINA, R. A. & KRAWINKLER, H. 2005. Hysteretic models that incorporate strength and stiffness deterioration. *Earthquake Engineering and Structural Dynamics*, 34**,** 1489-1511.

IERVOLINO, I. & CORNELL, C. A. 2005. Record selection for nonlinear seismic analysis of structures. *Earthquake Spectra*, 21**,** 685-713.

IERVOLINO, I. & GALASSO, C. 2009. REXEL 2.31 beta—tutorial, available at: http://www.reluis.it/doc/software/ REXEL_Tutorial_ENG.pdf.

IERVOLINO, I., GALASSO, C. & COSENZA, E. 2009. Spettri, Accelerogrammi e le Nuove Norme Tecniche per le Costruzioni. *Progettazione Sismica*, 1**,** 33-50, Gennaio-Aprile.

IERVOLINO, I., GALASSO, C. & COSENZA, E. 2010. REXEL: computer aided record selection for code-based seismic structural analysis. *Bulletin of Earthquake Engineering*, 8**,** 339-362.

IERVOLINO, I., MADDALONI, G. & COSENA, E. 2006a. Unscaled real record sets compliant with Eurocode 8. *First European Conference on Earthquake Engineering and Seismology (a joint event of the 13th ECEE & 30th General Assembly of the ESC).* Geneva, Switzerland, .

IERVOLINO, I., MADDALONI, G. & COSENZA, E. 2008. Eurocode 8 compliant real record sets for seismic analysis of structures. *Journal of Earthquake Engineering*, 12**,** 54 - 90.

IERVOLINO, I. & MANFREDI, G. 2008. A review of ground motion record selection strategies for dynamic structural analysis. *In: Oreste S. Bursi, David J. Wagg Editors,*

Modern Testing Techniques of Mechanical and Structural Systems, CISM Courses and Lectures, Springer, 52, 131-163.

IERVOLINO, I., MANFREDI, G. & COSENZA, E. 2006b. Ground motion duration effects on nonlinear seismic response. *Earthquake Engineering & Structural Dynamics,* 35**,** 21-38.

INOUE, T. & CORNELL, C. A. 1990. Seismic hazard analysis of multi-degree-of-freedom structures. *Reliability of Marine Structures Program Report No. RMS-8, Department of Civil and Environmental Engineering, Stanford University, California.*

ISOBE, D. & TSUDA, M. 2003. Seismic collapse analysis of reinforced concrete framed structures using the finite element method. *Earthquake Engineering & Structural Dynamics,* 32**,** 2027-2046.

JCSS 1995. Probabilistic Model Code, Part 3:Resistance Models. *Working Document JCSS-RACK-08-0 1-95*.

KABEYASAWA, T., MATSUMORI, T., KATSUMATA, H. & SHIRAI, K. 2005. Design of the full-scale six-story reinforced concrete wall-frame building for testing at E-Defense. *Proceedings of the First NEES/E-Defense Workshop on Collapse Simulation of Reinforced Concrete Building Structures,* PEER Rep. No. 2005/10, Pacific Earthquake Engineering Research Center, Univ. of California, Berkeley.

KADAS, K., YAKUT, A. & KAZAZ, I. 2011. Spectral Ground Motion Intensity Based on Capacity and Period Elongation. *Journal of Structural Engineering,* 137**,** 401-409.

KADID, A., YAHIAOUI, D. & CHEBILI, R. 2010. Behaviour of reinforced concrete buildings under simultaneous horizontal and vertical ground motions. *Asian Journal of Civil Engineering* 11**,** 463-476.

KAEWKULCHAI, G. & WILLAMSON, E. B. 2003. Progressive collapse behavior of planar frame structures. *Proceedings of the Response of Structures to Extreme Loading Conference, Toronto, Canada*.

KAEWKULCHAI, G. & WILLIAMSON, E. B. 2004. Beam element formulation and solution procedure for dynamic progressive collapse analysis. *Computers & Structures,* 82**,** 639-651.

KAEWKULCHAI, G. & WILLIAMSON, E. B. 2006. Modeling the Impact of Failed Members for Progressive Collapse Analysis of Frame Structures. *Journal of Performance of Constructed Facilities, ASCE,* 20**,** 375-383

KALKAN, E. & CHOPRA, A. 2011. Modal-pushoverbased ground-motion scaling procedure. *Journal of Structural Engineering (ASCE),* 138**,** 289-310.

KALKAN, E. & CHOPRA, A. K. 2010. Practical guidelines to select and scale earthquake records for nonlinear response history analysis of structures. *U.S. Geological Survey Open-File Report 2010-1068***,** 124.

KALKAN, E. & CHOPRA, A. K. 2012. Evaluation of Modal pushover-based scaling of one component of ground-motion: Tall buildings. *Earthquake Spectra,* 28**,** 1469-1493.

KALKAN, E. & KWONG, N. S. 2011. Documentation for Assessment of Modal Pushover-based Scaling Procedure for Nonlinear Response History Analysis of "Ordinary Standard" Bridges. *U.S. Geological Survey Open-File Report 2010-1328, 56 p.*

KAPPOS, A. J., CHRYSSANTHOPOULOS, M. K. & DYMIOTIS, C. 1999. Uncertainty analysis of strength and ductility of confined reinforced concrete members. *Engineering Structures,* 21**,** 195-208.

KAPPOS, A. J. & KYRIAKAKIS, P. 2000. A re-evaluation of scaling techniques for natural records. *Soil Dynamics and Earthquake Engineering,* 20**,** 111-123.

KARBASSI, A. 2010. *Performance-based seismic vulnerability evaluation of existing buildings in old sectors of Quebec.* Ph.D Dissertation, École de Technologie Supérieure (Université du Québec).

KARBASSI, A. & NOLLET, M. 2008. Application of the Applied Element Method to the Seismic Vulnerability Evaluation of Existing Buildings. *Canadian Society for Civil Engineering, 6th Structural Specialty Conference, Quebec City, QC,paper ST-401*.

KARTAL, M. E., BASAGA, H. B. & BAYRAKTAR, A. 2011. Probabilistic nonlinear analysis of CFR dams by MCS using Response Surface Method. *Applied Mathematical Modelling,* 35**,** 2752-2770.

KATAHIRA, N., ISOBE, D., INE, T. & KAJIWARA, K. Development Of macro-model seismic collapse simulator for framed structures using ASI-Gauss technique. The 14th World Conference on Earthquake Engineering October 12-17 2008 Beijing, China.

KATSANOS, E. I., SEXTOS, A. G. & MANOLIS, G. D. 2010. Selection of earthquake ground motion records: A state-of-the-art review from a structural engineering perspective *Soil Dynamics and Earthquake Engineering* 30**,** 157-169.

KEIICHIRO, S., YUKO, S., MOTOHIDE, T., YUICHI, M., SATOSHI, Y. & KAZUHIKO, K. 2009. Full scale shaking table collapse experiment on 4-story steel moment frame. *Behaviour of Steel Structures in Seismic Areas.* CRC Press.

KENNEDY, R. P., SHORT, S. A., MERZ, K. L., TOKARZ, F. J., IDRISS, I. M., POWER, M. S. & SADIGH, K. 1984. Engineering characterization of ground motion. Task I. Effects of characteristics of free-field motion on structural response. *Other Information: Portions are illegible in microfiche products.*

KHALIL, A. 2011. Enhanced Modeling of Steel Structures for Progressive Collapse Analysis Using Applied Element Method. *Journal of Performance of Constructed Facilities, ASCE*.

KIKUCHI, A., KAWAI, T. & SUZUKI, N. 1992. The rigid bodies-spring models and their applications to three-dimensional crack problems. *Computers & Structures,* 44**,** 469-480.

KIM, S. J. & ELNASHAI, A. S. 2008. *Seismic assessment of RC structures considering vertical ground motion.* Ph.D. thesis, University of Illinois.

KIM, S. J. & ELNASHAI, A. S. 2009. Characterization of shaking intensity distribution and seismic assessment of RC buildings for the Kashmir (Pakistan) earthquake of October 2005. *Engineering Structures,* 31**,** 2998-3015.

KIM, S. J., HOLUB, C. J. & ELNASHAI, A. S. 2011a. Analytical Assessment of the Effect of Vertical Earthquake Motion on RC Bridge Piers. *ASCE Journal of Structural Engineering,* 137**,** 252-260.

KIM, S. J., HOLUB, C. J. & ELNASHAI, A. S. 2011b. Experimental investigation of the behavior of RC bridge piers subjected to horizontal and vertical earthquake motion. *Engineering Structures,* 33**,** 2221-2235.

KIM, Y., KABEYASAWA, T., MATSUMORI, T. & KABEYASAWA, T. 2012. Numerical study of a full-scale six-story reinforced concrete wall-frame structure tested at E-Defense. *Earthquake Engineering & Structural Dynamics,* 41.

KRAMER, S. 1996. *Geotechnical earthquake engineering,* Upper Saddle River, N.J.: Prentice Hall.

KRAMER, S. L. & MITCHELL, R. A. 2006. Ground motion intensity measures for liquefaction hazard evaluation. *Earthquake Spectra,* 22.

KRAWINKLER, H. 2005. Van Nuys Hotel Building Testbed Report: Exercising Seismic Performance Assessment. *PEER Rep. No. 2005/11, Pacific Earthquake Engineering Research Center, Univ. of California, Berkeley*.

KRAWINKLER, H., ZAREIAN, F., LIGNOS, D. & IBARRA, L. 2009. Prediction of collapse of structures under earthquake excitations. *In: Papadrakakis M, Lagaros ND, Fragiadakis M, editors. 2nd International conference on computational methods in structural dynamics and earthquake engineering (COMPDYN 2009), Rhodes, Greece; June 22-24, 2009 [CD-ROM paper, Paper no. CD449]*.

KUPFER, H., HILSDORF, H. K. & RÜSCH, H. 1969. Behavior of Concrete under Biaxial Stresses. *ACI Journal,* 66**,** 656-666.

KURAMA, Y. C. & FARROW, K. T. 2003. Ground motion scaling methods for different site conditions and structure characteristics. *Earthquake Engineering & Structural Dynamics,* 32**,** 2425-2450.

KURODA, T., MEGURO, K. & WORAKANCHANA, K. 2004. Analysis of Confining Effect on Failure Behavior of Reinforced Concrete Structure. *13th World Conference on Earthquake Engineering,Vancouver, B.C., Canada*.

KWON, O.-S. & ELNASHAI, A. 2006. The effect of material and ground motion uncertainty on the seismic vulnerability curves of RC structure. *Engineering Structures,* 28**,** 289-303.

LEE, T.-H. & MOSALAM, K. M. 2005. Seismic demand sensitivity of reinforced concrete shear-wall building using FOSM method. *Earthquake Engineering and Structural Dynamics,* 34**,** 1719-1736.

LEE, T.-H. & MOSALAM, K. M. 2006. Probabilistic Seismic Evaluation of Reinforced Concrete Structural Components and Systems. *PEER Rep. No. 2006/04, Pacific Earthquake Engineering Research Center, Univ. of California, Berkeley.*

LIEL, A. & TUWAIR, H. 2010. A Practical Approach for Assessing Structural Resistance to Earthquake-Induced Collapse. *2010 ASCE Structures Congress, 19th Analysis and Computation Specialty Conference.*

LIEL, A. B. & DEIERLEIN, G. G. 2008. Assessing the Collapse Risk of California's Existing Reinforced Concrete Frame Structures: Metrics for Seismic Safety Decisions. *Blume Center Technical Report No. 166.*

LIEL, A. B., HASELTON, C. B. & DEIERLEIN, G. G. 2008. Comparative Assessment of Collapse Safety of Reinforced-Concrete Moment Frame Buildings. *The 14th World Conference on Earthquake Engineering October 12-17, 2008, Beijing, China.* October 12-17, 2008, Beijing, China.

LIEL, A. B., HASELTON, C. B. & DEIERLEIN, G. G. 2011. Seismic Collapse Safety of Reinforced Concrete Buildings. II: Comparative Assessment of Nonductile and Ductile Moment Frames. *Journal of Structural Engineering,* 137.

LIEL, A. B., HASELTON, C. B., DEIERLEIN, G. G. & BAKER, J. W. 2009. Incorporating modeling uncertainties in the assessment of seismic collapse risk of buildings. *Structural Safety,* 31**,** 197-211.

LIGNOS, D. & KRAWINKLER, H. 2009. Sidesway collapse of deteriorating structural systems under seismic excitations. *Report No. 172, The John A. Blume Earthquake Engineering Center, Stanford University, Stanford, CA.*

LIGNOS, D. & KRAWINKLER, H. 2011. Deterioration modeling of steel components in support of collapse prediction of steel moment frames under earthquake loading. *Journal of Structural Engineering,* 137**,** 1291-1302.

LIGNOS, D. G., KRAWINKLER, H. & WHITTAKER, A. S. 2011. Prediction and validation of sidesway collapse of two scale models of a 4-story steel moment frame. *Earthquake Engineering & Structural Dynamics,* 40**,** 807-825.

LIU, Y., XU, L. & GRIERSON, D. E. 2003. Performance of buildings under abnormal loading. *Proceedings of the Response of Structures to Extreme Loading Conference, Toronto, Canada.*

LU, X., LIN, X., MA, Y., LI, Y. & YE, L. 2008. Numerical Simulation for the Progressive Collapse of Concrete Building due to Earthquake. *Proc. the 14th World Conference on Earthquake Engineering.* Beijing, China.

LU, X., LIN, X. & YE, L. 2009. Simulation of structural collapse with Coupled Finite Element-Discrete Element Method *Proc. Computational Structural Engineering, Yuan Y, Cui JZ and Mang H(eds.).* Springer, Shanghai.

LU, Y. 1996. *Study of seismic behavior of reinforced concrete frames having vertical irregularities.* Doctoral dissertation, National Technical Univ. of Athens.

LU, Y. 2002. Comparative Study of Seismic Behavior of Multistory Reinforced Concrete Framed Structures. *Journal of Structural Engineering,* 128**,** 169-178.

LU, Y., TASSIOS, T. P., ZHANG, G.-F. & VINTZILEOU, E. 1999. Seismic Response of Reinforced Concrete Frames with Strength and Stiffness Irregularities. *ACI Struct. J.,* 96**,** 221-229.

LUCCHINI, A., MOLLAIOLI, F. & MONTI, G. 2011. Intensity measures for response prediction of a torsional building subjected to bi-directional earthquake ground motion. *Bulletin of Earthquake Engineering,* 9.

LUCO, N. 2002. *Probabilistic seismic demand analysis, SMRF connection fractures, and near-source effects.* Ph.D. thesis, Stanford University.

LUCO, N. & CORNELL, C. A. 2007. Structure-Specific Scalar Intensity Measures for Near-Source and Ordinary Earthquake Ground Motions. *Earthquake Spectra,* 23**,** 357-392.

LUCO, N., MANUEL, L., BALDAVA, S. & BAZZURRO, P. 2005. Correlation of damage of steel momentresisting frames to a vector-valued set of ground motion parameters. *9th International Conference on Structural Safety and Reliability.* Rome, Italy.

LUPOAE, M., BACIU, C., CONSTANTIN, D. & PUSCAU, H. 2011. Aspects Concerning Progressive Collapse of a Reinforced Concrete Frame Structure with Infill Walls. *Proceedings of the World Congress on Engineering, WCE 2011.* London, U.K.

LUPOAE, M. & BUCUR, C. 2009. Use of Applied Element Method to Simulate the Collapse of a Building. *SISOM 2009 and Session of the Commission of Acoustics, Bucharest 28-29 May*.

LYNN, K. M. & ISOBE, D. 2007. Structural collapse analysis of framed structures under impact loads using ASI-Gauss finite element method. *International Journal of Impact Engineering,* 34**,** 1500-1516.

MAEKAWA, K. 1991. *Nonlinear Analysis and Constitutive Models of Reinforced Concrete,* Tokyo, Gihodo Co. Ltd.

MARTINEZ-RUEDA, J. E. 1998. Scaling procedure for natural accelerograms based on a system of spectrum intensity scales. *Earthquake Spectra,* 14**,** 135-152.

MATLAB 2008 *version 7.6.0.234. Natick, Massachusetts: The MathWorks Inc.*

MATSUMORI, T., KIM, J. & KABEYASAWA, T. 2005. Shaking table test of a one-third-scale model of a six-story wall-frame R/C structure. *Proceedings of the First NEES/E-Defense Workshop on Collapse Simulation of Reinforced Concrete Building Structures,* PEER Rep. No. 2005/10, Pacific Earthquake Engineering Research Center, Univ. of California, Berkeley.

MCGUIRE, R. 2004. Seismic hazard and risk analysis. . *Berkeley: Earthquake Engineering Research Institute*.

MEDINA, R. A. & KRAWINKLER, H. 2005. Strength Demand Issues Relevant for the Seismic Design of Moment-Resisting Frames. *Earthquake Spectra,* 21**,** 415-439.

MEGURO, K. & HAKUNO, M. 1989. Fracture analyses of concrete structures by the modified distinct element method. *Structural Eng/Earthquake Eng,* 6**,** 283-294.

MEGURO, K. & HAKUNO, M. 1994. Application of the extended distinct element method for collapse simulation of a double-deck bridge. *Struc Eng/Earthquake Eng,* 10**,** 175-185.

MEGURO, K. & SATO, T. 1996. Simulation of collapse of structures due to the 1995 Great Hanshin earthquake. *Proceedings of the Eleventh World Conference on Earthquake Engineering, Acapulco, Mexico*.

MEGURO, K. & TAGEL-DIN, H. 1999a. Applied Element Method: A new efficient tool for design of structure considering its failure behavior. *5th U.S. National Conference on Lifeline Earthquake Engineering, Seattle, Washington, 12-14 Aug.*

MEGURO, K. & TAGEL-DIN, H. 1999b. Simulation of buckling and post-buckling behavior of structures using applied element method. *Bulletin of Earthquake Resistant Structure Research Center, IIS, University of Tokyo,* 32**,** 125-135.

MEGURO, K. & TAGEL-DIN, H. 2000. Applied Element Method for Structural Analysis: Theory and Application for Linear Materials. *Structural Eng./Earthquake Eng., International Journal of the Japan Society of Civil Engineers (JSCE)* 17**,** 21s-35s.

MEGURO, K. & TAGEL-DIN, H. 2001. Applied Element Simulation of RC Structures under Cyclic Loading. *Journal of Structural Engineering,* 127**,** 1295-1305.

MEGURO, K. & TAGEL-DIN, H. 2002. Applied Element Method Used for Large Displacement Structural Analysis. *Journal of Natural Disaster Science,* 24**,** 25-34.

MEHANNY, S. S. F. 1999. *Modeling and Assessment of Seismic Performance of Composite Frames with Reinforced Concrete Columns and Steel Beams.* Ph.D. Dissertation, Stanford University.

MEHANNY, S. S. F. 2009. A broad-range power-law form scalar-based seismic intensity measure. *Engineering Structures,* 31**,** 1354-1368.

MEHANNY, S. S. F. & DEIERLEIN, G. G. 2001. Seismic damage and collapse assessment of composite moment frames. *J. Struct. Eng,* 127**,** 1045-1053.

MIAO, Z. W., LU, X. Z., YE, L. P. & MA, Q. L. 2007. Simulation for the collapse of RC frame tall buildings under earthquake disaster. *Proc. International Symposium on Computational Mechanics (ISCM2007),* July 30-August 1, 2007, Beijing, China.

MIRZA, S. A., HATZINIKOLAS, M. & MACGREGOR, J. G. 1979. Statistical descriptions of strength of concrete. Journal of Structural Division. *ASCE* 105**,** 1021-37.

MITCHELL, M. 1991. *Engauge digitizer- digitizing software Version: 2.*

MOEHLE, J. P., ELWOOD, K. J. & SEZEN, H. 2002. Gravity load collapse of building frames during earthquakes. *ACI SP-197. Behavior and Design of Concrete Structures for Seismic Performance. American Concrete Institute***,** 215-238.

MOEHLE, J. P. & MAHIN, S. A. 1991. Observations on the behavior of reinforced concrete buildings during earthquakes. *ACI SP-127, Earthquake-resistant concrete structures inelastic response and design, S. K. Ghosh, ed., American Concrete Institute, Detroit, 67–89.,* 127**,** 67-90.

MOSALAM, K. M., TALAAT, M. & PARK, S. 2008. Modeling Progressive Collapse in Reinforced Concrete Framed Structures. *Proceedings of the 14th World Conference on Earthquake Engineering, Beijing, China, October 12-17, 8 pp.*

MOUSAVI, M., GHAFORY-ASHTIANY, M. & AZARBAKHT, A. 2011. A new indicator of elastic spectral shape for the reliable selection of ground motion records. *Earthquake Engineering & Structural Dynamics,* 40**,** 1403-1416.

MUNSHI, J. A. & GHOSH, S. K. 1998. Analyses of seismic performance of a code designed reinforced concrete building. *Engineering Structures,* 20**,** 608-616.

MWAFY, A. 2001. *Seismic performance of code-designed RC buildings.* Doctor of Philosophy, Imperial College London.

MWAFY, A. & ELNASHAI, A. 2006. Vulnerability of code-compliant RC buildings under multi-axial earthquake loading. *4th International Conference on Earthquake Engineering.* Taipei, Taiwan.

NAGAE, T., HAYASHI, S., IBARRA, L. & KRAWINKLER, H. 2005. Damage Process and collapse of RC frame structure- from the viewpoint of mechanism control. *Proceedings of the First NEES/E-Defense Workshop on Collapse Simulation of Reinforced Concrete Building Structures, PEER Rep. No. 2005/10, Pacific Earthquake Engineering Research Center, Univ. of California, Berkeley.*

NAKASHIMA, M., MATSUMIYA, T., LIU, D. & SUITA, K. 2004. Roles of large-scale test for assessment of seismic performance. *In:* FAJFAR, P. & KRAWINKLER, H. (eds.) *International Workshop on Performance-Based Seismic Design.* Bled, Slovenia.

NEWMARK, N. M. & HALL, W. J. 1978. Development of criteria for seismic review of selected nuclear power plants. *NUREG/CR-0098, Nuclear Regulatory Commission*.

NIST 2011. Selecting and Scaling Earthquake Ground Motions for Performing Response-History Analyses. *NIST GCR 11-917-15. Prepared by the NEHRP Consultants Joint Venture for the National Institute of Standards and Technology, Gaithersburg, Maryland*.

OKAMURA, H. & MAEKAWA, K. 1991. *Nonlinear Analysis and Constitutive Models of Reinforced Concrete,* Tokyo, Gihodo Co. Ltd.

OPENSEES 2005. Open system for earthquake engineering simulation. *Pacific Earthquake Engineering Research Center, http://opensees.berkeley.edu.*

OPENSEES 2010. Open system for earthquake engineering simulation. *Pacific Earthquake Engineering Research Center (PEER).*

PANDEY, B. & MEGURO, K. 2004. Simulation of Brick Masonry Wall Behavior under Inplane Lateral Loading Using Applied Element Method. *Proceedings on 13WCEE,Vancouver, Canada*.

PAPAZOGLOU, A. J. & ELNASHAI, A. S. 1996. Analytical and field evidence of the damaging effect of vertical earthquake ground motion. *Earthquake Eng. Struct. Dyn,* 25**,** 1109-1137.

PARK, Y. J., REINHORN, A. M. & KUNNATH, S. K. 1987. IDARC: Inelastic Damage Analysis of RC Frame-Shear Wall Structures. *Technical Report NCEER-87-0008, Center for Earthquake Engineering Research,State University of New York, Buffalo NY.*

PINTO, A., NEGRO, P. & TAUCER, F. 2004. Full-scale laboratory testing: Strategies and procedures to meet the needs of PBEE. *In:* FAJFAR, P. & KRAWINKLER, H. (eds.) *International Workshop on Performance-Based Seismic Design.* Bled, Slovenia.

PORTER, K. A., BECK, J. L. & SHAIKHUTDINOV, R. V. 2002. Sensitivity of Building Loss Estimates to Major Uncertain Variables. *Earthquake Spectra,* 18**,** 719- 743.

RAHNAMA, M. & KRAWINKLER, H. 1993. Effects of Soft Soil and Hysteresis Model on Seismic Demands. *The John Blume Earthquake Engineering Center, Stanford University,* Report No. 108.

RAPARLA, H. B., BODIGE, N. & KUMAR, R. P. 2011. 2D Numerical Modeling of Progressive Collapse during Earthquakes: A Case Study on RC Bare Frame. *Proceedings of International Conference on Advances in Civil Engineering, ACE-2011***,** 1-25.

REYES, J. & CHOPRA, A. 2012. Modal Pushover-Based Scaling of Two Components of Ground Motion Records for Nonlinear RHA of Structures. *Earthquake Spectra,* 28**,** 1243-1267.

RIDDELL, R. 2007. On Ground Motion Intensity Indices. *Earthquake Spectra,* 23**,** 147-173.

RISTIC, D., YAMADA, Y. & IEMURA, H. 1986. Stress-strain based modeling of hysteretic structures under earthquake induced bending and varying axial loads. *Research report no. 86-ST-01. Kyoto (Japan): School of Civil Engineering. Kyoto University*.

SALEM, H. M., EL-FOULY, A. K. & TAGEL-DIN, H. S. 2011. Toward an economic design of reinforced concrete structures against progressive collapse. *Engineering Structures,* 33**,** 3341-3350.

SASANI, M. 2008. Response of a reinforced concrete infilled-frame structure to removal of two adjacent columns. *Engineering Structures,* 30**,** 2478-2491.

SEISMOSOFT 2011. SeismoSignal v4.3.0. http://www.seismosoft.com/en/Download.aspx.

SEZEN, H., ELWOOD, K. J., WHITTAKER, A. S., MOSALAM, K. M., WALLACE, J. W. & STANTON, J. F. 2000. Structural engineering reconnaissance of the August 17, 1999 Earthquake: Kocaeli (Izmit), Turkey. *PEER Rep. No. 2000/09, Pacific Earthquake Engineering Research Center, Univ. of California, Berkeley*.

SEZEN, H. & MOEHLE, J. 2004. Shear strength model for lightly reinforced concrete columns. *Journal of Structural Engineering,* 130**,** 1692-1703.

SEZEN, H., WHITTAKER, A. S., ELWOOD, K. J. & MOSALAM, K. M. 2003. Performance of reinforced concrete buildings during the August 17, 1999 Kocaeli, Turkey earthquake, and seismic design and construction practise in Turkey. *Eng Struct,* 25**,** 103-114.

SHIH, C., WANG, Y.-K. & TING, E. C. 2004. Fundamentals of a Vector Form Intrinsic Finite Element: Part III. Convected Material Frame and Examples. *Journal of Mechanics,* 20**,** 133-143.

SHIRAI, K., MATSUMORI, T. & KABEYASAWA, T. 3-D dynamic collapse test of a six-story full-scale RC wall-frame building. Structural Engineering Research Frontiers, 2007 Long Beach, California, USA. ASCE, 1-10.

SHOME, N. 1999. *Probabilistic Seismic Demand Analysis of Nonlinear Structures.* Ph.D. thesis, Stanford University.

SHOME, N., CORNELL, C. A., BAZZURRO, P. & CARBALLO, J. E. 1998. Earthquakes, records and nonlinear responses. *Earthquake Spectra* 14**,** 469-500.

STAROSSEK, U. 2007. Typology of progressive collapse. *Engineering Structures,* 29**,** 2302-2307.

STEWART, J., CHIOU, S., BRAY, R., GRAVES, P., SOMERVILLE, G. & ABRAHAMSON, N. 2001. Ground motion evaluation procedures for performance-based design. *PEER report 2001/09, Pacific Earthquake Engineering Research Center, University of California, Berkeley*.

SUN, L., ZHOU, C. & FUJINO, Y. 2003a. *Collapse Simulation of RC Bridge Due to Earthquake ,The EQTAP Workshop, Shanghai, 2003.11*. [Online]. Available: <http://eqtap.edm.bosai.go.jp/useful_outputs/report/fujino/data/document/10_EQTAP_Collapse%20Simulation%20from%20Limin%20Sun_2003.pdf> [Accessed 10-8 2010].

SUN, L., ZHOU, C., QIN, D. & FAN, L. 2003b. Application of extended distinct element method with lattice model to collapse analysis of RC bridges. *Earthquake Engineering & Structural Dynamics,* 32**,** 1217-1236.

TAGEL-DIN, H. & MEGURO, K. 1999a. Applied element simulation for collapse analysis of structures. *Bulletin of Earthquake Resistant Structure Research Center, IIS, University of Tokyo,* 32**,** 113-123.

TAGEL-DIN, H. & MEGURO, K. 1999b. Simulation of Collapse Process of a Scaled RC Building Subjected to Base Excitation. *Proceedings of the 25th Japan Society of Civil Engineers (JSCE) Earthquake Engineering Symposium, Tokyo.*

TAGEL-DIN, H. & MEGURO, K. 2000a. Analysis of a Small Scale RC Building Subjected to Shaking Table Tests using Applied Element Method. *Proceedings of the 12th World Conference on Earthquake Engineering, New Zealand, January 30th - February 4th, 2000.*

TAGEL-DIN, H. & MEGURO, K. 2000b. Applied Element Method for Dynamic Large Deformation Analysis of Structures. *Structural Eng./Earthquake, JSCE,* 17**,** 215s-224s.

TAGEL-DIN, H. & MEGURO, K. 2000c. Nonlinear simulation of RC structures using Applied Element Method. *Structural Eng./Earthquake, JSCE,* 17**,** 137s-148s.

TALAAT, M. & MOSALAM, K. M. 2009. Modeling progressive collapse in reinforced concrete buildings using direct element removal. *Earthquake Engineering & Structural Dynamics,* 38**,** 609-634.

TALAAT, M. M. & MOSALAM, K. M. 2008. Computational Modeling of Progressive Collapse in Reinforced Concrete Frame Structures. *PEER Rep. No. 2007/10, Pacific Earthquake Engineering Research Center, Univ. of California, Berkeley*.

TING, E. C., SHIH, C. & WANG, Y.-K. 2004a. Fundamentals of a Vector Form Intrinsic Finite Element: Part I. Basic Procedure and A Plane Frame Element. *Journal of Mechanics,* 20**,** 113-122.

TING, E. C., SHIH, C. & WANG, Y.-K. 2004b. Fundamentals of a Vector Form Intrinsic Finite Element: Part II. Plane Solid Elements. *Journal of Mechanics,* 20**,** 123-132.

TOI, Y. & ISOBE, D. 1996. Finite element analysis of quasi-static and dynamic collapse behaviors of framed structures by the adaptively shifted integration technique. *Computers & Structures,* 58**,** 947-955.

TOTHONG, P. 2007. *Probabilistic Seismic Demand Analysis Using Advanced Ground Motion Intensity Measures, Attenuation Relationships, and Near Fault Effects.* Ph.D. thesis, Stanford University.

TOTHONG, P. & CORNELL., C. A. 2007. Probabilistic Seismic Demand Analysis Using Advanced Ground Motion Intensity Measures, Attenuation Relationships, and Near-Fault Effects. *Report No. PEER 2006/11*. Pacific Earthquake Engineering Research Center, University of California, Berkeley.

TOTHONG, P. & LUCO, N. 2007. Probabilistic seismic demand analysis using advanced ground motion intensity measures. *Earthquake Engineering & Structural Dynamics,* 36**,** 1837-1860.

TRIFUNAC, M. D. & BRADY, A. G. 1975. A study on the duration of strong earthquake ground motion *Bulletin of the Seismological Society of America,* 65**,** 581-626.

TUAN-NAM, T. & KASAI, K. 2012. Study on shaking-table experiment of a full-scale four-story steel building. *the 15th World Conference on Earthquake Engineering.* Lisbon.

UBC 1997. Uniform building code. *International Conference of Building officials, Whittier, California.*

UEHAN, F. & MEGURO, K. 2004a. Application of Numerical Simulation and Vibration Measurements for Seismic Damage Assessment of Railway Structures. *JSME International Journal Series C,* 47**,** 544-552.

UEHAN, F. & MEGURO, K. 2004b. Railway Structure Earthquake Damage Assessment Using Numerical Simulation and Vibration Measurement. *Quarterly Report of RTRI,* 45**,** 123-130.

VAMVATSIKOS, D. & CORNELL, C. A. 2002. Incremental dynamic analysis. *Earthquake Engineering & Structural Dynamics,* 31**,** 491-514.

VAMVATSIKOS, D. & CORNELL, C. A. 2005. Developing efficient scalar and vector intensity measures for IDA capacity estimation by incorporating elastic spectral shape information. *Earthq Eng Struct Dyn,* 1.

VAMVATSIKOS, D. & FRAGIADAKIS, M. 2010. Incremental dynamic analysis for estimating seismic performance sensitivity and uncertainty. *Earthquake Eng Struct Dyn,* 39**,** 141-163.

VASCONCELLOS REAL, M. D., FILHO, A. C. & MAESTRINI, S. R. 2003. Response variability in reinforced concrete structures with uncertain geometrical and material properties. *Nuclear Engineering and Design,* 226**,** 205-220.

VILLAVERDE, R. 2007. Methods to assess the seismic collapse capacity of building structures: state of the art. *Journal of Structural Engineering,* 133**,** 57-66.

VLASSIS, A. G. 2007. *Progressive collapse assessment of tall buildings.* Doctor of Philosophy, Imperial College London.

VON-THUN, J., ROCHIM, L., SCOTT, G. & WILSON, J. 1988. Earthquake ground motions for design and analysis of dams. *Earthquake Engineering and Soil Dynamics II - Recent advances in ground motion evaluation. New York: ASCE*.

WANG, C.-Y., WANG, R.-Z. & TSAI, K.-C. 2006. Numerical simulation of the progressive failure and collapse of structure under seismic and impact loading. *4th International Conference on Earthquake Engineering.* Taipei, Taiwan.

WANG, R.-Z., TSAI, K.-C. & LIN, B.-Z. 2011. Extremely large displacement dynamic analysis of elastic–plastic plane frames. *Earthquake Engineering & Structural Dynamics,* 40**,** 1515-1533.

WANG, R. Z., WU, C. L., TSAI, K. C., YANG, Y. S. & LIN, B. Z. Structural collapse analysis of framed structures under seismic excitation. The 14th World Conference on Earthquake Engineering 2008 Beijing, China.

WATSON-LAMPREY, E., HASELTON, C., LUCO, N., BAKER, J. & GOULET, C. A. 2008. Assessment of Ground Motion Selection and Modification (GMSM) Methods for Non-Linear Dynamic Analyses of Structures. *Geotechnical Earthquake Engineering and Soil Dynamics IV*.

WENG, Y.-T., TSAI, K.-C. & CHAN, Y.-R. 2010. A Ground Motion Scaling Method Considering Higher-Mode Effects and Structural Characteristics. *Earthquake Spectra,* 26**,** 841-867.

WIBOWO, H. 2009. *Progressive Collapse Analysis of Reinforced Concrete Bridges during Earthquakes.* Master of Applied Science, Carleton University.

WIBOWO, H. & LAU, D. T. 2009. Seismic progressive collapse: qualitative point of view. *Civil Engineering Dimension,* 11**,** 8-14.

WIBOWO, H., RESHOTKINA, S. S. & LAU, D. T. Modelling progressive collapse of RC bridges during earthquakes. CSCE Annual General Conference May 27-30 2009 St. John's, NL, Canada.

WORAKANCHANA, K., MAYORCA, P., GURAGAIN, R., NAVARATNARAJ, S. & MEGURO, K. 2008. 3-D Applied Element Method for PP-Band Retrofitted Masonry. *SEISAN KENKYU,* 60**,** 128-131.

XIANGUO, Y., JIARU, Q. & KANGNING, L. 2004. Shaking table test and dynamic response prediction on an earthquake-damaged RC building. *Earthquake Engineering and Engineering Vibration,* 3**,** 205-214.

YAHYAABADI, A. & TEHRANIZADEH, M. 2011. New scalar intensity measure for near-fault ground motions based on the optimal combination of spectral responses. *Scientia Iranica,* 18**,** 1149-1158.

YAKUT, A. & YALMAZ, H. 2008. Correlation of Deformation Demands with Ground Motion Intensity. *Journal of Structural Engineering,* 134**,** 1818-1828.

YAMADA, S., SUITA, K., TADA, M., KASAI, K., MATSUOKA, Y. & SHIMADA, Y. 2008. Collapse experiment on 4-story steel moment frame: Part 1 outline of test results. *Proceedings of the 14WCEE, Beijing, China*.

YANG, D., PAN, J. & LI, G. 2009. Non-structure-specific intensity measure parameters and characteristic period of near-fault ground motions. *Earthquake Engineering & Structural Dynamics,* 38**,** 1257-1280.

YIN, Y.-J. & LI, Y. 2010. Seismic collapse risk of light-frame wood construction considering aleatoric and epistemic uncertainties. *Structural Safety,* 32**,** 250-261.

ZAREIAN, F. & KRAWINKLER, H. 2007. Assessment of probability of collapse and design for collapse safety. *Earthquake Engineering & Structural Dynamics,* 36**,** 1901-1914.

ZAREIAN, F. & KRAWINKLER, H. 2009. Simplified performance-based earthquake engineering. *Report No. 169, The John A. Blume Earthquake Engineering Center, Stanford University, Stanford, CA.*

ZAREIAN, F., KRAWINKLER, H., IBARRA, L. & LIGNOS, D. 2010. Basic concepts and performance measures in prediction of collapse of buildings under earthquake ground motions. *The Structural Design of Tall and Special Buildings,* 19**,** 167-181.

ZAREIAN, F., KRAWINKLER, H., LIGNOS, D. G. & IBARRA, L. F. 2008. Predicting collapse of frame and wall structures. *The 14th World Conference on Earthquake Engineering October 12-17, 2008, Beijing, China.*

ZHANG, G. F. 1995. *Study of the seismic behavior of reinforced concrete frames with or without infills.* Doctoral dissertation, National Technical Univ. of Athens.

ZHANG, L.-M. & LIU, X.-L. 2008. Learning From The Wenchuan Earthquake: Key Problems In Collapse Analysis Of Structures *The 14th World Conference on Earthquake Engineering October 12-17.* Beijing, China

ZHANG, L. & LIU, X. 2000. Collapse Analysis of Reinforced Concrete Frame Structures Considering Collision Effects. *Proceedings of 12WCEE* 0289